NATIONAL TECHNICAL UNIVERSITY OF ATHENS

SCHOOL OF CIVIL ENGINEERING

DEPARTMENT OF WATER RESOURCES AND ENVIRONMENTAL ENGINEERING

LABORATORY OF HARBOUR WORKS

Propagation of Water Waves in Shallow Water with Emphasis on Fluid-Seabed Interactions: Advantages and Limitations of 2DH Numerical Techniques

PhD THESIS

VASILEIOS AFENTOULIS

Athens, December 2022

NATIONAL TECHNICAL UNIVERSITY OF ATHENS

SCHOOL OF CIVIL ENGINEERING

DEPARTMENT OF WATER RESOURCES AND ENVIRONMENTAL ENGINEERING

LABORATORY OF HARBOUR WORKS

Propagation of Water Waves in Shallow Water with Emphasis on Fluid-Seabed Interactions: Advantages and Limitations of 2DH Numerical Techniques

DISSERTATION
for the degree of Doctor of Philosophy
submitted to School of Civil Engineering of National Technical University of Athens

by
Vasileios Afentoulis
Defended in public:
28.11.2022
in Athens, Greece

Members of the Examining Committee:

Prof. Vasiliki Tsoukala	School of Civil Eng., NTUA	*Supervisor*
Prof. Kostas Belibassakis	School of Naval Archit., NTUA	*Adv. Committee*
Prof. Bijan Mohammadi	Université de Montpellier	*Adv. Committee*
Prof. Anastasios Stamou	School of Civil Eng., NTUA	
Prof. Theofanis Karambas	Dep. of Civil Eng., AUTh	
Assist. Prof. Achilleas Samaras	School of Civil Eng., D.U.Th	
Prof. Michel Benoit	EDF R&D (LNHE)	

ΕΘΝΙΚΟ ΜΕΤΣΟΒΙΟ ΠΟΛΥΤΕΧΝΕΙΟ

ΣΧΟΛΗ ΠΟΛΙΤΙΚΩΝ ΜΗΧΑΝΙΚΩΝ

ΤΟΜΕΑΣ ΥΔΑΤΙΚΩΝ ΠΟΡΩΝ ΚΑΙ ΠΕΡΙΒΑΛΛΟΝΤΟΣ

ΕΡΓΑΣΤΗΡΙΟ ΛΙΜΕΝΙΚΩΝ ΕΡΓΩΝ

Διάδοση Κυμάτων σε Ρηχά Νερά και Αλληλεπίδραση Ρευστού - Θαλάσσιου Πυθμένα: Πλεονεκτήματα και Περιορισμοί Υπολογιστικών Προσομοιώσεων με Μοντέλα Μέσου Βάθους

ΔΙΔΑΚΤΟΡΙΚΗ ΔΙΑΤΡΙΒΗ

ΒΑΣΙΛΕΙΟΣ ΑΦΕΝΤΟΥΛΗΣ

Αθήνα, Δεκέμβριος 2022

To my mother Maria
Στη μητέρα μου Μαρία

Abstract

This study seeks to assist in better understanding of non-cohesive sediments movement under wave-current actions. The core aim of the present dissertation is to develop novel, advanced 2DH numerical modelling techniques, and evaluate the advantages limitations of the existing ones, with the purpose of precisely simulating morphodynamic mechanisms over a variety of complex and irregular bathymetries, considering wave unsteady phenomena and several small-scale physical processes in the inner surf and swash zone. In addition, the advanced compound models, which were tailored within the context of the present research, served to assess the hydrodynamic and morphodynamic effects of a number of coastal defence types, such as submerged and emerged offshore-detached breakwaters, groynes and jetties.

To analyse general sediment phenomena in erosion-dominated and high-energy coasts, numerical assessments, based on available existing devices, were carried out in selected case studies in Greece. Furthermore, laboratory experimental data analysis and advanced coupled models were used to study the incipient motion of fine-sand and morphological evolution from dissipative to intermediate and reflective beach state.

Finally, inspired by the capacities and limitations of the existing numerical devices, the development of a novel and robust numerical model was achieved in purpose of practical applications. In particular, a process-based newly developed sediment transport model, with a quasi-3D approach for the assessment of suspended sediment transport, was utilized in tandem with a fully non-linear Boussinesq model to evaluate wave-current-sediment transport interactions in wave-dominated conditions, with and without the presence of coastal defences. In this context, novel 3D and 2D laboratory experimental investigations were exploited to corroborate the numerical predictions. The model validation against experimental measurements revealed that the main scope of the thesis was fulfilled satisfactorily.

In summary, this work unveils several fundamental aspects of fine sediment motion under the combined and unsteady action of waves and currents. It is believed that this research will help to further enhance our understanding of how 2DH modelling techniques can be applied in an extended range of coastal engineering problems, while it can be a valuable asset for engineers and scientists desiring to obtain accurate bed level evolution predictions.

Acknowledgments

I would like to express my gratitude to my supervisor and Director of Laboratory of Harbour Works (NTUA) Professor Vasiliki Tsoukala for giving me the opportunity to pursue this PhD thesis, and helping me in dealing with the research issues, that arose during every stage of my dissertation. It has been an honour and a privilege to collaborate with Professor Vasiliki Tsoukala for more than 11 years, starting from my undergraduate thesis in 2011. My heartfelt thanks also go to the co-supervisors Professor Kostas Belibassakis and Bijan Mohammadi. They were both aware of the progress of the PhD, through establishing a very good collaboration that encouraged me. Their comments were always apt and their contribution was catalytic since I have learnt a lot from their experience.

I would also like to thank Professor Constantinos Memos for his insightful remarks and comments, which helped me to progress my thesis. I fell also indebted to Professor Michel Benoit for hosting me in Ecole Centrale de Marseille and supervising a part of my PhD thesis. During this mobility program, I had the opportunity to develop several numerical techniques that were proven essential for the completion of my research work.

I am also grateful for the support that the research group of Laboratory of Harbour Works has provided to me and especially I would like to thank Andreas Papadimitriou for our collaboration and fruitful discussions. In addition, I would like to thank Dimitra Malliouri, Nikolas Martzikos, Eleftheria Kragiopoulou and Georgios Klonaris for the interaction and the collaboration all these years. I wish them all the best in their career.

Most of all, I would like to thank my family for everything they have offered me over these years, for their patience and the uninterrupted support to make my dreams come true.

Contents

Table of Figures

List of tables

Selected notations

a	Coefficient
A	Wave amplitude
C	Sediment concentration by mass or volume
C_a	Reference sediment concentration
c_x, c_y	Wave propagation velocities
ce	
d	Diameter of bed material
d_{50}	Median size of sediment
D	Deposition rate
D_*	Dimensionless particle size
Ca	Reference concentration
E	Erosion rate
f_c	Current friction coefficient
f_w	Wave friction coefficient
g	Gravitational acceleration
h	Water depth
H	Wave height
H_S	Significant wave height
H_{m0}	spectral significant wave height
N	Wave action density
K_c, K_l	Cross-shore and long-shore swash coefficients
K_t	Transmission coefficient
k_s	Roughness height
q	Sediment transport rate
R^b	Eddy-viscosity-type breaking term
R	Bottom friction term
Re_*	Shear Reynolds number
S_{xx}, S_{yy}	Radiation stresses
T	Wave period

T_p,	Peak wave period
u	Instantaneous horizontal velocity
$\bar{u}$	Mean horizontal velocity
u_w	Oscillatory horizontal velocity
U_C	Mean current velocity
u_*	Shear velocity
u_o	Scaling velocity
v	Velocity in y direction
v_o	Scaling velocity in y direction
$\bar{v}$	Mean velocity in y direction
w_s	Settling velocity
z	Vertical distance above the bottom
z_a	Reference height
β_e	Equilibrium angle
β	Parameter of sediment diffusivity
Δ_r	Ripple height
δ_w	Thickness of wave boundary layer
ε	Empirical sediment coefficient
ε_s	Sediment diffusivity
$\varepsilon_{s,c}$	Current-related sediment diffusivity coefficient
$\varepsilon_{s,w}$	Wave-related sediment diffusivity coefficient
ζ	Water level
η	Surface elevation
κ	Karman number
M	Horizontal flux
θ	Shields number
θ_c	Critical Shields number
ρ	Water density
ρ_s	Sediment density
τ	Shear stress
τ_c	Critical shear stress
v	Kinematic viscosity coefficient
v_t	Eddy viscosity
φ	Angle between wave and current

φ_μ	Internal friction angle
ψ	Univocal bed function
ω	Wave frequency

General operators

-	Time-average, steady component
$\sim$	Periodic component
$^{\rightarrow}$	Instantaneous component

Εκτενής Περίληψη

(Extended Abstract in Greek)

Διάδοση κυμάτων σε ρηχά νερά και αλληλεπίδραση ρευστού - θαλάσσιου πυθμένα: Πλεονεκτήματα και περιορισμοί υπολογιστικών προσομοιώσεων με μοντέλα μέσου Βάθους

του Βασίλειου Αφεντούλη

Εθνικό Μετσόβιο Πολυτεχνείο

Σχολή Πολιτικών Μηχανικών

Τομέας Υδατικών Πόρων και Περιβάλλοντος

Εργαστήριο Λιμενικών Έργων

Παρατηρώντας τους 15 από τους 20 μεγαλύτερους αστικούς ιστούς του κόσμου, μπορούμε να συμπεράνουμε πως τα παράκτια αστικά μέτωπα είναι οι περιοχές εκείνες που παρουσιάζουν την ολοένα και μεγαλύτερη αύξηση πυκνότητας πληθυσμού (Ranasinghe, 2016; Luijendijk et al., 2018). Σε παγκόσμια κλίμακα, οι παράκτιες ζώνες χαμηλής στάθμης συγκεντρώνουν το 10% του παγκόσμιου πληθυσμού (McGranahan et al., 2007). Πιο συγκεκριμένα, οι παράκτιες περιοχές φιλοξενούν περίπου 154 εκατομμύρια ανθρώπους, που ισοδυναμεί με το ένα τρίτο του πληθυσμού των μεσογειακών παράκτιων χωρών, ενώ εκτείνονται πάνω σε 46,000 χιλιόμετρα ακτογραμμής, το 54% των οποίων είναι βραχώδες και το 46% ιζηματογενές (Hénocque and Coccossis, 2001).

Τα παραλιακά συστήματα και οι χαμηλής στάθμης γειτονικές εκτάσεις, γνωστές και ως ακτές, περιλαμβάνουν όλες τις περιοχές γύρω από τη μέση στάθμη της θάλασσας. Μέχρι σήμερα, δεν υπάρχει παγκόσμιος κοινός ορισμός για τους όρους **ακτή** και **παράκτια ζώνη/περιοχή**, μία

έννοια που δίνει έμφαση στην ευρύτερη ζώνη ή την έκταση των παράκτιων οικοσυστημάτων (Nicholls et al., 2007). Όσον αφορά την έκθεση της σε πιθανή άνοδο της στάθμης της θάλασσας, ο όρος «παράκτια ζώνη χαμηλής στάθμης» έχει οριστεί ως «η συνεχόμενη περιοχή κατά μήκος της ακτής που βρίσκεται λιγότερο από 10 μέτρα πάνω από την επιφάνεια της θάλασσας» (Lichter et al., 2011).

Οι παράκτιες ζώνες και τα οικοσυστήματα που φιλοξενούνται σε αυτές καλύπτουν ένα ευρύ φάσμα βιοποικιλότητας και ανθρώπινων κοινωνικών δραστηριοτήτων. Αυτό το πολύπλοκο σύστημα διαφόρων φυσικών μεταβλητών είναι ιδιαίτερα εύθραυστο και εκτεθειμένο σε πολλαπλούς κινδύνους, όπως πλημμύρες, διάβρωση αμμωδών ακτών και καταστροφές υλικοτεχνικών υποδομών λόγω ακραίων υδρο-μετεωρολογικών φαινομένων, όπως καταιγίδες, έντονες βροχοπτώσεις και παλίρροιες (Plomaritis et al., 2018; Mori et al., 2019). Επιπλέον, οι σοβαρές περιβαλλοντικές κοινωνικές και οικονομικές επιπτώσεις στο θαλάσσιο περιβάλλον αναμένεται να είναι ακόμη πιο κρίσιμες στο εγγύς μέλλον, καθώς οι επιπτώσεις της κλιματικής αλλαγής μπορούν να επιδεινώσουν τα φαινόμενα αυτά. Περιβαλλοντικές διαταραχές, όπως η άνοδος της στάθμης της θάλασσας, οι αλλαγές στην ένταση των βροχοπτώσεων και των καταιγίδων, οι αυξημένες θερμοκρασίες, η οξίνιση των ωκεανών και η εξαφάνιση ειδών πανίδας και χλωρίδας είναι μερικές από τις προβλεπόμενες κλιματικές επιπτώσεις που θέτουν σε κίνδυνο την ισορροπία των παράκτιων συστημάτων.

Η διάβρωση των αμμωδών ακτών είναι μια αρκετά πολύπλοκη φυσική διαδικασία, καθώς περιλαμβάνει μια ανακατανομή των ιζημάτων από την επιφάνεια της παραλίας έως τα βαθιά ύδατα (Zhang et al,. 2004). **Η διάβρωση ακτών έχει σημαντικές επιπτώσεις στις υποδομές, τον τουρισμό και τη βιοποικιλότητα**, καθώς σε αστικοποιημένες παράκτιες περιοχές, οι αμμώδεις ή πετρώδεις παραλίες αποτελούν ένα σημαντικό ανάχωμα στην έντονη κυματική δράση (Almeida et al., 2012). Η διάβρωση της ακτογραμμής μπορεί να οριστεί ως η καθαρή απώλεια ιζημάτων σε μια συγκεκριμένη τομή του προφίλ πυθμένα, εντός μιας ορισμένης χρονικής κλίμακας ενδιαφέροντος (Castelle and Harley, 2020). Αυτό το φαινόμενο διάβρωσης μπορεί επίσης να σχηματοποιηθεί ως η αναρρίχηση της θάλασσας στην υποαέρια επιφάνεια του παράκτιου προφίλ (sub-aerial beach face), η οποία συχνά συνδέεται με υψηλές παλίρροιες και ενεργητικά κύματα (Senechal et al. 2020). Η παράκτια διάβρωση μπορεί επίσης να οριστεί ως μια υποχώρηση προς τη στεριά της θέσης της ακτογραμμής. Οι επιπτώσεις αυτού του ελλείμματος όγκου ιζημάτων συνδέονται με παράκτιες διεργασίες, όπως η παρουσία υπολοίπων ακτών (beach scarps), η υποσκαφή αμμόλοφων, βράχων και υποδομών.

Οι παράκτιες καταιγίδες συχνά οδηγούν σε αποσταθεροποίηση του παράκτιου συστήματος, μέσω της εντατικοποίησης του κυματικού κλίματος και πεδίου παράκτιων ρευμάτων, συντελώντας παράλληλα στην αύξηση του ύψους της στάθμης της θάλασσας. Αυτοί οι μηχανισμοί αναμορφώνουν τη γεωμετρία του θαλάσσιου πυθμένα και τη θέση ακτογραμμής, μετακινώντας μεγάλες ποσότητες άμμου προς τα βαθιά ύδατα. Το κύμα καταιγίδας, ή αλλιώς τα διακεκριμένα γεγονότα κυμάτων υψηλής ενέργειας, παράγουν υδροδυναμικά μοτίβα που είναι καθοριστικά για την εξέλιξη της μορφολογίας του βυθού. Συγκεκριμένα, τα παράκτια ρεύματα επαναφοράς (undertow) που παράγονται υπό την επίδραση των ακριών κυματισμών, μπορούν να κατευθύνουν μεγάλες ποσότητες ιζήματος προς τα βαθιά ύδατα (Toldo, 2006; Guimarães et al., 2014). Επιπλέον, για ιδιαίτερα ακραίες καιρικές συνθήκες και συνθήκες κυμάτων, μπορεί να σημειωθεί καθαρή απώλεια ιζήματος κατά μήκος του ενεργού προφίλ παραλίας (από την επιφάνεια της παραλίας ή τα μέγιστα των θινών μέχρι το βάθος κλεισίματος (Valiente et al., 2018)) . Οι διεργασίες διάβρωσης κατά τη διάρκεια ακραίων καταιγίδων μικρής περιόδου αντιπροσωπεύουν ένα ολοένα και πιο έντονο πρόβλημα για τη σταθερότητα του παράκτιου συστήματος, καθώς για ένα μεγάλο και απότομο έλλειμμα στο ισοζύγιο ιζημάτων, μπορεί να χρειαστούν δεκαετίες ώστε αυτό να αναπληρωθεί. **Στην περίπτωση αυτών των γεγονότων μικρής περιόδου, η μορφολογική εξέλιξη της γεωμετρίας του πυθμένα είναι ευθέως ανάλογη με την ποσότητα της εισερχόμενης κυματικής ενέργειας** στην παράκτια ζώνη ενώ οι χρονικές κλίμακες μορφολογίας μεταβάλλονται μέχρι να επιτευχθεί ένα νέο σημείο ισορροπίας μεταξύ εισερχόμενης στην παράκτια ζώνη κυματικής ενέργειας και μεταβολής του πυθμένα (Afentoulis et al., 2017).

Οι πρόσφατες καταγραφές ακραίων καταιγίδων και κυμάτων, που σημειώθηκαν κατά τη διάρκεια του χειμώνα 2013 - 2014 κατά μήκος των ευρωπαϊκών ακτών, είχαν ως συνέπεια τη θεαματική υποχώρηση της ακτογραμμής προς την ξηρά μέσα σε χρονικό διάστημα μόλις λίγων ημερών. Κατά τη διάρκεια αυτής της περιόδου, η ακτογραμμή μήκους 110 χιλιομέτρων της Νοτιοδυτικής Γαλλίας βρέθηκε εκτεθειμένη στις πιο έντονες κυματικές συνθήκες των τελευταίων 18 χρόνων (**Error! Reference source not found.**). Θεαματικές αλλαγές στις μετεωρολογικές και κυματικές συνθήκες έχουν επίσης εντοπιστεί στην Ελλάδα τα τελευταία χρόνια, προκαλώντας σημαντικές παράκτιες πλημμύρες και διαβρωτικά φαινόμενα. Το Σχήμα στην Εικόνα 2 δείχνει τις καταστροφικές ζημιές λόγω των ισχυρών καταιγίδων που σημειώθηκαν το 2013 στο νησί της Κρήτης στην Ελλάδα. Οι παράκτιες πλημμύρες οδήγησαν σε καταστροφές υποδομών και υπερπήδηση κυμάτων στο επίπεδο του παράκτιου μετώπου, φαινόμενο που συνοδεύτηκε από υποχώρηση της ακτογραμμής κατά δεκάδες μέτρα.

Εικόνα 1 Παράκτια διάβρωση και καταστροφές υποδομών στη νοτιοδυτική πλευρά της Γαλλίας το χειμώνα του 2013/2014

Εικόνα 2 Φαινόμενα Καταιγίδας στο Ρέθυμνο (2019)

Εκτός από τις επιπτώσεις των φυσικών διεργασιών κοντά στην ξηρά, οι ανθρωπογενείς επιπτώσεις και οι άναρχες υποδομές μπορούν να εντείνουν τη συνεχιζόμενη παράκτια διάβρωση. Προβλήτες και άλλα εμπόδια που μεταβάλλουν την στερεομεταφορά, αντανακλαστικοί κάθετοι τοίχοι που επιταχύνουν τη μετακίνηση προς τα βαθιά ύδατα, μεγάλων ποσοτήτων άμμου (Seabergh and Kraus, 2003), καθώς και η καταστροφή της βλάστησης κατά μήκος της ακτής αποτελούν βασικές αιτίες της εντατικοποίησης της διάβρωσης των ακτών σε παγκόσμια κλίμακα τόσο μεσοπρόθεσμα όσο και μακροπρόθεσμα (Gabriel Ruiz-Martínez et al., 2016). Επιπλέον, παράγοντες που δυσχεραίνουν την ισορροπία του παράκτιου συστήματος και εντατικοποιούν τη διάβρωση είναι η παρακράτηση ιζημάτων στα φράγματα, η μετατόπιση εκβολών ποταμού, καθώς και η οικοδόμηση επί επιφανειακών και υπόγειων ρευμάτων (Bird et al., 1996; Waters et al., 2016). Περίπου 15 km^2 ετησίως είναι η εκτιμώμενη χαμένη παράκτια έκταση στην Ευρώπη λόγω της διάβρωσης (van Rijn, 2011). **Κατά τα επόμενα χρόνια, παράγοντες όπως η αστικοποίηση, η αύξηση του πληθυσμού με την παράλληλη αύξηση της κατασκευαστικής δραστηριότητας αναμένεται πως θα ενισχύσουν τις διαβρωτικές τάσεις, προσθέτοντας μεγαλύτερη πίεση στην ήδη φθίνουσα παροχή ιζημάτων.**

Ποικίλες στρατηγικές αλλά και μία σειρά από παράκτια έργα σχεδιάζονται από τους μηχανικούς σήμερα ώστε να επιτευχθεί η προστασία ευάλωτων παράκτιων περιοχών. Πρόσφατες μελέτες έχουν εξετάσει την απόδοση αυτών των έργων σχετικά με την επίδραση τους στην διατήρηση της θέσης της ακτογραμμής ή ακόμα και την προώθηση αυτής (Pranzini et al., 2015 ;· Servold et al., 2017). Μία σειρά από έργα μηχανικού, που έχουν ως στόχο την αντιμετώπιση των φαινομένων διάβρωσης, μεσοπρόθεσμα παρουσιάζουν τα ακριβώς αντίθετα του αναμενομένου αποτελέσματα, καθώς ευθύνονται και για την εντατικοποίηση προβλημάτων διάβρωσης στη γειτνίαση των κατασκευών (Douglas et al. 2003).

Σήμερα, αρκετές χώρες έχουν υιοθετήσει νομοθεσίες για την προστασία του φυσικού παράκτιου περιβάλλοντος, που επιβάλλει περιορισμούς στις κατασκευαστικές δραστηριότητες κοντά στην ακτή και υποχρεώνει την εκτέλεση μελετών περιβαλλοντικών επιπτώσεων. Ωστόσο, κατά τις προηγούμενες δεκαετίες η διάβρωση αντιμετωπίστηκε ημιεμπειρικά και αποσπασματικά, ενώ δεν ελήφθησαν τα απαραίτητα μέτρα, αφού οι παράκτιες περιοχές θεωρούνταν ως ένα περιβάλλον σχετικά σταθερό, και επομένως οι επιπτώσεις στο σήμερα είναι ιδιαιτέρα έντονες.

Η πλειονότητα των επεμβάσεων για τη διασφάλιση της σταθερότητας της ακτής, βασίζεται στην τοποθέτηση κατασκευών «σκληρής» προστασίας. Τα έργα αυτά περιλαμβάνουν έξαλους, χαμηλής στέψης ή ύφαλους κυματοθραύστες, κάθετους ως προς την ακτογραμμή προβόλους, θωράκιση ακτών με φυσικούς ή τεχνητούς ογκόλιθους. Επιπλέον, παρατηρείται πως τα τελευταία χρόνια η υιοθέτηση πιο ήπιων λύσεων για την προστασία ακτών αποτελεί μία στρατηγική που κερδίζει συνεχώς έδαφος, Τέτοιες λύσεις αφορούν στη χρησιμοποίηση φιλικών προς το περιβάλλον μέσων, όπως οι ξύλινες κατασκευές και γεω-σωλήνων, η ενίσχυση της παράκτιας βλάστησης και η φύτευση κατάλληλων δενδρυλλίων που σταθεροποιούν το παράκτιο έδαφος, καθώς και η αναπλήρωση των ακτών με αμμώδη ή πετρώδη ιζήματα μεγάλης διαμέτρου.

Η μαθηματική προσομοίωση φυσικών παράκτιων διεργασιών, όπως η διάδοση των κυμάτων, η υδροδυναμική κυκλοφορία, η στερεομεταφορά και η εξέλιξη μορφολογίας, είναι ένα ουσιαστικό εργαλείο για την πρόβλεψη της παράκτιας μορφοδυναμικής και κατ' επέκταση της πρόληψης του φαινομένου διάβρωσης, Τα μαθηματικά μοντέλα προσομοίωσης παρέχουν επίσης **χρήσιμα συμπεράσματα για το κατά πόσο η απόδοση των παράκτιων έργων**, συναρτήσει της θέσης και της φύσης τους, είναι η ικανή να συγκρατήσει ή ακόμα και να προωθήσει προς τη θάλασσα την θέση της ακτογραμμής.

Διαφορετικοί τύποι αριθμητικών μοντέλων συναντώνται στη βιβλιογραφία της παράκτιας μηχανικής, για την πρόβλεψή της υδροδυναμικής κυκλοφορίας και της μορφοδυναμικής κοντά στην ακτή. Σύμφωνα με τον Roelvink (2011), τα υπάρχοντα μοντέλα μπορούν να χωριστούν σε τρεις κατηγορίες:

1) Μοντέλα παράκτιων προφίλ, όπου το ενδιαφέρον έγκειται στις εγκάρσιες διεργασίες της ακτής (Roelvink and Brøker, 1993; Schoonees and Theron, 1995).
2) Μοντέλα ακτογραμμής και εξέλιξη αυτής βασισμένα σε διακριτικά προφίλ διασταυρώσεων, όπου οι μικρής χωρικής και χρονικής κλίμακας διακυμάνσεις αμελούνται (GENESIS, UNIBEST και LITPACK), (Szmytkiewicz et al., 2000).
3) Μοντέλα παράκτιων φυσικών διεργασιών δισδιάστατα, όπου λαμβάνονται υπόψη οι μεταβολές μικρής κλίμακας (Nicholson et al., 1997).

Η παρούσα διδακτορική εργασία αφορά στη μελέτη της διάδοσης των κυμάτων σε ρηχά νερά και τη μελέτη των αλληλεπιδράσεων ρευστού – θαλάσσιου αμμώδους πυθμένα, υπό ασταθείς ροές, καθώς και στα πλεονεκτήματα και περιορισμούς υπολογιστικών προσομοιώσεων με μοντέλα παράκτιων φυσικών διεργασιών δισδιάστατα(μέσου βάθους). **Οι βασικοί στόχοι που τέθηκαν στα πλαίσια αυτής της διδακτορικής συμπυκνώνονται στην παρακάτω λίστα:**

(1) Η εφαρμογή και η σύγκριση των υφιστάμενων αριθμητικών εργαλείων παράκτιας μηχανικής, προκειμένου να αξιολογηθεί η απόδοση, η εφαρμογή και οι ιδιότητές τους.

(2) Η ανάπτυξη νέων αριθμητικών μοντέλων και εργαλείων για την προσομοίωση της παράκτιας διάδοσης κυμάτων και μηχανισμών μεταφοράς ιζημάτων.

(3) Η επαλήθευση της αποτελεσματικότητας των μοντέλων σε σχέση με τον βαθμό ακρίβειας πρόβλεψης της μορφολογίας του βυθού και η σύγκριση των αποτελεσμάτων με πειραματικά ευρήματα και μετρήσεις πεδίου.

(4) Η εφαρμογή επιλεγμένων εργαλείων και αριθμητικών μοντέλων για τη μελέτη υδρο-μορφοδυναμικών διεργασιών σε παράκτιες ζώνες όπου κυριαρχεί η διάβρωση.

Πυρήνα του παρόντος έργου αποτελεί **η αριθμητική διερεύνηση των υδροδυναμικών επιδράσεων στους μηχανισμούς διάβρωσης και απόθεσης** μη συνεκτικών ιζημάτων, καθώς και η επίδραση αυτών στην εξέλιξη της ακτογραμμής, λαμβάνοντας υπόψη την παρουσία θαλάσσιων κατασκευών, όπως ένα παράλληλο σύστημα έξαλών ή ύφαλων. κυματοθραυστών, ή προβόλων. Στο πλαίσιο του παρόντος διδακτορικού αναλύθηκαν διεξοδικά μια σειρά από περιπτώσεις και εφαρμογές παράκτιας μηχανικής, σχετικά με τις αλληλεπιδράσεις ροής του βυθού σε επικλινείς παραλίες και την αποτελεσματικότητα των παράκτιων κατασκευών στον έλεγχο των φαινομένων διάβρωσης. Ιδιαίτερη έμφαση δόθηκε στις υδρο-μορφοδυναμικές διεργασίες στην εσωτερική ζώνη θραύσης και αναρρίχησης - surf και swash zone, όπου ο μηχανισμός μεταφοράς ιζημάτων είναι ακόμα ασαφής (Afentoulis et al., 2022 ; Pourzangbar et al., 2022) και μια σειρά από περιορισμούς χαρακτηρίζουν τα υπάρχοντα αριθμητικά μοντέλα κυμάτων-ρευμάτων-βαθυμετρικής εξέλιξης. Οι αριθμητικές προβλέψεις των αλληλεπιδράσεων κύματος-ρεύματος και οι μορφολογικές αποκρίσεις, με ή χωρίς την παρουσία παράκτιων δομών, εξακολουθούν να συνδέονται με σημαντική αβεβαιότητα που σχετίζεται με την εξαιρετικά μη γραμμική φύση αυτών των φυσικών διεργασιών. Σε προηγούμενες μελέτες (Kobayashi et al., 2000; Karambas and Koutitas, 2002; Ding and Wang, 2008; Gallerano et al. 2016; Klonaris et al., 2016; Malej et al., 2019, Bouvier et al., 2019; Hieu et al., 2020), είτε η υδροδυναμική επίλυση δε λαμβάνει υπόψη της τα χαρακτηριστικά ανάκλασης και μετάδοσης

(π.χ. διαπερατότητα) των παράκτιων κατασκευών, είτε οι προσεγγίσεις μεταφοράς ιζήματος που χρησιμοποιήθηκαν δεν είναι κατάλληλες για την καταγραφή των μη γραμμικών επιδράσεων του κύματος στη στερεομεταφορά και προσομοίωση των τρισδιάστατων χαρακτηριστικών των φορτίων μεταφοράς αιωρούμενων ιζημάτων. Οι χρονικές κλίμακες ενδιαφέροντος που εξετάστηκαν στα πλαίσια της παρούσας διδακτορικής διατριβής ποικίλλουν από μερικές ώρες έως αρκετούς μήνες.

Για τις ανάγκες αυτής της εργασίας, χρησιμοποιήθηκαν τρία διαφορετικά προηγμένα αριθμητικά μοντέλα με στόχο την καλύτερη κατανόηση των διεργασιών υδρο-μορφοδυναμικής κοντά στην ακτή, τα οποία περιγράφονται στη συνέχεια. Αυτά τα εργαλεία εφαρμόστηκαν για την πρόβλεψη της μορφολογίας του θαλάσσιου πυθμένα σε περιοχές μελέτης, όπου εμφανίζονται υδρο-μορφοδυναμικά φαινόμενα υψηλής έντασης. Επιπλέον, αναπτύχθηκαν νέοι αλγόριθμοι και μοντέλα από τον συγγραφέα αυτής της διατριβής για την περαιτέρω διερεύνηση και μελέτη των υδροδυναμικών παραμέτρων και της μεταφοράς ιζημάτων σε όλη την εσωτερική παράκτια ζώνη. Ιδιαίτερο βάρος δόθηκε, εδώ, στις ανάγκες για βέλτιστη και πιο αποτελεσματική προσομοίωση της επίδρασης της κυματογενής δράσης στον αμμώδη βυθό, μειώνοντας τον υπολογιστικό φόρτο. **Συνοψίζοντας, η παρούσα διατριβή περιλαμβάνει την εξέλιξη υπαρχόντων και την ανάπτυξη νέων αριθμητικών μοντέλων βασισμένων σε σύγχρονες μεθόδους επίλυσης προβλημάτων υδροδυναμικής και μορφοδυναμικής.**

Για τη διερεύνηση των υδροδυναμικών χαρακτηριστικών κοντά στην ακτή, ακολουθήθηκαν δύο διαφορετικές αριθμητικές προσεγγίσεις. **Η πρώτη προσέγγιση βασίστηκε στη χρησιμοποίηση ενός υδροδυναμικού μοντέλου που βασίζεται στις δισδιάστατες μη γραμμικές εξισώσεις ρηχών νερών** (NSWE) (Marche and Bonneton 2006), (Marche et al.2007). Το κύριο πλεονέκτημα αυτής της αριθμητικής προσέγγισης είναι ότι τα γεγονότα θραύσης μπορούν να μοντελοποιηθούν μέσω του αναπτύγματος της ελεύθερης επιφάνειας και της ασυνέχειας ρεύματος (Bonneton et al. 2010). Σημειώνεται, ωστόσο, ότι εδώ δεν λαμβάνονται υπόψη τα φαινόμενα διασποράς, κάτι που αποτελεί βασικό περιορισμό αυτής της μεθοδολογίας. Στο πλαίσιο αυτής της προσέγγισης, προγραμματίστηκε και εφαρμόστηκε ένας αριθμητικός κυματιστήρας - wavemaker, για τη διάδοση ακανόνιστων κυμάτων χρησιμοποιώντας κατευθυντικά φασματικά δεδομένα. Ο τρόπος κίνησης του ιζήματος αξιολογήθηκε χρησιμοποιώντας δύο διαφορετικές μεθόδους που λαμβάνουν υπόψη τη μη γραμμική επίδραση των κυμάτων στην υδροδυναμική κυκλοφορία και κατ’ επέκταση στο μηχανισμό στερεομεταφοράς. Για τις ανάγκες της προσομοίωσης αυτών των μηχανισμών μορφολογίας ένα νέο αριθμητικό μοντέλο αναπτύχθηκε στα πλαίσια της παρούσας διατριβής.

Η δεύτερη αριθμητική προσέγγιση έγκειται στη χχρησιμοποίηση ενός πλήρως μη γραμμικού κυματικού και υδροδυναμικού μοντέλου **Boussinesq** (Madsen et al. 1997; Kennedy et al. 2001), για τις περιοχές μελέτης που εκτείνονται από βαθιά έως ρηχά ύδατα, ώστε να καταστεί δυνατή η ακριβής προσομοίωση **φαινομένων διασποράς ακονόνιστων κυματισμών σε σύνθετες βαθυμετρίες.** Πιο συγκεκριμένα, το μη γραμμικό μοντέλο τύπου Boussinesq, FUNWAVE-TVD (Shi et al. 2012), εφαρμόστηκε με στόχο την προσομοίωση της διάδοσης κύματος και της υδροδυναμικής κυκλοφορίας σε μεταβατικές παράκτιες ζώνες και συσχετίστηκε με ένα νέο ημι-τρισδιάστατο μοντέλο μεταφοράς ιζήματος και μορφολογίας που αναπτύχθηκε στα πλαίσια της παρούσας μελέτης για την επίλυση της μη γραμμικής επίδρασης των κυμάτων στη μεταφορά ιζήματος. Επιπλέον, εφαρμόστηκε μια τρισδιάστατη προσέγγιση για την εκτίμηση της μεταφοράς ιζήματος με αιωρούμενο φορτίο προκειμένου να περιγράφει η κατακόρυφη δομή της συγκέντρωσης ιζήματος.

Επιπρόσθετα, μελετήθηκαν πολλές βασικές φυσικές διεργασίες για τη μοντελοποίηση μεταφοράς ιζήματος, όπως το κατώφλι έναρξης κίνησης ιζήματος, το τρισδιάστατο προφίλ συγκέντρωσης αιωρούμενου ιζήματος, η συγκέντρωση ισορροπίας ή κορεσμού κοντά στον πυθμένα και η μέση κατά βάθος συγκέντρωση αιωρούμενων ιζημάτων υπό την παρουσία κυμάτων, ρευμάτων ή λόγω του συνδυασμού δύο. Οι αριθμητικές μέθοδοι που ενσωματώθηκαν σε αυτή την έρευνα περιλαμβάνουν εξισώσεις για ασταθείς ή παλιρροϊκές ροές σε μια μη επίπεδη κοίτη ιζήματος, την τροχιακή ταχύτητα κύματος κοντά στον πυθμένα της θάλασσας, τον συντελεστή τριβής για τα κύματα, τη ταχύτητα καθίζησης των λεπτών κόκκων άμμου, την οριακή τάση διάτμησης στον πυθμένα των κόκκων άμμου λόγω της δράσης των ρευμάτων ή/και των κυμάτων, το φορτίο πυθμένα και ο συνολικός ρυθμός μεταφοράς ιζήματος.

Επιπλέον, δόθηκε ιδιαίτερη προσοχή στη διερεύνηση της δυναμικής των ιζημάτων στη ζώνη αναρρίχησης - swash, καθώς ο μηχανισμός αυτός παρουσιάζει μεγάλο ενδιαφέρον για τα έργα μηχανικού στην παράκτια ζώνη. Η δυναμική του swash καθορίζει τη θέση της ακτογραμμής, και επομένως η ακριβής μελέτη των φυσικών διεργασιών σε αυτή την περιοχή συμβάλλει στην αξιολόγηση της απόδοσης των παράκτιων έργων προστασίας όσον αφορά στην ικανότητά τους να διατηρήσουν ή να προωθήσουν την ακτογραμμή προς τη θάλασσα.

Δομή διδακτορικής διατριβής

Η παρούσα διδακτορική διατριβή απαρτίζεται από πέντε (5) ενότητες/κεφάλαια εκτών οποίων το κεφάλαιο 1 αποτελεί την εισαγωγή, ενώ τα βασικά συμπεράσματα και οι προτάσεις μελλοντικής έρευνας παρουσιάζονται στο κεφάλαιο 5. Η ολοκληρωμένη ανάλυση, μέσω αριθμητικών επιλύσεων, των φαινομένων μεταφοράς ιζημάτων σε πραγματικές συνθήκες και σε περιοχές όπου παρατηρούνται διαβρωτικές τάσεις με χρήση των διαθέσιμων και υπαρχουσών ρουτίνων παρουσιάζεται στο κεφάλαιο 2. Επιπρόσθετα, στο κεφάλαιο 3 παρουσιάζεται η εργαστηριακή και πειραματική διερεύνηση υδρο-μορφολογικών συνθηκών υπό πολυσχιδείς/σύνθετες βαθυμετρίες χωρίς την παρουσία έργων, κάνοντας χρήση νέων συνδυαστικών μοντέλων με στόχο τη διερεύνηση της βαθυμετρικής εξέλιξης και των υποσταδίων ακτής (από απορροφητική (dissipative) σε ανακλαστική μορφή ακτής και αντίστροφα). Στο κεφάλαιο 4 παρουσιάζεται ένα νέο συζευγμένο αριθμητικό μοντέλο για την ανάπτυξη του οποίου ελήφθησαν υπόψη όλα τα συμπεράσματα που εξήχθησαν κατά τα προηγούμενα στάδια της έρευνας (κεφάλαια 2-3). Συγκεκριμένα αναπτύχθηκε ένα μοντέλο μεταφοράς ιζήματος, βασιζόμενο σε μια 3D προσέγγιση για την προσομοίωση της μεταφοράς ιζήματος σε αιώρηση, ενώ αυτό συνδυάστηκε με ένα πλήρως μη γραμμικό μοντέλο Boussinesq για την αξιολόγηση των δράσεων κύματος-ρεύματος στην παράκτια ζώνη. Σε αυτό το πλαίσιο, αξιοποιήθηκαν 3D και 2D εργαστηριακές πειραματικές έρευνες για να επιβεβαιωθούν οι αριθμητικές προβλέψεις. Η δομή της παρούσας διδακτορικης διατριβής παρουσιάζεται στην Εικόνα 4

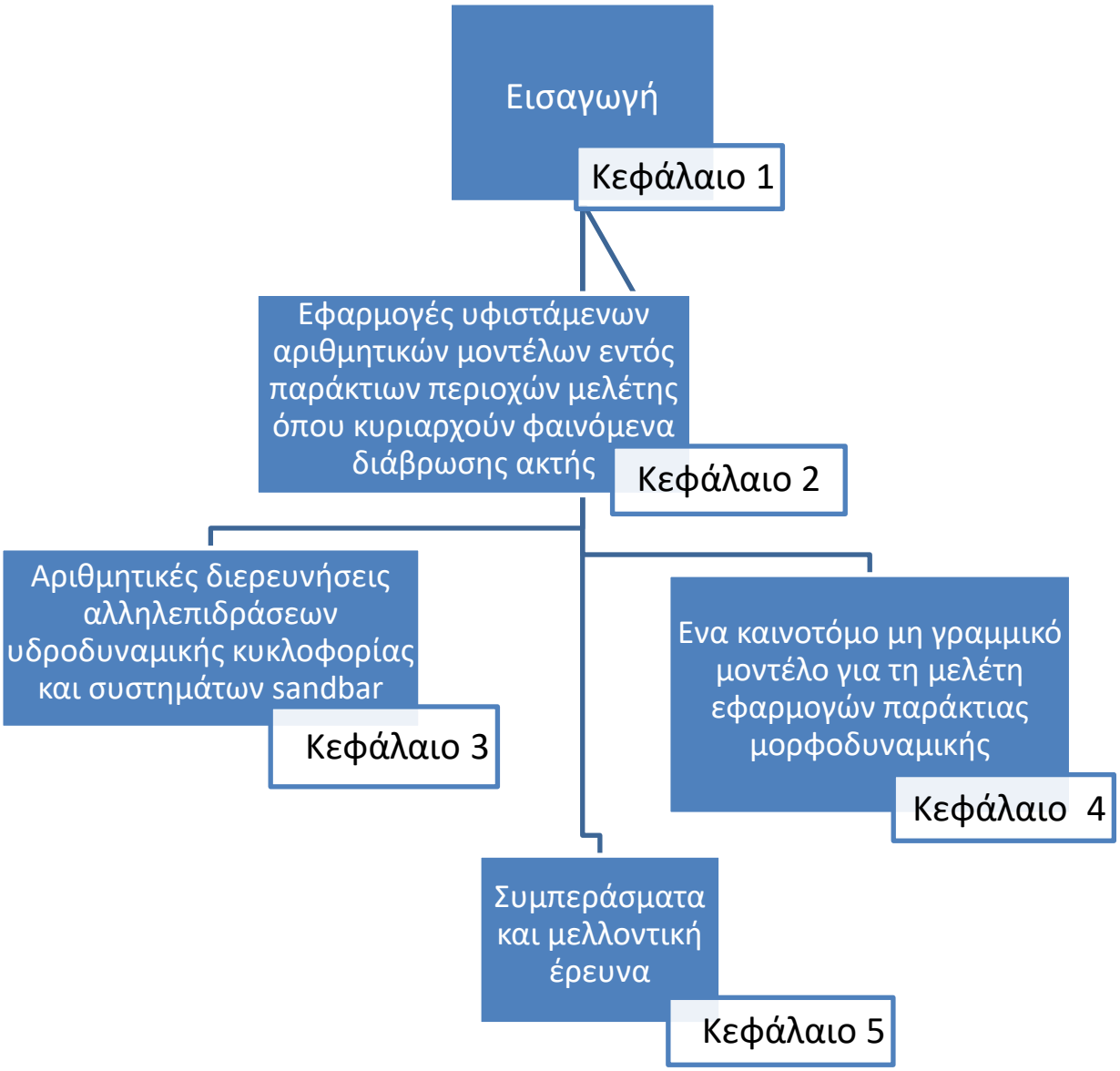

Εικόνα 3 Απεικόνιση της δομής της διατριβής με τη μορφή διαγράμματος.

Εφαρμογές υφιστάμενων αριθμητικών μοντέλων εντός παράκτιων περιοχών μελέτης όπου κυριαρχούν φαινόμενα διάβρωσης ακτής

Η ενότητα αυτή αναφέρεται στο κεφάλαιο 2 της παρούσας διδακτορικής διατριβή (Coastal area models and applications in erosion-dominated areas**)**. Υφιστάμενα αριθμητικά εργαλεία χρησιμοποιήθηκε σε αυτό το στάδιο για την προσομοίωση των φαινομένων διάδοσης κυμάτων, υδροδυναμικής κυκλοφορίας, αλληλεπιδράσεων κύματος-ρεύματος, μεταφοράς ιζημάτων και μορφολογίας σε περιοχές με έντονα μορφοδυναμικά φαινόμενα. Τα αριθμητικά αποτελέσματα παρέχουν σημαντικές παρατηρήσεις και συμπεράσματα σχετικά με τις διεργασίες των βαθυμετρικών αλλαγών που προκαλούνται από κύματα – καταιγίδων, ακραίων μετεωρολογικών φαινομένων, αλλά και τον μηχανισμό της παράκτιας ΄άμυνας΄ για τον έλεγχο της διάβρωσης και τη διατήρηση της ακεραιότητας και ισορροπίας του παράκτιου περιβάλλοντος. Τα μοντέλα που χρησιμοποιήθηκαν εδώ είναι: η σουίτα MIKE21 DHI και το μοντέλο XBeach. Επιπλέον, μια αριθμητική φόρμουλα για την εξέλιξη της μορφολογίας του βυθού της θάλασσας, που αναπτύχθηκε από τους Bouharguane και Mohammadi (2013) χρησιμοποιήθηκε για την προσομοίωση της δυναμικής των ιζημάτων υπό ή χωρίς την παρουσία παράκτιων έργων.

Τα πρόσφατα καταγεγραμμένα ακραία φαινόμενα καταιγίδας και κυμάτων στις ευρωπαϊκές ακτές προκάλεσαν θεαματική διάβρωση της ακτογραμμής την τελευταία δεκαετία (Castelle et al. 2015). Ομοίως, στην παρούσα περιοχή μελέτης - την παραλιακή πόλη του Ρεθύμνου, στην Ελλάδα, σημειώθηκαν μεγάλες πλημμύρες και ακραία κυματικά φαινόμενα τα τελευταία χρόνια, με αποτέλεσμα να καταγραφούν σοβαρές ζημιές σε υποδομές κυρίως στην Παλιά Πόλη του Ρεθύμνου και σημαντικά φαινόμενα διάβρωσης στις ανατολικές ως προς αυτήν περιοχές (Makropoulos et al., 2014b; Kragiopoulou et al., 2016; Tsoukala et al., 2016).

Χαρακτηριστικά της περιοχής μελέτης

Η υπό μελέτη περιοχή βρίσκεται στο Νομό Ρεθύμνου, που είναι ένας από τους τέσσερις Νομούς της Κρήτης στην Ελλάδα (Εικόνα 4). Το Ρέθυμνο είναι παραθαλάσσια πόλη και ο πληθυσμός της ανέρχεται σε 32.468 κατοίκους με πυκνότητα πληθυσμού 140 /km^2. Ως η τρίτη σε πληθυσμό αστική περιοχή στο νησί της Κρήτης, αναπτύσσονται εμπορικές, διοικητικές, πολιτιστικές και τουριστικές δραστηριότητες κατά μήκος της βόρειας ακτής όπου βρίσκεται η πόλη. Το μέσο απόλυτο υψόμετρο είναι 15 m (Makropoulos et al., 2014a). Η περιοχή μελέτης περιλαμβάνει το λιμάνι του Ρεθύμνου, που βρίσκεται στη Βόρεια περιοχή της Κρήτης εντός του ομώνυμου

κόλπου και την παρακείμενη παράκτια περιοχή στα ανατολικά (συνολική έκταση περίπου 19 km^2) με μήκος ακτογραμμής περίπου 8,8 km και μέγιστο βάθος ίσο με 30 m, σε απόσταση ίση με 1.9 km από την ακτή.

Οι πλημμύρες ήταν πάντα ένα σημαντικό ζήτημα (Chondros et al., 2021) για την παραλιακή πόλη του Ρεθύμνου. Σημαντικές ζημιές καταγράφηκαν τα τελευταία χρόνια κυρίως στο κέντρο της πόλης και στις ανατολικές περιοχές χαμηλής στάθμης. Επιπλέον, οι αλλαγές στις συνθήκες ανέμου, πιθανώς λόγω κλιματικών αλλαγών, προκαλούν καταιγίδες που μπορούν να συνδυαστούν με έντονους κυματισμούς και ισχυρά παράκτια ρεύματα.

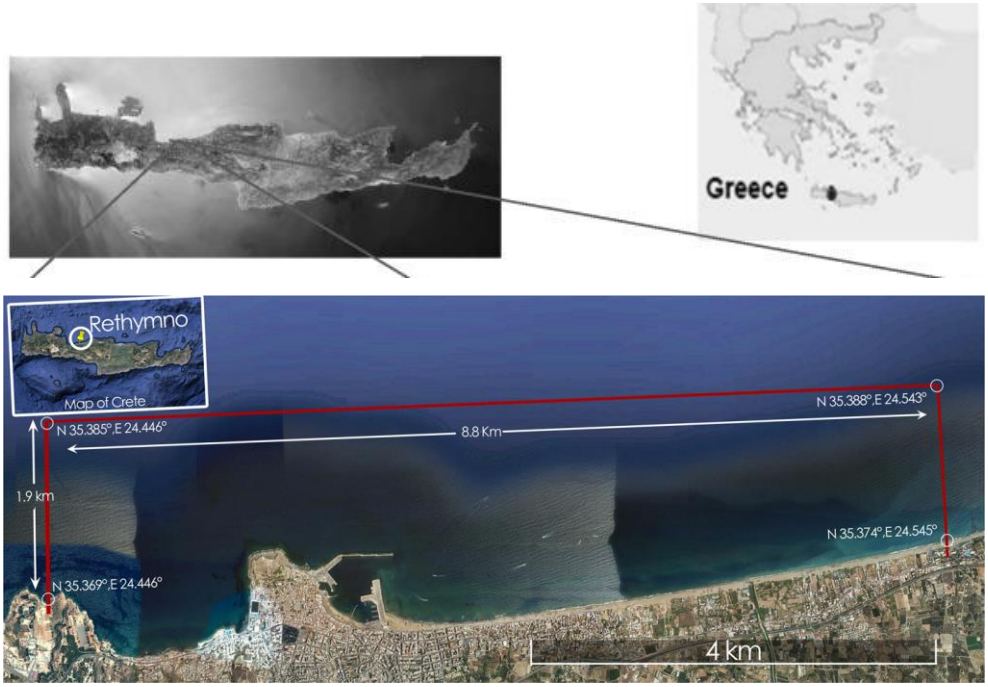

Εικόνα 4 Περιοχή μελέτης στο Ρέθυμνο - Satellite image from Google Earth 31/08/2015 (Google Earth Engine Team 2015).

Για τις ανάγκες της παρούσας έρευνας, αναλύθηκαν δεδομένα αιολικής και κυματικής δράσης, προκειμένου να προσδιοριστούν οι κυματικές συνθήκες που επικρατούν στις υπεράκτιες περιοχές του Ρεθύμνου, τα δεδομένα αυτά ανακτήθηκαν από την εργασία των Tsoukala et al., 2016 και Velikou et al., 2014 - CCSEAWAVS project. Πιο συγκεκριμένα, χρησιμοποιώντας τα διαθέσιμα δεδομένα υπεράκτιων κυμάτων, επιτεύχθηκε η κατηγοριοποίηση των φαινομένων καταιγίδας, προκειμένου να συσχετιστούν με αντίστοιχους παράγοντες τρωτότητας των ακτών. Η ταξινόμηση πραγματοποιήθηκε με βάση πέντε κατηγορίες: I - Ασθενής, II - Μέτρια, III-Σημαντική, IV - Σοβαρή και V – Ακραία (Πίνακας 1). Ο όρος ‘καταιγίδα’ ορίστηκε εδώ, ως το

γεγονός που υπερβαίνει ένα ελάχιστο σημαντικό ύψος κύματος (Hs > 2 m) και με ελάχιστη διάρκεια 6 ωρών (Li et al., 2014, Michele et al., 2007).

ΔΕΔΟΜΕΝΑ 2000–2100						
Κατηγορίες	**H_s εύρος [m]**	**T_p εύρος [s]**	**Μέσο H_s [m]**	**Μέση T_p [s]**	**Μέση διάρκεια [h]**	**Αριθμός γεγονότων**
I Ασθενής	2.0–5.3	6.4–10.1	2.5	7.7	14.13	823
II Μέτρια	2.0–5.0	6.7–9.9	2.7	8.0	42.03	94
III Σημαντική	2.0–6.0	6.9–10.3	3.0	8.2	61.84	13
IV Σοβαρή	2.0–5.4	6.4–10.0	3.2	8.2	81.38	8
V Ακραία	2.0–5.0	7.8–9.7	4.2	9.1	72.00	1

Πίνακας 1 Χαρακτηριστικά κυμάτων καταιγίδας, περίοδος 2000–2100 για βόρεια διεύθυνση προσπίπτοντος κυματισμού στην περιοχή του Ρεθύμνου (Martzikos et al., 2018).

Στο πλαίσιο αυτό, πραγματοποιήθηκε η ακριβής πρόβλεψη και προσομοίωση των παράκτιων φυσικών διεργασιών, με χρήση αριθμητικών μοντέλων, για την εκτίμηση της τρωτότητας της ακτής σε σχέση με τα επιλεγμένα σενάρια καταγίδας. Τα μοντέλα MIKE 21 (DHI 2015a, b) και XBeach (Roelvink et al. 2009; Smit et al. 2010) χρησιμοποιήθηκαν για την προσομοίωση της διάδοσης κυμάτων, των ρευμάτων που προκαλούνται από τα κύματα, της μεταφοράς ιζημάτων και της μορφολογίας, υπό ακραίες κυματικές συνθήκες στην παράκτια ζώνη του Ρέθυμνο. Αυτά τα αριθμητικά μοντέλα 2DH μπορούν να εξάγουν διάφορες παραμέτρους κυμάτων, όπως ύψη κύματος, ταχύτητες σωματιδίων, μέσες χρονικές ταχύτητες - Eulerian, τάσεις ακτινοβολίας, ροές υπόγειων υδάτων, ρυθμούς μεταφοράς ιζημάτων και μορφολογικές αλλαγές στον πυθμένα της θάλασσας. Σε προηγούμενες μελέτες (Lončar et al., 2016; Ruiz de Alegria-Arzaburu et al., 2011), αυτά τα μοντέλα συνδυάστηκαν μέσω μιας μεθόδου αλυσίδας, στην οποία οι υπολογισμοί υπεράκτιων κυμάτων MIKE 21 χρησίμευσαν ως είσοδος στην προσομοίωση με το μοντέλο XBeach των φυσικών φαινομένων κοντά στην ακτή. Στο πλαίσιο της παρούσας διατριβής, ακολουθήθηκε μια διαφορετική προσέγγιση, καθώς τα δύο αυτά μοντέλα εφαρμόστηκαν με σκοπό τη διερεύνηση των ίδιων υδρο-μορφοδυναμικών παραμέτρων (χαρακτηριστικά κύματος και κυματογενών ρευμάτων, μεταφοράς ιζήματος μέσω φορτίου αιώρησης και πυθμένα, βαθυμετρική εξέλιξη) και στη συνέχεια αξιολογήθηκαν σχετικά με την ικανότητά τους να προβλέπουν τις υδροδυναμικές διεργασίες και τη μεταφορά ιζημάτων συγκρίνοντας τα αποτελέσματά τους σε όλο το μήκος της θαλάσσιας προς μελέτη ζώνης από τα βαθιά έως τα ρηχά ύδατα. Με αυτόν τον τρόπο, η απόδοση κάθε μοντέλου μπορεί να αξιολογηθεί, ενώ η συμφωνία μεταξύ των αποτελεσμάτων των δύο μοντέλων παρέχει ένα υψηλό βαθμό αξιοπιστίας στη μελέτη των φυσικών διεργασιών. Τα παρακάτω σχήματα (Εικόνα 5, Εικόνα 6) αποτυπώνουν τη χωρική κατανομή της ταχύτητας ρεύματος κατά μήκος της ακτής όπως αυτή υπολογίστηκε μέσα από τις αριθμητικές αναλύσεις. Τα αριθμητικά αποτελέσματα

των δύο μοντέλων επικυρώνουν την ύπαρξη ενός έντονου παράλληλου προς την ακτή κυματογενούς ρεύματος προς τα δυτικά, που προκαλείται από τα σενάρια καταιγίδας Β και ΒΑ, που αποτελεί κυρίαρχο παράγοντα για την κίνηση των ιζημάτων. Επιπλέον, τα αριθμητικά αποτελέσματα υποδεικνύουν την παρουσία ισχυρών ρευμάτων επαναφοράς (rip currents) στην ανατολική προσήνεμη πλευρά του κύριου κυματοθραύστη, τα οποία προκαλούν έντονα φαινόμενα διάβρωσης μέσω της μεταφοράς μεγάλης ποσότητας ιζήματος από τα ρηχά στα βαθιά ύδατα. Τέλος, οι τιμές που αφορούν στις μέσες τιμές των ταχυτήτων μέσου βάθους όπως αυτές υπολογίσθηκαν στις εξόδους των δύο μοντέλων, παρουσιάζουν καλή συσχέτιση μεταξύ τους, καθώς δεν υπερβαίνουν την απόλυτη τιμή των 2 m/s. Ωστόσο, τα δύο μοντέλα παρουσιάζουν επίσης σημαντικές διαφορές, που συνοψίζονται στα εξής:

1. Έλλειψη πληροφοριών σχετικά με την υπεράκτια υδροδυναμική κυκλοφορία στα αποτελέσματα του μοντέλου XBeach.
2. Τα αποτελέσματα των κυματογενών ταχυτήτων παρουσιάζουν ακανόνιστα μοτίβα (patterns) στην περίπτωση του XBeach, ενώ τα αποτελέσματα του MIKE 21 παρουσιάζουν καλά ρυθμισμένα μοτίβα ρεύματος κοντά στην ακτή. Γεγονός που οφείλεται στην πιο ομαλή κατανομή των αποτελεσμάτων της κυματικής διάδοσης (Κεφάλαιο 2 : Figure 2-10).
3. Αν και για το σενάριο καταιγίδας ΒΑ, τα αποτελέσματα της διάδοσης του ρεύματος προς τα δυτικά είναι παρόμοια μεταξύ των δύο μοντέλων, για το σενάριο καταιγίδας Ν, τα αποτελέσματα του XBeach παρουσιάζουν μια έντονη υδροδυναμική διαγώνια κίνηση, κάτι που έρχεται σε αντίθεση με τα αποτελέσματα του MIKE 21, τα οποία παρουσιάζουν μία κυρίως υδροδυναμική κίνηση κατά μήκος της ακτής.

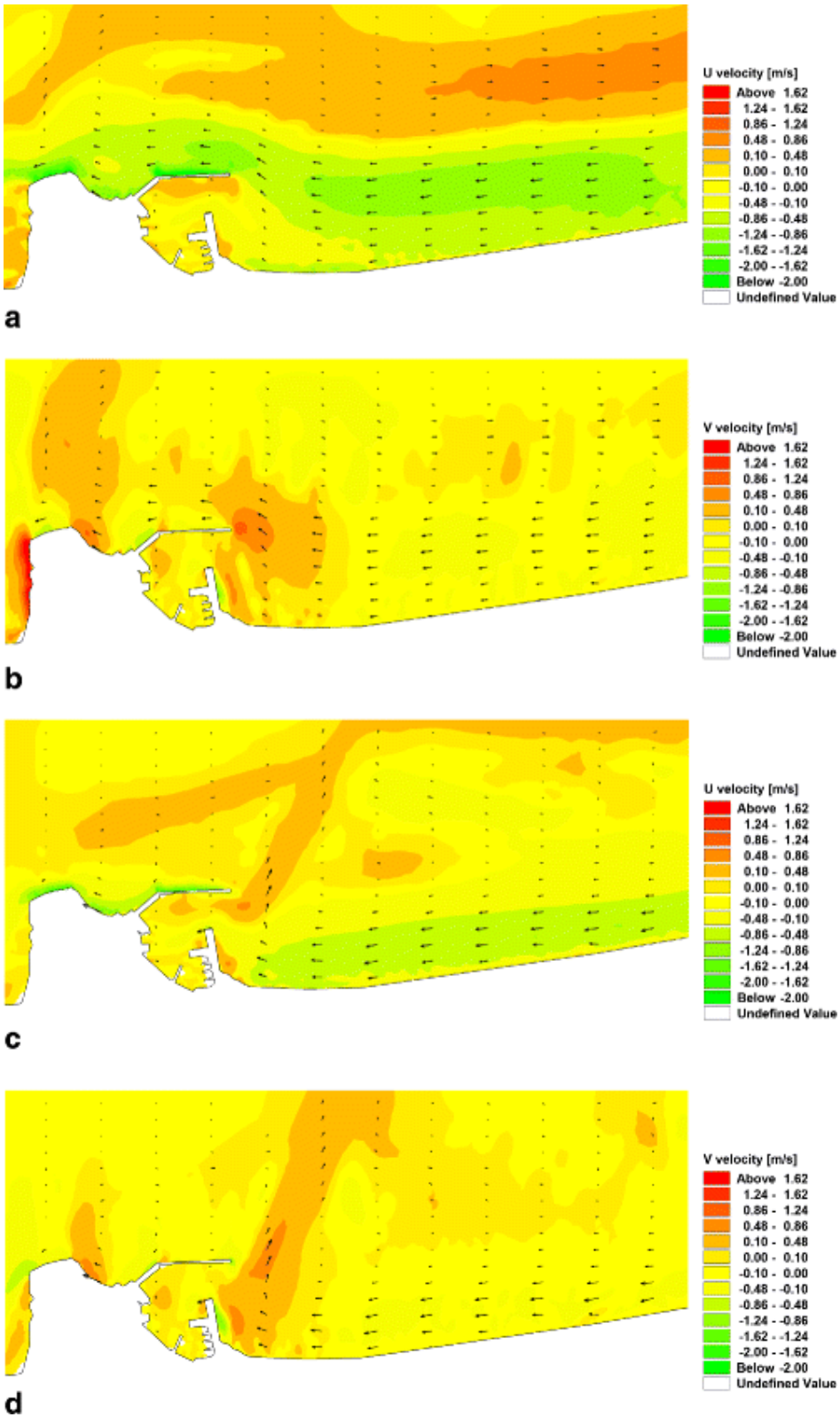

Εικόνα 5 a,b) Σενάριο βόρειας καταιγίδας (IV Σοβαρή)- Χωρική κατανομή της ταχύτητας ρεύματος κατά μήκος της ακτής U και της κάθετης προς την ακτή ταχύτητας V - μοντέλο MIKE 21 FM HD. γ,δ) Σενάριο βορειοανατολικής καταιγίδας - Χωρική κατανομή της ταχύτητας ρεύματος κατά μήκος της ακτής U και της κάθετης προς την ακτή ταχύτητας V - μοντέλο MIKE 21 FM HD.

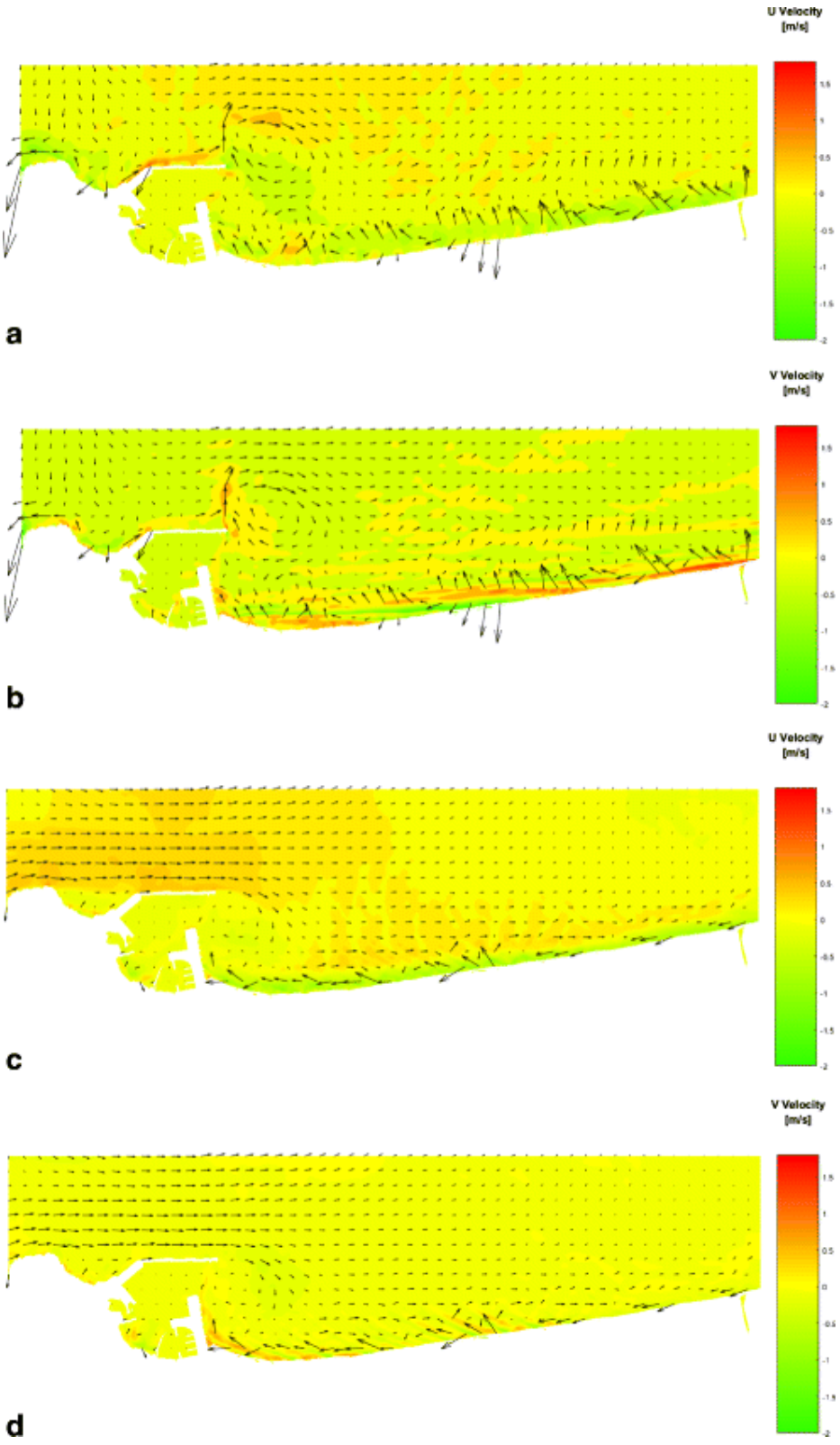

Εικόνα 6 Σενάριο βόρειας καταιγίδας (IV Σοβαρή) - Χωρική κατανομή της ταχύτητας ρεύματος κατά μήκος της ακτής U και της κάθετης προς την ακτή ταχύτητας V - μοντέλο XBeach. γ,δ) Σενάριο βορειοανατολικής καταιγίδας - Χωρική κατανομή της ταχύτητας ρεύματος κατά μήκος της ακτής U και της κάθετης προς την ακτή ταχύτητας V - μοντέλο XBeach.

Προτεινόμενες λύσεις βασιζόμενες σε αριθμητικές προσομοιώσεις

Η υπάρχουσα διάταξη του λιμανιού είναι ιδιαίτερα ευάλωτη σε έντονα καιρικά φαινόμενα, ενώ επιπλέον, οι μετατοπίσεις ιζημάτων που διερευνήθηκαν αριθμητικά οδηγούν μεγάλους όγκους ιζήματος, που αποθηκεύεται στην περιοχή ανατολικά του υπήνεμου κυματοθραύστη, να μετακινηθούν εντός της λιμενολεκάνης. Αυτή η διαδικασία μπορεί να οδηγήσει σε μια επακόλουθη μείωση του βάθους πυθμένα στην εισόδου του λιμανιού, εμποδίζοντας τον διάπλου. Επιπλέον, η υψηλή έντασης στερεομεταφορά πυροδοτεί σημαντικά φαινόμενα διάβρωσης στις παρακείμενες ανατολικές ακτές. Προκειμένου να ελεγχθούν αυτά τα φαινόμενα μεταφοράς ιζημάτων, προτάθηκε μια εναλλακτική διάταξη λιμανιού, συμπεριλαμβανομένων κυματοθραυστών με καμπύλο σχήμα ενισχυμένο με θωράκιση αποτελούμενη από ογκόλιθους XBlocks. Επιπλέον, αξιολογήθηκε η διαμόρφωση λύσης ενός συστήματος ύφαλων κυματοθραυστών για την καταπολέμηση των φαινομένων διάβρωσης στην ανατολική παράκτια περιοχή. Η Εικόνα 7 απεικονίζει την ενίσχυση του κυματοθραύστη καθώς και τη σχεδίαση του προβλεπόμενου συστήματος ύφαλων αποσπασμένων κυματοθραυστών κατά μήκος της ακτής.

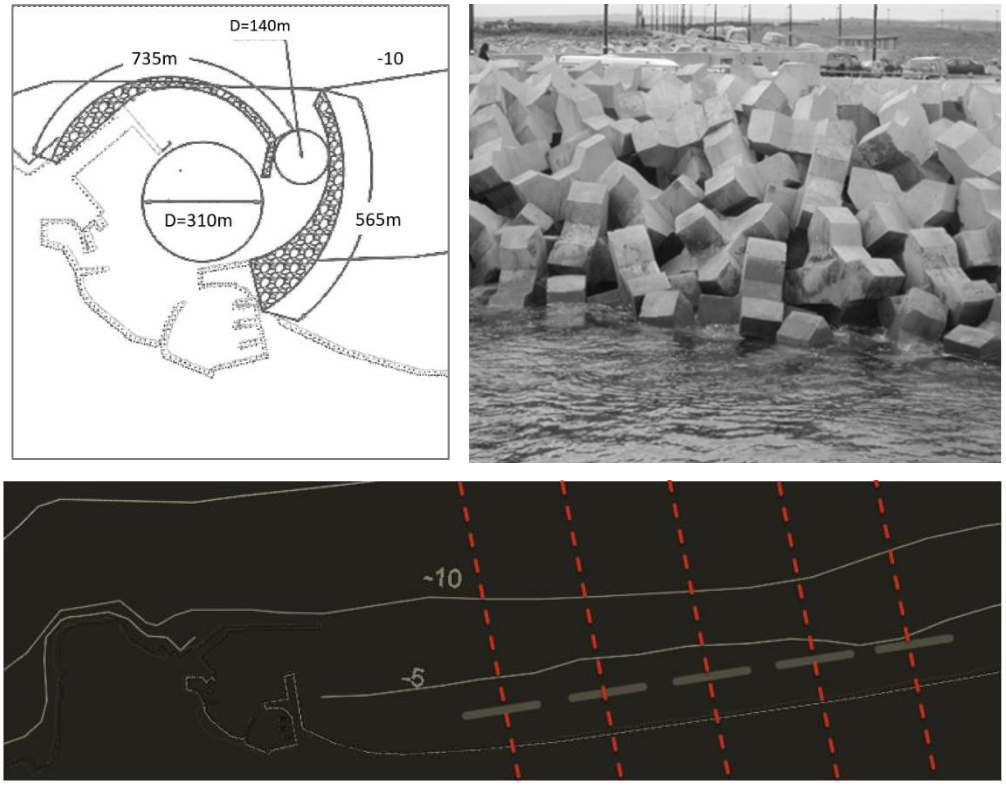

Εικόνα 7 Πάνω: Μεταβολή των γεωμετρικών ιδιοτήτων του λιμανιού του Ρεθύμνου και ενίσχυση του κυματοθραύστη με Xblocs. Κάτω: Σχέδιο του προβλεπόμενου συστήματος αποσπασμένων κυματοθραυστών κατά μήκος της ακτής.

Η απόκριση της προτεινόμενης διάταξης του λιμένα έναντι της υδρομορφοδυναμικής που προκαλείται από καταιγίδες, προσομοιώθηκε προκειμένου να διερευνηθούν τα μοτίβα μεταφοράς ιζημάτων και να εκτιμηθεί η τάση απόθεσης στην είσοδο του λιμανιού. Για τη δυσμενέστερη περίπτωση του σεναρίου βόρειου ανέμου, οι αριθμητικές προσομοιώσεις πραγματοποιήθηκαν χρησιμοποιώντας την αλυσίδα λογισμικού MIKE 21 SW-HD-ST. Με την αναμόρφωση των κυματοθραυστών μεταβάλλεται η κατεύθυνση της υδροδυναμικής κυκλοφορίας και επιτυγχάνεται επαρκής ηρεμία της λιμενολεκάνης. Τα αποτελέσματα προσομοίωσης της διάδοσης κυμάτων δείχνουν μια ομαλή μετατροπή των τιμών του ύψους κύματος προς τις περιοχές με ρηχά νερά (Εικόνα 8). Τα κύματα δεν επηρεάζουν τη λεκάνη του λιμανιού και η περιοχή μπροστά από τον προσήνεμο κυματοθραύστη είναι επαρκώς προστατευμένη. Τα διανύσματα ταχύτητας ρευμάτων ακολουθούν διαφορετικά μοτίβα, σε σχέση με την υφιστάμενη διάταξη (Εικόνα 5, Εικόνα 6), γεγονός που οδηγεί σε ήπιες χωρικές μεταβολές ταχύτητας. Οι αλλαγές της μορφολογίας πυθμένα και τα μοτίβα των ροών μεταφοράς ιζήματος κατά την επιλεγμένη προσομοίωση ακραίας καταιγίδας, απεικονίζονται στην Εικόνα 9. Η μορφολογική εξέλιξη δείχνει ότι η συσσωρευμένη ποσότητα ιζήματος μπροστά από την είσοδο εμφανίζεται σημαντικά μειωμένη, όπως ήταν αναμενόμενο από τα υδροδυναμικά αποτελέσματα.

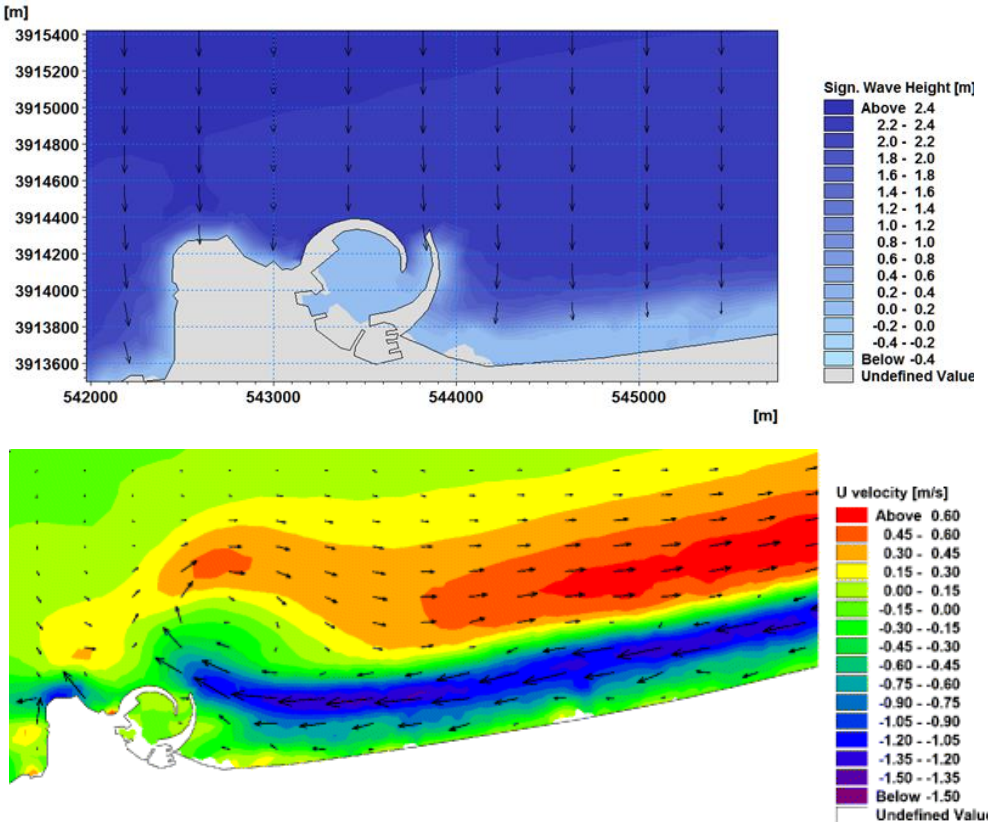

Εικόνα 8 Αποτελέσματα προσομοίωσης της διάδοσης κυμάτων και υδροδυναμική κυκλοφορία - Σενάριο βόρειας καταιγίδας (IV Σοβαρή).

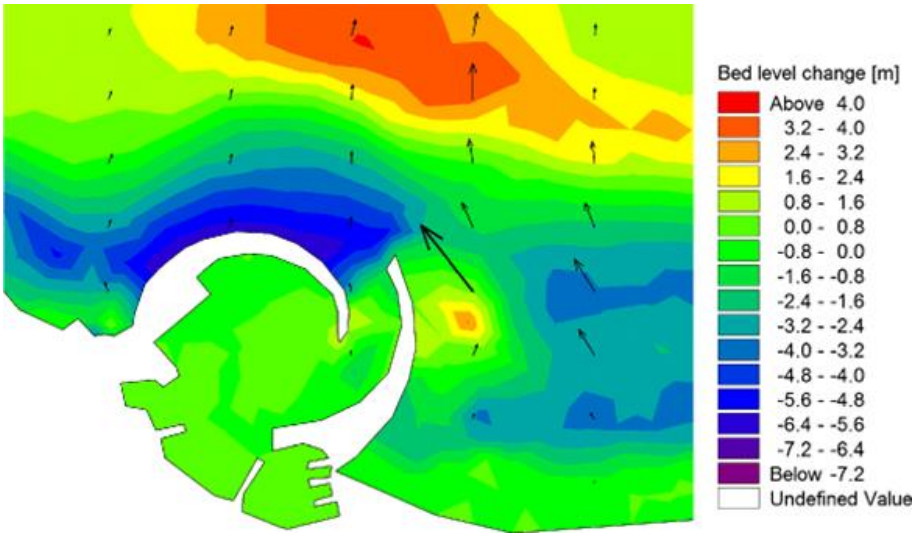

Εικόνα 9 Εξέλιξη βαθυμετρίας - Σενάριο βόρειας καταιγίδας (IV Σοβαρή).

Παράλληλα με την εφαρμογή των μοντέλων XBeach και MIKE21, για τη βελτιστοποίηση των γεωμετρικών ιδιοτήτων των ύφαλων κυματοθραυστών χρησιμοποιήθηκε η αριθμητική ρουτίνα των Bouharguane and Mohammadi (2013). Η ρουτίνα αυτή εφαρμόστηκε σε ένα αντιπροσωπευτικό βαθυμετρικό προφίλ κάθετο προς την ακτογραμμή, στην ανατολική περιοχή του Ρεθύμνου. Οι παράμετροι εισόδου του μοντέλου των Bouharguane and Mohammadi

(2013), προέρχονται από τα αποτελέσματα εξόδου του μοντέλου MIKE21 σε ένα βάθος 18 μέτρων, για το σενάριο Βόρειας Καταιγίδας (IV Σοβαρή) H_S = 4.95 m, T_p = 9.65 s. Η συγκεκριμένη ρουτίνα βασίζεται σε εξισώσεις ρηχών υδάτων και εφαρμόστηκε εδώ για τη διερεύνηση των αλληλεπιδράσεων ρευστού - θαλάσσιου πυθμένα, χρησιμοποιώντας αρχές ελαχιστοποίησης (Mohammadi and Bouchette, 2014). Για την προστασία της ακτής στα ανατολικά του Ρεθύμνου επιλέχθηκε η λύση που αφορά στην τοποθέτηση παράλληλων προς την ακτή κυματοθραυστών χαμηλής στέψης (+0,4 σε σχέση με τη μέση επιφάνεια της θάλασσας). Η μεταβλητή που αφορά στην απόσταση αυτών ως προς την ακτή βελτιστοποιήθηκε αξιοποιώντας τα αποτελέσματα εξόδου της ρουτίνας των Bouharguane and Mohammadi (2013), βέλτιστη απόσταση θεωρήθηκε εκείνη που οδηγεί στην ελάχιστη διάβρωση κατά μήκος του επιλεγόμενου βαθυμετρικού προφίλ. Η Εικόνα 10 απεικονίζει τη μορφολογική εξέλιξη του βυθού για τρεις διαφορετικές τοποθεσίες (απόσταση από την ακτή) του κυματοθραύστη, μετά από την περίοδο των 72 ωρών - σενάριο δυσμενέστερων συνθηκών (H_S = 4.95 m, T_p = 9.65 s). Η απόσταση των 200 m από την ακτογραμμή αποδείχθηκε βέλτιστη .

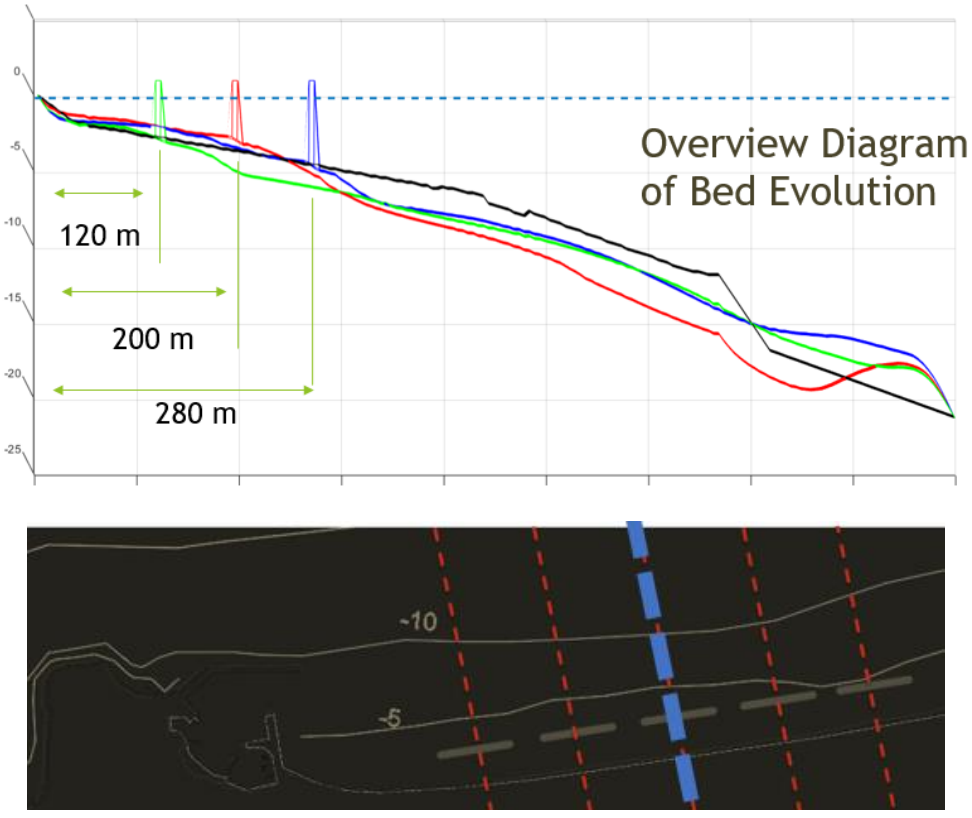

Εικόνα 10 Επάλληλες εξελίξεις βυθού για τις τρεις επιλεγμένες διαμορφώσεις με μεταβλητή απόσταση κυματοθραύστη από την ακτή - σενάριο Βόρειας Καταιγίδας (IV Σοβαρή) (H_S = 4.95 m, T_p = 9.65 s).

Σε αυτή την ενότητα που αναφέρεται στο κεφάλαιο 2 της παρούσας διδακτορικής διατριβή (Coastal area models and applications in erosion-dominated areas), εφαρμόστηκαν

διαφορετικές μεθοδολογίες και αριθμητικές προσεγγίσεις για τη διερεύνηση φυσικών διεργασιών κοντά στην ξηρά, όπως η διάδοση κυμάτων, η υδροδυναμική και η μορφοδυναμική. Η τρωτότητα των ακτών που προκαλείται από καταιγίδες αναλύθηκε για την περιοχή μελέτης του Ρεθύμνου στην Ελλάδα, όπου αξιολογήθηκαν διάφορες λύσεις (διαμορφώσεις παράκτιων κατασκευών), μέσω προηγμένης αριθμητικής μοντελοποίησης (μοντέλα : XBeach , MIKE21 και η ρουτίνα των Bouharguane and Mohammadi (2013)), ως προς την ικανότητά τους να απομειώνουν τις καταστροφικές συνέπειες των κυμάτων καταιγίδας.

Τα αποτελέσματα που προέκυψαν δείχνουν ότι το παράκτιο σύστημα στην περιοχή έρευνας μας είναι εκτεθειμένο σε έντονη διάβρωση λόγω ενεργητικών κυμάτων και ισχυρών υδροδυναμικών ρευμάτων. Η κύρια κατεύθυνση της μετατόπισης των ιζημάτων προσδιορίστηκε με ακρίβεια(Afentoulis et al, 2017), καθώς, όπως έχει παρατηρηθεί, μεγάλοι όγκοι ιζημάτων μετατοπίζονται από περιοχές υψηλής ενέργειας σε περιοχές χαμηλής κυματικής ενέργειας κατά τη διάρκεια ακραίων μετεωρολογικών γεγονότων. Η συμφωνία μεταξύ των αποτελεσμάτων των δύο μοντέλων (XBeach – MIKE21) παρέχει περισσότερη εμπιστοσύνη στην εκτίμηση των δράσεων φυσικών παράκτιων διεργασιών. Ωστόσο, όπως αναμενόταν, υπάρχουν ορισμένες αποκλίσεις μεταξύ των παραμέτρων εξόδων των δύο μοντέλων, λόγω των διαφορετικών δυνατοτήτων και της διαφορετικής φύσης τους: Το μοντέλο XBeach παρέχει πληροφορίες για τις διεργασίες σε περιοχές κοντά στην ακτή, ενώ το MIKE 21 προσομοιώνει καλύτερα τη μετατροπή των πληροφοριών από βαθιά νερά σε ρηχά υδάτινες περιοχές(Κεφάλαιο 2- Figure 2-10 : Figure 2-14 a, b) North-Eastern Storm Scenario - Spatial distribution of sediment transport total load x and y component - XBeach model. c, d) North-Eastern Storm Scenario - Spatial distribution of sediment transport total load x and y component - XBeach model).

Τα ευρήματά της παρούσας έρευνας υποδεικνύουν ότι η προτεινόμενη λύση αναμόρφωσης της διάταξης λιμένα με καμπυλωτούς και ενισχυμένους κυματοθραύστες παρέχει ικανοποιητική ηρεμία λιμενολεκάνης, λόγω μείωσης της προσπίπτουσας κυματικής δράσης, μεταβάλλοντας παράλληλα τις κατευθύνσεις μετατόπισης ιζημάτων. Όσον αφορά τον σχεδιασμό του συστήματος κυματοθραυστών, τα αποτελέσματα που προέκυψαν δείχνουν ευνοϊκές τάσεις για συσσώρευση ιζήματος κοντά στην ακτογραμμή, για μία απόσταση από την ακτή ίση με 200 m. Η μεθοδολογία που παρουσιάζεται εδώ μπορεί να αποτελέσει ένα σημαντικό εργαλείο για την αξιολόγηση των επιπτώσεων ακραίων καταιγίδων σε περιοχές μελέτης που αντιμετωπίζουν προβλήματα διάβρωσης. Ειδικότερα, τα αριθμητικά μοντέλα που εφαρμόστηκαν, μπορούν να βοηθήσουν μηχανικούς και επιστήμονες που επιθυμούν να

λάβουν ακριβείς προβλέψεις εξέλιξης της γεωμετρίας πυθμένα σε πολύπλοκες βαθυμετρίες και υπό την παρουσία έργων, βελτιώνοντας παράλληλα το σχεδιασμό και τη διαμόρφωσή των παράκτιων κατασκευών.

Αριθμητικές διερευνήσεις αλληλεπιδράσεων υδροδυναμικής κυκλοφορίας και συστημάτων sandbar

Η ενότητα αυτή αναφέρεται στο κεφάλαιο 3 της παρούσας διδακτορικής διατριβή (Numerical assessments of sandbar systems and rip channel dynamics**).** Η μορφολογική εξέλιξη του βυθού της θάλασσας υπό τη συνδυασμένη δράση κυμάτων και ρευμάτων έχει μελετηθεί εκτενώς στη βιβλιογραφία, αλλά μέχρι σήμερα το φαινόμενο αυτό δεν είναι ακόμη πλήρως κατανοητό στο σύνολό του. Ιστορικά, πραγματοποιήθηκαν πολλές μελέτες για τη διερεύνηση της διόδου μεταφοράς ιζημάτων και τη δημιουργία/μετατόπιση διαφορετικών μορφών ράβδων άμμου (Sandbars), (Sleath, 1984; Nielsen 1992; Deigaard and Fredsøe, 1992; Soulsby, 1997; Van Rijn 1993, 2007). Λόγω της πολύπλοκης φύσης αυτών των φαινομένων, είναι δύσκολο να ερμηνευθούν αυστηρά οι μηχανισμοί τους με μια γραμμική θεωρία. Οι ροές ιζήματος μπορούν να δημιουργηθούν και να οδηγηθούν από το συνδυασμό σταθερών ροών (ρεύματα) και ταλαντωτικών ροών (κύματα). Ωστόσο, πολλές άλλες διαδικασίες πρέπει να ληφθούν υπόψη, όπως οι διακυμάνσεις της μέσης στάθμης της θάλασσας (παλίρροια, wave setup), τα φαινόμενα θραύσης και η επίδραση της κλίσης και της μορφής της βαθυμετρίας (Camenen and Larroudé, 2003).

Οι Wright και Short (1984) χρησιμοποίησαν μεγάλο αριθμό μετρήσεων πεδίων για δεδομένα κυμάτων, ρευμάτων και μορφολογίας πυθμένα ώστε να πραγματοποιήσουν το πιο ευρέως αποδεκτό σύστημα ταξινόμησης ακτών. Η έννοια των δύο τελικών σταδίων ακτής (απορροφητική/dissipative (D) και ανακλαστική/reflective (R)), βασίζεται στη μεταβολή των σχετικών υδροδυναμικών συνθηκών και της παράλληλης αλληλεπίδρασης ρευστού - θαλάσσιου πυθμένα. Μία ακτή dissipative (D) ή ήπιων κλίσεων, χαρακτηρίζεται από υδροδυναμικές συνθήκες με μεγάλες περιόδους κυμάτων χαμηλής ενέργειας, και από την απουσία θαλάσσιων ρευμάτων επαναφοράς (rip currents), ενώ παράλληλα είναι το αποτέλεσμα κυμάτων που διαχέονται προοδευτικά, καθώς αυτά εισέρχονται σε μια ευρεία ζώνη θράυσης. Η ανακλαστική ακτή (R) στερείται οποιωνδήποτε χαρακτηριστικών διάχυσης, καθώς οι ανισορροπίες λόγω θραύσης περιορίζονται στη ζώνη υψηλής ανύψωσης, κοντά στην επιφάνεια της παραλίας. Έντονα ρεύματα επαναφοράς παρατηρούνται σε ανακλαστικές ακτές, καθοδηγούμενα από έντονες βυθομετρικές κλίσεις. Η Εικόνα 11 παρουσιάζει σχηματικά τα διάφορα στάδια και υποστάδια εξέλιξης κατάστασης ακτών, από απορροφητική σε ανακλαστική ακτή με βάση το έργο των Short and Woodroffe, 2009.

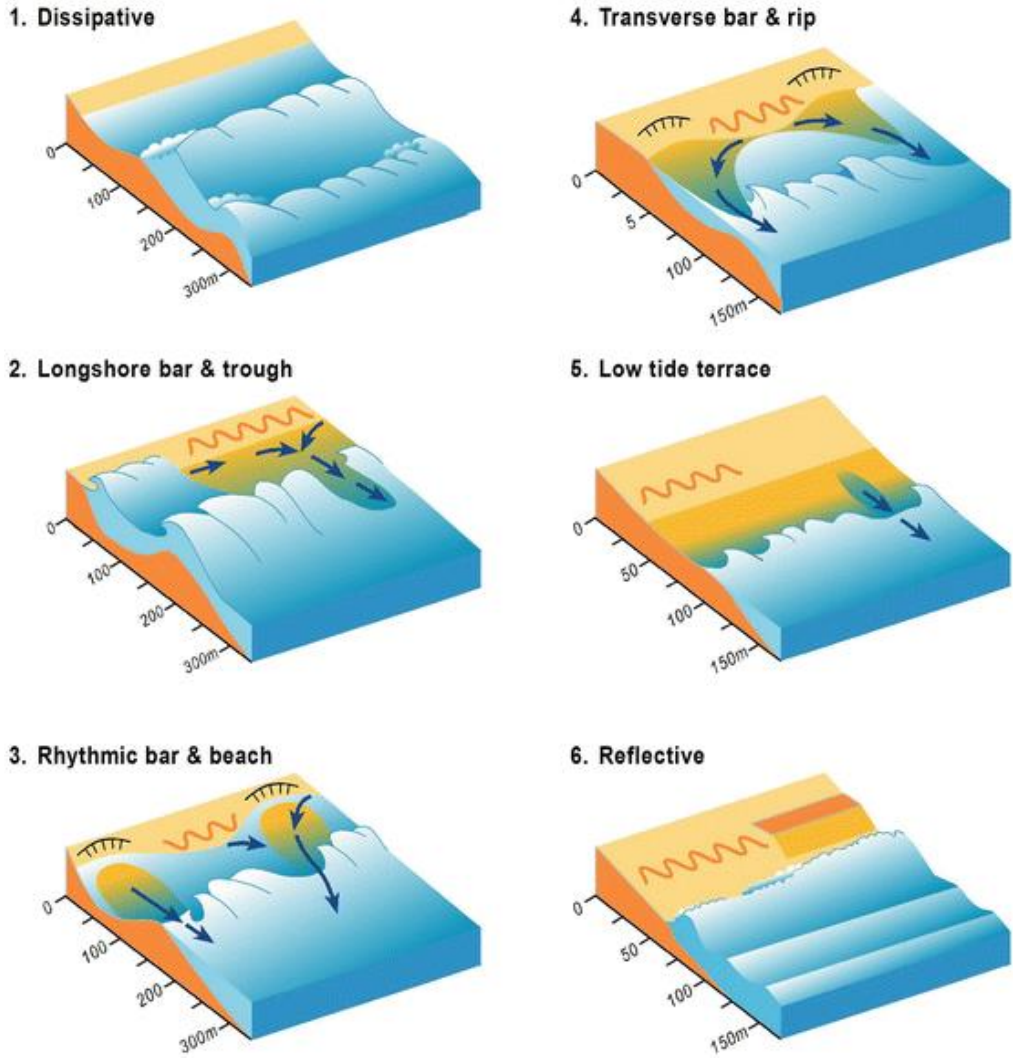

Εικόνα 11 Σχηματική απεικόνιση σταδίων μετάβασης από απορροφητική σε ανακλαστική ακτή, ενδιάμεσα στάδια : 2. Παράλληλη προς την ακτή ράβδος, 3. Ρυθμική ράβδος και ακτή, 4.Εγκάρσια ράβδος και ρεύμα επαναφοράς, 5 . Επίπεδο χαμηλής παλίρροιας (Short and Woodroffe, 2009).

Οι Castelle et al. (2010) πραγματοποίησαν ένα τρισδιάστατο εργαστηριακό πείραμα (Εικόνα 12) για τη διερεύνηση των μηχανισμών ρευμάτων επαναφοράς υπό μεταβαλλόμενο αμμώδη πυθμένα, στις εγκαταστάσεις ARTELIA /SOGREAH (LHF, G-INP, Γαλλία), βασισμένο στην εργασία των Wright και Short (1984). Εφαρμόστηκαν αποθετικές και διαβρωτικές συνθήκες ακανόνιστων κυματισμών, ενώ τα πειράματα περιλαμβάναν όλα τα στάδια εξέλιξης ακτής**. Τα αποτελέσματα έδειξαν ότι ο ρυθμός μεταβολής και η ακολουθία των κυματικών χαρακτηριστικών στον κυματιστήρα, έχει άμεση επίπτωση στην μεταβολή της γεωμετρίας πυθμένα. Με άλλα λόγια μεταβάλλοντας μέσα σε μικρό χρονικό διάστημα (1-3 ώρες) τις επικρατούσες <u>ενεργητικές</u> κυματικές συνθήκες, η βαθυμετρική εξέλιξη επιταχύνεται σημαντικά καθώς ο αμμώδης πυθμένας δεν προλαβαίνει να ΄αγγίξει' το σημείο ισορροπίας που αντιστοιχεί στις εκάστοτε συνθήκες κύματος.** Αυτό ήταν το πρώτο τρισδιάστατο

εργαστηριακό πείραμα που παρείχε εκτενείς μετρήσεις υδροδυναμικής και μορφοδυναμικής ακτής σε όλα τα στάδια και υποστάδια μετάβασης. Η διερεύνηση των υδρομορφοδυναμικών φαινομένων αποκάλυψε την έντονη αλληλεπίδραση μεταξύ πολλών μηχανισμών ανάδρασης που σχετίζονται με τις κυκλοφορίες ρευμάτων επαναφοράς καθοδηγούμενα από τα κύματα, τη μεταφορά ιζημάτων και την εξέλιξη του βυθού.

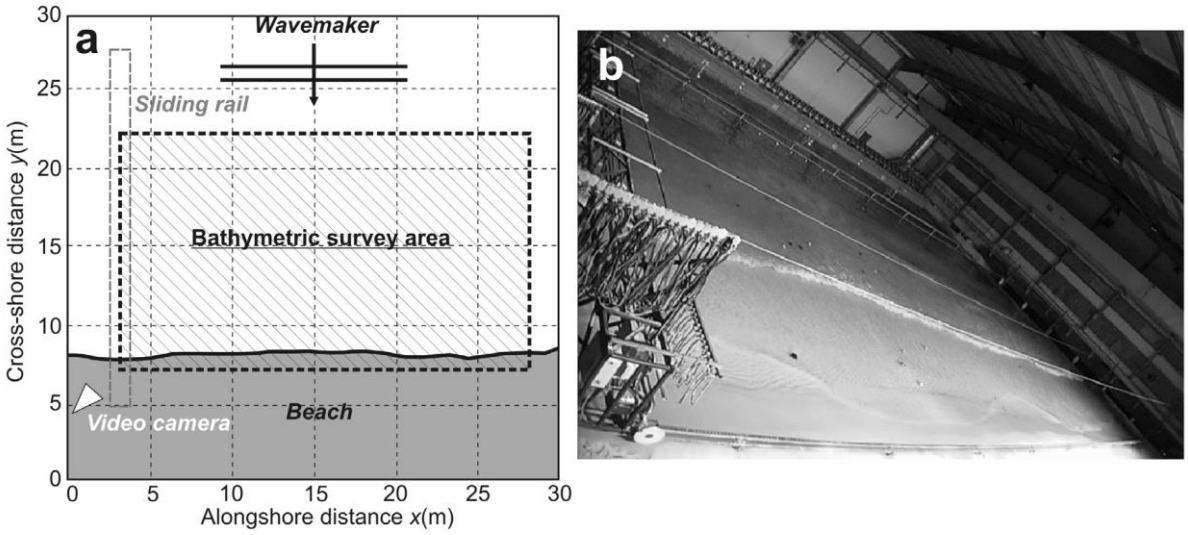

Εικόνα 12 Πειραματική διάταξη και εγκαταστάσεις για τις φυσικές προσομοιώσεις των Castelle et al., 2010.

Αριθμητική αξιολόγηση των αλληλεπιδράσεων υδροδυναμικής κυκλοφορίας – αμμώδους βυθού χρησιμοποιώντας αρχές ελαχιστοποίησης

Για την αριθμητική μελέτη αυτού του φαινομένου αλληλεπίδρασης υδροδυναμικής κυκλοφορίας - αμμώδους πυθμένα, αξιοποιήθηκε ένα αριθμητικό μοντέλο βασισμένο τόσο σε εξισώσεις ρηχών νερών, όσο και σε μια μαθηματική προσέγγιση για την πρόβλεψη βαθυμετρικής εξέλιξης, χρησιμοποιώντας αρχές ελαχιστοποίησης (Bouharguane and Mohammadi, 2013; Mohammadi and Bouchette, 2014). Οι αρχές ελαχιστοποίησης έχουν χρησιμοποιηθεί αρκετές φορές στο παρελθόν για το σχεδιασμό προστατευτικών έργων κατά της παράκτιας διάβρωσης (Azerad et al., 2005), (Isebe et al., 2008). Σε αντίθεση με τα προγενέστερα έργα, όπου οι προς μελέτη δομές ήταν ανεξάρτητες από το χρόνο, η παρούσα μέθοδος προχωρά ένα βήμα παραπέρα δίνοντας τη δυνατότητα στη δομή να αλλάζει με το χρόνο. **Αξίζει να σημειωθεί ότι η θεμελιώδης υπόθεση αυτής της προτεινόμενης μεθόδου είναι το γεγονός ότι η βαθυμετρία προσαρμόζεται στη ροή με κάποιο είδος βέλτιστης μεταφοράς άμμου προκειμένου να ελαχιστοποιηθεί μία έκφραση ενέργειας.** Οι χρονικές

κλίμακες ενδιαφέροντος είναι κάτω από ένα μήνα και οι ανακτήσεις μεταξύ καταιγίδων ή εποχιακών και διαχρονικών μεταβλητών είναι εκτός του πεδίου εφαρμογής.

Για τις ανάγκες των αριθμητικών προσομοιώσεων αξιοποιήθηκε η περίπτωση της πειραματικής διάταξης που περιεγράφηκε προηγουμένως (Εικόνα 12) με μέσο βάθος νερού h_0= 0,765 m, προκειμένου να συγκριθούν τα αριθμητικά υπολογισμένα και πειραματικά μετρηθέντα υδροδυναμικά και μορφοδυναμικά χαρακτηριστικά. Οι ίδιες κυματικές συνθήκες με αυτές του πειράματος εφαρμόστηκαν στο ανοιχτό όριο, επομένως, η συνολική διάρκεια της κυματικής δράσης (96,4 ώρες) χωρίστηκε σε 2 φάσεις, τις 62 ώρες της ακολουθίας κυμάτων απόθεσης με συνθήκες Η-ήπιων κύματος (Hs = 18 cm / T p = 3,5 s) και 34,4 ώρες της διαβρωτικής ακολουθίας με συνθήκες Ε-ενεργού κύματος (Hs = 23 cm / T p = 2,3 s).

Για την εκτίμηση της δυναμικής μεταφοράς ιζημάτων και την εξέλιξη του προφίλ της ακτής, το κυματικό κλίμα των πειραμάτων αναπαράχθηκε αριθμητικά. Μόνο η περιοχή μεταξύ 6 ≤ x ≤ 26 m λήφθηκε υπόψη, όπου εκτείνεται ο αμμώδης πυθμένας και όπου πραγματοποιήθηκαν πειραματικές μετρήσεις (Εικόνα 12). Οι Εικόνα 13 και Εικόνα 14 αποτυπώνουν τη σύγκριση πειράματος – μοντέλου αναφορικά με την εξέλιξη βαθυμετρίας κατά τη διάρκεια ήπιων/αποθετικών κυματισμών (accretive wave sequence) και ενεργητικών κυματισμών (erosive wave sequence). Το πιο εντυπωσιακό χαρακτηριστικό αυτών των αποτελεσμάτων, είναι ότι η χρονική εξέλιξη της γεωμετρίας πυθμένα, ακολουθεί την ίδια ακολουθία με αυτή του πειράματος.

Κατά την πρώτη φάση, παρατηρήθηκε μία συνολική τάση απόθεσης (accretion) με παράλληλη αύξηση του ύψους/στάθμης του αμμώδους πυθμένα (bottom elevation) για μια χρονική περίοδο 62 ωρών ήπιων και μακρών κυμάτων (Hm0 = 18 cm / T p = 3,5 s). Κατά τη διάρκεια αυτού του σταδίου, τα αριθμητικά αποτελέσματα δείχνουν μια μετατόπιση των ιζημάτων προς την ακτή με παράλληλη έντονη διάβρωση στην περιοχή των βαθέων υδάτων (offshore) (x ≤10 m)(Εικόνα 13). Για το σενάριο αυτής της ήπιας κυματικής ακολουθίας, η σύγκριση της αριθμητικά υπολογιζόμενης βαθυμετρίας με αυτή του πειράματος, δείχνει ότι η απόθεση στην περίπτωση των αριθμητικών ευρημάτων είναι πιο έντονη και επεκτείνεται περαιτέρω προς τη βαθιά ύδατα.

Σχετικά με το δεύτερο στάδιο μεταξύ 62 ≤T ≤96,4 ωρών με συνθήκες Ε-ενεργού κύματος και βραχείας περιόδου κύματος (Hm0 = 23 cm / T p = 2,3 s), προκύπτει μια συνολική τάση διάβρωσης, για την περίπτωση των αριθμητικών προβλέψεων. Όπως παρατηρείται στην Εικόνα 14, το σύστημα ράβδων άμμου (sandbar system) μετατοπίστηκε προς τα βαθιά ύδατα. Η

σύγκριση με τα πειραματικά δεδομένα, αποδεικνύει ότι η διάβρωση είναι λιγότερο έντονη προς την ακτή στην περίπτωση του αριθμητικού μοντέλου και η συγκέντρωση ιζήματος στο τμήμα x ≤6 είναι υψηλότερη από αυτή του πειράματος.

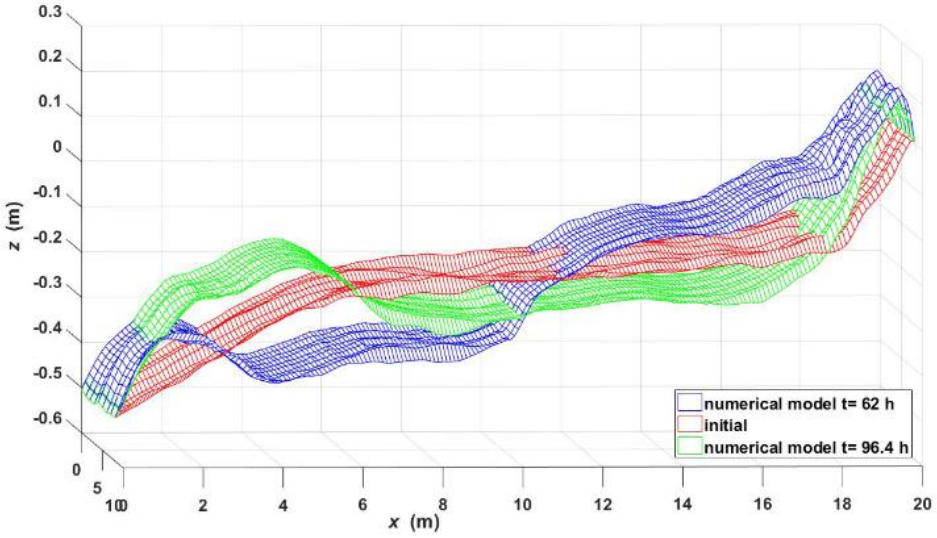

Εικόνα 13 Πειραματικά και αριθμητικά αποτελέσματα εξέλιξης βαθυμετρίας κατα τη διάρκεια ήπιων/αποθετικών κυματισμών (accretive wave sequence), χρησιμοποιώντας την αριθμητική φόρμουλα των Bouharguane and Mohammadi, 2013.

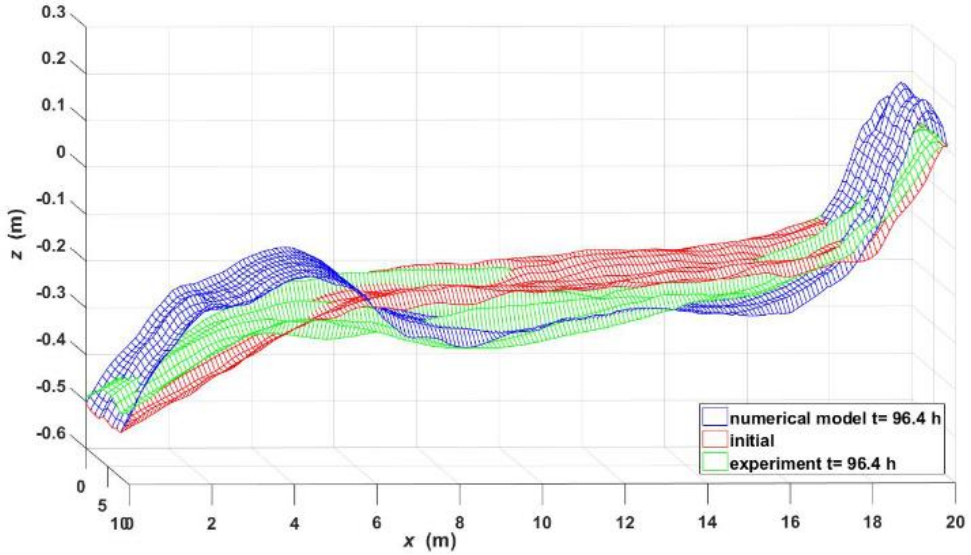

Εικόνα 14 Πειραματικά και αριθμητικά αποτελέσματα εξέλιξης βαθυμετρίας κατα τη διάρκεια ενεργητικών κυματισμών (erosive wave sequence), χρησιμοποιώντας την αριθμητική φόρμουλα των Bouharguane and Mohammadi, 2013.

Αριθμητικές προσομοιώσεις για την αξιολόγηση μηχανισμών μεταφοράς ιζημάτων σε ρηχό και σύνθετο θαλάσσιο πυθμένα με βάση ημι-ασταθείς προσεγγιστικές σχέσεις.

Μία δεύτερη αριθμητική προσέγγιση, βασισμένη στις συμβατικές σχέσεις για τη δυναμική των ιζημάτων, χρησιμοποιήθηκε εδώ για την προσομοίωση των υδροδυναμικών συνθηκών και της βαθυμετρικής εξέλιξης υπό διαβρωτικές και αποθετικές κυματικές ακολουθίες. Για τις υδροδυναμικές προβλέψεις, εφαρμόστηκε μια ρουτίνα που λύνει τις δισδιάστατες μη γραμμικές εξισώσεις ρηχών νερών (NSWE) (Marche and Bonneton, 2006), (Marche et al., 2007). Στα πλαίσια της παρούσας διδακτορικής διατριβής αναπτύχθηκε ένας αριθμητικός κυματιστήρας - wave-maker για τη προσομοίωση της γένεσης ακανόνιστων κυμάτων χρησιμοποιώντας κατευθυντικά φασματικά δεδομένα. Ο μηχανισμός κίνησης ιζήματος αξιολογήθηκε, μέσω ενός αριθμητικού μοντέλου που αναπτύχθηκε στα πλαίσια της παρούσας διατριβής (Afentoulis et al., 2019), χρησιμοποιώντας ημι-ασταθείς σχέσεις που λαμβάνουν υπόψη τη μη γραμμική επίδραση των κυμάτων στην υδροδυναμική κυκλοφορία και κατ'επέκταση στο μηχανισμό στερεομεταφοράς (Ribberink 1998 ; Camenen and Larson's 2005, 2007, 2008 ; Soulsby 1997) (Κεφάλαιο 3 : Formulas of Ribberink and Camenen – Larson και Formula of Soulsby-Van Rijn). Τα αποτελέσματα των δύο παραπάνω αριθμητικών μεθόδων συγκρίθηκαν με τα πειραματικά ευρήματα των Castelle et al. (2010).

Η Εικόνα 15 απεικονίζει το πεδίο κυματογενών ρευμάτων μετά από 1, 7, 30 και 60 ώρες δράσης κύματος, και τις αντίστοιχες βυθομετρικές αλλαγές στο χρόνο αυτό, υπό συνθήκες ήπιων και μακρών κυμάτων (Hm0 = 18 cm / T p = 3,5 s). Η εξέλιξη του ιζηματογενούς πυθμένα είναι πιο έντονη στις ζώνες όπου εμφανίζονται σημαντικές χωρικές διαβαθμίσεις της ταχύτητας. Κοντά στην ακτή, τα ρεύματα με προσανατολισμό προς τα ανοιχτά είχαν ως αποτέλεσμα την αλλαγή της βυθομετρικής ομοιομορφίας ως προς την παράκτια κατεύθυνση (Along-shore uniformity), με συναφείς συνθήκες διάβρωσης κοντά στα πλευρικά όρια. Αξίζει να αναφερθεί πως η αρχική γεωμετρία με σταθερή κλίση ακτής δεν είναι ΄ρεαλιστική΄, επομένως το σύστημα κύματος-ρεύματος-θαλάσσιου βυθού τείνει να βρει μια ισορροπία αλλάζοντας τις βαθυμετρικές κλίσεις κοντά στην ακτή. Ως εκ τούτου, παρατηρούνται τρισδιάστατα χαρακτηριστικά στη μορφολογία του πυθμένα μετά από 30 ώρες κυματικής δράσης (three-dimensional structure of rhythmic topography). Αυτή η γεωμετρία μεταβάλει την υδροδυναμική κυκλοφορία κατά μήκος της ακτής, όπου παρατηρούνται ρεύματα με ταχύτητα 0,1 m/s. Παρατηρείται ακόμα πως δεν υπάρχουν σημαντικές μεταβολές στη γεωμετρία του πυθμένα μεταξύ 30 και 60 ωρών και συμπεραίνεται ότι ο ρυθμός βαθυμετρικής μεταβολής ήταν αρχικά υψηλός και επιβραδύνθηκε καθώς πλησίαζε η ισορροπία ως προς τις

επικρατούσες κυματικές συνθήκες. Κοντά στο στάδιο ισορροπίας, σχετικά ασθενείς ταχύτητες περίπου 0,07 m/s χαρακτηρίζουν το επαγόμενο από το κύμα πεδίο ρεύματος.

Η Εικόνα 16 απεικονίζει το πεδίο κυματογενών ρευμάτων μετά από 1, 5, 15 και 30 ώρες δράσης κύματος, και τις αντίστοιχες βυθομετρικές αλλαγές στο χρόνο αυτό, υπό συνθήκες Ε-ενεργού κύματος και βραχείας περιόδου κύματος (Hm0 = 23 cm / T p = 2,3 s). Η εξέλιξη του ιζηματογενούς πυθμένα είναι πιο έντονη στις ζώνες όπου εμφανίζονται σημαντικές χωρικές διαβαθμίσεις της ταχύτητας. Παρατηρείται μια έντονη κίνηση ιζήματος προς το ανοιχτό όριο κατά τη διάρκεια της διαβρωτικής ακολουθίας. Η ένταση και η κατεύθυνση των ρευμάτων που προκαλούνται από τα κύματα είναι καθοριστικές για τις μορφολογικές αλλαγές του βυθού της θάλασσας. Η υδροδυναμική ροή χαρακτηρίζεται από ένα ρεύμα επαναφοράς, με ταχύτητα 0,1 m/s.

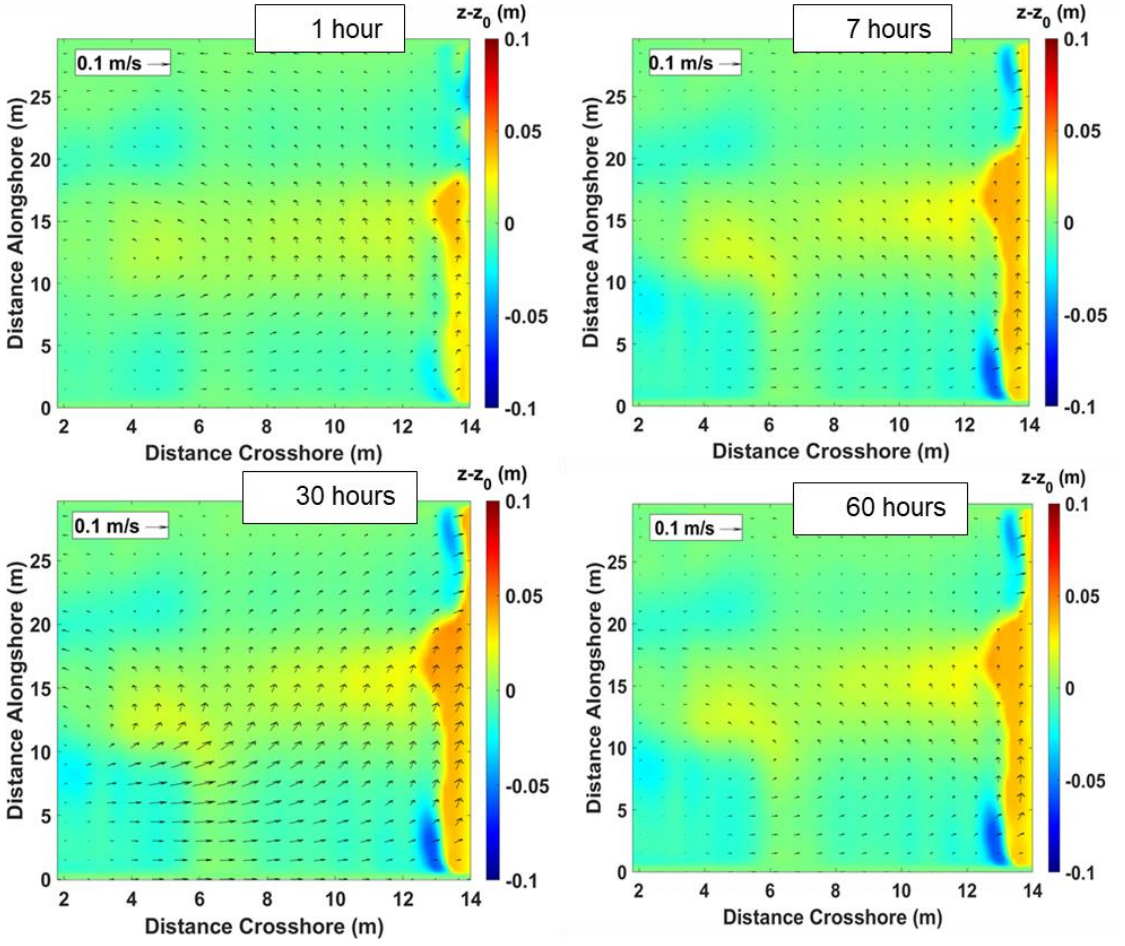

Εικόνα 15 Αριθμητικά αποτελέσματα εξέλιξης βαθυμετρίας και υδροδυναμικής κυκλοφορίας κατα τη διάρκεια ήπιων κυματισμών (accretive wave sequence) (Hm0 = 18 cm / T p = 3,5 s).

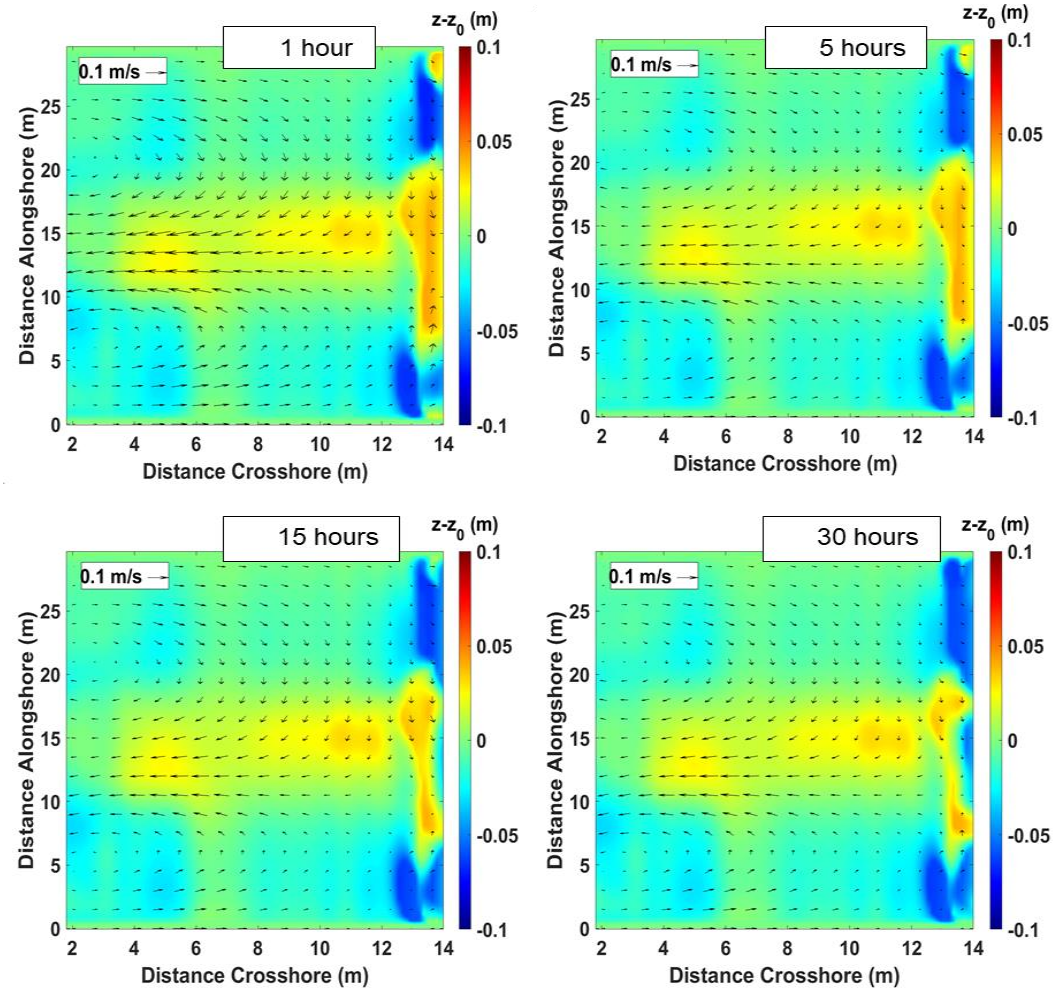

Εικόνα 16 Αριθμητικά αποτελέσματα εξέλιξης βαθυμετρίας και υδροδυναμικής κυκλοφορίας κατα τη διάρκεια ενεργητικών κυματισμών (erosive wave sequence) (Hm0 = 23 cm / T p = 2,3 s).

Η εξέλιξη του βυθού στο τέλος της αυξητικής και διαβρωτικής ακολουθίας χρησιμοποιώντας τις σχέσεις των Ribberink και Camenen – Larson παρουσιάζεται στην Εικόνα 17 (Κεφάλαιο 3 : Formulas of Ribberink and Camenen – Larson και Formula of Soulsby-Van Rijn). Οι αλλαγές του βυθού στο τέλος κάθε σταδίου είναι της ίδιας τάξης μεγέθους με αυτές των πειραμάτων, αποδεικνύοντας με αυτό το τρόπο το κυρίαρχο ρόλο των υδροδυναμικών μοτίβων στη μορφολογία της ακτής. Οι παρατηρούμενες αποκλίσεις της τελικής γεωμετρίας του πυθμένα πειράματος και μοντέλου, είναι μεταξύ -0,1 m και +0,1 m. Επομένως, επιτεύχθηκε μια καλή συμφωνία μεταξύ των πειραματικών και αριθμητικών αποτελεσμάτων

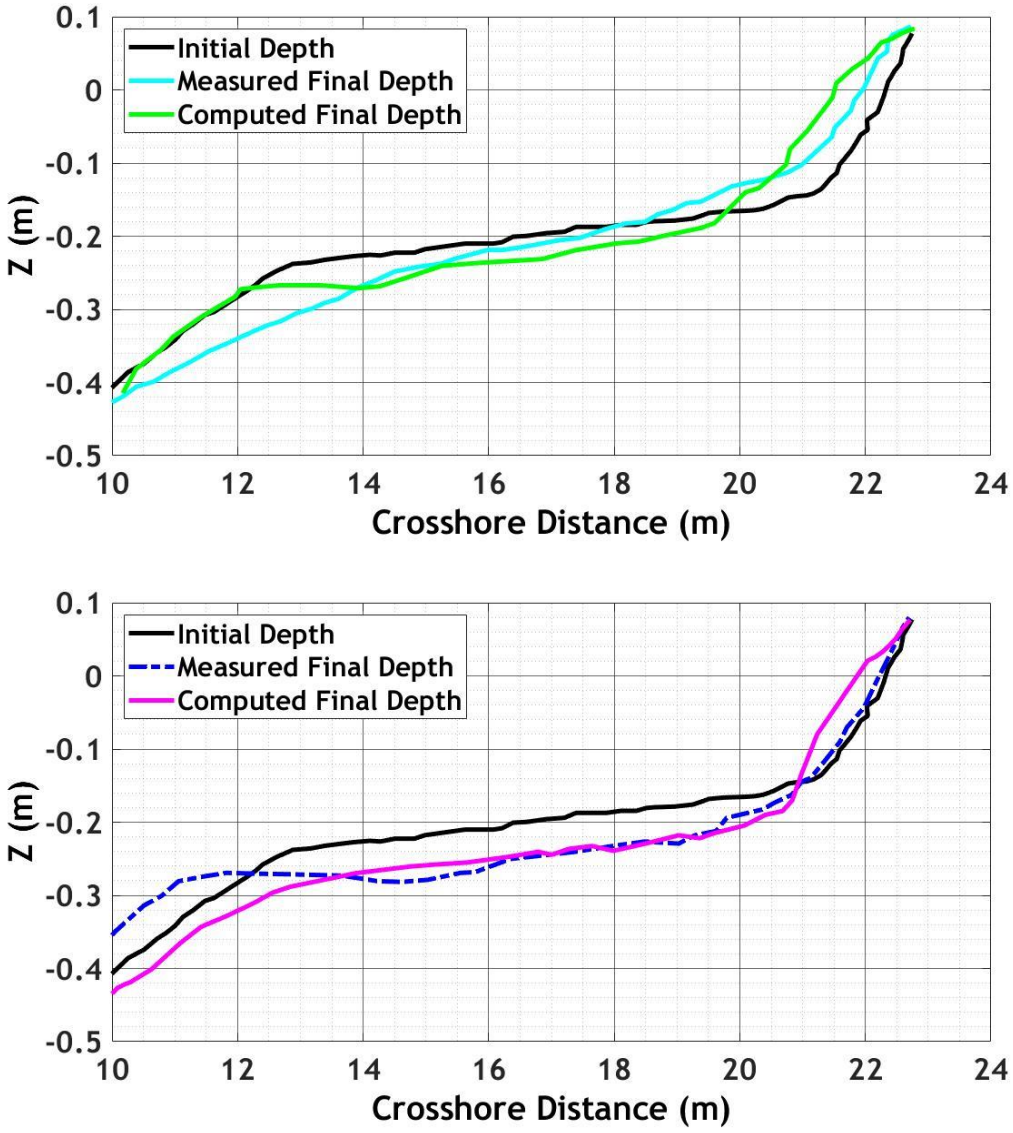

Εικόνα 17 Πειραματικά και αριθμητικά αποτελέσματα εξέλιξης βαθυμετρίας κατά τη διάρκεια ήπιων/αποθετικών κυματισμών (accretive wave sequence) (πάνω) και ενεργητικών κυματισμών (erosive wave sequence) (κάτω), χρησιμοποιώντας μία αριθμητική φόρμουλα βασισμένη στις συμβατικές σχέσεις για τη δυναμική των ιζημάτων.

Όπως έχει ήδη συζητηθεί προηγουμένως σε αυτή τη διατριβή, το κύριο αντικείμενο έρευνας είναι η ανάπτυξη ενός αξιόπιστου εργαλείου για την αξιολόγηση της παράκτιας μεταφοράς ιζημάτων και της μορφολογίας. Η πολυπλοκότητα και η αβεβαιότητα των διαφόρων παράκτιων φυσικών διεργασιών είναι τόσο έντονη που οι προβλέψεις ροών ιζήματος μπορούν να θεωρηθούν ικανοποιητικές, ακόμα και αν εμπεριέχουν ένα μεγάλο συντελεστή αβεβαιότητας, ειδικά εάν πρόκειται για μετρήσεις πεδίου. Ωστόσο, στις μέρες μας, οι σύγχρονες τεχνικές ολοκληρωμένης διαχείριση παράκτιων ζωνών και ακτών απαιτούν μία ρεαλιστική εκτίμηση των φορτίων ιζημάτων, παρά το αυξημένο επίπεδο αβεβαιότητας.

Ως εκ τούτου, σε αυτή την ενότητα, που αναφέρεται στο κεφάλαιο 3 της παρούσας διδακτορικής διατριβή (Numerical assessments of sandbar systems and rip channel dynamics), έγινε μια προσπάθεια να αυξήσουμε την ικανότητά κατανόησης της αλληλεπίδρασης κύματος-αμμώδους πυθμένα χωρίς την παρουσία παράκτιων έργων. Τα αριθμητικά αποτελέσματα επιβεβαιώθηκαν σε σχέση με τα πειραματικά ευρήματα των Michaellet et al., (2013), ενώ χρησιμοποιήθηκαν δύο διακριτές προσεγγίσεις για την αξιολόγηση της μορφοδυναμικής των ακτών και ιδιαίτερα της επίδρασης των μεταβολών του κλίματος των κυμάτων στη μορφολογία. Η πρώτη αριθμητική μέθοδος (Numerical assessment of flow-seabed interactions using minimization principles.), η οποία χρησιμοποιήθηκε εδώ, βασίζεται σε αρχές ελαχιστοποίησης για την αξιολόγηση της παράκτιας μορφολογίας (Bouharguane and Mohammadi, 2013; Mohammadi and Bouchette, 2014). Αυτή η αριθμητική μέθοδος παρείχε αξιόπιστα αποτελέσματα, σχετικά με τον προσδιορισμό των ζωνών, στις οποίες επικρατεί απόθεση ή διάβρωση. Ωστόσο, ο περιορισμός αυτού του μοντέλου σε σχέση με την αναπαραγωγή ενός ρεαλιστικού κυματικού κλίματος, δυσχεραίνει την ακριβή προσομοίωση ρευμάτων κοντά στην ακτή. Όσον αφορά την πρόβλεψη τελικής γεωμετρίας πυθμένα, επιτεύχθηκε μία ικανοποιητική συμφωνία μεταξύ των αριθμητικά υπολογισμένων και των μετρούμενων παραμέτρων. Αυτό μπορεί να οδηγήσει στο συμπέρασμα ότι η συγκεκριμένη αριθμητική τεχνική μπορεί να παρέχει ακριβή πρόβλεψη για μονοδιάστατες εφαρμογές μέσου βάθους (1DH cross-shore), με ή χωρίς την παρουσία παράκτιων έργων.

Ένα ακόμα αριθμητικό σύνθετο μοντέλο (Numerical approaches for the evaluation of sediment transport mechanisms on a shallow sloping sea bottom based on quasi-steady approximations.), χρησιμοποιήθηκε σε αυτή την ενότητα για τη διερεύνηση υδροδυναμικών και μορφοδυναμικών φαινομένων δισδιάστατων εφαρμογών μέσου βάθους 2DH, με βάση τις μη γραμμικές εξισώσεις ρηχών υδάτων (NSWE), ενώ παράλληλα για τις ανάγκες του σύνθετου μοντέλου, στα πλαίσια της παρούσας διδακτορικής εργασίας αναπτύχθηκε ένα νέο μοντέλο μεταφοράς ιζήματος και μορφολογίας, που συζεύχθηκε με το υδροδυναμικό μοντέλο. Αυτή η αριθμητική μέθοδος μπορεί να επιτύχει την πρόβλεψη της συνδυασμένης δράσης κυμάτων - ρευμάτων και την αξιολόγηση των επιδράσεων μη γραμμικών κυμάτων στους ρυθμούς μεταφοράς ιζημάτων. Με τη χρήση του συζευγμένου μοντέλου διερευνήθηκαν οι διαδικασίες διάδοσης κύματος κοντά στην ακτή, η υδροδυναμική κυκλοφορία, η μεταφορά ιζήματος και η μορφολογία. Οι χάρτες της κατανομής ύψους κύματος που εξήχθησαν δείχνουν μια καλή συμφωνία σε σύγκριση με τα πειραματικά δεδομένα, αν και η παρατηρούμενη θραύση κύματος που προσημειώθηκε αποκλειστικά μέσω της δυναμικής ανισορροπίας λόγω μεταβολής του βάθους, έχει ως αποτέλεσμα ένα λιγότερο ενεργητικό κυματικό πεδίο κοντά

στην ακτή, σε αντίθεση με αυτό του πειράματος. Η υδροδυναμική κυκλοφορία οδηγεί τις ιζηματογενείς ροές, ενώ η υπολογισμένη τελική γεωμετρία πυθμένα είναι σύμφωνη με αυτό του πειράματος. **Ωστόσο, αυτή η προσέγγιση κατέδειξε την ανάγκη να ενσωματωθεί ένα πιο σύνθετο υδροδυναμικό και κυματικό μοντέλο για τη μελέτη των μη γραμμικών κυμάτων, των χαρακτηριστικών διασποράς, και της ροής, το οποίο παρουσιάζεται στη συνέχεια.**

Ένα καινοτόμο μη γραμμικό μοντέλο για τη μελέτη εφαρμογών παράκτιας μορφοδυναμικής

Τα αριθμητικά μοντέλα που βασίζονται στην ανάλυση της φάσης των κυματισμών, είναι σε θέση να επιλύσουν πολλές από τις προαναφερθείσες σημαντικές διαδικασίες μετασχηματισμού κυμάτων στις μεταβατικές ζώνες από τα βαθιά στα ρηχά ύδατα, ωστόσο συχνά συνδέονται με σημαντικούς περιορισμούς, π.χ. με ήπια κλίση πυθμένα (για μοντέλα που βασίζονται στις εξισώσεις κύματος ήπιας κλίσης) και ικανοποίηση της προσέγγισης των εξισώσεων ρηχών νερών. **Σε αυτό το σημείο αξίζει να αναφερθεί ότι τα μοντέλα ανάλυσης φάσης, τα οποία βασίζονται σε εξισώσεις ρηχών νερών, θέτουν σημαντικούς περιορισμούς στο μέγιστο σχετικό βάθος *kh* (*k* ο αριθμός κύματος και *h* βάθος) που μπορεί να προσεγγιστεί**. Στην περίπτωση υψηλών τιμών *kh*, οι κατακόρυφες επιταχύνσεις ή η διασπορά κυμάτων δεν μπορούν να παραβλεφθούν και η χρήση εξισώσεων ρηχών υδάτων για τον υπολογισμό των υδροδυναμικών παραμέτρων καθίσταται ανακριβής. Από βαθιά έως ρηχά νερά, τα φαινόμενα διασποράς μη γραμμικών κυμάτων μπορούν να προσομοιωθούν ικανοποιητικά χρησιμοποιώντας μοντέλα τύπου Boussinesq (Madsen et al., 1997; Kennedy et al., 2001) καθώς είναι ιδιαίτερα ακριβή ως προς την επίλυση κυματικών φαινομένων σε αβαθή ύδατα, όπως αυτών της διάθλασης και της περίθλασης (Do, 2020). **Ωστόσο, μέχρι πρόσφατα, η εφαρμογή τους στην υδροδυναμική μοντελοποίηση ήταν περιορισμένη λόγω του υψηλού υπολογιστικού κόστους, καθιστώντας τη χρήση τους σε πρακτικές εφαρμογές σχεδόν αδύνατη**. Σήμερα, αρκετά μοντέλα τύπου Boussinesq σε συνδυασμό με μια αριθμητική ρουτίνα υπολογισμού μεταφοράς ιζήματος, κατάλληλη για εφαρμογές παράκτιας μηχανικής, μπορούν να συναντηθούν στη βιβλιογραφία της ακτομηχανικής (Kobayashi et al., 2001; Karambas, 2002; Karambas, 2012; Gallerano et al. 2016, Klonaris et al., 2016; Malej et al., 2019). Με βάση αυτή την ιδέα, διαφορετικές έρευνες έχουν προβλέψει σε ένα βαθμό την εξέλιξη της ακτογραμμής και τη μορφολογία της ακτής στη γειτνίαση κυματοθραυστών Και άλλων παράκτιων έργων προστασίας (Du et al., 2010; Karambas and Samaras, 2017; Bouvier et al., 2019; Hieu et al., 2020).

Μέχρι σήμερα, οι αριθμητικές προβλέψεις των αλληλεπιδράσεων κύματος-ρεύματος και οι μορφολογικές αποκρίσεις, με ή χωρίς την παρουσία παράκτιων δομών, εξακολουθούν να χαρακτηρίζονται από σημαντικό βαθμό αβεβαιότητας που σχετίζεται με την υψηλή μη γραμμική φύση αυτών των φυσικών διεργασιών. Στις προαναφερθείσες μελέτες, είτε η υδροδυναμική επίλυση δεν λαμβάνει υπόψη τα χαρακτηριστικά ανάκλασης και απορρόφησης (π.χ. διαπερατότητα) των κυματοθραυστών και των κατακόρυφων εμποδίων, είτε οι προσεγγίσεις που χρησιμοποιήθηκαν για τη μεταφορά ιζήματος δεν είναι κατάλληλες για την καταγραφή των μη γραμμικών επιδράσεων του κύματος στη στερεομεταφορά και για την προσομοίωση των τρισδιάστατων χαρακτηριστικών των φορτίων μεταφοράς αιωρούμενων ιζημάτων. Στην παρούσα μελέτη, ένα πλήρως μη γραμμικό μοντέλο Boussinesq - FUNWAVE-TVD (Shi et al., 2012) για την προσομοίωση της διάδοσης κύματος και της υδροδυναμικής κυκλοφορίας συνδυάστηκε με ένα ημί - τρισδιάστατο μοντέλο στερεομεταφοράς και μορφολογίας, το οποίο αναπτύχθηκε από το συγγραφέα αυτής της μελέτης. Έτσι, εκμεταλλευόμενοι την ικανότητα του μοντέλου FUNWAVE να παρέχει πληροφορίες σχετικά με την ανάκλαση και τη συμπεριφορά μετάδοσης κυμάτων και χρησιμοποιώντας προηγμένες προσεγγίσεις μεταφοράς ιζημάτων, συμπεριλαμβανομένων πτυχών της ασταθούς στερεομεταφοράς, αυτή η μελέτη επιδιώκει να μειώσει την αβεβαιότητα που σχετίζονται με τις υδρομορφοδυναμικές προβλέψεις. Ιδιαίτερη προσοχή δόθηκε στον ρόλο της δυναμικής μεταφοράς ιζημάτων σε όλη τη ζώνη swash, ενσωματώνοντας τεχνικές προσομοίωσης αυτών των μηχανισμών στο μορφοδυναμικό μοντέλο, ενώ παράλληλα χρησιμοποιήθηκαν προηγμένες τεχνικές για τη μοντελοποίηση των τρισδιάστατων μοτίβων αιωρούμενων ροών - φορτίου ιζήματος και ενσωμάτωσης μη γραμμικών και ασταθών επιδράσεων κυμάτων στην επίλυση του φορτίου πυθμένα. Ο βασικός σκοπός είναι η ανάπτυξη ενός ολοκληρωμένου μοντέλου που μπορεί να χρησιμοποιηθεί σε ένα ευρύ φάσμα εφαρμογών παράκτιας μηχανικής, τόσο για ήπιες λύσεις προστασίας (αναπλήρωση παραλιών, διαχείριση αμμόλοφων, αποστράγγιση) όσο και για τεχνικές έργων πολιτικού μηχανικού (σχεδιασμός κάθετων προβόλων, κυματοθραυστών, θωράκισης, προβλητών).

Επιπλέον, προκειμένου να διασφαλιστεί η αξιοπιστία της αριθμητικής προσέγγισής, το σύνθετο μοντέλο εξετάστηκε υπό πέντε διακριτές πειραματικές περιπτώσεις, καλύπτοντας ένα ευρύ φάσμα εφαρμογών παράκτιας μηχανικής τόσο σε κλίμακα φυσικού μοντέλου, όσο και σε κλίμακα πεδίου, παρέχοντας σημαντικές πληροφορίες για τη μορφολογική απόκριση της αμμώδους ακτής στη συνδυασμένη δράση κυμάτων και ρευμάτων.

Εφαρμογές μονοδιάστατης ροής

Η πρώτη σειρά συγκρίσεων αναφέρεται στην πειραματική διαδικασία που πραγματοποιήθηκε στο Grosser Wellenkanal στο Αννόβερο στα πλαίσια του έργου EU SAFE (Dette et al., 2002). Εδώ, αναπαράχθηκε το τεστ B2 της πειραματικής σειράς προκειμένου να αξιολογηθούν τα αποτελέσματα του αριθμητικού συζευγμένου μοντέλου. Εφαρμόστηκαν ακανόνιστα κύματα (Hs=1,20 m και Tp=5,5 s), για συνολική διάρκεια 23 ωρών. Η αρχική βαθυμετρία χαρακτηρίζεται από το θεωρητικό προφίλ ισορροπίας Bruun (Bruun, 1954; Dean, 1977). Η σύνοψη των πειραματικών δεδομένων κυμάτων και βαθυμετρίας που χρησιμοποιήθηκαν ως είσοδος για την αριθμητική προσομοίωση δίνεται στον Πίνακα 2.

Πίνακας 2 Παρουσίαση πειραματικών δεδομένων κυμάτων και βαθυμετρίας για το τεστ B2 των Dette et al. (2002).

H_s (m)	**1.20**
T_p (s)	**5.5**
Βάθος νερού στο κυματιστήρα (m)	**5.0**
D_{50} (mm)	**0.30**
Διάρκεια (h)	**23**
Κλίση	**μη σταθερή**

Η σύγκριση των αποτελεσμάτων πειράματος και αριθμητικού μοντέλου παρουσιάζεται παρακάτω. Αξίζει να αναφερθεί πως ιδιαίτερα ικανοποιητική συμφωνία παρατηρήθηκε τόσο ως προς την προσομοίωση των κυματικών φαινομένων (θράυση, ρήχωση, Εικόνα 18) όσο και σε σχέση με την επίλυση των ιζηματογενών φορτίων και της τελικής γεωμετρίας πυθμένα. Το αριθμητικό συζευγμένο μοντέλο αναπαρήγαγε επιτυχώς τις κορυφές της κατανομής του φορτίου ιζήματος κατά μήκος του προφίλ της ακτής (Εικόνα 20). Σε σχέση με την τελική βαθυμετρία (Εικόνα 19), ο σχηματισμός αμμώδους ράβδου προβλέφθηκε με ακρίβεια, αν και το μοντέλο υπερεκτιμά τη διάβρωση της ακτογραμμής στη ζώνη αναρρίχησής (swash). Τα επόμενα σχήματα παρουσιάζουν τις παραμέτρους εξόδου σε σύγκριση με τις πειραματικές μετρήσεις.

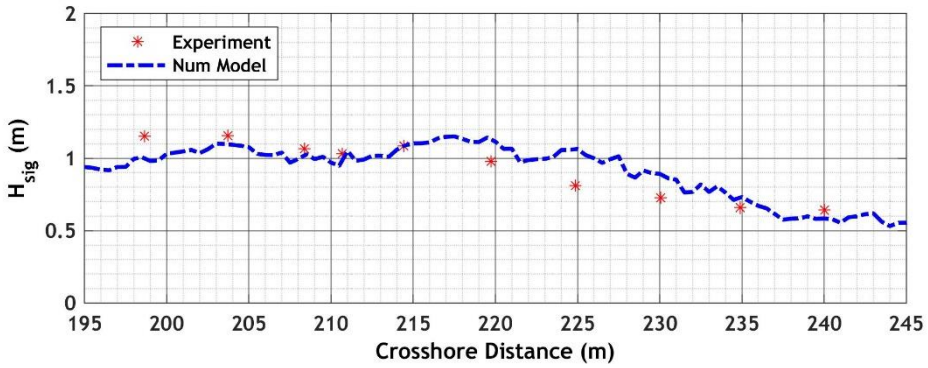

Εικόνα 18 Αριθμητικά και πειραματικά αποτελέσματα κατανομής σημαντικού ύψους κύματος - test case B2 in Dette et al. (2002).

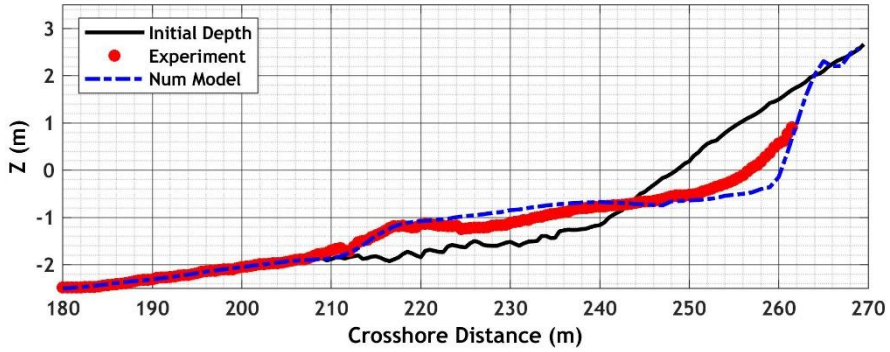

Εικόνα 19 Αριθμητικά και πειραματικά τελικής γεωμετρίας πυθμένα - test case B2 in Dette et al. (2002).

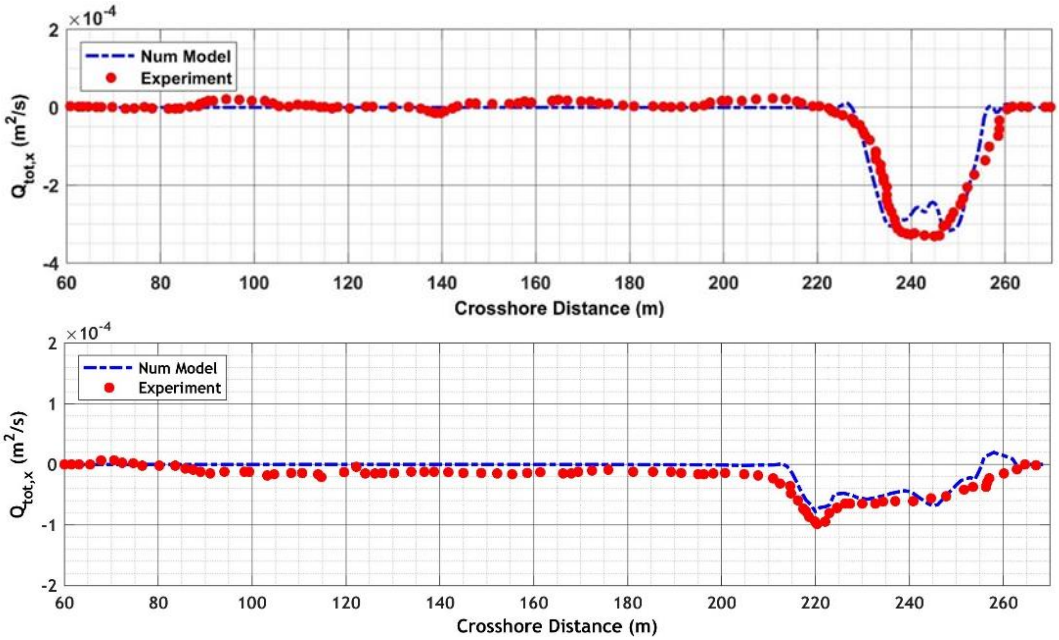

Εικόνα 20 Αριθμητικά και πειραματικά αποτελέσματα ιζηματογενών φορτίων - test case B2 in Dette et al. (2002).

Η δεύτερη σειρά συγκρίσεων αναφέρεται στο έργο Hydralab III SANDS (Scaling and Analysis and New instrumentation for Dynamic bed testS). Το συγκεκριμένο πείραμα πραγματοποιήθηκε στο

Canal de Investigacion y Experimentacion Maritima (CIEM) στο Universidad Politecnica de Cataluña (UPC), στη Βαρκελώνη, και τα πειραματικά ευρήματα παρουσιάστηκαν στη μελέτη των Alsina et al. (2012). Η σύνοψη των πειραματικών δεδομένων κυμάτων και βαθυμετρίας που χρησιμοποιήθηκαν ως είσοδος για την αριθμητική προσομοίωση δίνεται στον παρακάτω πίνακα. Η αρχική υπολογισμένη και μετρημένη κατανομή σημαντικού ύψους κύματος μετά από 21,15 ώρες κυματικής δράσης απεικονίζονται στο Σχήμα της Εικόνα 21. Το αρχικό προφίλ ακτής, καθώς και τα υπολογισμένα και μετρημένα τελικά προφίλ στις 21,15 ώρες φαίνονται επίσης στην Εικόνα 21. Η παρούσα περίπτωση αντιστοιχεί σε διαβρωτικές συνθήκες κοντά στη ζώνη swash λόγω του αρχικού ανακλαστικού προφίλ παραλίας που, με τη σειρά του, εξαναγκάζει σημαντικές ποσότητες ιζήματος να μετακινηθούν σε βαθύτερα ύδατα. Το μοντέλο FUNWAVE-TVD εκτίμησε με ακρίβεια την κατανομή ύψους κύματος ακτής λόγω της υψηλής τάξης μη γραμμικότητας. Ωστόσο, πρέπει να σημειωθεί ότι ορισμένες αποκλίσεις μεταξύ των μετρήσεων και των αριθμητικών αποτελεσμάτων εμφανίζονται στην περιοχή όπου το βάθος του νερού είναι μικρότερο από 0,5 m. Ένα γεγονός θραύσης λαμβάνει χώρα αμέσως στη θέση x = 20 m που οδηγεί στο σχηματισμό της εσωτερικής ράβδου άμμου.

Πίνακας 3 Παρουσίαση πειραματικών δεδομένων κυμάτων και βαθυμετρίας - SANDS test (Alsina et al., 2012).

H_s (m)	0.53
T_p (s)	4.14
Βάθος νερού στο κυματιστήρα (m)	2.47
D_{50} (mm)	0.25
Διάρκεια (h)	21.15
Κλίση	1:10

Τα αριθμητικά αποτελέσματα του μοντέλου μεταφοράς ιζημάτων παρουσιάζουν καλή συστοιχία σε σχέση με τα πειραματικά αποτελέσματα, καθώς επιτεύχθηκε ακριβής πρόβλεψη του σχηματισμού ‘σκαλοπατιού’ – beach step. Συνολικά, η εξέλιξη του βαθυμετρικού σχήματος με την πάροδο του χρόνου ακολουθεί την ίδια πορεία με αυτή του πειράματος. Ωστόσο, μπορεί να ανιχνευθεί κάποια απόκλιση της τάξης του ± 0,10 cm στη ζώνη swash και surf.

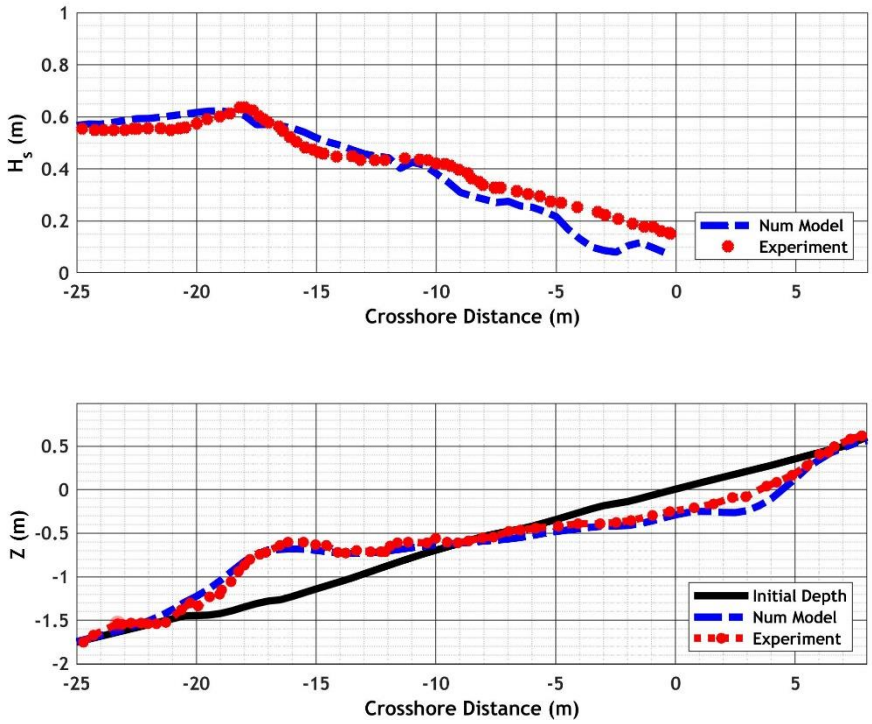

Εικόνα 21 Αριθμητικά και πειραματικά αποτελέσματα κατανομής σημαντικού ύψους κύματος και τελικής γεωμετρίας πυθμένα - SANDS test Alsina et al. (2012).

Εφαρμογές δισδιάστατης ροής

Το φυσικό μοντέλο που σχεδιάστηκε και παρουσιάστηκε από τους Baidei et al. (1994) επιλέχθηκε εδώ ως πείραμα αναφοράς για τη μελέτη μεταφοράς ιζημάτων κοντά στην ξηρά και τις μορφολογικές επιδράσεις των κάθετων προς την ακτή προβόλων (groynes) σε μια αρχικώς ευθύγραμμη ακτογραμμή, η οποία ήταν εκτεθειμένη σε ακανόνιστα κύματα με γωνία πρόσπτωσης 11,6 μοιρών. Το τεστ NT2 της πειραματικής μελέτης αναπαράχθηκε αριθμητικά στο πλαίσιο της παρούσας εργασίας. Η διάμεση διάμετρος των κόκκων του αμμώδους υλικού (D50) ήταν 0,12 mm και η αρχική ομοιόμορφη κλίση της παραλίας ήταν 1:10. Το Σχήμα της Εικόνα 22 απεικονίζει το πεδίο κυματογενών ρευμάτων μετά από 1 ώρα κυματικής δράσης. Η κάθετη προς την ακτή κατασκεύη αλλάζει την κατεύθυνση των παραθαλάσσιων ρευμάτων στη γειτνίασή της, καθώς μειωμένες ταχύτητες μπορούν να φανούν στην υπήνεμη πλευρά της. Τα εγγύς παράκτια ρεύματα έχουν μέγιστη ταχύτητα περίπου ίση με 0,1 m/s. Επιπλέον, παρατηρούνται ταχύτητες προσανατολισμένες προς τα ανοιχτά, που αντανακλώνται από την παραλία, με μέγιστη ταχύτητα 0,06 m/s. Τα φαινόμενα ανάκλασης στην περιοχή του groyne είναι περιορισμένα, λόγω της εφαρμογής εσωτερικών στρωμάτων απορρόφησης που αντιπροσωπεύουν την τριβή ροής και τη διάχυση ενέργειας μέσα στη σώμα του groyne.

Η Εικόνα 23 δείχνει την τελική εξέλιξη του πυθμένα μετά από 12 ώρες δράσης κυμάτων. Η ανοδική συσσώρευση ιζήματος συμβάλλει στην προώθηση της ακτογραμμής προς τη θάλασσα, ενώ η έλλειψη ιζημάτων στην υπήνεμη πλευρά της δομής οδηγεί σε υποχώρηση της ακτογραμμής. Συνολικά, τα αριθμητικά ευρήματα παρουσιάζουν αρκετά καλή συσχέτιση με τα πειραματικά αποτελέσματα, όπως φαίνεται στην Εικόνα 23. Η υπολογισμένη τελική θέση της ακτογραμμής είναι σχεδόν πανομοιότυπη με αυτή του πειράματος, με κάποιες μικρές αποκλίσεις που συναντώνται κοντά στα πλευρικά όρια.

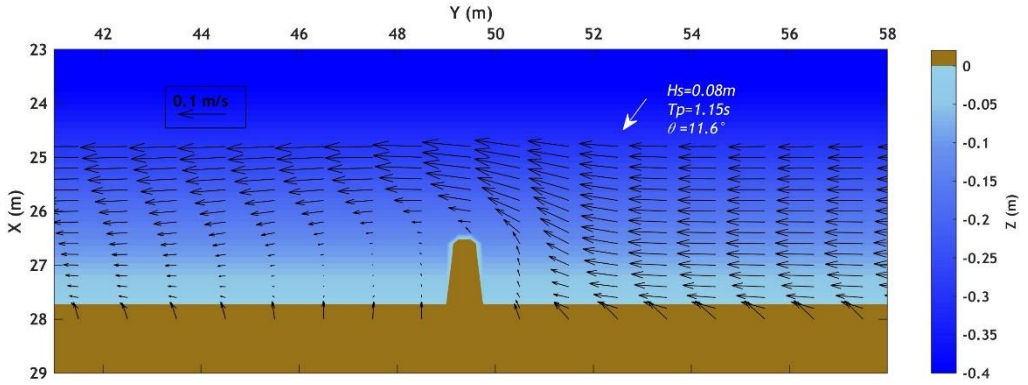

Εικόνα 22 Αριθμητικά και πειραματικά αποτελέσματα κυματογεννών παράκτιων ρευμάτων - Test NT2 Baidei et al. (1994).

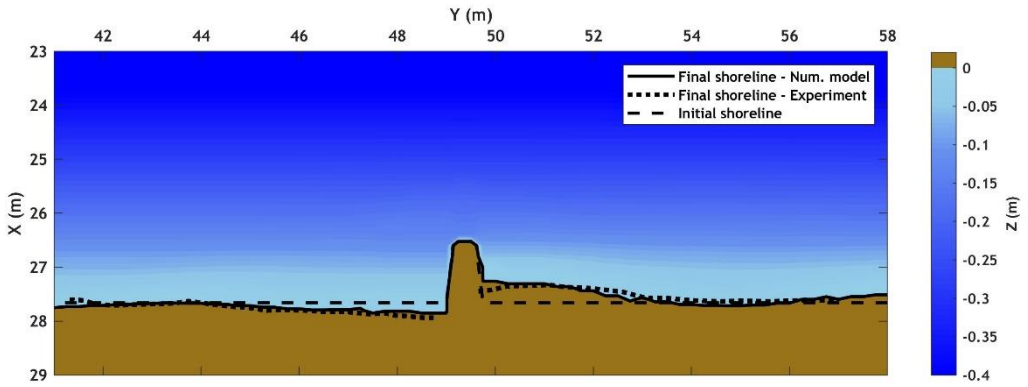

Εικόνα 23 Αριθμητικά και πειραματικά αποτελέσματα εξέλιξης πυθμένα - Test NT2 Baidei et al. (1994).

Οι μελέτες των Deltares/Delft Hydraulics (1997) και Bos et al. (1996) αναλύθηκαν σχετικά με την εξέταση της επίδρασης ενός αποσπασμένου κυματοθραύστη στην παράκτια υδρομορφοδυναμική, χρησιμοποιώντας προσεγγίσεις αριθμητικής μοντελοποίησης. Αυτή η εργασία χρησιμοποιήθηκε ως μελέτη αναφοράς για την επικύρωση του αριθμητικού μας μοντέλου σε συνθήκες πεδίου. Αυτή η εφαρμογή παρουσιάζει ιδιαίτερα μεγάλο ενδιαφέρον, καθώς η συμπεριφορά του μοντέλου μπορεί να διαφέρει ως προς την ικανότητα

προσομοίωσης εργαστηριακών δοκιμών και συνθηκών πεδίου. Έχει αποδειχθεί ότι η επίτευξη ισορροπίας πυθμένα είναι πιο αργή στο πεδίο από ό,τι σε συνθήκες εργαστηρίου, όπου η χρήση λεπτόκοκκου ιζήματος μπορεί να προκαλέσει πρόσθετα προβλήματα κλίμακας (Gorrick et al., 2014). Ως εκ τούτου, η παρούσα εφαρμογή αντιστοιχεί σε συνολική διάρκεια 50 ημερών, η οποία θεωρείται επαρκής περίοδος για τη διερεύνηση της ικανότητας του μοντέλου να καταγράφει τις αλληλεπιδράσεις ρευστού-θαλάσσιου πυθμένα. Εφαρμόστηκαν ακανόνιστα κύματα στα βαθιά νερά με Hs=2,00 m και Tp=8,0 s.

Η Εικόνα 24 δείχνει ένα στιγμιότυπο της υπολογιζόμενης αριθμητικά στιγμιαίας ανύψωσης ελεύθερης επιφάνειας. Οι διεργασίες κοντά στην ακτή που μπορούν να εντοπιστούν σε αυτό το σχήμα είναι οι ρήχωση, περίθλαση στην προστατευμένη περιοχή καθώς και το wave run-up και run-down. Η θραύση του κύματος πάνω από τον κυματοθραύστη μπορεί να παρατηρηθεί στα X = 400m. Το αρχικό πεδίο κυματογενών ρευμάτων μετά από 1 ημέρα κυματικής δράσης, απεικονίζεται στην Εικόνα 25. Ένας σχηματισμός δύο στροβιλισμών μπορεί να παρατηρηθεί στην υπήνεμη πλευρά του κυματοθραύστη. Αυτός ο σχηματισμός δημιουργείται λόγω της χωρικής μεταβολής της μέσης στάθμης της θάλασσας μεταξύ εκτεθειμένης και προστατευμένης από τους κυματισμούς περιοχής, η οποία ωθεί τα φαινόμενα περίθλασης με επακόλουθη ώθηση των ρευμάτων προς το κάτω μέρος της κατασκευής. Παράλληλα, ασθενή ρεύματα επαναφοράς με ταχύτητα 0,2 m/s μπορούν να εντοπιστούν, μεταξύ των πλευρικών ορίων του μοντέλου και της κατασκευής, ενώ ταχύτητες προσανατολισμένες προς τα ανοιχτά, της τάξης των 0,75 m/s, ανιχνεύονται κοντά στην ακτή.

Η Εικόνα 25 δείχνει την αλλαγή του βυθού μετά από 10 ημέρες και τα σχετικά κυματογενή ρεύματα. Πίσω από το κυματοθραύστη, η ακτογραμμή εκτείνεται προς τη θάλασσα και μία αρχική μορφή - τόμπολο αρχίζει να σχηματίζεται. Η βαθυμετρία μετά από 50 ημέρες δράσης κυμάτων απεικονίζεται στο σχήμα της Εικόνα 27. Μπορεί να παρατηρηθεί ότι δεν υπάρχουν σημαντικές διαφορές στη γεωμετρία του βυθού της θάλασσας μεταξύ του διαστήματος 10 και 50 ημερών. Συνάγεται έτσι το συμπέρασμα ότι ο αρχικός ρυθμός μεταβολής ήταν αρχικά υψηλός και επιβραδύνθηκε καθώς πλησίαζε η μορφοδυναμική ισορροπία για τις συγκεκριμένες επικρατούσες αρχικές συνθήκες. Κοντά στο στάδιο ισορροπίας, σχετικά ασθενείς ταχύτητες περίπου 0,3 m/s χαρακτηρίζουν το επαγόμενο από το κύμα πεδίο ρευμάτων. Κατά τη διάρκεια αυτής της φάσης, τα κύματα αποσβένουν στη σκιά του κυματοθραύστη λόγω της παρουσίας του tombolo, με αποτέλεσμα ένα λιγότερο ενεργητικό πεδίο ρεύματος στην προστατευόμενη περιοχή. Συνεπώς, καθώς οι ταχύτητες είναι σχετικά ανίσχυρες σε αυτό το στάδιο, οι ροές των ιζημάτων είναι ασήμαντες και δεν υπάρχει

αξιοσημείωτη αλλαγή στη γεωμετρία του βυθού. Η συμφωνία μεταξύ των παρόντων αποτελεσμάτων και των αντίστοιχων δεδομένων της μελέτης του Deltares/Delft Hydraulics (1997) φαίνεται αρκετά ικανοποιητική, όσον αφορά την τελική ακτογραμμή και την παρατηρούμενη διάβρωση στις εκτεθειμένες περιοχές του πεδίου.

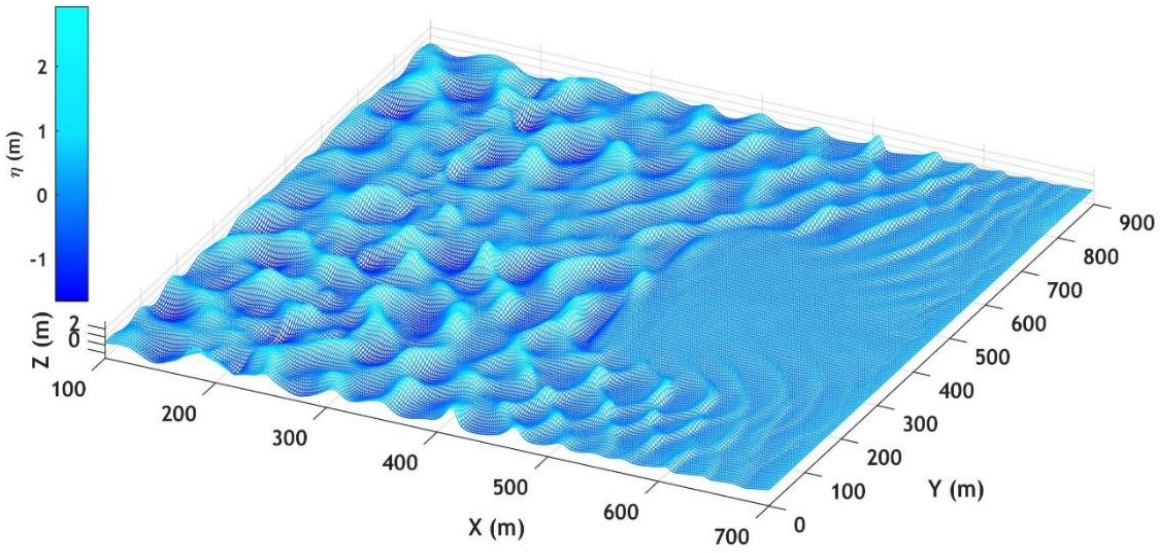

Εικόνα 24 Αριθμητικά αποτελέσματα της υπολογιζόμενης αριθμητικά στιγμιαίας ανύψωσης ελεύθερης επιφάνειας (Hs=2,00 m, Tp=8,0 s).

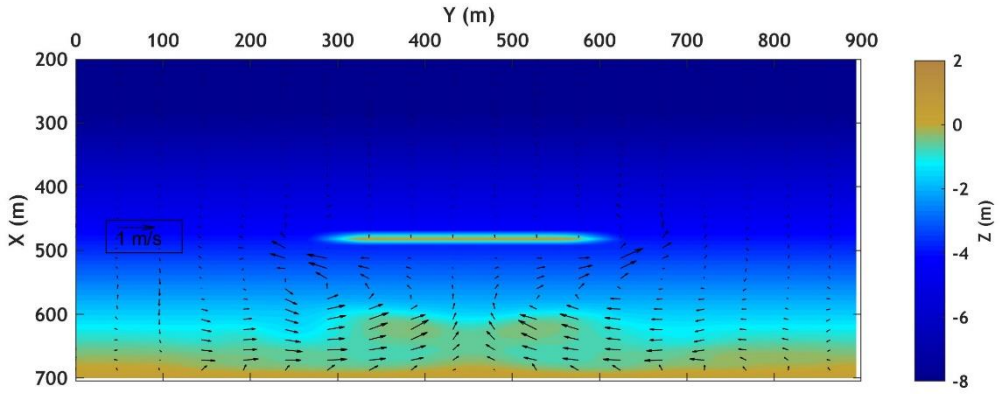

Εικόνα 25 Αριθμητικά αποτελέσματα κυματογενών παράκτιων ρευμάτων και εξέλιξη βαθυμετρίας μετά από 1 ημέρα κυματικής δράσης (Hs=2,00 m, Tp=8,0 s).

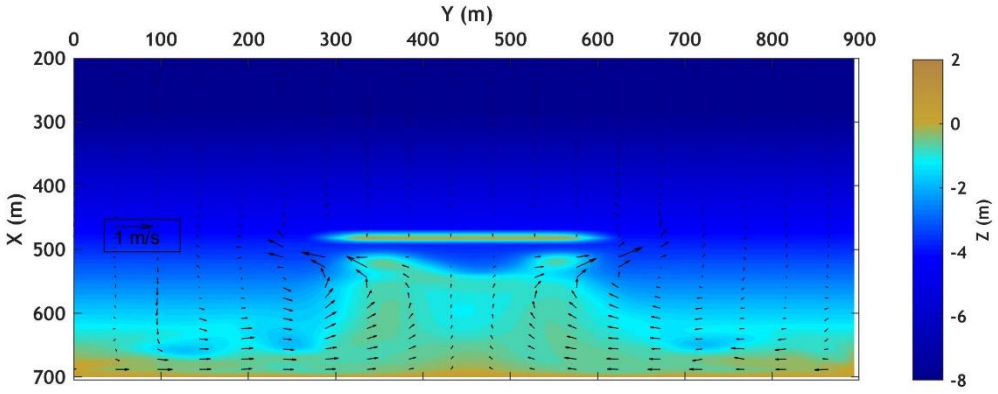

Εικόνα 26 Αριθμητικά αποτελέσματα κυματογενών παράκτιων ρευμάτων και εξέλιξη βαθυμετρίας μετά από 10 ημέρες κυματικής δράσης (Hs=2,00 m, Tp=8,0 s).

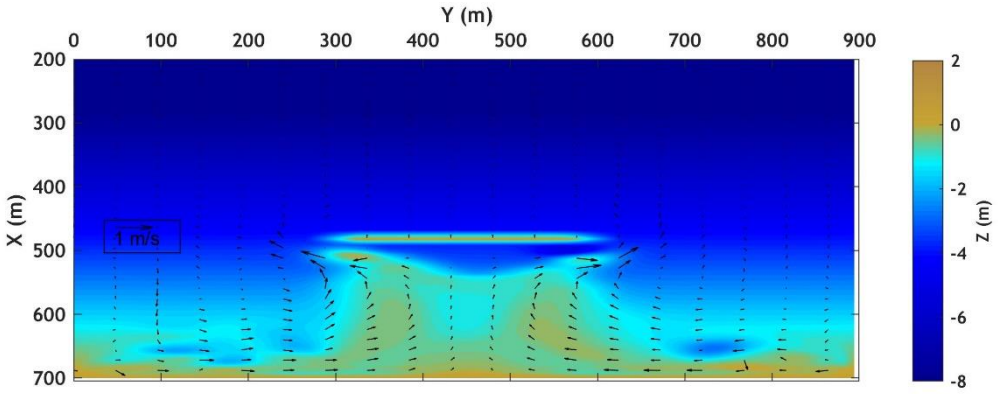

Εικόνα 27 Αριθμητικά αποτελέσματα κυματογενών παράκτιων ρευμάτων και εξέλιξη βαθυμετρίας μετά από 50 ημέρες κυματικής δράσης (Hs=2,00 m, Tp=8,0 s).

Το προτεινόμενο μοντέλο χρησιμοποιήθηκε και για τη διερεύνηση των υδροδυναμικών και μορφοδυναμικών προτύπων και μορφολογίας στην περιοχή ενός ύφαλου αποσπασμένου κυματοθραύστη. Αυτές οι κατασκευές μπορούν να οδηγήσουν σε μείωση της ενέργειας των κυμάτων μέσω της καθοδηγούμενης από τη μεταβολή βάθους θραύσης κυμάτων, και η απόκριση της ακτογραμμής στον ύφαλο κυματοθραύστη διέπεται από υδροδυναμικές διεργασίες όπως το wave setup και τα onshore mass flux (Ranasinghe et al., 2010). Προκειμένου να αξιολογηθεί η επίδραση των ύφαλων κυματοθραυστών στη μορφολογία της ακτής, η μελέτη των Cáceres et al. (2005) χρησιμοποιήθηκε ως σημείο αναφοράς. Το ύψος της στέψης του κυματοθραύστη ορίστηκε στα -0,5 m και η κατασκευή τοποθετήθηκε σε απόσταση 230 m από την ακτή. Η βαθυμετρική εξέλιξη υπολογίστηκε για διάρκεια 200 ωρών, ενώ χρησιμοποιήθηκε ένας συντελεστής μορφολογικής επιτάχυνσης (Morfac = 15) για τη μείωση του υπολογιστικού κόστους.

Η υπολογισμένη βαθυμετρία και το σχετικό πεδίο ρευμάτων μετά από 200 ώρες κυματικής δράσης παρουσιάζονται στο Σχήμα της Εικόνα 28. Τα αποτελέσματα του μοντέλου συμφωνούν καλά με τα ευρήματα των Cáceres et al. (2005), καθώς το ολοκληρωμένο μοντέλο πέτυχε να αναπαράγει όλα τα μορφολογικά και υδροδυναμικά μοτίβα πίσω από τον κυματοθραύστη και μέχρι την ακτή. Για άλλη μια φορά μπορούν να εντοπιστούν δύο συμμετρικές δίνες εκτός της προστατευμένης περιοχής, ενώ μέσα από τα κενά επικρατούν ισχυρά αποκλίνοντα διαβρωτικά ρεύματα, με ταχύτητα 0,8 m/s. Η συνολική εξέλιξη του πυθμένα αποκαλύπτει τη διάβρωση κοντά στη δομή, ενώ η ακτογραμμή αυξάνεται και ο σχηματισμός προεξέχοντος μπορεί να παρατηρηθεί.

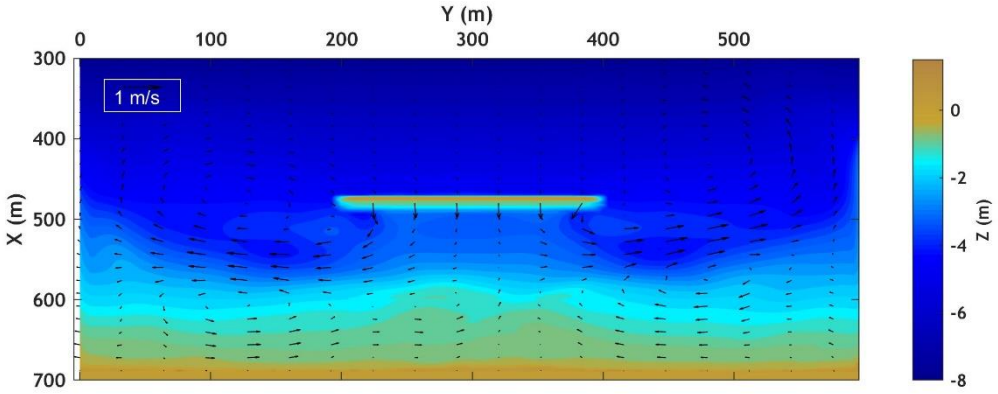

Εικόνα 28 Αριθμητικά αποτελέσματα κυματογενών παράκτιων ρευμάτων και εξέλιξη βαθυμετρίας μετά από 200 ώρες κυματικής δράσης.

Βασικά συμπεράσματα

Η διάβρωση των ακτών αποτελεί ένα παγκόσμιο πρόβλημα, που προκαλείται από φυσικές διεργασίες αλλά και από ανθρωπογενείς δραστηριότητες. Η επιλογή του κατάλληλου τύπου προστασίας για τον έλεγχο της διάβρωσης των ακτών είναι το αντικείμενο μιας ενεργού συζήτησης σε πολλές χώρες του κόσμου, καθώς μία ευρεία γκάμα από τεχνικές ήπιας κλίμακας, καθώς και μεγάλων έργων πολιτικού μηχανικού μπορούν να επιστρατευτούν για την αντιμετώπιση του φαινομένου. Η επιλογή, σύλληψη και διαστασιολόγηση αυτών των έργων απαιτεί τη χρήση προβλέψεων μορφοδυναμικής υψηλού υπολογιστικού κόστους, για την εκτίμηση της επίδρασης κάθε εναλλακτικής λύσης στο παράκτιο σύστημα. Τα τελευταία χρόνια, η επιστημονική έρευνα έχει στραφεί στην εφαρμογή προηγμένων αριθμητικών τεχνικών για τη διερεύνηση της απόδοσης και της αποτελεσματικότητας αυτών των κατασκευών (ήπιων ή μη), όσον αφορά την ικανότητά τους να ελαχιστοποιούν τις τάσεις διάβρωσης. Ως εκ τούτου, η παρούσα διδακτορική διατριβή μπορεί να θεωρηθεί ως μέρος αυτού του ερευνητικού πεδίου. **Αυτή η μελέτη επιδιώκει να βοηθήσει στην καλύτερη κατανόηση της κίνησης των μη συνεκτικών ιζημάτων υπό τη δράση κυματορεύματος. Βασικός στόχος είναι η ανάπτυξη προηγμένων τεχνικών αριθμητικής μοντελοποίησης, προκειμένου να προσομοιωθούν με ακρίβεια μορφοδυναμικοί μηχανισμοί σε ένα μεγάλο εύρος από ακανόνιστες βαθυμετρίες, λαμβάνοντας υπόψη φαινόμενα αστάθειας κυμάτων, καθώς και άλλες φυσικές διεργασίες μικρής κλίμακας στην εσωτερική ζώνη θραύσης και swash.**

Ως μία διαδικασία βιβλιογραφικής ανασκόπησης, πραγματοποιήθηκε η ανάλυση των υπαρχόντων αριθμητικών συσκευών και εργαλείων καθώς ως προς τις δυνατότητες τους να προβλέπουν φαινόμενα μεταφοράς ιζημάτων σε περιοχές μελέτης με ιδιαίτερο μορφολογικό ενδιαφέρον (Κεφάλαιο 1). Αρκετές μεθοδολογίες και αριθμητικές προσεγγίσεις εφαρμόστηκαν για τη διερεύνηση φυσικών διεργασιών κοντά στην ακτή, όπως η διάδοση κυμάτων, η υδροδυναμική κυκλοφορία και μορφοδυναμική. Η τρωτότητα των ακτών που προκαλείται από κύματα καταιγίδας αναλύθηκε για την περιοχή μελέτης του Ρεθύμνου στην Ελλάδα. Για την περιοχή αυτή αξιολογήθηκαν διάφορες τεχνικές λύσεις προστασίας (διαμορφώσεις παράκτιων έργων), μέσω προηγμένης αριθμητικής μοντελοποίησης, ως προς την ικανότητά τους να απομειώνουν τις καταστροφικές συνέπειες ακραίων φαινομένων καταιγίδας. Η διάδοση των κυμάτων και τα υδρομορφοδυναμικά μοτίβα εκτιμήθηκαν μέσω δύο διακριτών αριθμητικών μοντέλων: MIKE 21 και XBeach, ενώ έγινε σύγκριση μεταξύ των παραμέτρων εξόδου τους. Η εφαρμογή των μοντέλων αυτών είχε ως στόχο την αξιολόγηση της ικανότητάς αυτών να

προσομοιώνουν με ακρίβεια φυσικές διεργασίες κοντά στην ακτή, υπό ακραία φαινόμενα καταιγίδας. Αποδείχθηκε ότι η συνεργατική αριθμητική μοντελοποίηση MIKE 21 και XBeach μπορεί να εφαρμοστεί σε μεγάλη κλίμακα (τομέας συνολικής επιφάνειας 14 km^2) για την αξιόπιστη προσομοίωση των υδρο-μορφοδυναμικών συνθηκών υπό ακραίες συνθήκες καταιγίδας. Τα αριθμητικά υπολογισμένα πεδία μεταφοράς ιζήματος και ρευμάτων, έδειξαν παρόμοια χαρακτηριστικά (κύρια κατεύθυνση και ένταση ταχυτήτων και φορτίων), η οποία επιβεβαιώνει την εγκυρότητα της αριθμητικής τεχνικής.

Η επιλεγμένη προσέγγιση παρουσίασε και ορισμένους περιορισμούς, που σχετίζονται με την οιονεί γραμμική φύση των αριθμητικών μοντέλων MIKE21 και XB, στα οποία η υδροδυναμική κυκλοφορία υπολογίζεται μέσω από μία τεχνικής ‘μέσων κυματισμών’(wave-averaged approach). Πιο συγκεκριμένα, το XBeach σε λειτουργία surf beat βασίζεται στην επίλυση του μέσου όρου βραχέων κυμάτων και ομάδας κυματισμών, η οποία προσθέτει σημαντικές δυσκολίες στην πρόβλεψη μη γραμμικών αλληλεπιδράσεων κυμάτων-ρευμάτων, καθώς και ενδο-κυματικών επιδράσεων στην υδροδυναμική και μορφολογία. Επιπλέον, τα φαινόμενα περίθλασης και διασποράς δεν μπορούν να προσομοιωθούν επαρκώς από το μοντέλο XB σε λειτουργία surfbeat.

Επιπλέον, το μοντέλο MIKE21 λαμβάνει υπόψη πιο σύνθετες φυσικές διεργασίες, όπως η θραύση στα ανοιχτά (white capping) και η μη γραμμική μεταφορά ενέργειας μεταξύ των διαφορετικών συνιστωσών ενός φάσματος κύματος. Ωστόσο, όπως και στην περίπτωση του μοντέλου XB, αυτή η συσκευή παρέχει μια προσέγγιση βασισμένη σε ‘μέσο΄ κύματισμό (wave-averaged approach) για την αξιολόγηση των υδρο-μορφοδυναμικών χαρακτηριστικών, καθώς το υδροδυναμικό πεδίο καθοδηγείται από τις τάσεις ακτινοβολίας που υπολογίζονται μέσω του μοντέλου φασματικών κυμάτων. Αυτή η μέθοδος θέτει σημαντικούς περιορισμούς στην ακριβή πρόβλεψη φαινομένων κυμάτων κοντά στην ακτή, όπου λαμβάνουν χώρα έντονα μη γραμμικά φαινόμενα (ανάκλαση, ‘τρισδιαστοσιοποίηση’ κύματος, κυματική διασπορά).

Επιπρόσθετα, η εργαστηριακή και πειραματική διερεύνηση υδρο-μορφολογικών συνθηκών υπό πολυσχιδείς βαθυμετρίες χωρίς την παρουσία έργων με νέα συνδυαστικά μοντέλα, παρείχε χρήσιμα συμπεράσματα ως προς τους μηχανισμούς βαθυμετρικής εξέλιξης και μετάβασης μεταξύ των επιμέρους σταδίων, από απορροφητική σε ενδιάμεση και ανακλαστική μορφή ακτής (κεφάλαιο 3). Τα λεπτομερή μορφοδυναμικά πειραματικά δεδομένα που συλλέχθηκαν από τους Castelle et al., (2010) και Michallet et al., (2013) χρησίμευσαν εδώ ως σημαντικό σημείο αναφοράς για τις αριθμητικές επιλύσεις. Προκειμένου να επιτευχθεί μία

καλή κατανόηση αυτών των φυσικών διεργασιών, χρησιμοποιήθηκαν δύο διακριτές προσεγγίσεις για την αξιολόγηση των μηχανισμών μορφοδυναμικής και ιδιαίτερα της επίδρασης των μεταβολών κυματικού κλίματος στη μορφολογία ακτής. Η πρώτη προσέγγιση, η οποία χρησιμοποιήθηκε εδώ, βασίζεται σε αρχές ελαχιστοποίησης για την αξιολόγηση της μορφολογίας πυθμένα. Η θεμελιώδης υπόθεση αυτής της μεθόδου είναι το γεγονός ότι ο ιζηματογενής πυθμένας προσαρμόζεται στην υδροδυναμική ροή με κάποιο είδος βέλτιστης μεταφοράς άμμου προκειμένου να ελαχιστοποιηθεί μία έκφραση ενέργειας. Η βέλτιστη μεταφορά θεωρείται εδώ ως η ελάχιστη αλλαγή στο σχήμα της βαθυμετρίας. Αυτή η αριθμητική μέθοδος παρείχε αξιόπιστα αποτελέσματα, σχετικά με τον προσδιορισμό των παράκτιων ζωνών, στις οποίες επικρατεί απόθεση ή διάβρωση. Ωστόσο, ο περιορισμός αυτού του μοντέλου που έγκειται στην αναπαραγωγή ενός ρεαλιστικού κυματικού κλίματος (εξετάστηκαν μόνο κάθετα προς την ακτή κύματα), δυσχεραίνει την προσομοίωση των υδροδυναμικών μοτίβων που παρατηρήθηκαν κατά την πειραματική διαδικασία. Όσον αφορά την αριθμητικά υπολογιζόμενη τελική γεωμετρία πυθμένα (alongshore averaged profiles), επιτεύχθηκε μία σχετικά καλή συμφωνία μεταξύ των αριθμητικών κα πειραματικών παραμέτρων. Αυτό μπορεί να οδηγήσει στο συμπέρασμα ότι αυτή η συγκεκριμένη αριθμητική τεχνική που βασίζεται σε αρχές βελτιστοποίησης μπορεί να παρέχει ακριβής προβλέψεις για μονοδιάστατες εφαρμογές ακτομηχανικής 1DH.

Επιπλέον, στο κεφάλαιο 3, παρουσιάστηκε ένα επιπλέον σύνθετο αριθμητικό μοντέλο για τη διερεύνηση υδροδυναμικών και μορφοδυναμικών φαινομένων 2DH, με βάση τις μη γραμμικές εξισώσεις ρηχών υδάτων (NSWE) ενώ αναπτύχθηκε στα πλαίσια της παρούσας διατριβής ένα νέο μοντέλο μεταφοράς ιζήματος βασιζόμενο σε μη-ασταθής σχέσεις για την αριθμητική επίλυση των ιζηματογενών φορτίων. Αυτή η τεχνική παρείχε σημαντικές πληροφορίες σχετικά με την εμφάνιση ακανόνιστων μοτίβων κυματογενών ρευμάτων (ρεύματα παράλληλα προς την ακτή ή ρεύματα επαναφοράς). Συνολικά, επιτεύχθηκε μια καλή συμφωνία μεταξύ των πειραματικών και των αριθμητικών αποτελεσμάτων, καθώς η βαθυμετρική εξέλιξη ακολούθησε με ακρίβεια τις μεταβολές κυματικού κλίματος.

Λαμβάνοντας υπόψη όλα τα παραπάνω, και με βάση την ενδελεχή καταγραφή αναφορικά με τις δυνατότητες και τους περιορισμούς των υπαρχουσών αριθμητικών εργαλείων, η παρούσα έρευνα προχώρησε ένα βήμα παραπέρα με την ανάπτυξη ενός νέου και προηγμένου συνδυαστικού αριθμητικού μοντέλου για πρακτικές και επιστημονικές εφαρμογές (κεφάλαιο 4). Συγκεκριμένα αναπτύχθηκε ένα μοντέλο μεταφοράς ιζήματος, βασιζόμενο σε μια 3D προσέγγιση για την προσομοίωση της μεταφοράς ιζήματος σε αιώρηση, ενώ αυτό

συνδυάστηκε με ένα πλήρως μη γραμμικό μοντέλο Boussinesq για την αξιολόγηση των δράσεων κύματος-ρεύματος στην παράκτια ζώνη. Η χρήση αυτού του μοντέλου επίλυσης φάσης έδωσε μια καλή περιγραφή όλων των φυσικών διεργασιών μετασχηματισμού κυμάτων και υδροδυναμικής κυκλοφορίας στα ρηχά νερά: ρήχωση, θραύση κύματος, wave run-up and run-down , δισδιάστατα ρεύματα που προκαλούνται από κύματα σε πολύπλοκες βαθυμετρίες, φαινόμενα διασπορά, λοξότητα και ασυμμετρία, αλληλεπίδραση κύματος ρεύματος. Αυτά τα χαρακτηριστικά αποδείχθηκαν ιδιαίτερα σημαντικά για την ακριβή εκτίμηση της μεταφοράς ιζήματος και των μορφολογικών διεργασιών. Ως εκ τούτου, το πλήρως μη γραμμικό μοντέλο Boussinesq-FUNWAVE-TVD συσχετίστηκε άμεσα με ένα ημί- τρισδιάστατο μοντέλο μεταφοράς ιζήματος και μορφολογίας, το οποίο αναπτύχθηκε από τον συγγραφέα της παρούσας διατριβής. Αυτή η συσκευή λαμβάνει υπόψη τις μη γραμμικές διεργασίες μεταφοράς ιζημάτων, με την παράλληλη ενσωμάτωση των ασταθών κυματικών επιδράσεων στο φορτίου πυθμένα. Ιδιαίτερη προσοχή δόθηκε στο ρόλο της δυναμικής μεταφοράς ιζημάτων κατά μήκος της ζώνης αναρρίχησής (swash), ενώ χρησιμοποιήθηκαν προηγμένες αριθμητικές τεχνικές για τη μοντελοποίηση των τρισδιάστατων μοτίβων φορτίου αιώρησης. Το συζευγμένο μη γραμμικό μοντέλο επικυρώθηκε διεξοδικά σε σχέση με εργαστηριακά δεδομένα και άλλες αριθμητικές έρευνες. Σε αυτό το πλαίσιο, αξιοποιήθηκαν 3D και 2D εργαστηριακές πειραματικές έρευνες για να επιβεβαιωθούν οι αριθμητικές προβλέψεις. Η επιβεβαίωση της αξιοπιστίας του αριθμητικού μοντέλου έναντι των πειραματικών μετρήσεων αποκάλυψε ότι ο κύριος σκοπός της διατριβής εκπληρώθηκε ικανοποιητικά.

Παράλληλα, διερευνήθηκαν μία σειρά από επιμέρους παράκτιες φυσικές διεργασίες όπως η μορφοδυναμική στη ζώνη αναρρίχησης, καθώς επίσης, προβλέφθηκε με ακρίβεια ο σχηματισμός ράβδων άμμου (sandbars) που προκαλούνται από τη θραύση κύματος κοντά στην ακτή. Παρόλα αυτά απαιτούνται περαιτέρω έρευνες για : 1) τη μοντελοποίηση της μορφολογίας αμμοκυματίων (ripples) χρησιμοποιώντας λεπτότερα πλέγματα και αλληλουχίες μεταβαλλόμενων κυματισμών, 2) την προσομοίωση φαινομένων απόθεσης (accretion) κοντά στην ακτή και στη ζώνη αναρρίχησης , η οποία απαιτεί την αριθμητική προσομοίωση των υπόγειων νερών σε βαθύτερα στρώματα. Επιπλέον, προκειμένου να επεκταθεί το πεδίο εφαρμογής του συζευγμένου μη γραμμικού μοντέλου , ο ρόλος της μεταφοράς αιολικού ιζήματος θα πρέπει να ληφθεί υπόψη, ιδιαίτερα σε περιπτώσεις διάβρωσης αμμόλοφων .

Λαμβάνοντας υπόψη όλα τα παραπάνω, το παρουσιαζόμενο έργο μπορεί να αποτελέσει πολύτιμο υλικό για μηχανικούς και επιστήμονες που επιθυμούν να αποκτήσουν ακριβείς

προβλέψεις εξέλιξης αμμώδη πυθμένα σε πολύπλοκες βαθυμετρίες και υπό την παρουσία ενός μεγάλου εύρους τύπων κατασκευών παράκτιας προστασίας, τόσο σε πειραματικό όσο και σε πραγματικό πεδίο.

Στοιχεία καινοτομίας

Η παρούσα διδακτορική εργασία επιδιώκει να συνδράμει στην περαιτέρω εξέλιξη των μέσων κατανόησης και διερεύνησης παράκτιων φυσικών διεργασιών μέσω της εφαρμογής προηγμένης αριθμητικής μοντελοποίησης. Βασικός στόχος είναι η παραγωγή αξιόπιστων προβλέψεων βαθυμετρικής εξέλιξης του αμμώδους πυθμένα, αναπτύσσοντας νέες τεχικές προσομοίωσης της δυναμικής μεταφοράς ιζημάτων και δίνοντας ιδιαίτερη έμφαση στη μη συνεκτική κίνηση ιζημάτων υπό δράσεις κυματορεύματος. Στο συγκεκριμένο ερευνητικό έργο εντοπίζονται μία σειρά από καινοτόμα στοιχεία:

- Μια εκτενής ανάλυση υφιστάμενων υπολογιστικών εργαλείων παρουσιάζεται στα επόμενα κεφάλαια, της οποίας γενικός στόχος είναι η αξιολόγηση των αρχών προσομοίωσης που βασίζονται σε εξισώσεις μέσου βάθους και οι οποίες χρησιμοποιούνται ευρέως σε προβλήματα μορφολογίας ακτών. Για αυτό το σκοπό, πραγματοποιήθηκε η αξιολόγηση των διαθέσιμων συσκευών/μοντέλων, σε σχέση με την ικανότητά τους να παρέχουν ακριβείς και αξιόπιστες προβλέψεις βαθυμετρικής εξέλιξης. Δύο διαφορετικά υπολογιστικά εργαλεία χρησιμοποιήθηκαν για την προσομοίωση των φυσικών διαδικασιών κοντά στην ακτή, όπως η διάδοση κυμάτων, η υδροδυναμική κυκλοφορία, η αλληλεπίδραση κύματος-ρεύματος, η μεταφορά ιζημάτων και η μορφολογία. Πιο συγκεκριμένα, σε επιλεγμένες περιοχές μελέτης, διερευνήθηκαν υδρο-μορφοδυναμικά μοτίβα μέσω του λογισμικού MIKE 21 και XBeach, ενώ οι μορφολογικές εξελίξεις στη γειτνίαση παράλληλων ύφαλων κυματοθραυστών προσομοιώθηκαν μέσω μιας αριθμητικής φόρμουλας βασισμένης σε αρχές ελαχιστοποίησης. Μέσα από την παρούσα ερευνητική διαδικασία, εξήχθησαν πολύτιμα συμπεράσματα σχετικά με τους περιορισμούς και τα πλεονεκτήματα των υπαρχουσών τεχνικών μοντελοποίησης μέσου βάθους.

- Επιπλέον στα πλαίσια της παρούσας διατριβής, επιτεύχθηκε η δημιουργία ενός καινοτόμου αριθμητικού εργαλείου για εφαρμογές ακτομηχανικής. Πιο συγκεκριμένα, ένα ημί--τρισδιάστατο μοντέλο μεταφοράς ιζήματος και μορφολογίας που λαμβάνει υπόψη τα ασταθή και μη γραμμικά υδροδυναμικά φαινόμενα, αναπτύχθηκε από το συγγραφέα της εργασίας. Ιδιαίτερη προσοχή δόθηκε στον ρόλο της δυναμικής μεταφοράς ιζημάτων κατά μήκος της ζώνης διαβροχής (swash) και της εσωτερικής ζώνης θραύσης (surf), ενσωματώνοντάς τα στοιχεία αυτά στην αριθμητική προσομοίωση. Παράλληλα, χρησιμοποιήθηκαν προηγμένες τεχνικές για την

προσομοίωση τρισδιάστατων μοτίβων αιωρούμενων ροών ιζήματος και την ανάλυση των μη γραμμικών και ασταθών επιδράσεων κυμάτων στον ρυθμό μεταφοράς ιζήματος μέσω φορτίου πυθμένα.

- Το νέο αυτό μοντέλο μεταφοράς ιζημάτων συζεύχτηκε με ένα πλήρως μη γραμμικό κυματικό μοντέλο τύπου Boussinesq (FUNWAVE-TVD), με σκοπό την αξιόπιστη προσομοίωση των υδροδυναμικών φαινομένων και την παροχή ακριβών προβλέψεων εξέλιξης της γεωμετρίας αμμώδους πυθμένα, για μία ευρεία γκάμα χρονικών και χωρικών κλίμακων ενδιαφέροντος. Επομένως, η καινοτομία του παρόντος έργου συνίσταται στην ελαχιστοποίηση της αβεβαιότητας σχετικά με τα αποτελέσματα υδρο/μορφοδυναμικών προσομοιώσεων, η οποία συχνά συναντάται στις παραμέτρους εξόδου των υφιστάμενων υπολογιστικών εργαλείων.

- Επιπρόσθετα, ο ρόλος των δομών παράκτιας προστασίας (πρόβολοι/Groynes, έξαλοι ή ύφαλοι κυματοθραύστες) αξιολογήθηκε ενδελεχώς ως προς την προστασία που αυτές παρέχουν στις υπο-διάβρωση αμμώδης ακτές, εφαρμόζοντας το νέο συζευγμένο υπολογιστικό μοντέλο. Μέσω αυτής της διαδικασίας επιτεύχθηκε ένας διττός στόχος που αφορά στην αξιολόγηση του μοντέλου σε σχέση με την προσομοίωση των κυματικών και μορφοδυναμικών χαρακτηριστικών στη γειτνίαση παράκτιων έργων, ενώ παράλληλα διερευνήθηκε πλήρως και ο ρόλος των ίδιων των κατασκευών σχετικά με την ικανότητα αυτών να εμποδίζουν τα φαινόμενα διάβρωσης. Ιδιαίτερη έμφαση δόθηκε στη μελέτη της μεταβολής κυματικού πεδίου και μορφοδυναμικών χαρακτηριστικών, όπως αυτή παρατηρείται στις περιοχές ανάντη και κατάντη των παράκτιων έργων προστασίας. Βασική επιδίωξη του ερευνητή ήταν να διατηρηθεί η υπολογιστική πολυπλοκότητα σε λογικά επίπεδα μέσω της χρήσης τεχνικών μορφολογικής επιτάχυνσης και την εκμετάλλευση υπολογιστικών τεχνικών παράλληλων σχημάτων. Ως εκ τούτου, η χρήση του ολοκληρωμένου αριθμητικού μοντέλο μπορεί να καταστεί δυνατή για ένα ευρύ φάσμα πρακτικών εφαρμογών ακτομηχανικής (αναπλήρωση ακτών, κατασκευή προβολών και κυματοθραυστών, Βυθοκορήσεις…), αποφεύγοντάς έτσι τη δημιουργία ενός ακόμη ερευνητικού εργαλείου που εφαρμόζεται αποκλειστικά σε προβλήματα εργαστηριακού τύπου.

- Μια ακόμα πτυχή καινοτομίας της διατριβής συνίσταται στο γεγονός ότι οι αλληλεπιδράσεις παράκτιων ρευμάτων και θαλάσσιου πυθμένα μελετήθηκαν διεξοδικά για κυματικές ακολουθίες διάβρωσης και απόθεσης (beach down-state and

up-state transitions). Για το σκοπό αυτό αναπτύχθηκαν και χρησιμοποιήθηκαν επιπλέον υπολογιστικά μοντέλα βασιζόμενα σε αρχές ελαχιστοποίησης αλλά και σε παραδοσιακές φόρμουλες μεταφοράς ιζήματος, αποκαλύπτοντας σημαντικές πτυχές εξέλιξης μορφολογίας ακτής υπό την επίδραση διαβρωτικών και μη κυματισμών, για τα στάδια μετάβασης μεταξύ ενός ανακλαστικού τύπου ακτής και μίας ακτής ήπιας κλίσης (Dissipative) . Για τις ανάγκες της συγκεκριμένης έρευνας, οι πειραματικές μετρήσεις ενός τρισδιάστατου φυσικού μοντέλο, χρησιμοποιήθηκαν ως σημείο αναφοράς προκειμένου να επιβεβαιωθούν οι δύο διακριτές τεχνικές προσομοίωσης που εφαρμόστηκαν για τις προβλέψεις των αλληλεπιδράσεων κύματος-αμμώδους πυθμένα. Χρήσιμα συμπεράσματα εξήχθησαν μέσα από τα αριθμητικά και πειραματικά αποτελέσματα που απέδειξαν πως οποιαδήποτε προδιαγεγραμμένη αλλαγή στις συνθήκες κύματος αύξησε δραστικά τον ρυθμό μεταβολής μορφολογίας

Βιβλιογραφικές αναφορές

Afentoulis, V., Eleftheria, K., Eleni, S., Evangelos, M., Archontia, L., Christos, M., & Vasiliki, T. (2017). Coastal Processes Assessment Under Extreme Storm Events Using Numerical Modelling Approaches. Environmental Processes, 4(3), 731-747.

Almeida, L. P., Vousdoukas, M. V., Ferreira, Ó., Rodrigues, B. A., & Matias, A. (2012). Thresholds for storm impacts on an exposed sandy coastal area in southern Portugal. Geomorphology, 143, 3-12.

Alsina, J. M., Cáceres, I., Brocchini, M., & Baldock, T. E. (2012). An experimental study on sediment transport and bed evolution under different swash zone morphological conditions. Coastal Engineering, 68. https://doi.org/10.1016/j.coastaleng.2012.04.008

Badiei, P., Kamphuis, J. W., & Hamilton, D. G. (1994). Physical experiments on the effects of groins on shore morphology. In Coastal Engineering 1994 (pp. 1782-1796).

Bird, E. C. (1996). Coastal erosion and rising sea-level. In Sea-Level Rise and Coastal Subsidence (pp. 87-103). Springe Blumberg, A. F. "A primer for ECOMSED." Mahwah NJ: Hydro Qual Inc (2002): 1-194. r, Dordrecht.

Bouharguane, A., & Mohammadi, B. (2013). Minimisation principles for the evolution of a soft sea bed interacting with a shallow sea. International Journal of Computational Fluid Dynamics, 26(3), 163-172.

Bouvier, C., Castelle, B., & Balouin, Y. (2019). Modeling the impact of the implementation of a submerged structure on surf zone sandbar dynamics. Journal of Marine Science and Engineering, 7(4). https://doi.org/10.3390/jmse7040117

Castelle, B., & Harley, M. (2020). Extreme events: impact and recovery. In Sandy Beach Morphodynamics (pp. 533-556).

Castelle, B., Marieu, V., Bujan, S., Splinter, K. D., Robinet, A., Sénéchal, N., & Ferreira, S. (2015). Impact of the winter 2013–2014 series of severe Western Europe storms on a double-barred sandy coast: Beach and dune erosion and megacusp embayments. Geomorphology, 238, 135-148.

de Alegria-Arzaburu, Amaia Ruiz, Jon J. Williams, and Gerhard Masselink. "Application of XBeach to model storm response on a macrotidal gravel barrier." Coastal Engineering Proceedings 32 (2011): 39-39.

Deigaard, R., Justesen, P., & Fredsøe, J. (1991). Modelling of undertow by a one-equation turbulence model. Coastal Engineering, 15(5-6), 431-458.

Dette, H. H., Larson, M., Murphy, J., Newe, J., Peters, K., Reniers, A., & Steetzel, H. (2002). Application of prototype flume tests for beach nourishment assessment. Coastal Engineering, 47(2). https://doi.org/10.1016/S0378-3839(02)00124-2

DHI, J. (2015). Mike 21 2d modelling of coast and sea. URL http://www. mikepoweredbydhi. com/products/mike-21.

Do, J. D., Jin, J. Y., Hyun, S. K., Jeong, W. M., & Chang, Y. S. (2020). Numerical investigation of the effect of wave diffraction on beach erosion/accretion at the Gangneung Harbor, Korea. Journal of Hydro-Environment Research, 29. https://doi.org/10.1016/j.jher.2019.11.003

Douglas Shields, F., Knight, S. S., Morin, N., & Blank, J. (2003). Response of fishes and aquatic habitats to sand-bed stream restoration using large woody debris. Hydrobiologia, 494(1), 251-257.

Guimarães, P. V., Farina, L., & Toldo Jr, E. E. (2014). Analysis of extreme wave events on the southern coast of Brazil. Natural Hazards and Earth System Sciences, 14(12), 3195-3205.

Hénocque, Y., & Coccossis, H. (2001). White paper coastal zone management in the Mediterranean.

Hieu, P. D., Phan, V. N., Nguyen, V. T., Nguyen, T. V., & Tanaka, H. (2020). Numerical study of nearshore hydrodynamics and morphology changes behind offshore breakwaters under actions of waves using a sediment transport model coupled with the SWASH model. Coastal Engineering Journal, 62(4), 553-565.

Karambas, T. v., & Samaras, A. G. (2017). An integrated numerical model for the design of coastal protection structures. Journal of Marine Science and Engineering, 5(4). https://doi.org/10.3390/jmse5040050

Kennedy, A. B., Kirby, J. T., Chen, Q., & Dalrymple, R. A. (2001). Boussinesq-type equations with improved nonlinear performance. Wave Motion, 33(3). https://doi.org/10.1016/S0165-2125(00)00071-8

Kragiopoulou, E. V., Skarlatou, S., Lykou, A., Makropoulos, C., & Tsoukala, V. K. (2016). Assessing coastal zone response under extreme storm events for flood risk management. The case study of Rethymno, Greece. In 13th International conference on protection and restoration of the environment Mykonos Island, Greece.

Li, F., et al. "Probabilistic modelling of extreme storms along the Dutch coast." Coastal Engineering 86 (2014): 1-13.

Lichter, M., Vafeidis, A. T., Nicholls, R. J., & Kaiser, G. (2011). Exploring data-related uncertainties in analyses of land area and population in the “Low-Elevation Coastal Zone”(LECZ). Journal of Coastal Research, 27(4), 757-768.

Lončar, G., Bekić, D., Babić, M., Grbić, N., & Pranjić, V. (2016). A morphodynamic stability analysis of gravel beach cross-section by 1D numerical model. Građevinar, 68(02.), 113-124.

Luijendijk, A., Hagenaars, G., Ranasinghe, R., Baart, F., Donchyts, G., & Aarninkhof, S. (2018). The state of the world’s beaches. Scientific reports, 8(1), 1-11.

Madsen, P. A., Sørensen, O. R., & Schäffer, H. A. (1997). Surf zone dynamics simulated by a Boussinesq type model. Part I. Model description and cross-shore motion of regular waves. Coastal Engineering, 32(4). https://doi.org/10.1016/S0378-3839(97)00028-8

Makropoulos, C., Tsoukala, V. K., Lykou, A., Chondros, M., Manojlovic, N., & Vojinovic, Z. (2014, March). Extreme and rare events in coastal regions due to climate change—a case study application in Rethymno. In Int. Conf. ADAPTto CLIMATE (pp. 27-28).

Makropoulos, C., Tsoukala, V., Belibassakis, K. A., Lykou, A., Chondros, M., Gourgoura, P., & Nikolopoulos, D. (2015). Managing flood risk in coastal cities through an integrated modelling framework supporting stakeholders'involvement: the case of rethymno, Crete. 36th IAHR World Congrees.

Marche, F., & Bonneton, P. (2007). A simple and efficient well-balanced model for 2DH bore propagation and run-up over a sloping beach. In Coastal Engineering 2006: (In 5 Volumes) (pp. 998-1010).

Marche, F., Bonneton, P., Fabrie, P., & Seguin, N. (2007). Evaluation of well-balanced bore-capturing schemes for 2D wetting and drying processes. International Journal for Numerical Methods in Fluids, 53(5), 867-894.

McGranahan, G., Balk, D., & Anderson, B. (2007). The rising tide: assessing the risks of climate change and human settlements in low elevation coastal zones. Environment and urbanization, 19(1), 17-37.

Michallet, H., Castelle, B., Barthélemy, E., Berni, C., & Bonneton, P. (2013). Physical modeling of three-dimensional intermediate beach morphodynamics. Journal of Geophysical Research: Earth Surface, 118(2), 1045-1059.

Michele C, Salvadori G, Passoni G, Vezzoli R (2007) A multivariate model of sea storms using copulas. Coast Eng 54(10):734–751

Mohammadi, B., & Bouchette, F. (2014). Extreme scenarios for the evolution of a soft bed interacting with a fluid using the Value at Risk of the bed characteristics. Computers & Fluids, 89, 78-87.

Mori, N., Yasuda, T., Arikawa, T., Kataoka, T., Nakajo, S., Suzuki, K., ... & Webb, A. (2019). 2018 Typhoon Jebi post-event survey of coastal damage in the Kansai region, Japan. Coastal Engineering Journal, 61(3), 278-294.

Nicholls, R. J., Wong, P. P., Burkett, V., Codignotto, J., Hay, J., McLean, R., ... & Saito, Y. (2007). Coastal systems and low-lying areas.

Nicholson, J., et al. "Intercomparison of coastal area morphodynamic models." Coastal Engineering 31.1-4 (1997): 97-123.

Nielsen, P. (1992). Coastal bottom boundary layers and sediment transport (Vol. 4). World scientific.

Plomaritis, T. A., Ferreira, Ó., & Costas, S. (2018). Regional assessment of storm related overwash and breaching hazards on coastal barriers. Coastal Engineering, 134, 124-133.

Pourzangbar, A., & Brocchini, M. (2022). A new process-based, wave-resolving, 2DH circulation model for the evolution of natural sand bars: The role of nearbed dynamics and suspended sediment transport. Coastal Engineering, 177, 104192.

Pranzini, E., Wetzel, L., & Williams, A. T. (2015). Aspects of coastal erosion and protection in Europe. Journal of coastal conservation, 19(4), 445-459.

Ranasinghe, R. (2016). Assessing climate change impacts on open sandy coasts: A review. Earth-science reviews, 160, 320-332.

Roelvink, D. (2011). A guide to modeling coastal morphology (Vol. 12). world scientific.

Roelvink, D., Reniers, A., Van Dongeren, A. P., De Vries, J. V. T., McCall, R., & Lescinski, J. (2009). Modelling storm impacts on beaches, dunes and barrier islands. Coastal engineering, 56(11-12), 1133-1152.

Roelvink, Jan A., and I. Brøker. "Cross-shore profile models." Coastal Engineering 21.1-3 (1993): 163-191.

Ruiz-Martínez, G., Mariño-Tapia, I., Baldwin, E. G. M., Casarín, R. S., & Ortiz, C. E. E. (2016). Identifying coastal defence schemes through morphodynamic numerical simulations along the northern coast of Yucatan, Mexico. Journal of Coastal Research, 32(3), 651-669.

Schoonees, J. S., and A. K. Theron. "Evaluation of 10 cross-shore sediment transport/morphological models." Coastal Engineering 25.1-2 (1995): 1-41.

Seabergh, W. C., & Kraus, N. C. (2003). Progress in management of sediment bypassing at coastal inlets: natural bypassing, weir jetties, jetty spurs, and engineering aids in design. Coastal Engineering Journal, 45(04), 533-563.

Senechal, N., & de Alegría-Arzaburu, A. R. (2020). Seasonal imprint on beach morphodynamics. Sandy Beach Morphodynamics, 461-486.

Servold, K. P., Webb, B. M., & Douglass, S. L. (2017). Effects of low-crested living shoreline breakwaters on wave setup. In Coastal Structures and Solutions to Coastal Disasters 2015: Resilient Coastal Communities (pp. 421-431). Reston, VA: American Society of Civil Engineers.

Shi, F., Kirby, J. T., Harris, J. C., Geiman, J. D., & Grilli, S. T. (2012). A high-order adaptive time-stepping TVD solver for Boussinesq modeling of breaking waves and coastal inundation. Ocean Modelling, 43, 36-51.

Sleath, J. F. (1984). Sea bed mechanics.

Smit, P. B., Stelling, G. S., Roelvink, D., van Thiel de Vries, J., McCall, R., van Dongeren, A., ... & Jacobs, R. (2010). XBeach: Non-hydrostatic model. Delft University of Technology and Deltares.

Soulsby, R. (1997). Dynamics of marine sands.

Short, A. D., & Woodroffe, C. D. (2009). The coast of Australia. Cambridge University Press.

Toldo Jr, E. E., Nicolodi, J. L., Almeida, L. E. S. B., Corrêa, I. C. S., & Esteves, L. S. (2006). Coastal dunes and shoreface width as a function of longshore transport. Journal of Coastal Research, 390-394.

Tsoukala, V. K., Chondros, M., Kapelonis, Z. G., Martzikos, N., Lykou, A., Belibassakis, K., & Makropoulos, C. (2016). An integrated wave modelling framework for extreme and rare events for climate change in coastal areas–the case of Rethymno, Crete. Oceanologia, 58(2), 71-89.

Van Rijn, L. C. (2011). Coastal erosion and control. Ocean & Coastal Management, 54(12), 867-887.

Velikou, K., Tolika, K., Anagnostopoulou, C., Tegoulias, I., & Vagenas, C. (2014). High resolution climate over Greece: assessment and future projections. In 12th International Conference on Meteorology, Climatology and Atmospheric Physics (COMECAP 2014), Heraklion.

Waters, C. N., Zalasiewicz, J., Summerhayes, C., Barnosky, A. D., Poirier, C., Gałuszka, A., ... & Wolfe, A. P. (2016). The Anthropocene is functionally and stratigraphically distinct from the Holocene. Science, 351(6269).

Wright, L. D., & Short, A. D. (1984). Morphodynamic variability of surf zones and beaches: a synthesis. Marine geology, 56(1-4), 93-118.

Zhang, K., Douglas, B. C., & Leatherman, S. P. (2004). Global warming and coastal erosion. Climatic change, 64(1), 41-58.

1 Introduction

1.1 Context and research areas

Including to 15 of the world's 20 megalopolis, the coastlines are among the most populated areas in the world (Ranasinghe, 2016; Luijendijk et al., 2018). Worldwide, Low-laying coastal zones concentrate 10% of the global population (McGranahan et al., 2007). The coastal areas host about 154 million people, which is equivalent to one third of the population of Mediterranean coastal countries, along about 46,000 km of shoreline, 54% of which is rocky and 46% is sedimentary (Hénocque and Coccossis, 2001). Littoral systems and low-lying areas, also known as coasts, include all the areas close to mean sea level. In a general sense, there is no global definition for the coast and the coastal zone/area, where the latter put emphasis on the area or extent of the coastal ecosystems (Nicholls et al., 2007). Regarding the exposure to potential sea level rise, the term 'low-lying coastal zone' has been defined as "the contiguous area along the coast that is less than 10 m above sea level" (Lichter et al., 2011).

Coasts are important zones in natural ecosystems, often home to a wide range of biodiversity and human social activities. This complex system of natural variables is particularly fragile and exposed to multiple risks, including flooding, shoreline erosion and infrastructural damages due to extreme hydro-meteorological events: storm surges, heavy precipitation and very high tides (Plomaritis et al., 2018; Mori et al., 2019). Furthermore, the severe environmental social and economic impacts in the marine environment are expected to become even more critical in the near future, as climate-driven effects can aggravate the problem. Environmental disruptions, such as sea level rise, changes in precipitation and storm intensity, increased temperatures, ocean acidification, disappearance of species are some of the projected climate effects that put coastal systems at a significant risk.

Over the last few years, there has been an increasing amount of discussion in the literature, which draws attention to the hindcasting and forecasting of the physical parameters of coastal systems, highlighting a strong link between climate change effects and coastal hazards (Nicholls et al., 2007; Wang et al., 2014; Toimil et al., 2017; Brown et al., 2013). The role of two parameters related to change of climate, such as the potential rise of the sea water level and the increasing frequency of extreme storm coastal storms, has been thoroughly analysed. According to the 5th

Assessment Report (AR5) of the Intergovernmental Panel on Climate Change, the global sea level rise within 80 years to range between 0.50 and 0.98 m with regards to the 1986–2005 period, in the case of the highest emission RCP 8.5 scenario (Church et al., 2013). Furthermore, a high amount of studies has been dedicated to investigating the effects of a storm on coastal environment during the last few years (Barnard et al., 2014; Hondula and Dolan, 2010; Klemas, 2009; Rangel Buitrago and Anfuso, 2011; Sanchez-Vidal et al., 2012), (Walker and Basco, 2011; Massey et al., 2011). The definition of a coastal storm is considered very challenging, since it requires the combination of several parameters regarding the atmospheric conditions, water level, tidal cycle, as well as the time of a storm beginning and how long it is active (Martzikos et al., 2021). Harley (2017) in his detailed analysis, provided a new definition for the coastal storm as a "meteorologically-induced disturbance to the local maritime conditions (i.e. waves and/or water levels) that has the potential to significantly alter the underlying morphology and expose the backshore to waves, currents and/or inundation".

Coastal Vulnerability Indices (CVI) can be utilized to identify potential impacts of sea storms based on the characteristics of a number of physical drivers and physical or socioeconomic factors (i.e., wave height, tidal heights, subsidence, potential sea water rise, historical data of shoreline retreat, dune geometry, beach slope, population density, land use) (Grases et al., 2020). However, these indicators cannot consider the role of nearshore hydro-morphodynamics, and therefore a quantitative assessment of shoreline movement and flooding conditions cannot be provided. Although, they can be utilized to assess whether the study area is resilient or susceptible to a specific risk within a geographical domain and even at different time scales.

1.1.1 Costal Hazards:

1.1.1.1 Inundations

Coastal floods are amongst the most destructive natural hazards affecting urban zones adjacent to the shorelines. During recent years, an increasing number of extreme meteorological events has been recorded, storm surges, wave setup and high tides that trigger intense coastal flooding events, affecting hundreds of millions of people. Figure 1-1 shows the frequency of flooding along U.S. Coasts, through the comparison between the recorded events of 1950-1959 and 2010-2015 (Sweet et al., 2014). Extreme coastal water levels may lead to considerable impacts in densely populated low-lying coastal areas. Coastal flooding usually occurs during high tides

and storms that force water masses toward the shore. Effects of coastal flooding also include road closures, less stormwater drainage capacity, deterioration of infrastructure, and intrusion of saltwater to drinking water. In addition, these impacts can affect human health, as deterioration of water infrastructure and saltwater intrusion can put people at the high risk of being exposed to harmful chemicals.

Flood hazard is rarely a function of one process alone but comprises multiple drivers, including energetic waves, extreme coastal water levels, heavy precipitation, and high river discharge (Ganguli and Merz, 2019). These extreme flooding events are largely natural, however human influence on the nearshore environment can exacerbate coastal inundation (Ramsay and Bell, 2008). Anthropogenic unplanned infrastructures and poor governance are additional factors that increase flood risk, while massive development in coastal margins increases the consequences of coastal hazards. Managing this escalating risk over the near future is a significant challenge for planning authorities worldwide. Inundation and flooding affect a number of socioeconomic sectors such as freshwater resources, agriculture and forestry, fisheries and aquaculture, health, biodiversity, settlements/infrastructure, recreation and tourism.

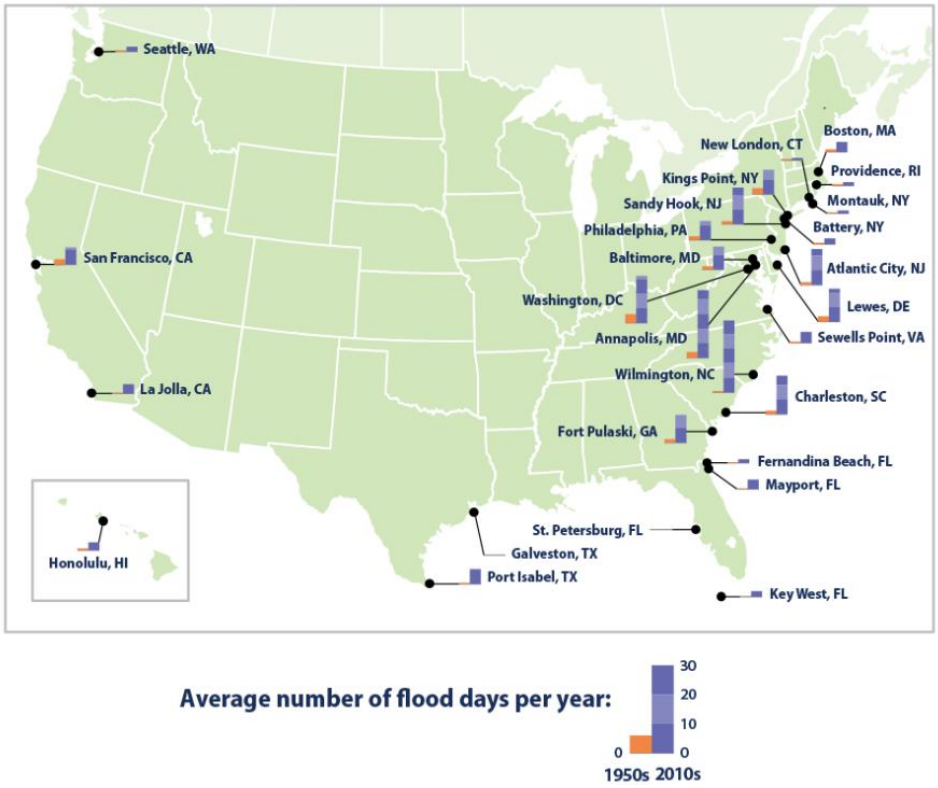

Figure 1-1 Frequency of recorded flooding along U.S. coasts, 2010-2015 versus 1950-1959 (Sweet et al., 2014).

1.1.1.2 Shoreline Erosion

Erosion of sandy coasts is a completely different physical process from inundation, as it involves a redistribution of sediment from the beach face to offshore depths (Zhang et al. 2004). Coastal erosion has significant impacts on infrastructure, tourism, and biodiversity, while there are no considerable effects on the other sectors that can be affected by coastal flooding, such as fisheries and aquaculture, agriculture and forestry or freshwater resources, according to the study of Nicholls et al. (2011). In urbanized coastal zones, sand or gravel beaches form an important buffer between storm attack and property (Almeida et al., 2012). In basic terms, shoreline erosion can be defined as the net loss of sediments over a particular vertical (2D) crosshore section of the bottom profile within a specific timescale of interest (Castelle and Harley, 2020). This erosion phenomenon can be manifested by the overwash of the subaerial beachface, which is often associated with high tides and large wave set-ups (Senechal et al. 2020). The coastal erosion can also be defined as a landward retreat of the shoreline position. The effects of this deficit of sediment budget concerns nearshore processes such as the presence of beach scarps and the undermining of dunes, cliffs and any back-shore infrastructure that may be situated.

Coastal storms are often associated with a destabilization of the littoral system, while natural processes involving waves, currents, sea level variability and wind forcing can seriously affect the nearshore system by reshaping the shoreline and moving large amounts of sand offshore. Storm surge, breaking events of high energetic waves and high wave set-up drive hydrodynamic patterns which are determinants for the evolution of seabed morphology. In particular, the nearshore undertow or rip currents (Afentoulis et al., 2016) can drive large amounts of sediment from high to low wave energy areas (Toldo, 2006; Guimaraes et al., 2014). Furthermore, for particularly extreme weather and wave conditions, a net loss of sediment might take place along the active beach profile (from the beach face or dune maxima down to closure depth). The erosion processes during short-period extreme storms represents a growing problem in the long term for stability of littoral system, as an immense and abrupt deficit of sediment may take decades to be recovered). In the case of these short-period events, the morphological evolution of the bottom geometry is directly proportional to the amount of the incoming wave energy in the coastal zone (Afentoulis et al., 2017).

The recent records of extreme storms and wave events, which were encountered during the winter of 2013 - 2014 along the European coasts, have as a consequence spectacular landward

retreat of the shoreline within a time interval of a few days. During that period, the 110-km coastline of Southwestern France was exposed to the most intense wave conditions over the last 18 years (Figure 1-2). Spectacular changes in meteorological and wave conditions were also identified in Greece over the last few years, triggering significant coastal flooding and erosive events. (Figure 1-3)

An equally significant aspect of beach erosion has been experienced in United States, where coastal erosion is responsible for about $500 million per year concerning coastal property loss, including damage to structures and loss of land. More than $150 million are spent every year on beach nourishment and other shore protection solutions (Dean et al., 2008). In addition to shoreline retreat, about 325 km^2 of coastal wetlands are lost in an annually basis, which is equivalent to seven football fields disappearing every hour of every day (Dahl and Stedman, 2013.). Figure 1-4 shows an overview of cliff erosion caused by a storm-induced energetic wave field along the West Coast of U.S.A.

Figure 1-2 Images of the severe damaged sea defences and coastal erosion during the extreme storm events of the winter 2013/2014 in SW France.

Figure 1-3 Damages of coastal infrastructures and intense beach erosion due to high energetic storm events; Crete, Greece 2013.

Figure 1-4 Cliff erosion is a common storm-induced hazard along the West Coast in USA. (Source: https://toolkit.climate.gov)

Besides the effects of nearshore physical processes, anthropogenic unplanned infrastructures can intensify the ongoing coastal erosion, as jetties and other obstacles to longshore transport, reflective vertical walls that accelerate offshore sand bar migration (Seabergh and Kraus, 2003), as well as devegetation along coasts are key causes of beach erosion intensification in the long term (Gabriel Ruiz-Martínez et al., 2016). Moreover, erosion is also produced due to sediment bypassing at dams, elimination of river bed quarrying, and other changes in river sediment supply to the coastal zone (Bird et al., 1996; Waters et al., 2016.). About 15 km2 per year is the estimated lost coastal area in Europe due to marine erosion (van Rijn, 2011). During next coming years, urbanization, population growth and increase in construction activity will grow this coastal risk, adding more pressure to an already dwindling sediment supply.

1.1.2 Coastal Protection Solutions

The EUROSION study (2004) suggests opposing coastal erosion by restoring the sediment balance in every coastal cell, which can be defined as a part that contains a complete cycle of erosion, accretion, sediment sources and sinks as well as the transport paths involved (Niesing, 2005). Furthermore, in the CONSCIENCE project (2010) coastal cells are analysed by investigating the sand volume accumulated in large-scale and small-scale coastal cells at various study areas (van Rijn, 2011). It should be noted that the strategic planning for the management of our littoral environment is implicitly based on the studying of the nearshore processes that are responsible for the evolution of coastal morphology (Williams et al., 2017; Reeve and Spivak, 2001).

Government policies or private actors define the response to the physical processes, while the institutional, legal, technological and financial aspects of the implemented strategies to control coastal erosion can be summarized in Figure 1-5. Each point inside the pyramid with a specific weighting represents every plan that can be employed to control coastal erosion (Figure 1-5 C). Defence is often costly and frequently temporary, consisting of hard and soft engineering techniques (Pranzini and Williams, 2013; Pranzini et al., 2015). Moreover, the management of retreat - structures, including the movement, demolition, or degradation of infrastructures is a decision that is becoming more frequent nowadays. However, ‘Greater attention is now being paid to the advantages of retreating from the coast as an adaptation strategy, rather than implementing defences to resist shoreline change in situ’ (Nordstrom et al., 2015). Finally, Sacrifices or no active intervention is a third strategy that can be followed when the implementation of other policies is not feasible.

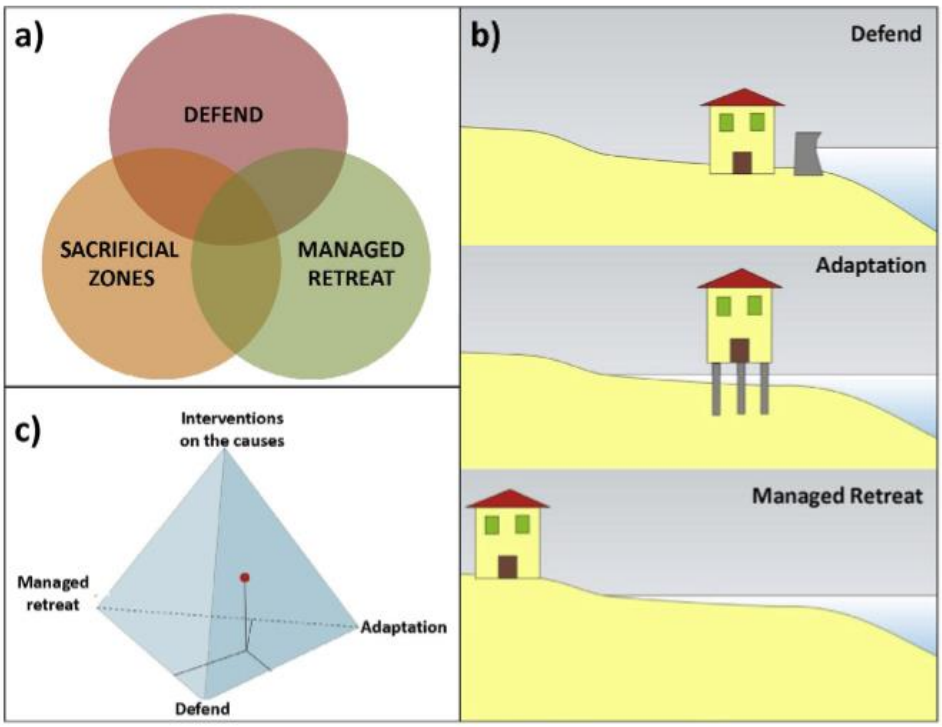

Figure 1-5 Standard strategies available to Government w.r.t. coastal erosion. b). Defend, Adapt and Retreat strategies. c) Adaptation with a further axis. (Williams et al. 2017).

While coastal defence structures are built to protect vulnerable areas, recent studies have analyzed the performance of these works to maintain shoreline position or to advance it (Pranzini et al. 2015; Servold et al. 2017). It has long been known that the engineering projects, which aim to deal with beach erosion issues, they are also responsible for intensifying problems at nearby locations (side - effects). Douglas et al. (2003) presents analytical examples of these side effects; 1 billion m^3 of sediment is removed from the American coasts due to engineering works during the past century.

Nowadays, many countries have created legislations to protect natural coastal environments, that enforces restrictions on construction activities close to the shore and oblige the execution of impact assessment studies. However, during the previous decades, no serious measures were decided since the coastal areas was considered as an environment that is relatively stable. Until now, the majority of coastal interventions to ensure the beach stability based on the “hard” protection concept. The effect of these structures upon the coastal environment was treated semi-empirically and fragmentarily.

1.1.2.1 Soft engineering protection solutions

The choice of an appropriate type of structures is the object of an active discussion in many countries, as 'soft' and 'hard' engineering techniques can be used to deal with beach erosion. Nowadays, coastal management is shifting towards soft techniques or nature-based coastal defence. Sandscaping and sand dunes, mangroves, seagrass, coral and shellfish reefs, reinforcement of vegetated and unvegetated dunes by a rocky core can be utilized to improve the stability of coastal environment (Vikolainen et al. 2017; Morris et al. 2018). Figures 1-6 – 1-8 show distinct nature- based solutions that have been already discussed in the literature of coastal engineering. Mangroves provide an effective natural protection against erosion, while they can also reduce flood risk and damages. Furthermore, the geotextile tube technology has been employed in recent years for flood and water control, but it can also be used to control beach erosion (Koerner and Koerner, 2006; Muthukumaran and Ilamparuthi, 2006). These devices can also be located within the surf zone to decrease the incoming wave energy, contributing to a depth-induced breaking of the incident waves. The Geotube® containers for instance are a proven solution that contributes to rebuild beaches and reclaim land from water masses for recreational, residential or industrial purposes and for half the cost of armour stone or riprap.

Applying soft-engineered measures requires ongoing and regular monitoring and maintenance. The efficiency of nature-based techniques for shoreline stabilization, such as vegetation and biogenic reefs is the object of an active debate and sceptical comments were available in the literature (Garcia et al. 2018). Finally, in order to reduce the uncertainty and risk, nature-based and hardened/improved infrastructure can be combined to form the optimal solution (Schoonees et al., 2019; Silva et al., 2017)

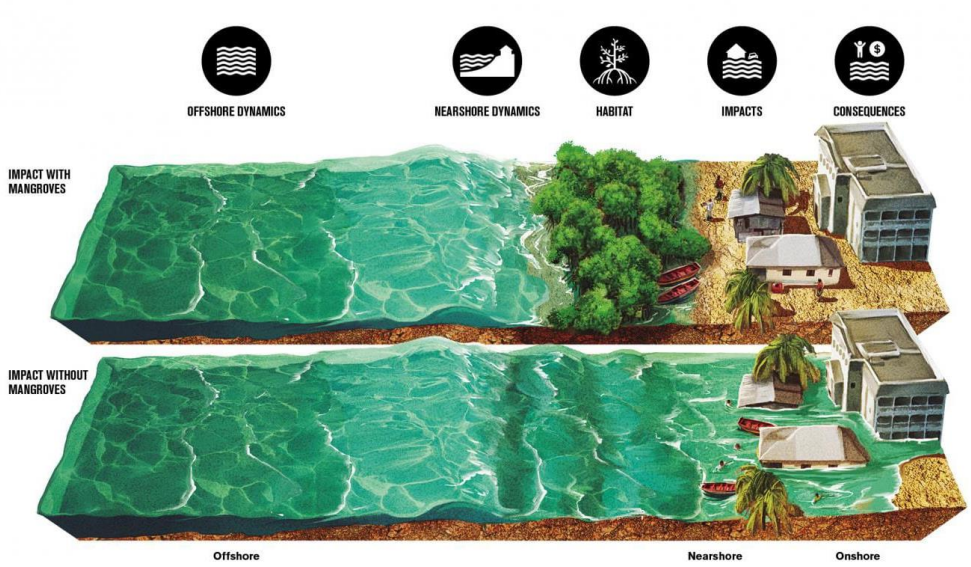

Figure 1-6 This illustration shows the impact of storm surge on coastal infrastructure and people with and without mangrove forests. (Credit: © World Bank and Punto Aparte)

Figure 1-7 Section of a geotextile tube which placed along the beach to reinforce the sand dune (Source: Geotubes®)

1.1.2.2 Hard engineering protection solutions

Coastal protection hard structures are related to the construction of large structures made of concrete or natural stones such as detached emerged or submerged breakwaters and groynes, seawalls, revetments. They have been employed worldwide to control coastal erosion and to provide protection against flooding phenomena to the inland (Charlier and De Meyer, 1989; van Rijn, 2013; Nordstrom, 2014; Pranzini et al., 2015; Servold et al., 2017). The presence of breakwaters results in a significant reduction of the wave energy reaching the sheltered area of the structure. The reduced wave agitation, in combination with the altered nearshore breaking wave-induced current field, create the appropriate conditions for sediment deposition while simultaneously enabling shoreline advance. It should be noted that emerged breakwaters have

been used at a lesser extent the last decades as a protection solution due to their impact on the aesthetics of coastal landscape. Hence, submerged structures provide a good compromise between the need to reduce the wave energy close to the shore and the aim to ensure landscape preservation and a good water quality though the exchange of water between offshore and inshore areas. However, the underlaying processes of shoreline response to submerged breakwater structures are not yet fully understood, due to limited available data concerning the performance of prototype-submerged structures (Ranasinghe et al., 2010).

Moreover, groynes, another commonly used coastal protection structure, are employed to retain the beach and maintain the stability of the littoral system. Sediment deposition occurred on the updrift side of a groyne due to wave diffraction, while erosion can be observed on the downdrift side. To avoid downdrift erosion a groyne field comprised of multiple groynes is often selected as an optimal protection solution (Baelus et al., 2019). A groyne system contributes to the seaward advance of shoreline by hindering wave-induced nearshore currents, deflecting energetic tidal currents, and intercepting longshore littoral drift (Bakker et al., 1970). The hydrodynamic and morphodynamic characteristics around groynes and breakwaters are partly known based on laboratory studies, field observations, and numerical investigations (van Rijn, 2011). However, the effects of these structures on the evolution of nearshore hydrodynamics and morphodynamics is still not yet fully understood.

Alternatively, high-strength precast concrete can be utilized as solution for protecting littoral systems and halting beach erosion. That type of structures (Figure 1-8) has generated an increased interest and acceptance in the coastal engineering community. Different patents of artificial reef barriers consist of precast concrete as available, such as Wave Attenuation Devices®, Reef Balls™ and Beach Prisms™. An important advantage precast has is that it's environmentally friendly, unlike the surplus armored vehicles, old steel barges, trawlers and tugboats that are sometimes used to create artificial reefs.

It should be mentioned that hard structures are effective in the short-term, but they are often costly, and their long-term sustainability has come under growing critique (Betzold, 2017). The implementation of hard structures to oppose coastal erosion, can have negative impacts on littoral systems due to interfering processes operating at a wide spatial scale of several kilometres (Pilkey and Young, 2010, Neal et al., 2017, Rangel-Buitrago et al., 2017). To avoid such negative experiences, correct application of adequate management policy is required to

preserve ecosystems as well as socio-economic activities and above all a real time monitoring of the performance of these structures is required.

Figure 1-8 Artificial Reefs & Coastal Restoration Inc.'s patented Wave Attenuation Device. (Source NPCA and Living Shoreline Solutions Inc).

1.1.3 Nearshore processes and predictive numerical modelling

The modelling of nearshore physical processes, such as the propagation of surface gravity waves, hydrodynamic circulation, sediment transport and morphology, is an essential key in order to predict coastal morphodynamics, as outlined throughout this thesis.

1.1.3.1 Surface waves

Waves play an important role in stirring up sediments from the bed level, as well as forcing current motions such as alongshore currents, rip currents, and mass-transport (or streaming) velocities, which carry the sediments. Waves can be generated either locally, known as wind-sea, due to the impact of local winds blowing for a specific distance (the fetch), and time (the duration); or as swell, which results from distant storms and often has a longer wavelength and less spread in period and direction than a locally generated sea (Soulsby, 1997). Other type of waves can also be encountered in coastal regions, such as infragravity waves, tsunamis or tidal surges. For the needs of this study only wind-generated surface gravity waves, sea and swell, were considered.

'At deeper water these waves are only weakly non-linear and as a consequence the wave field can characterized as a summation of a large number of independent wave components resulting in a Gaussian sea state creating an irregular wave field' (Roelving, 2011). While waves propagate from offshore to shallow water regions, depth-induced non-linearities appear, associated with a reduction of wave propagation speed due to bottom dissipation. The latter results in the reduction of the incoming wave energy through the shoaling effect. Wave refraction and diffraction are also nearshore physical processes that appear while incident waves interact with shallow water depths.

In addition, wave breaking is a physical phenomenon of high importance regarding its impact on hydrodynamic patterns and subsequently on sediment dynamics. In a large scale, wave breaking results in energy dissipation, which is the result of many local hydrodynamic phenomena, ultimately leading to dissipation due to small scale viscous effects. Different criterions can be found in the literature for the identification of the conditions under which wave breaking take place, based on limiting steepness, limiting wave height on a horizontal or sloping bed, local non-linearities, Froude number, hybrid slope/vertical velocity (Bacigaluppi et al. 2019). Wave breaking drive shear instabilities that are responsible for the generation of nearshore flows and the initiation of motion of sediment particles. This process is the most significant energy input into wave-dominated coastal environments and particularly in a region known as the surf zone. This zone is that part of the shoreface extending from the seaward boundary of wave breaking to the swash zone.

Deigaard et al. (1991) demonstrated that the breaking wave-induced bed shear-stresses in the surf zone do not differ significantly from those of unbroken offshore waves, but they exhibit an important wave to-wave variability, so that occasional large values could prevail. Thus, the neglect of wave breaking processes may lead to an underestimate of suspended sediment concentrations in the upper half of the water column throughout the nearshore zone.

1.1.3.2 Hydrodynamic circulation

Tidal motions, wind stresses, atmospheric pressure gradients, wave-induced forces, river outflows, large-scale water surface slopes and horizontal density gradients associated with oceanic circulations can result in the generation of sea-currents (Soulsby 1997). Close to the coast, wave-induced currents are especially intense, whereas further offshore combinations of

tidal and meteorological forcing dominate. The modelling of breaking wave-induced nearshore circulation such as alongshore currents, and rip currents is an object of active research nowadays. A big variety of modelling techniques have been used, based on depth-integrated equations. These include phase resolving (e.g., Chen et al., 2003; Clark et al., 2011), group-averaged (Reniers et al., 2004), or fully phase-averaged models (Geiman et al. 2011). However, it should be noted that these techniques are unfortunately not satisfactory adapted for large-scale continental shelf processes, which are driven by stratification, making it difficult to model cross-shore transport processes uniformly from the beach to the shelf break (Michaud et al. 2012).

When waves travel with a normal angle of incidence towards the coast, they drive complex circulation cells and rip currents throughout the surf zone. On the other hand, waves that approach the coast obliquely, they responsible for the generation of an alongshore littoral drift. Despite the alongshore and crosshore currents, attention should be focused on the undertow. Nadaoka et al. (1982) and Stive (1980, 1983) revealed the existence of seaward velocities under the wave trough during wave breaking, while shoreward velocities were observed in the vertical layer above the wave trough. Assuming no net flow over the vertical, the time-averaged return flow occurs under the wave trough level can be defined as undertow (van Rijn 1993), which is responsible for the transfer of significant sediment masses offshore in the surf zone.

Currents both stir up and transport sediments, hence the sediment trajectories globally follow the current circulation. Although, because the sediment transport fluxes depend non-linearly on the current velocities, and also due to the effect of wave-stirring, the direction of long-term net sediment transport may differ from the residual current direction.

1.1.3.3 Combined current and waves

Close to the shore, wave propagation can be affected by the existence of strong currents, that alter wave characteristics. Especially, opposing currents have an important effect on wave steepness even to the point of breaking (Chawla and Kirby, 1999). On the other hand, following currents enlarge wave troughs and thereby wave lengths, resulting in a wave height reduction. Van der Kaaij and Nieuwjaar - (1987) found that following currents reduce the velocities near the bed and near the water surface while they increase intermediate depth velocities. This phenomenon is especially pronounced in case of a weak current and a high wave. On the

contrary opposing currents contribute to the reduction of near bed velocities, increasing the velocities of water particles close to the surface.

1.1.3.4 Sediment transport

In coastal zones once the sediments are detached can be transported by gravity, wind, water, or a combination of the above. When the near bed shear velocity exceeds a critical value, which is responsible for the initiation of motion, bed materials start be rolling or sliding and interacting with the bed. Regular or irregular jumps of sediments may occur for intense bed shear velocities. For the values of shear velocities than exceed sediment falling velocities, sediment particles are lifted towards the water surface driven by turbulent forces. The transport of particles that correspond to the sliding is referred in the literature to as 'bed load transport', whilst the transport that corresponds to the lifting is widely known as 'suspended load transport'. Moreover, the transport of very fine slit suspended materials of 50 μm is called 'wash load'. These materials are in near-permanent suspension and, therefore, are transported through the stream without deposition.

1.1.3.4.1 Threshold of motion

The threshold motion condition of the sediment materials can be defined by estimating the balance between the forces tending to move sediments the forces contrasting this motion. The following forces are imposed on the particles: forces which tend to move the grain (drag and lift force); force that tries to keep the grain in its place (gravity force) (Figure 1-9). This approach considered by Armanini 2018 and it was initially derived from the classical theory originally proposed by Shields (1936) under the assumption of homogeneous, non-cohesive particles lying on a quasi-horizontal and -straight bed. In the case of sloping beds, different processes must be taken into consideration, such as avalanching or repose angle, especially close to the swash zone where the slope effect is dominant.

The threshold of motion of sediments is an essential factor in most types of computation and numerical modeling concerned with sediment response to hydrodynamics. It is required in applications involving scour around vertical maritime structures; sea bed morphology investigations; bed load transport (especially of coarser sediments); and entrainment of finer sediments into suspension

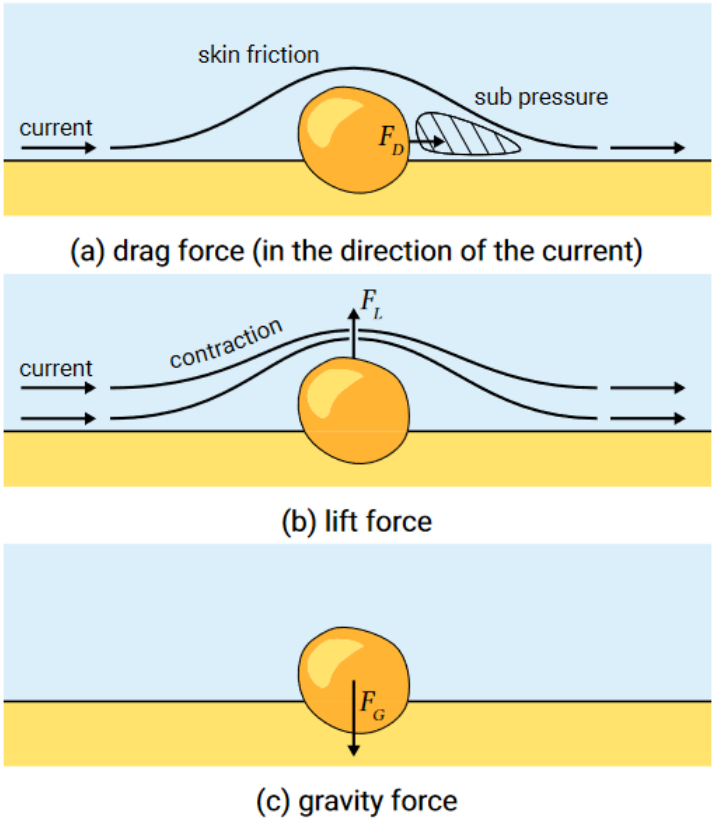

Figure 1-9 Scheme of the forces acting on an individual grain on a streambed. Particles are considered non-cohesive (Bosboom and Stive 2021)

1.1.3.4.2 Bed load

Bagnold (1956) defines the bed-load transport as that in which the continuous contacts of the materials with the bed are limited by the effect of gravity, whilst the suspended-load transport is determined as that in which the excess weight of the sediments is supported by random successions of upward forces, triggered by turbulent eddies. Einstein (1950), however, stated a different approach. He defines the bed-load transport as the transport of particles in a narrow layer of 2 particle diameters thick, above the bed by sliding, rolling, or jumping in a longitudinal distance of a few particle diameters. The bed layer is defined as a layer in which the turbulent mixing is low without any influence on the sediment particles, and therefore suspension of sediments is impossible in the bed-load layer. Further, Einstein considers that the distance travelled by bed-load particle is a constant distance of 100 particle diameters, independent of the hydrodynamic conditions, the transport rate and the bed characteristics.

According to the ISO-standard definitions (ISO 4363), bed load is the motion of the sediment in almost continuous contact with the bed, carried forward by rolling, sliding or hoping. Van Rijn (1984) based on the equations of motions of individual bed-load particles and computed the

saltation characteristics and the particle velocity as a function of the hydrodynamic conditions and the particle size for plane bed conditions. Figure 1-10 show a schematic view of bed load mechanism and the equilibrium of shear stress applied on sediment particles. The results of his analysis show that the bed load transport is weakly affected by particle sizes, this conclusion is in line with other previous investigations about the particle size's impact on sediment fluxes (Figure 1-11). The difference between the fluid shear stresses and the critical shear stresses gives the magnitude of the bed load transport according to the study of van Rijn (1993).

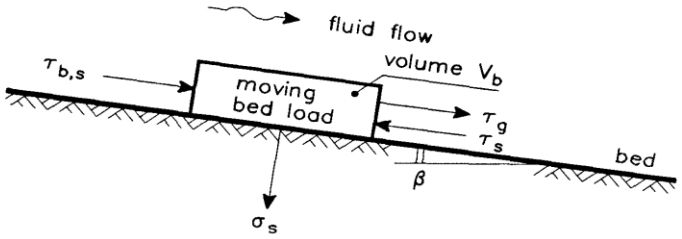

Figure 7.2.13 Stresses at base of bed load

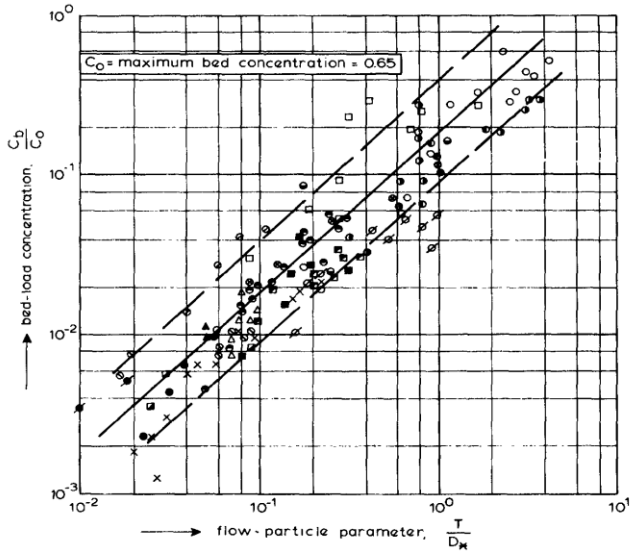

Figure 1-10 Stresses at base of bed load (van Rijn 1993)

d_{50} (μm)	D_* (-)	$\tau_{b,cr}$ (N/m²)	T (-)	q_b (m²/s)	
				Eq. (7.2.44)	Eq. (7.2.45)
600	15.2	0.30	7.3	$5.2\ 10^{-5}$	$6.5\ 10^{-5}$
700	17.7	0.35	6.1	$4.7\ 10^{-5}$	$5.6\ 10^{-5}$
800	20.2	0.40	5.3	$4.5\ 10^{-5}$	$5.0\ 10^{-5}$
900	22.8	0.47	4.3	$3.8\ 10^{-5}$	$3.9\ 10^{-5}$
1000	25.3	0.55	3.5	$3.2\ 10^{-5}$	$3.1\ 10^{-5}$

Table 1 Bed load transport rates according to van Rijn (1993).

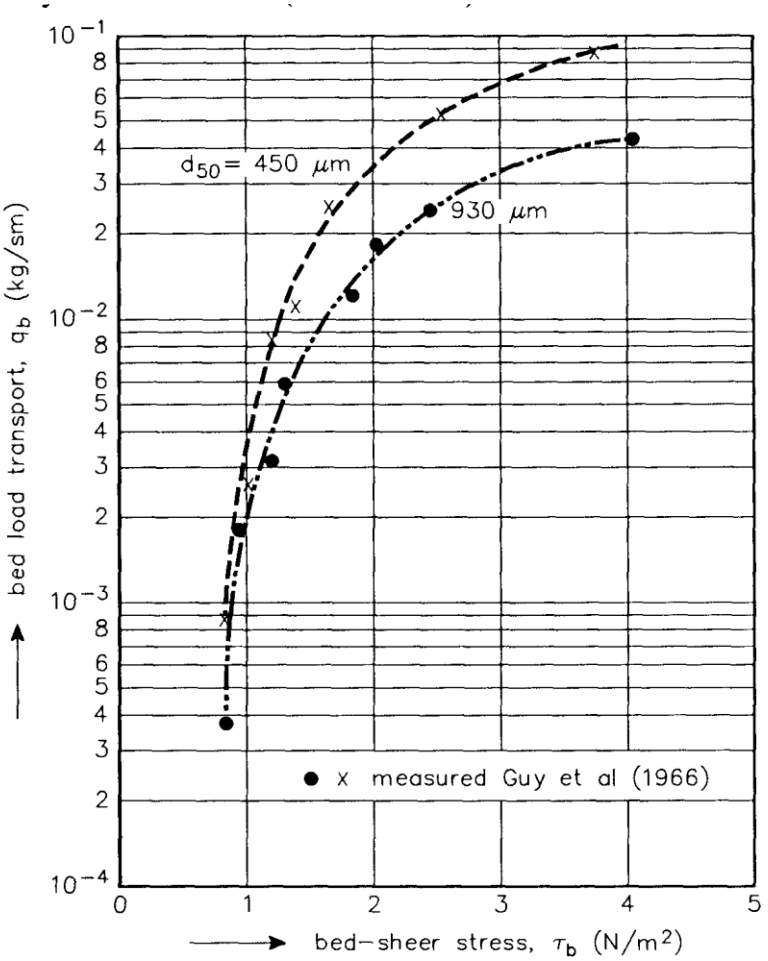

Figure 1-11 Influence of grain size on bed load transport rate (Guy et al. 1966)

1.1.3.4.3 Suspended load

For current velocities or wave values significantly above the threshold of motion, sand is entrained off the bed and into suspension, where it is carried at the same speed as the current. When this happens, the proportion of sediment carried in suspension is generally much larger than that being carried simultaneously as bedload, and hence the suspended load is an important contribution to the total sediment transport rate. An important factor in the design of cooling water intakes for power stations is prevention of ingress of suspended sediment, for which calculations of the concentrations and grain sizes at the height of the intake are required.

When bed-shear velocity exceeds the particle fall velocity, the grains can be lifted to a specific level at which the upward turbulent forces will be comparable to or higher than the submerged particle weight, where random particle trajectories appear because of turbulent fluctuations. Globally, the behavior of the suspended sediment particles is described in terms of the sediment concentration, which can be expressed as the solid volume per unit fluid volume or the solid

mass per unit fluid volume (Figure 1-12). Experimental observation showed that the suspended sediment concentrations decrease with distance up from the bed (van Rijn 1984). An important part of morphological computations with suspended sediment transport is the usage of a reference concentration as a bed-boundary condition, which distinguish bed load and suspended load van Rijn (1984, 1993). This resembles also to the theory introduced by Einstein (1950), who defined the bed-load transport in a layer of two particle diameters.

While bed load is assumed to instantaneously adapt to the local hydrodynamic conditions, suspended load responds in a time and space lag manner, related to the time that the suspended particle needs to reach the bed. Two methods have been widely used to describe the mechanism of suspended load transport: the sediment transport rates that consider the combine action of waves and currents and the diffusion- advection equation. The spreading of suspended sediments due to random motions and by turbulence is termed diffusion, whilst the spreading due to gradients of time-averaged velocity components is termed advection. The latter method was utilized for the needs of the present thesis.

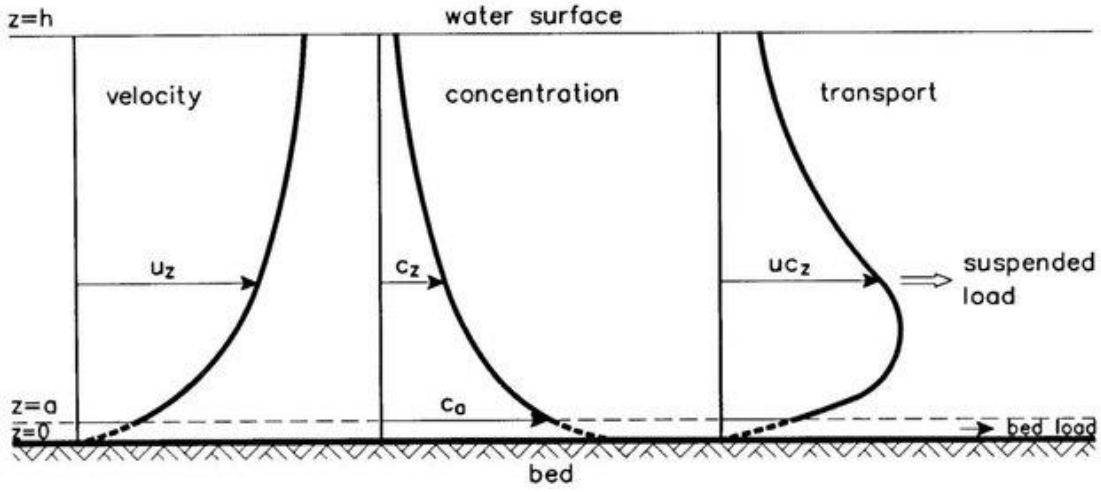

Figure 1-12 Definition sketch suspended load transport by Van Rijn (1993).

1.1.3.5 Morphology - Sediment Continuity.

Morphological changes vary at a different and slower rate as compared to the short-term variations of hydrodynamics. Thus, the estimation of bathymetry update requires to keep a budget of the sediment fluxes that have been derived by averaging the instantaneous flow parameters. These sediment transport fluxes are often integrated over a number of time steps,

which corresponds to several wave periods. In order to estimate bathymetry update the sediment mass conservation (Exner) equation can be employed. Effectively:

$$\frac{\partial z_b}{\partial t} = \frac{-1}{1-n_p} \nabla \cdot q_{tot} \ , \tag{1.1}$$

where, n_p is the sediment porosity, $\boldsymbol{q_{tot}}$=($q_{tot,x}, q_{tot,y}$)denotes the total volumetric sediment transport rate equal to the sum of suspended and bed load transport rate and z_b is the local bottom elevation

The Exner equation was originally developed to describe morphological changes in terms of sediment mass conservation in rivers (Exner, 1925). The effect of the bed slope on sediment transport has been included in this equation by and Karambas et al. (2002) further analyzed it. Paola et al. (2006) derived another Watanabe (1988) and Leont'yev (1996) form of the standard Exner equation for sediment mass balance that considers effects of tectonic uplift and subsidence, soil formation and creep, compaction, and chemical precipitation and dissolution. Wolinski (2009) has refocused the generalized Exner equations in relation to coastal areas. Based on his work, Deng et al. (2017) introduce two types of Exner equations: the generalized Exner equation based on the sediment column at a specific point and the shoreline Exner equation based on a cross-shore profile of the shoreface which explicitly includes interconnections between external sediment fluxes, shoreline position, and relative sea-level changes.

1.1.4 Coastal area numerical approaches: 2DH models

Different types of numerical predictive models can be encountered in the literature of coastal engineering for the evaluation of nearshore hydrodynamics and morphodynamics. According to Roelvink (2011), the existing models can be described as been in three categories:

1) Coastal profile models, where the focus is on the cross-shore processes, while long-shore variability is neglected (Roelvink and Brøker, 1993; Schoonees and Theron, 1995);
2) Coastline models and shoreline evolution based on distinctive cross-shore profiles, where short-term fluctuations of the profile are smoothed out and bar behaviour is not considered (GENESIS, UNIBEST and LITPACK), (Szmytkiewicz et al., 2000);

3) Coastal area models, where alongshore and cross-shore variabilities are considered (Nicholson et al., 1997).

Hydro-morphological models had been developed since 1980 (Nicholson et al., 1997). Amongst them, devices that employ an unstructured flexible mesh can be utilized in order to describe thoroughly the geometry of solid boundaries in a coastal zone. These devices provide different resolution levels between offshore and nearshore regions, in order to keep a low computational cost. Some of these models are listed below:

- Delft3D (Deltares, 2014);
- XBeach (Roelvink et al., 2009);
- FUNWAVE-TVD (Shi et al. 2012)
- MIKE DHI (Pietrzak et al., 2002);
- Telemac (Villaret, 2010);
- ECOMSED (Blumberg, 2002);
- ADCIRC (Luettich and Westerink, 2004);
- ROMS (Warner et al., 2008);
- Wallingford, COHERENS (Luyten et al., 2006).

The above numerical models, used for the simulation of nearshore processes, can be distinguished in two board categories, concerning their approaches to incorporate wave effects. Those that are based on the spectrum concept (or phase averaged) as well as on models based on the momentum concept (or phase resolving). These distinct approaches have been highlighted (Hotlhiujsen, 2003) for the numerical investigation of the dominant processes governing wave transformation. In particular:

1. The phase-averaged approach describes wave propagation in the spatial and time domain nature using the variance-density spectrum, which is the Fourier transformation of the auto-covariance function of free-surface elevation. The most notoriously used models following this approach are 3rd generation spectral wave models (Benoit et al., 1996, Group WAMDI, 1988). Due to the complex nature of wind-nearshore waves, the usage of a deterministic approach to describing the sea surface elevation is generally not feasible for large-scale analyses (Rusu and Soares, 2013). Thus, many efforts have been made during the recent years to describe wave propagation in the frequency

domain, rather than in time-domain. Third-generation models, such as the WAM, MIKE21 -SW and SWAN are based on the spectral concept. The physical processes that can be assessed are wave refraction, shoaling, reflection, wave-induced setup, wave-wave interactions, depth-induced breaking, bottom friction, wind energy transfers and whitecapping. Furthermore, a phase-decoupled method, to consider wave diffraction, was implemented by Holthuijsen et al. (2003).

2. The phase resolving deterministic approach describing properties of the wave field in the spatial and temporal domain at a fine resolution. The spatial step is often a small fraction of the wavelength. In this category, models solving the mild slope, shallow water (SWE) or Boussinesq equations have been employed. The prediction of the surface gravity waves by means of the phase resolving models has proven, in the recent years, to be a valuable tool in simulating waves propagating from deep to shallow water. These devices give reliable predictions in comparisons with filed or experimental data.

Within the framework of the present work, several advanced existing numerical devices were utilized, such as MIKE21 DHI, XBeach and FUNWAVE – TVD, for the investigation of nearshore physical processes, with a special focus on wave-current-sediment interactions and they were applied in study areas where erosion phenomena are particularly intense. Figure 1-13 illustrates an example of numerical outputs of Mike 21 HD concerning the current field in the vicinity of harbour structures in the city of Rethymno in Greece (Afentoulis et al. 2017). The usage of the above numerical tools provided significant insights and conclusions that contributed to the development of new numerical hydro-morphodynamic models in the context of the present dissertation.

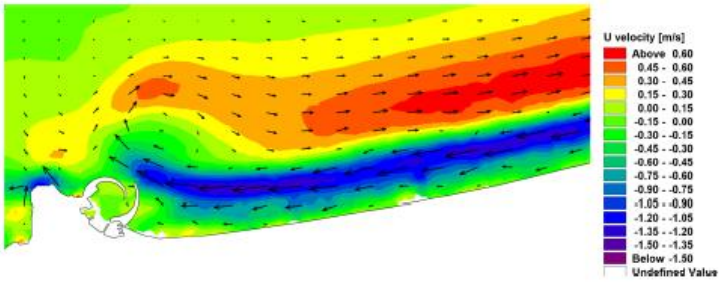

Figure 1-13 MIKE21 HD results: U velocity contours and net velocity vectors for a reshaped harbour layout (Afentoulis et al. 2017).

1.2 Objectives and research questions

The present dissertation concerns the study of wave propagation in shallow water and the study of fluid – seabed interactions under unsteady flows. The main purpose is the numerical investigation of hydrodynamic effects on the erosion and deposition mechanisms of non-cohesive sediments, as well as their impact on coastline evolution, taking into account the presence of maritime structures, such as a shore parallel system of emerged or submerged breakwaters, groynes and jetties. A variety of test cases and coastal engineering applications, regarding flow seabed interactions in sloping beaches and the efficiency of coastal structures to control erosion phenomena, were thoroughly analysed in this research. Special focus was placed on the hydro-morphodynamic processes in the inner surf and swash zone, where the mechanism of sediment transport is still unclear and a number of uncertainties and limitations are associated with the existing waves-currents-bathymetric evolution numerical models. The time scales of interest vary from a couple of hours to several months.

For the needs of this work, several advanced existing numerical tools and models were utilized to better understand nearshore hydro-morphodynamics processes. These devices were applied to predict bed morphology in study areas, where intense erosion phenomena appear. Furthermore, new algorithms and models were developed by the author of this dissertation for the assessment of hydrodynamic parameters and sediment transport dynamics throughout the inner surf and swash zone. A further research was based, herein, on the needs for optimal and more effective simulation of the flow impact on the sea bottom reducing the computational burden. Thus, this thesis involves the development and the evolution of existing or new numerical models based on modern methods for solving flow problems.

The already developed state-of-the-art models that were employed here are the MIKE21 DHI suite, XBeach and FUNWAVE –TVD model. In addition, a numerical formulation for sea--bed evolution, developed by Bouharguane and Mohammadi (2013) was applied to evaluate sediment dynamics with and without the presence of coastal defences. Initially, short time scale wave events, which can have a serious impact on the reshaping of coastline, were analysed within our research. These phenomena relate to climate and seasonal changes and to the manifestation of extreme events, storms and floods with a parallel increase of the meteorological tide.

For the evaluation of hydrodynamic characteristics nearshore, two different numerical approaches were followed. A model that solves the two-dimensional non-linear shallow water equations (NSWE) in conservative form was initially used (Marche and Bonneton 2006),(Marche et al.2007). The main advantage of this numerical approach is that breaking events can be modelled as the development of a free surface and current discontinuity (Bonneton et al. 2010).It is noted, however, that dispersion effects are not considered, which a limitation of this approach is. A wave-maker was developed and implemented for the generation of irregular waves using directional spectral data. These irregular waves can be obtained by superposing a series of wave components with different frequencies and directions, using random phases.

Thereafter, in deep to shallow water, dispersive nonlinear wave effects were simulated satisfactorily using a Boussinesq approach (Madsen et al. 1997; Kennedy et al. 2001). In the present study, a highly nonlinear Boussinesq model (Shi et al. 2012) tasked with the simulation of wave propagation and hydrodynamic circulation was directly coupled to a newly developed quasi 3-D sediment transport and morphology model., since these equations are sufficiently accurate in resolving nearshore wave phenomena, such as refraction and diffraction (Do 2019).

Several key approaches for sediment transport modelling were studied, such as the threshold motion, the suspended sediment concentration profile, the equilibrium or saturation concentration near the bottom and the depth-averaged suspended sediment concentration under the presence of waves, currents or due to the combined action of both environmental forces. The numerical methods incorporated in this research, include formulae for: the drag coefficient for unsteady or tidal flows on a non- flat bed of sediment, wave orbital velocity at the sea bed, the friction coefficient for waves, bottom dissipation in combined wave and current flow, the settling velocity of fine sand grains, the threshold bed shear-stress of sand grains due to the action of currents and/or waves, the bedload and total transport rate of sand under currents and/or waves, and the longshore transport of sediment. In addition, a 3-D approach for the estimation of the suspended load sediment transport was implemented in order to describe the vertical structure of the sediment concentration.

Furthermore, special attention was given to the investigation of swash sediment dynamics, as their role is of high interest for engineering applications. Swash dynamics determine the shoreline position, thus the precise evaluation of the natural processes in this zone contribute in the performance evaluation of coastal defence structures in terms of their capacity to maintain or advance the shoreline seaward.

1.2.1 Research Goals

Based on the above objectives the goals of the thesis are:

(1) The application and comparison between existing coastal engineering numerical devices and software suites, in order to evaluate their performance, capacity and properties.

(2) The development of new numerical models and tools, based on previous codes and algorithms, for the simulation of coastal wave propagation and sediment transport mechanisms.

(3) The verification of the model's capacity and efficiency to accurately predict seabed morphology and the validation against experimental results and real-filed measurements.

(4) The application of selected devices and numerical models in order to assess hydro-morphodynamic processes in erosion-dominated coastal zones.

1.2.2 Research Questions

Moreover, the present PhD dissertation aims at providing answers to the following research questions:

(1) How existing numerical models and software suites perform in terms of the prediction of nearshore complex morphological processes, influenced by the unsteady impact of the wave-current combined action and how they consider coastal structures effects?

(2) What are the key approaches for the modelling of beach up-state or down-state transitions and the prediction of sandbar systems and rip channels behaviour?

(3) How to develop time-dependent techniques for fine sediment transport modelling, including non-linear wave effects in nearshore region and swash zone, for practical purposes (e.g., to improve the approaches of sediment simulation in 2DH/3D model)?

(4) How coupled numerical modelling techniques can incorporate the role of coastal structures/obstacles on the mechanisms of wave propagation, wave-induced current, sediment transport by waves and currents, and bed morphology evolution.

1.3 Innovative points

This thesis seeks to assist in better understanding of nearshore physical processes and the application of advanced numerical modelling, for the simulation of nearshore sediment transport dynamics, with a special focus on non-cohesive sediment movement under wave-current actions. The following innovative aspects are included:

- An extensive review is provided in this work, whose overall objective is to evaluate existing 2DH modeling techniques that are currently been utilized in coastal morphology problems. A complete assessment of available devices was made, in terms of their capacities to provide accurate and reliable predictions of bathymetric evolution. This analysis contains a plethora of modeling suites that was employed for the simulation of nearshore physical processes, such as wave propagation, hydrodynamic circulation, wave-current interaction, sediment transport and morphology. Therefore, in selected case studies, hydro-morphodynamic patterns were investigated through MIKE 21 and XBeach software, whilst seabed morphological evolutions in the vicinity of detached submerged breakwaters were simulated by means of a minimization principles-based numerical formulation. Valuable insights were gained about the limitations and advantages of existing 2DH coastal area modeling approaches.
- Inspired by the capacities and limitations of the existing numerical devices, the development of a novel and robust numerical model was achieved in purpose of practical applications. In particular, a quasi-3-D sediment transport and morphology model that fully considers unsteady and nonlinear hydrodynamic effects, was developed and introduced in the context of the present dissertation. Special attention was given to the role of sediment transport dynamics across the swash and inner surf zone, incorporating them in the numerical device. In addition, advanced numerical techniques were utilized to simulate three-dimensional patterns of suspended load fluxes and consider wave nonlinear and unsteady effects on bed load transport rate. This new predictor was tailored for the Suspended Sediment Transport based on the solution of the three-dimensional convection-diffusion (mass-balance) equation for the sediment concentration.
- This newly tailored sediment transport predictor was coupled to a fully nonlinear Boussinesq wave driver (FUNWAVE-TVD), for the purpose of performing reliable computations and providing accurate predictions of bed level evolution, across various timescales of interest. Therefore, the innovation of the proposed approach

consists in reducing the uncertainty in hydro-morphodynamic simulations, which is often associated with the existing and available numerical tools that can be encountered in the literature of coastal engineering. In a rigorous modelling framework, this study provides a series of tools and algorithms that assist the modeller to analyse model sensitivity, undertake parameter optimisation and quantify parameter-induced uncertainty. In order to verify the model's performance and corroborate the applied formulations, the compound model was validated thoroughly against a number of laboratory data and other numerical investigations.

- Furthermore, the role of several coastal protection structures (Groynes, emerged or submerged breakwaters) was rigorously evaluated in terms of their capacity to control beach erosion. A particular effort was made to keep the computational complexity at a reasonable level by utilizing morphological acceleration techniques and exploiting computational techniques of parallel schemes. It was, therefore, demonstrated that this newly developed integrated model can be utilized to a wide range of maritime engineering applications, both for soft engineering (beach replenishment, sand dune management, drainage) and hard engineering techniques (design of groynes, breakwaters, seawalls, revetments).
- A further innovation aspect of the dissertation consists of the fact that the beach down-state and up-state transitions were investigated via different numerical approaches, unveiling important discoveries about morphodynamic effects of rip current systems. In that regard, measurements of a 3D physical experiment were utilized as benchmark in order to corroborate two distinct simulation techniques that were applied herein for the predictions of wave-sandy bed interactions over an initial shallow sloping bottom.

1.4 Thesis organization

This thesis in all has five chapters:

- (1) Chapter one, this introduction, presents the research issues, background and overviews of wave, current circulation and sediment transport modelling, as well as techniques and strategies to control beach erosion. Objectives and research questions were proposed.
- (2) Chapter two, presents the applications of several existing coastal area models in erosion-dominated areas. This chapter also provides numerical observations on sediment dynamics under waves and currents using MIKE21 and XBeach devices,

while a novel numerical approach based on minimization principles were applied to optimize the form of coastal defences. General features and limitations of available process-based models are summarized.

- (3) Chapter three is about sediment transport phenomena associated with the presence of sandbars and rip channels. Numerical techniques were developed in order to predict beach up-state and down-state transitions, while the numerical findings were qualitatively validated against experimental data. A special focus was placed on the incipient motion of fine-sand particles under combined waves and currents and seabed evolutions. For this purpose, minimization principles and advanced formulas for the estimations of sediment fluxes were employed, while the hydrodynamic solution was based non-linear shallow water equations.
- (4) Chapter four develops a 2DH model for morphodynamic simulations under wave-current interactions, inspiring by the capacities and limitations of the already existing numerical process-based models, that have been discussed in previous chapters. The new sediment transport model accounts for unsteady wave effects and swash zone morphodynamics, and it was coupled to a fully nonlinear Boussinesq wave model, providing integrated predictions of bed level evolution, across various timescales of interest. This novel model was validated thoroughly against laboratory data and other numerical investigations. Discussions are made on the impact of several coastal structures and configurations on nearshore morphology.
- (5) Chapter five summarizes the whole work, gives answers to the pre-defined research questions and makes suggestions for future study.

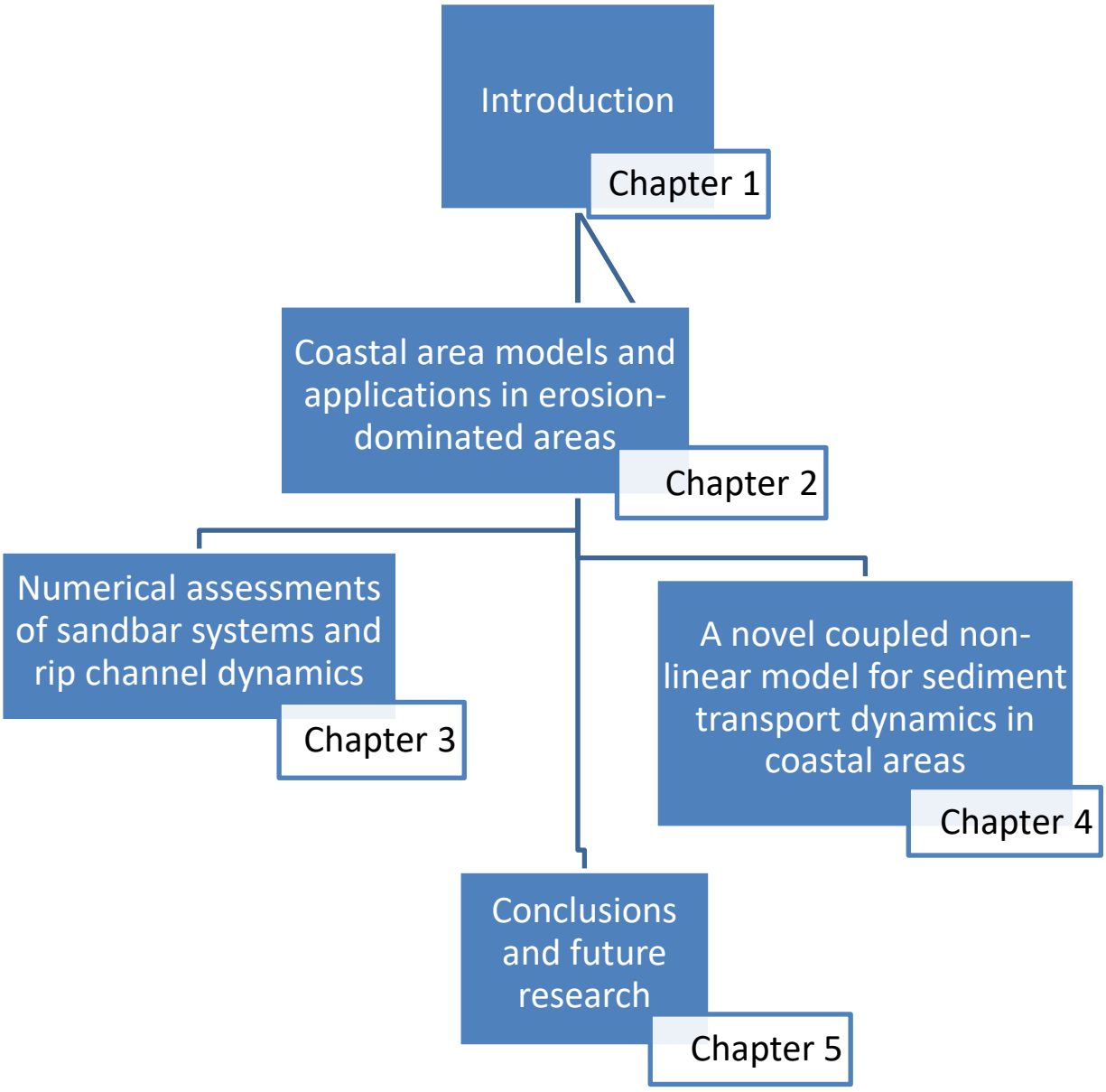

Figure 1-14 Thesis structure.

References

Afentoulis, V., Tsoukala, V., & Mohammadi, B. (2016). Experimental and numerical modeling of fluid-seabed interaction in shallow water. Coastal Engineering Proceedings, (35), 18-18.

Afentoulis, V., Eleftheria, K., Eleni, S., Evangelos, M., Archontia, L., Christos, M., & Vasiliki, T. (2017). Coastal Processes Assessment Under Extreme Storm Events Using Numerical Modelling Approaches. Environmental Processes, 4(3), 731-747.

Afentoulis, V., Papadimitriou, A., Tsoukala, V., & Benoit, M. (2019). Numerical Approaches for the Evaluation of Sediment Transport Mechanisms on a Shallow Sloping Sea Bottom. In First International Scientific Conference on Design and Management of Harbor, Coastal and Offshore Works.

Almeida, L. P., Vousdoukas, M. V., Ferreira, Ó., Rodrigues, B. A., & Matias, A. (2012). Thresholds for storm impacts on an exposed sandy coastal area in southern Portugal. Geomorphology, 143, 3-12.

Armanini, A. (2018). Initiation of Sediment Motion. In Principles of River Hydraulics (pp. 49-76). Springer, Cham.

Bacigaluppi, P., Ricchiuto, M., & Bonneton, P. (2020). Implementation and evaluation of breaking detection criteria for a hybrid Boussinesq model. Water waves, 2(2), 207-241.

Baelus, L., Lanckriet, T., Bolle, A., Szengel, V., & Van Quickelborne, E. (2019). Design of a Groyne Field to Counteract Beach Erosion at Wenduine, Belgium. Coastal Structures 2019, 347-355.

Bakker, W. T., & Joustra, D. S. (1970). The history of the Dutch coast in the last century. In Coastal Engineering 1970 (pp. 709-728).

Bagnold, R. A. (1956). The flow of cohesionless grains in fluids. Philosophical Transactions of the Royal Society of London. Series A, Mathematical and Physical Sciences, 249(964), 235-297.

Barnard, P. L., van Ormondt, M., Erikson, L. H., Eshleman, J., Hapke, C., Ruggiero, P., ... & Foxgrover, A. C. (2014). Development of the Coastal Storm Modeling System (CoSMoS) for predicting the impact of storms on high-energy, active-margin coasts. Natural hazards, 74(2), 1095-1125.

Benoit, M., Marcos, F., & Becq, F. (1997). Development of a third generation shallow-water wave model with unstructured spatial meshing. In Coastal Engineering 1996 (pp. 465-478).

Betzold, C., & Mohamed, I. (2017). Seawalls as a response to coastal erosion and flooding: a case study from Grande Comore, Comoros (West Indian Ocean). Regional Environmental Change, 17(4), 1077-1087.

Bird, E. C. (1996). Coastal erosion and rising sea-level. In Sea-Level Rise and Coastal Subsidence (pp. 87-103). Springe Blumberg, A. F. "A primer for ECOMSED." Mahwah NJ: Hydro Qual Inc (2002): 1-194. r, Dordrecht.

Brown, S., Nicholls, R. J., Woodroffe, C. D., Hanson, S., Hinkel, J., Kebede, A. S., ... & Vafeidis, A. T. (2013). Sea-level rise impacts and responses: a global perspective. In Coastal hazards (pp. 117-149). Springer, Dordrecht.

Castelle, B., & Harley, M. (2020). Extreme events: impact and recovery. In Sandy Beach Morphodynamics (pp. 533-556).

Charlier, R. H., & De Meyer, C. P. (1989). Coastal defense and beach renovation. Ocean and Shoreline Management, 12(5-6), 525-543.

Chawla, A., & Kirby, J. T. (1999). Experimental study of wave breaking and blocking on opposing currents. In Coastal Engineering 1998 (pp. 759-772).

Chen, Q., Kirby, J. T., Dalrymple, R. A., Shi, F., & Thornton, E. B. (2003). Boussinesq modeling of longshore currents. Journal of Geophysical Research: Oceans, 108(C11).

Chondros, M., Metallinos, A., Papadimitriou, A., Memos, C., & Tsoukala, V. (2021). A coastal flood early-warning system based on offshore sea state forecasts and artificial neural networks. Journal of marine science and engineering, 9(11), 1272.

Church, J. A., Clark, P. U., Cazenave, A., Gregory, J. M., Jevrejeva, S., Levermann, A., ... & Unnikrishnan, A. S. (2013). “Chapter 13: Sea Level Change” in Climate Change 2013: The Physical Science Basis: Contribution of Working Group I to the Fifth Assessment Report of the Intergovernmental Panel on Climate Change.

Clark, D. B., Feddersen, F., & Guza, R. T. (2011). Modeling surf zone tracer plumes: 2. Transport and dispersion. Journal of Geophysical Research: Oceans, 116(C11).

Dahl, T. E., & Stedman, S. M. (2013). Status and trends of wetlands in the coastal watersheds of the Conterminous United States 2004 to 2009. US Department of the Interior, US Fish and Wildlife Service and National Oceanic and Atmospheric Administration, National Marine Fisheries Service.

Dean, R. G., Davis, R. A., & Erickson, K. M. (2008). Beach Nourishment: A Guide for Local Government Officials: Beach Nourishment with Emphasis on Geological Characteristics Affecting Project Performance. National Oceanic and Atmospheric Administration (NOAA), Coastal Services Center.

Deigaard, R., Justesen, P., & Fredsøe, J. (1991). Modelling of undertow by a one-equation turbulence model. Coastal Engineering, 15(5-6), 431-458.

Deltares. (2014). User Manual Delft3D-Flow.

Deng, Junjie, et al. "Morphogenetic modelling of coastal and estuarine evolution." Earth-Science Reviews 171 (2017): 254-271.

Douglas, S.L., Bobe, A., Chen, Q.J. (2003), The amount of sand removed from. Americas beaches by engineering works, Coastal Sediments 2003.

Einstein, H. A. (1950). The bed-load function for sediment transportation in open channel flows (No. 1026). US Department of Agriculture.

Exner, Felix M. "Uber die wechselwirkung zwischen wasser und geschiebe in flussen." Akad. Wiss. Wien Math. Naturwiss. Klasse 134.2a (1925): 165-204.

Garcia-Lozano, C., & Pintó, J. (2018). Current status and future restoration of coastal dune systems on the Catalan shoreline (Spain, NW Mediterranean Sea). Journal of coastal conservation, 22(3), 519-532.

Geiman, J. D., Kirby, J. T., Reniers, A. J. H. M., & MacMahan, J. H. (2011). Effects of wave averaging on estimates of fluid mixing in the surf zone. Journal of Geophysical Research: Oceans, 116(C4).

Guimarães, P. V., Farina, L., & Toldo Jr, E. E. (2014). Analysis of extreme wave events on the southern coast of Brazil. Natural Hazards and Earth System Sciences, 14(12), 3195-3205.

Grases, A., Gracia, V., García-León, M., Lin-Ye, J., & Sierra, J. P. (2020). Coastal flooding and erosion under a changing climate: implications at a low-lying coast (Ebro Delta). Water, 12(2), 346.

Group, T. W. (1988). The WAM model—A third generation ocean wave prediction model. Journal of Physical Oceanography, 18(12), 1775-1810.

Harley, M. (2017). Coastal storm definition. Coastal Storms: Processes and Impacts, edited by: Ciavola, P. and Coco, G., John Wiley and Sons, Chichester, UK, 1-21.

Hénocque, Y., & Coccossis, H. (2001). White paper coastal zone management in the Mediterranean.

Hondula, D. M., & Dolan, R. (2010). Predicting severe winter coastal storm damage. Environmental Research Letters, 5(3), 034004.

Holthuijsen, L. H., Herman, A., & Booij, N. (2003). Phase-decoupled refraction–diffraction for spectral wave models. Coastal Engineering, 49(4), 291-305.

Klemas, V. V. (2009). The role of remote sensing in predicting and determining coastal storm impacts. Journal of Coastal Research, 25(6), 1264-1275.

Koerner, G. R., & Koerner, R. M. (2006). Geotextile tube assessment using a hanging bag test. Geotextiles and Geomembranes, 24(2), 129-137.

Lichter, M., Vafeidis, A. T., Nicholls, R. J., & Kaiser, G. (2011). Exploring data-related uncertainties in analyses of land area and population in the “Low-Elevation Coastal Zone”(LECZ). Journal of Coastal Research, 27(4), 757-768.

Leont'yev, I. O. (1996). Numerical modelling of beach erosion during storm event. Coastal Engineering, 29(1-2), 187-200.

Luettich, R. A., & Westerink, J. J. (2004). Formulation and numerical implementation of the 2D/3D ADCIRC finite element model version 44. XX (p. 74). Chapel Hill, NC, USA: R. Luettich.

Luijendijk, A., Hagenaars, G., Ranasinghe, R., Baart, F., Donchyts, G., & Aarninkhof, S. (2018). The state of the world's beaches. Scientific reports, 8(1), 1-11.

Luyten, Patrick, et al. "A new version of the European public domain code COHERENS." European Operational Oceanography: Present and Future 474 (2006).

Massey, T. C., Wamsley, T. V., & Cialone, M. A. (2011). Coastal storm modeling-system integration. In Solutions to Coastal Disasters 2011 (pp. 99-108).

Martzikos, N. T., Prinos, P. E., Memos, C. D., & Tsoukala, V. K. (2021). Statistical analysis of Mediterranean coastal storms. Oceanologia, 63(1), 133-148.

McGranahan, G., Balk, D., & Anderson, B. (2007). The rising tide: assessing the risks of climate change and human settlements in low elevation coastal zones. Environment and urbanization, 19(1), 17-37.

Michaud, H., Marsaleix, P., Leredde, Y., Estournel, C., Bourrin, F., Lyard, F., ... & Ardhuin, F. (2012). Three-dimensional modelling of wave-induced current from the surf zone to the inner shelf. Ocean Science, 8(4), 657-681.Mori, N., Yasuda, T., Arikawa, T., Kataoka, T., Nakajo, S., Suzuki, K., ... & Webb, A. (2019). 2018 Typhoon Jebi post-event survey of coastal damage in the Kansai region, Japan. Coastal Engineering Journal, 61(3), 278-294.

Morris, R. L., Konlechner, T. M., Ghisalberti, M., & Swearer, S. E. (2018). From grey to green: Efficacy of eco-engineering solutions for nature-based coastal defence. Global change biology, 24(5), 1827-1842.

Muthukumaran, A. E., & Ilamparuthi, K. (2006). Laboratory studies on geotextile filters as used in geotextile tube dewatering. Geotextiles and Geomembranes, 24(4), 210-219.

Nadaoka, K., & Kondoh, T. (1982). Laboratory measurements of velocity field structure in the surf zone by LDV. Coastal Engineering in Japan, 25(1), 125-145.

Nicholls, R. J., Wong, P. P., Burkett, V., Codignotto, J., Hay, J., McLean, R., ... & Saito, Y. (2007). Coastal systems and low-lying areas.

Nicholls, R. J. (2011). Planning for the impacts of sea level rise. Oceanography, 24(2), 144-157.

Nicholson, J., Broker, I., Roelvink, J. A., Price, D., Tanguy, J. M., & Moreno, L. (1997). Intercomparison of coastal area morphodynamic models. Coastal Engineering, 31(1-4), 97-123.

Niesing, H. (2005). EUROSION: Coastal erosion measures, knowledge and results acquired through 60 studies. Proceedings 'Dunes and Estuaries, 421-431.

Nordstrom, K. F., Armaroli, C., Jackson, N. L., & Ciavola, P. (2015). Opportunities and constraints for managed retreat on exposed sandy shores: Examples from Emilia-Romagna, Italy. Ocean & Coastal Management, 104, 11-21.

Paola, C., & Voller, V. R. (2005). A generalized Exner equation for sediment mass balance. Journa Pietrzak, J., Jakobson, J. B., Burchard, H., Vested, H. J., & Petersen, O. (2002). A three-dimensional hydrostatic model for coastal and ocean modelling using a generalised topography following co-ordinate system. Ocean Modelling, 4(2), 173-205.

l of Geophysical Research: Earth Surface, 110(F4).

Pietrzak, Julie, et al. "A three-dimensional hydrostatic model for coastal and ocean modelling using a generalised topography following co-ordinate system." Ocean Modelling 4.2 (2002): 173-205.

Pilkey, O. H., & Young, R. (2010). The rising sea. Island Press

Pranzini, E., & Williams, A. T. (Eds.). (2013). Coastal erosion and protection in Europe.

Pranzini, E., Wetzel, L., & Williams, A. T. (2015). Aspects of coastal erosion and protection in Europe. Journal of coastal conservation, 19(4), 445-459.

Plomaritis, T. A., Ferreira, Ó., & Costas, S. (2018). Regional assessment of storm related overwash and breaching hazards on coastal barriers. Coastal Engineering, 134, 124-133.

Ranasinghe, R. W. M. R. J. B., Larson, M., & Savioli, J. (2010). Shoreline response to a single shore-parallel submerged breakwater. Coastal Engineering, 57(11-12), 1006-1017.

Ranasinghe, R. (2016). Assessing climate change impacts on open sandy coasts: A review. Earth-science reviews, 160, 320-332.

Rangel-Buitrago, N., & Anfuso, G. (2011). An application of Dolan and Davis (1992) classification to coastal storms in SW Spanish littoral. Journal of Coastal Research, 1891-1895.

Rangel-Buitrago, N., Williams, A., Anfuso, G., Arias, M., & Gracia, A. (2017). Magnitudes, sources, and management of beach litter along the Atlantico department coastline, Caribbean coast of Colombia. Ocean & coastal management, 138, 142-157.

Reeve, D. E., & Spivack, M. (2001). Stochastic prediction of long-term coastal evolution. WIT Transactions on The Built Environment, 58.

Reniers, A. J., Roelvink, J. A., & Thornton, E. B. (2004). Morphodynamic modeling of an embayed beach under wave group forcing. Journal of Geophysical Research: Oceans, 109(C1).

Roelvink, D., Reniers, A., Van Dongeren, A. P., De Vries, J. V. T., McCall, R., & Lescinski, J. (2009). Modelling storm impacts on beaches, dunes and barrier islands. Coastal engineering, 56(11-12), 1133-1152.

Roelvink, D. (2011). A guide to modeling coastal morphology (Vol. 12). world scientific.

Roelvink, J. A., & Brøker, I. (1993). Cross-shore profile models. Coastal Engineering, 21(1-3), 163-191.

Ruiz-Martínez, G., Mariño-Tapia, I., Baldwin, E. G. M., Casarín, R. S., & Ortiz, C. E. E. (2016). Identifying coastal defence schemes through morphodynamic numerical simulations along the northern coast of Yucatan, Mexico. Journal of Coastal Research, 32(3), 651-669.

Rusu, Eugen, and C. Guedes Soares. "Modeling waves in open coastal areas and harbors with phase-resolving and phase-averaged models." Journal of Coastal Research 29.6 (2013): 1309-1325.

Sanchez-Vidal, A., Canals, M., Calafat, A. M., Lastras, G., Pedrosa-Pàmies, R., Menéndez, M., ... & Alcoverro, T. (2012). Impacts on the deep-sea ecosystem by a severe coastal storm. PLoS one, 7(1), e30395.

Schoonees, J. S., & Theron, A. K. (1995). Evaluation of 10 cross-shore sediment transport/morphological models. Coastal Engineering, 25(1-2), 1-41.Schoonees, T., Mancheño, A. G., Scheres, B., Bouma, T. J., Silva, R., Schlurmann, T., & Schüttrumpf, H. (2019). Hard structures for coastal protection, towards greener designs. Estuaries and Coasts, 42(7), 1709-1729.

Seabergh, W. C., & Kraus, N. C. (2003). Progress in management of sediment bypassing at coastal inlets: natural bypassing, weir jetties, jetty spurs, and engineering aids in design. Coastal Engineering Journal, 45(04), 533-563.

Senechal, N., & de Alegría-Arzaburu, A. R. (2020). Seasonal imprint on beach morphodynamics. Sandy Beach Morphodynamics, 461-486.

Servold, K. P., Webb, B. M., & Douglass, S. L. (2017). Effects of low-crested living shoreline breakwaters on wave setup. In Coastal Structures and Solutions to Coastal Disasters 2015: Resilient Coastal Communities (pp. 421-431). Reston, VA: American Society of Civil Engineers.

Shi, F., Kirby, J. T., Harris, J. C., Geiman, J. D., & Grilli, S. T. (2012). A high-order adaptive time-stepping TVD solver for Boussinesq modeling of breaking waves and coastal inundation. Ocean Modelling, 43, 36-51.

Shields, A. (1936). Anwendung der Aehnlichkeitsmechanik und der Turbulenzforschung auf die Geschiebebewegung. PhD Thesis Technical University Berlin.

Silva, R., Lithgow, D., Esteves, L. S., Martínez, M. L., Moreno-Casasola, P., Martell, R., ... & Rivillas, G. D. (2017, June). Coastal risk mitigation by green infrastructure in Latin America. In Proceedings of the Institution of Civil Engineers-Maritime Engineering (Vol. 170, No. 2, pp. 39-54). Thomas Telford Ltd.

Stive, M. J. F. (1980). Velocity and pressure field of spilling breakers. In Coastal Engineering 1980 (pp. 547-566).

Stive, M. J. F. (1985). A scale comparison of waves breaking on a beach. Coastal engineering, 9(2), 151-158.

Soulsby, R. (1997). Dynamics of marine sands.

Sweet, W., Park, J., Marra, J., Zervas, C., & Gill, S. (2014). Sea level rise and nuisance flood frequency changes around the United States.

Szmytkiewicz, M., Biegowski, J., Kaczmarek, L. M., Okroj, T., Ostrowski, R., Pruszak, Z., ... & Skaja, M. (2000). Coastline changes nearby harbour structures: comparative analysis of one-line models versus field data. Coastal Engineering, 40(2), 119-139.

Toimil, A., Losada, I. J., Camus, P., & Díaz-Simal, P. (2017). Managing coastal erosion under climate change at the regional scale. Coastal Engineering, 128, 106-122.

Toldo Jr, E. E., Nicolodi, J. L., Almeida, L. E. S. B., Corrêa, I. C. S., & Esteves, L. S. (2006). Coastal dunes and shoreface width as a function of longshore transport. Journal of Coastal Research, 390-394.

Valiente, N. G., Masselink, G., Scott, T., Conley, D., & McCarroll, R. J. (2019). Role of waves and tides on depth of closure and potential for headland bypassing. Marine Geology, 407, 60-75.

van der Kaaij, T., & Nieuwjaar, M. W. C. (1987). Sediment transport concentrations and sediment transport in case of irregular non-breaking waves with a current.

Van Rijn, L. C. (1984). Sediment transport, part I: bed load transport. Journal of hydraulic engineering, 110(10), 1431-1456.

Van Rijn, L. C. (1993). Principles of sediment transport in rivers, estuaries and coastal seas (Vol. 1006, pp. 11-3). Amsterdam: Aqua publications.

van Rijn, L. C. (2011). Coastal erosion and control. Ocean & Coastal Management, 54(12), 867-887.

van Rijn, L. C. V., Ribberink, J. S., Werf, J. V. D., & Walstra, D. J. (2013). Coastal sediment dynamics: recent advances and future research needs. Journal of hydraulic research, 51(5), 475-493.

Villaret, C., Hervouet, J. M., Kopmann, R., Merkel, U., & Davies, A. G. (2013). Morphodynamic modeling using the Telemac finite-element system. Computers & Geosciences, 53, 105-113.

Vikolainen, V., Flikweert, J., Bressers, H., & Lulofs, K. (2017). Governance context for coastal innovations in England: the case of sandscaping in North Norfolk. Ocean & coastal management, 145, 82-93.

Walker, R. A., & Basco, D. R. (2011). Application of coastal storm impulse (COSI) parameter to predict coastal erosion. Coastal Engineering Proceedings, (32), 23-23.

Wang, B., Pan, S. Y., Ke, R. Y., Wang, K., & Wei, Y. M. (2014). An overview of climate change vulnerability: a bibliometric analysis based on Web of Science database. Natural hazards, 74(3), 1649-1666.

Warner, John C., et al. "Development of a three-dimensional, regional, coupled wave, current, and sediment-transport model." Computers & geosciences 34.10 (2008): 1284-1306.

Watanabe, A., and M. Dibajnia. "Numerical modeling of nearshore waves, cross-shore sediment transport and beach profile change." Proc. IAHR Symp. on Mathematical Modelling of Sediment Transport In the Coastal Zone. 1988.

Waters, C. N., Zalasiewicz, J., Summerhayes, C., Barnosky, A. D., Poirier, C., Gałuszka, A., ... & Wolfe, A. P. (2016). The Anthropocene is functionally and stratigraphically distinct from the Holocene. Science, 351(6269).

Williams, A. T., Rangel-Buitrago, N., Pranzini, E., & Anfuso, G. (2018). The management of coastal erosion. Ocean & Coastal Management, 156, 4-20.

Wolinsky, M. A., & Murray, A. B. (2009). A unifying framework for shoreline migration: 2. Application to wave-dominated coasts. Journal of Geophysical Research: Earth Surface, 114(F1).

Zhang, K., Douglas, B. C., & Leatherman, S. P. (2004). Global warming and coastal erosion. Climatic change, 64(1), 41-58.

2 Coastal area models and applications in erosion-dominated areas

2.1 Context

Coastal zone is a significant geographical and particular region, since it gathers a wide range of social-human's activities and appears to be a complex as well as fragile system of natural variables. Coastal communities are increasingly at risk from serious coastal hazards, such as shoreline erosion and flooding related to extreme hydro-meteorological events: storm surges, heavy precipitation, tsunamis and tides. Coastal defence predisposed to coastline recession, due to the action of high tides and increased wave energy nearshore, may involve various protection structures to reduce or at least to mitigate shoreline erosion problems. Therefore, it is necessary to describe the driving mechanisms, which contribute to the destabilization of coastal environment. Within the context of the present research, a comprehensive analysis of hydro-morphodynamic phenomena was effectuated in study areas where intense erosion or sedimentation problems occur, applying advanced existing numerical devices.

A plethora of existing and new numerical devices was employed for the simulation of wave propagation, hydrodynamic circulation, wave-current interactions, sediment transport and morphology. The results of this study provide valuable insights into the mechanisms of storm-induced bathymetric changes and the performance of coastal defences to control beach erosion and maintain landscape integrity respecting a functional design and environmental or aesthetic values, within the context of an integrated coastal zone management. The state-of-the-art models that were employed here are: the MIKE21 DHI suite and XBeach model. In addition, a numerical formulation for sea--bed evolution, developed by Bouharguane and Mohammadi (2013) was utilized to assess sediment dynamics with and without the presence of coastal structures.

2.2 The investigation of form and processes in the coastal zone under extreme storm events - the case study of Rethymno, Greece

The recently recorded extreme storm and wave events in the European coast caused spectacular erosion of the shoreline (Castelle et al. 2015). Similarly, in our case study - the coastal city of Rethymno, in Greece, major flood and extreme wave events were encountered during the last few years, resulting in serious damages mainly on the Old Town of Rethymno and the east low-laying areas followed by significant erosion phenomena (Makropoulos et al. 2014b; Kragiopoulou et al. 2016; Tsoukala et al. 2016). Rethymno city was one of the eleven case study areas of PEARL (Preparing for Extreme And Rare events in coastal regions) project, an EU funded research project, which aims at developing adaptive risk management strategies for coastal communities focusing on extreme hydro-meteorological events, with a multidisciplinary approach integrating social, environmental and technical research and innovation so as to increase the resilience of coastal regions all over the world.

2.2.1 Case Study characteristics

The area under study is located at the Prefecture of Rethymno, which is one of the four Prefectures of Crete in Greece. Rethymno is a coastal city and its population stands at 32,468 inhabitants with a density of 140 population/km2. As the third most populous urban area in the island of Crete, commercial, administrative, cultural and tourist activities are being developed along the north coast where the city is located. The mean absolute altitude is 15 m (Makropoulos et al. 2014a). The case study area includes the port of Rethymno, located in the Northern area of Crete within the homonymous bay and the adjacent coastal area on the east (a total area of about 19 km2) with a coastline length of approximately 8.8 km (Figure 2-1) and a maximum depth equal to 30 m.

Flooding has always been an important issue for the coastal city of Rethymno. Major flood events were encountered throughout the years, resulting in serious damages mainly in city centre and the east low-lying areas. In addition, changes in wind conditions, potentially due to climatic changes, lead to a more frequent occurrence of storm events. The extreme weather conditions of strong winds drive storm waves that can be combined with flash floods from ephemeral streams. These storm-induced flooding usually occurs through three basic processes: 1) overflowing or inundation, (2) wave overtoppin, causing floods intermittently due to the wave run-up (3) barrier breaching.

Energetic wave conditions close to the land trigger violent wave overtopping discharges along the windward breakwaters of the harbour, as shown in Figure 2-2 - Figure 2-3, affecting the stability of breakwaters and port facilities as well as human safety. An additional severe effect of wave overtopping is the flood inundation of the harbour's surface area and the surrounding roads. The quantities of seawater (Figure 2-2) that penetrates from the west (Parking area) during those storm events, overflows the harbour's surface area, as well as the wider coastal area, causing disruption to loading and unloading operations, damage to the port facilities and the cargo, traffic problems and damage to coastal shops and restaurants.

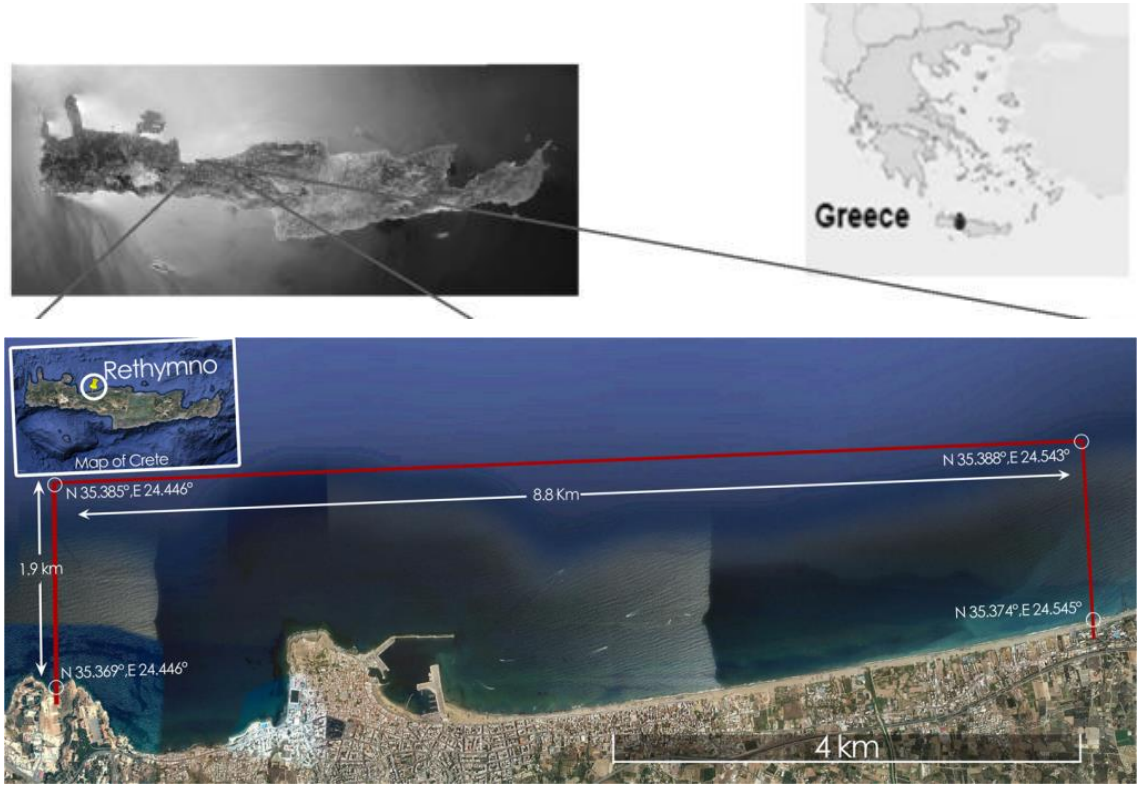

Figure 2-1 Location, coordinates and size of the case study area - Satellite image from Google Earth 31/08/2015 (Google Earth Engine Team 2015)

Moreover, the adjacent sandy beaches are exposed to intense erosion, spoiling the coastal site and affecting the tourism's contribution to local economy. The coastal bed is comprised mostly of fine sand, with a median sediment diameter of D_{50} =0.15 mm, which was used for the morphological simulations. These fine sand materials render the coast especially vulnerable against erosive wave sequences, as sand particles can be easily transported due to their light

special specific weight. A shoreline retreat of several meters has been observed in recent years, which can be validated by available field measurements and satellite photos (Karambas, 2010).

The combined occurrence of extreme hydro-meteorological events poses a real threat to Rethymno's community, while it emphasizes the need for specific actionable roadmaps that will enhance the existing infrastructure and operational strategies against the danger of flood. A multidisciplinary approach, involving monitoring of swash dynamics on structures and beaches, evaluation of land-use and land-cover change due to urban expansion and unplanned construction, implementation of soft and nature-based techniques is required to prevent floods and subsequent coastal erosion. This wide range of actions is necessary for helping stakeholders to identify areas that are sensitive to floods and also to define efficient flood management strategies and socio-economic measures for Rethymno.

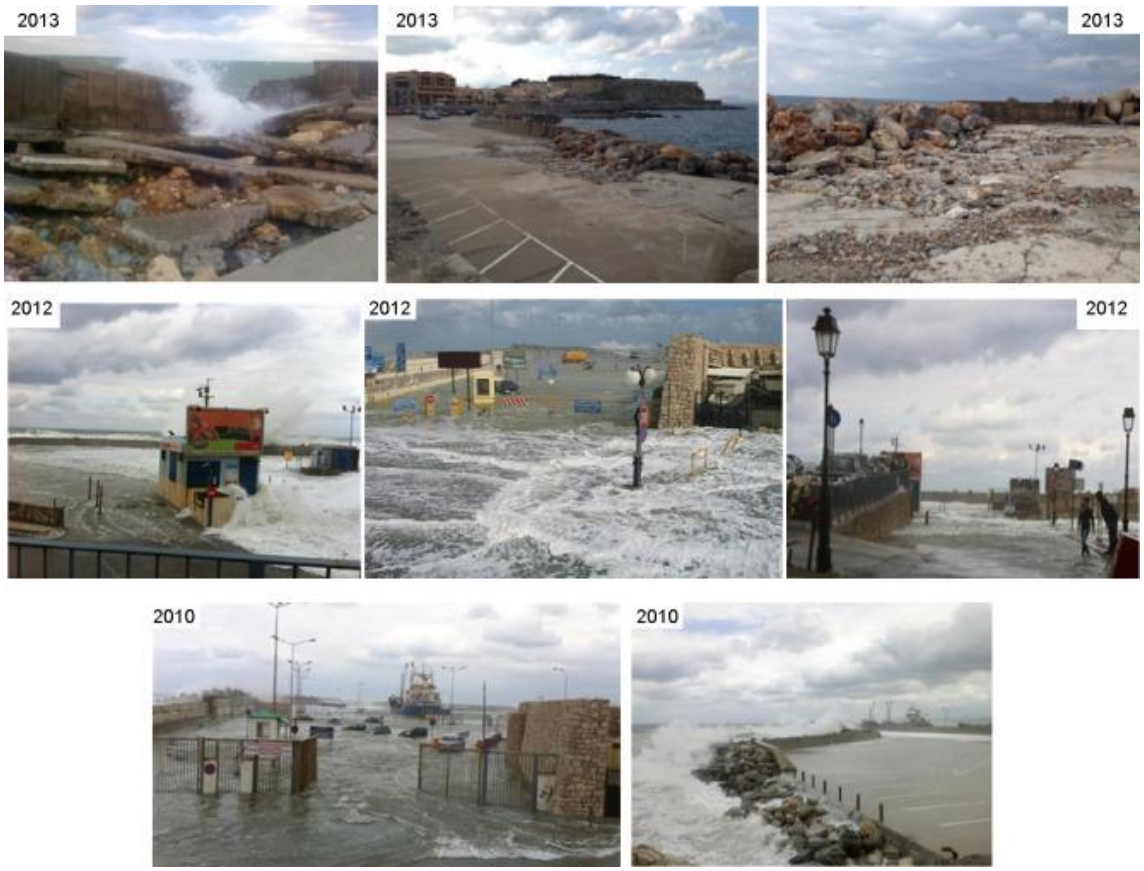

Figure 2-2 Recent floods at the harbour area of Rethymno (2010–2013).

Figure 2-3 Recent floods at the harbour area of Rethymno (2019).

2.2.2 Prevailing environmental conditions

For the needs of our research, a number of wind and wave hindcast and forecast data were analysed in order to determine the wave prevailing conditions at the offshore areas of Rethymno, these data were retrieved from the work of Tsoukala et al., 2016 and they had initially been presented in the study of Velikou et al., 2014 - CCSEAWAVS project. In those projects, wind regional and local measurements were utilized to force a global wave model in the north offshore zone of our study area and a 3-level SWAN-based scheme was uilized (Athanassoulis et al., 2014), the nested areas are illustrated in Figure 2-4. This technique was developed in the framework of Thales project CCSEAWAVS (Prinos, 2014), which aimed to estimate the effects of climate change on sea level and wave climate of the Greek seas, the coastal vulnerability and the safety of coastal and marine structures. This simulation scheme used past and future projections climatic wind fields for the estimation of wave characteristics with resolution 0.2 * 0.2 degrees in the Mediterranean basin. These data provided boundary information for repeating the simulation using a finer mesh 0.05*0.05 degrees inside an Eastern Mediterranean subsection. Then, a high-resolution 0.005*0.005 degrees mesh was applied in

the selected coastal region of Rethymno. Details of the methodology were described in Athanassoulis et al. (2015).

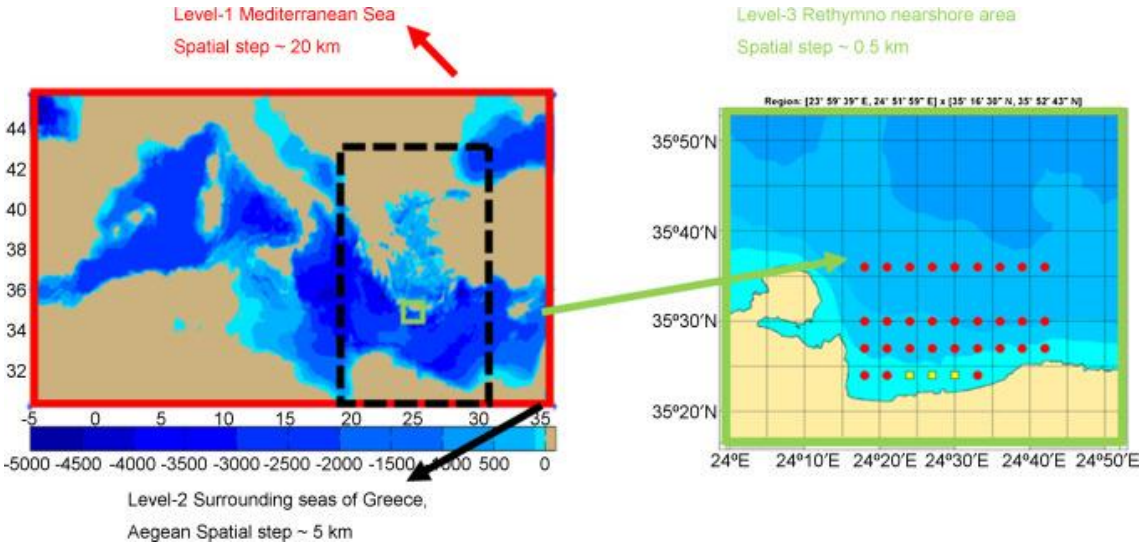

Figure 2-4 Estimation of offshore wave characteristics using a 3-level downscaling approach (Tsoukala et al., 2016).

The distribution of significant wave height, wave peak period and mean wave direction in a water depth of about 100 meters in the offshore area of our case study, for one past (1961-2000) and two bi-centurial future periods (2001-2050, 2051-2100) is shown in Figure 2-5. Overall, the projected future distributions remain very close to those of the past period. Some weak but noticeable discrepancies can be identified during period 2051-2100, with higher occurrence of waves originating from the North sector. Although relatively small, this probability shift towards southward waves can be significant due to the North-facing orientation of Rethymno coast.

Using the available offshore wave data, a categorization of storm events was achieved, in order to treat the storm surges in-group and not individually and, associating them with respective factors of coastal vulnerability for the needs of the present research. This was done by following the definition and identification of the storms through the energy content as proposed by Dolan and Davis (1992). The classification was accomplished into five classes: I - weak, II - moderate, III- significant, IV - severe and V - extreme. The first step before applying this approach was the characterization of the forcing. A storm can be defined as the event exceeding a minimum significant wave height (e.g. Hs > 2 m) and with a minimum duration of 6 h (Li et al., 2014, Michele et al., 2007).

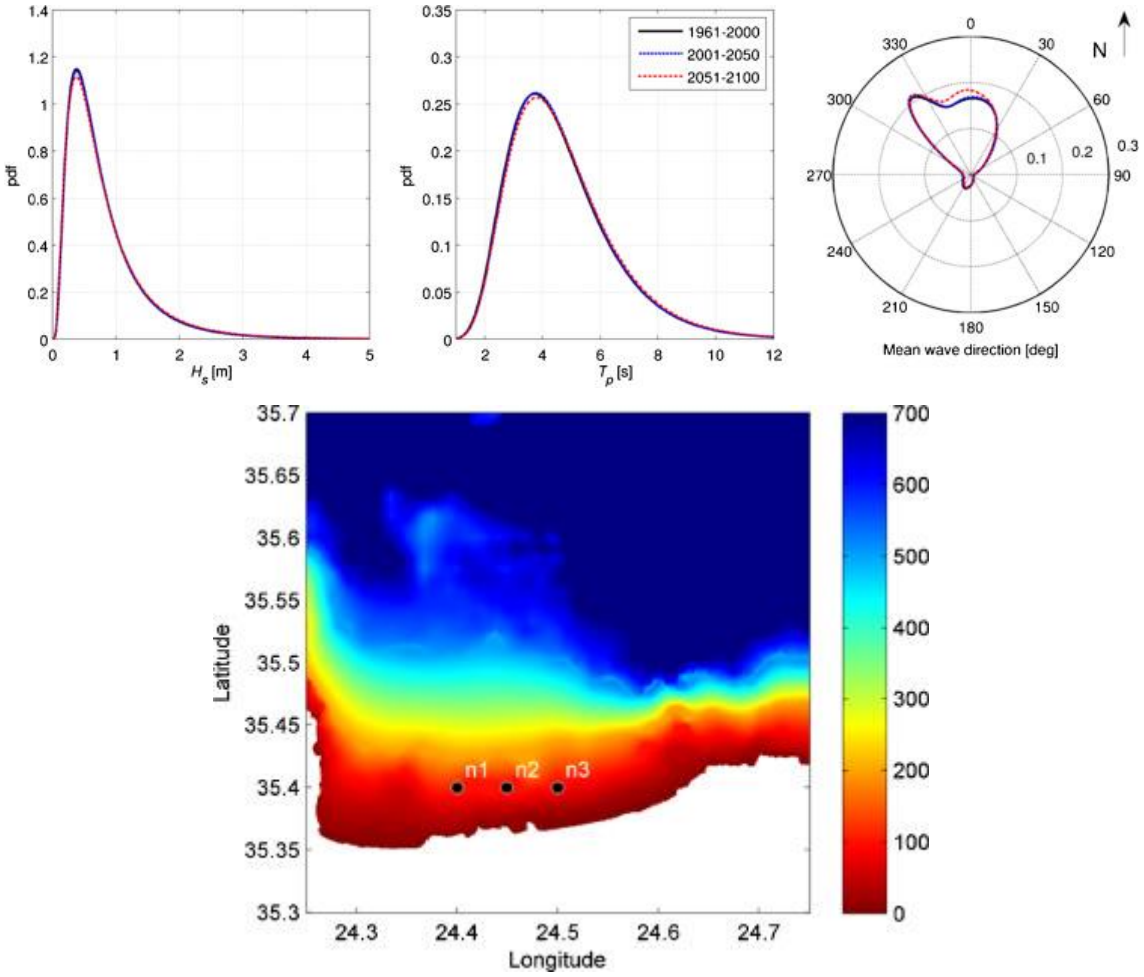

Figure 2-5 Probability density functions for the significant wave height Hs (left panel), peak wave period Tp (central panel) and mean wave direction (right panel), for three time periods at points ni,i = 1–3(down) (Tsoukala et al., 2016).

The threshold of significant wave height (Hs) was considered here to be 2 m in order to describe rare events with only 10% of total wave heights and thus defined as the 90th percentile of the data set (Rangel-Buitrago and Anfuso, 2011). The energy content of each event can then be estimated as follows:

$$E = \int_{t1}^{t2} H_S^2 dt$$

Where, (*t1–t2*) is the storm duration and H_s is always greater than H_s threshold.

The above analysis was divided into two periods: 1960-2000 (past climate) and 2000-2100 (future climate). The results of the average wave height, period and duration in n2 grid point, of Figure 2-5, for each storm class are given in the following Tables. Furthermore, Martzikos and Afentoulis, 2017, carried out a further analysis and categorization of storms in this coastal area.

North wind direction 1960–2000							
Storm class		H_s range [m]	T_p range [s]	Average H_s [m]	Average T_p [s]	Average duration [h]	No. of events
I	Weak	2.0–4.6	6.2–9.4	2.5	7.7	14.20	318
II	Moderate	2.0–5.7	6.5–10.0	2.9	8.1	34.50	27
III	Significant	2.0–4.6	7.5–9.6	3.6	8.1	44.25	4
IV	Severe	2.0–5.6	6.7–10.7	3.3	8.3	72.50	6
V	Extreme	–	–	–	–	–	0

Table 2 Storm events for the period 1960–2000 N direction.

North wind direction 2000–2100							
Storm class		H_s range [m]	T_p range [s]	Average H_s [m]	Average T_p [s]	Average duration [h]	No. of events
I	Weak	2.0–5.3	6.4–10.1	2.5	7.7	14.13	823
II	Moderate	2.0–5.0	6.7–9.9	2.7	8.0	42.03	94
III	Significant	2.0–6.0	6.9–10.3	3.0	8.2	61.84	13
IV	Severe	2.0–5.4	6.4–10.0	3.2	8.2	81.38	8
V	Extreme	2.0–5.0	7.8–9.7	4.2	9.1	72.00	1

Table 3 Storm events for the period 2000–2100 N direction.

Northwest wind direction 1960–2000							
Storm class		H_s range [m]	T_p range [s]	Average H_s [m]	Average T_p [s]	Average duration [h]	No. of events
I	Weak	2.5–4.6	6.2–9.4	2.5	7.7	11.40	10

Table 4 Storm events for the period 1960–2000 NW direction.

Northwest wind direction 2000–2100							
Storm class		H_s range [m]	T_p range [s]	Average H_s [m]	Average T_p [s]	Average duration [h]	No. of events
I	Weak	2.0–4.6	6.2–9.4	2.5	7.7	10.55	33
II	Moderate	2.0–5.7	6.5–10.0	3.0	8.1	39.00	1

Table 5 Storm events for the period 2000–2100 NW direction.

Northeast wind direction 1960–2000							
Storm class		H_s range [m]	T_p range [s]	Average H_s [m]	Average T_p [s]	Average duration [h]	No. of events
I	Weak	2.0–2.8	6.2–9.4	2.3	7.7	10.55	24
II	Moderate	2.0–3.1	6.5–10.0	2.6	8.1	24.00	14
III	Significant	2.0-3.7	6.9-11.0	2.8	8.4	31.00	8

Table 6 Storm events for the period 1960–2000 NE direction.

Northeast wind direction 2000–2100							
Storm class		H_s range [m]	T_p range [s]	Average H_s [m]	Average T_p [s]	Average duration [h]	No. of events
I	Weak	2.0–2.9	6.2–9.4	2.3	7.7	10.55	24
II	Moderate	2.0–3.5	6.5–10.0	2.6	8.1	24.00	14
III	Significant	2.0-3.8	7.0-11.2	2.9	8.4	31.00	8

Table 7 Storm events for the period 2000–2100 NE direction.

For the investigation of nearshore morphodynamics, the necessary wave condition at the offshore boundary of the local geographical area were derived from a downscaling approach, based on the transformation of global wind fields carrying the effect of climate change and affecting nearshore wave conditions. The obtained offshore wave parameters (directional spectrum) presented in the study of Tsoukala et al., 2016 were used to determine the input parameters of the nearshore models (MIKE21 and XBeach) which were applied for the transformation of the offshore information to shallower regions, up to the coast. The overall duration of the selected storm surge scenarios is equal to the real duration of specific storm events as obtained in a previous study (Kragiopoulou et al. 2016), in which four storm scenarios have been identified as worst-case.

Two selected scenarios accounting for the largest incoming wave energy, attributable to North and North-East incident wave directions, were selected and simulated within the present study, considering that the coastline is well protected from waves incoming from the north-west direction because of the presence of the jetties and the nearby hill. Thus, the N-direction storm event with highest identified significant wave height (H_S *= 4.95 m)* and storm duration (*D = 72 h)*, and the NE-direction storm event with highest identified significant wave height (H_S *= 2.66* m) and storm duration (*D = 24 h)*, are selected to be simulated. The basic characteristics of the two storm scenarios are listed below in Table 8, while the energy density spectra for the incident waves of the respective scenarios are illustrated in Figure 2-6

Direction	H_S range (m)	T_p range (s)	H_S Average (m)	T_p Average (s)	Event Duration (h)
N	2.46-4.95	7.84-9.65	4.18	9.07	72
NE	2.07-2.66	6.78-8.96	2.41	8.16	24

Table 8 Characteristic storm events in the case study area.

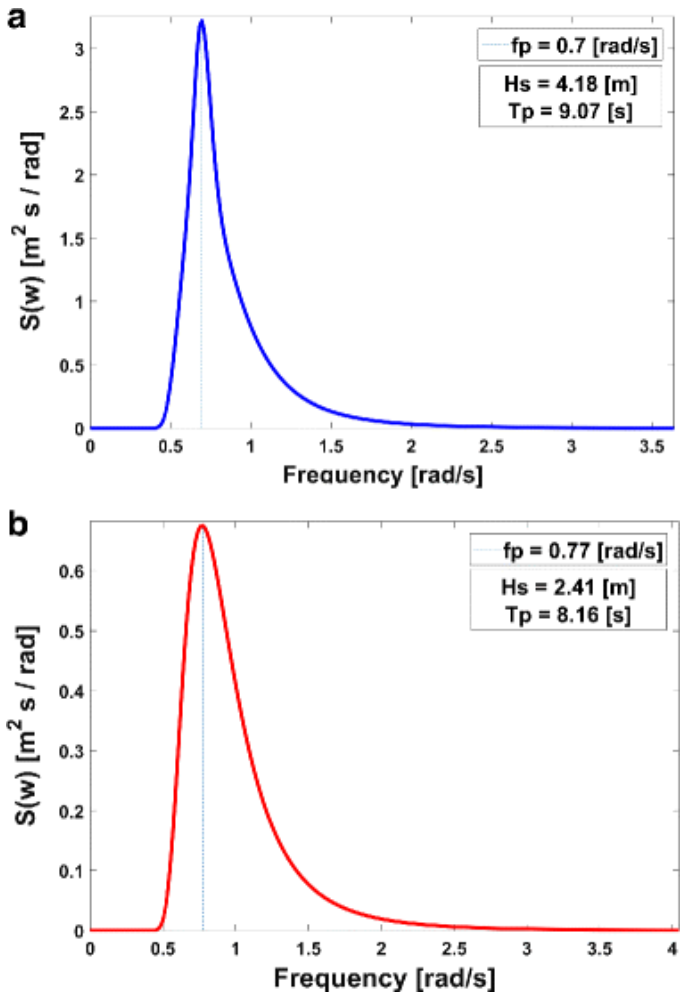

Figure 2-6 Energy density spectra for the average input wave characteristics for (a) the North Storm Scenario and (b) the North-East Storm Scenario (Afentoulis et al., 2017).

2.2.3 Coastal Processes Assessment Using Numerical Modelling Approaches

Within this context, the precise assessment of coastal physical processes, using advanced numerical models, was carried out to estimate the vulnerability of the coast. MIKE 21 (DHI 2015a, b) and XBeach (Roelvink et al. 2009; Smit et al. 2010) models were employed to simulate wave propagation, wave-induced currents, sediment transport and morphology, under extreme wave conditions in the coastal zone of Rethymno. These 2DH-numerical models can output several wave parameters, such as wave heights, velocities of particles, time-averaged eulerian velocities, radiation stresses, groundwater discharges, sediment transport rates and morphological changes of the sea bottom. In previous studies, these models were combined through a nesting method, in which MIKE 21 offshore wave calculations served as an input to XBeach simulation in the nearshore area (Carevic et al. 2016; Ruiz de Alegria-Arzaburu et al. 2011). Here, a different approach was followed. The models were tested on their ability to assess hydrodynamic processes and sediment transport by comparing their results. In such manner,

the performance of each model can be evaluated, while agreement between the two models results provides reliability in the assessment of physical processes.

2.2.3.1 Models description and set-up

2.2.3.1.1 MIKE21 Coupled Model FM

MIKE 21 by DHI Water and Environment is a state of the art numerical model, used here to evaluate waves, hydrodynamics, sediment transport and equivalent bed evolution, through the coupling of its SpectralWaves (SW) module with the Hydrodynamics (HD) and Sediment Transport (ST) aspects of the MIKE 21 Coupled Model FM . This process-based numerical model has been used extensively in a variety of coastal engineering applications, with and without the presence of coastal protection structures. The MIKE21 Coupled model FM suite includes several complementary numerical models and tools three of which were used for the purpose of this research:

- MIKE21 SW, a 3rd generation spectral wave model based on the conservation of the wave action balance, suited for the propagation and transformation of waves in the coastal zone.
- MIKE21 HD, a depth-averaged hydrodynamic model based on the Reynolds averaged Navier-Stokes equations of motion (RANS), for the description of the nearshore circulation.
- MIKE21 ST, a sand transport and morphology updating model, used to calculate sediment transport rates and ultimately the morphological bed evolution.

These devices are directly coupled, allowing for the interaction between waves and currents and the effect of bed level changes in waves and hydrodynamics. The calculations are performed in an unstructured finite element mesh, which is especially suitable for calculations with a high degree of flexibility, reducing the computational burden and offering a more precise representation of the coastline and complex topography features. In the following subsections the governing equations of each model will be presented.

2.2.3.1.2 MIKE21 SW model

MIKE 21 SW model is a 3rd generation spectral wave model suited for the propagation of waves in the oceanic scale and in nearshore areas. The governing equation of the model is based on the principle of conservation of the wave action-balance, which reads in Cartesian coordinates:

$$\frac{\partial N}{\partial t} + c_x \frac{\partial N}{\partial x} + c_y \frac{\partial N}{\partial y} + c_\sigma \frac{\partial N}{\partial \sigma} + c_\theta \frac{\partial N}{\partial \theta} = \frac{S}{\sigma} \tag{2.1}$$

where $N(x,y,\sigma,\vartheta,t)$ is the wave action density, c_x, c_y are the propagation velocities in the spatial domain, c_σ is the propagation velocity in the frequency domain and c_θ is the propagation velocity in the directional domain. All the aforementioned transfer velocities are computed according to the linear wave theory . In the right part of Equation (13) the term *S* denotes the source and sink terms of the energy balance equation (e.g. generation due to wind, white-capping dissipation, non-linear wave interactions, depth-induced breaking etc).

The discretization in the geographical and spectral domain is carried out using a finite volume cell-centered method. In frequency space, a logarithmic discretization is used, whereas in the directional space an equidistant division is used. The time integration is performed based on a fractional step approach. The propagation step is at the first level solved without taking the source terms into account, utilizing an explicit Euler scheme. To deal with severe stability restrictions, a multi-sequence integration scheme is implemented, allowing for the use of large time steps for the wave propagation and spectrum evolution. On the second level the source term integration step is solved using an implicit method.

2.2.3.1.3 MIKE21 HD model

The hydrodynamic and transport model MIKE21 HD is based on the solution of the depth-integrated shallow water equations, expressed by the continuity and momentum equations in the Cartesian space:

$$\frac{\partial h}{\partial t} + \frac{\partial h\bar{u}}{\partial x} + \frac{\partial h\bar{v}}{\partial y} = hS \tag{2.2}$$

$$\begin{aligned}\frac{\partial h\bar{u}}{\partial t} + \frac{\partial h\bar{u}^2}{\partial x} + \frac{\partial h\bar{u}\bar{v}}{\partial y} &= f\bar{v}h - gh\frac{\partial \eta}{\partial x} - \frac{h}{\rho}\frac{\partial p_a}{\partial x} - \frac{gh^2}{2\rho}\frac{\partial \rho}{\partial x} \\ &+ \frac{\tau_{sx}}{\rho} - \frac{\tau_{bx}}{\rho} - \frac{1}{\rho}\left(\frac{\partial S_{xx}}{\partial x} + \frac{\partial S_{xy}}{\partial y}\right) + \frac{\partial}{\partial x}(hT_{xx}) + \frac{\partial}{\partial y}(hT_{xy}) + hu_s S\end{aligned} \tag{2.3}$$

$$\begin{aligned}\frac{\partial h\bar{v}}{\partial t} + \frac{\partial h\bar{u}\bar{v}}{\partial x} + \frac{\partial h\bar{v}^2}{\partial y} &= f\bar{u}h - gh\frac{\partial \eta}{\partial y} - \frac{h}{\rho}\frac{\partial p_a}{\partial y} - \frac{gh^2}{2\rho}\frac{\partial \rho}{\partial y} \\ &+ \frac{\tau_{sx}}{\rho} - \frac{\tau_{bx}}{\rho} - \frac{1}{\rho}\left(\frac{\partial S_{xy}}{\partial x} + \frac{\partial S_{yy}}{\partial y}\right) + \frac{\partial}{\partial x}(hT_{xy}) + \frac{\partial}{\partial y}(hT_{yy}) + hv_s S\end{aligned} \tag{2.4}$$

Where h is the total depth of the water column, $\bar{u}$ and $\bar{v}$ are the depth-averaged velocity components in the x and y direction respectively, η is the surface elevation, f is the Coriolis

parameter, ρ is the water density, S_{xx}, S_{yy}, S_{xy}, are components of the radiation stress tensor, p_a is the atmospheric pressure, S being the magnitude of point sources, with u_s, v_s being the velocity vectors of the point discharge and T_{xx}, T_{yy}, T_{xy} denoting lateral stresses including viscous, turbulent friction and differential advection.

2.2.3.1.4 MIKE21 ST model

MIKE 21 ST model calculates the sediment transport rates and the morphological bed evolution either in a pure current case, or under the combined effect of waves and currents. The model is valid for sand grains and often overestimates shingle-sized material transport rates. For the case of wave and current induced sediment transport, the rates are calculated by linear interpolation on an externally formed sediment transport table. The core of this utility is a quasi three-dimensional sediment transport model (STPQ3D). The model calculates the instantaneous and time-averaged hydrodynamics and sediment transport in the two horizontal directions.

The determination of the bed level evolution is the rate of bed level change $\frac{\partial z}{\partial t}$ at the element cell centers. This parameter is obtained by solving the well-known equation of sediment continuity, denoted as Exner equation:

$$\frac{\partial z}{\partial t} = -\frac{1}{(1-n)}\left(\frac{\partial q_x}{\partial x} + \frac{\partial q_y}{\partial y} - \Delta S\right) \quad (2.5)$$

Where n is the sediment porosity, S_x, S_y is the total load sediment transport rates in the x and y direction respectively and ΔS is a sediment source or sink term. The new bed level is then obtained by a forward in time differential scheme.

2.2.3.1.4.1 MIKE21 SETUP

The aforementioned MIKE21 modules were applied on a triangulated flexible mesh generated on the wet part of the case study area, while the bathymetrical data were interpolated over this computational domain, as shown in Figure 2-1, and covering a total surface of 14 km^2.

Figure **2-7** shows the initial bathymetry used in the model runs. Initial conditions for the storms events are waves which enter the computational domain through the northern boundary, as it is presented in Figure 2-8. Different levels of spatial resolution were applied in order to capture wave non-linear effects close to the shore with a wide spatial step offshore, while keeping the computational cost at a minimum. The ST module simulated sediment transport phenomena due to the combined action of wave and currents, and predicted the

morphological evolution of the seabed. In the model run, the sediment particles are treated as non-cohesive, representing uniform sand with porosity of 0.4 and size of 0.2 mm, the main input parameters that were used for MIKE21 and XBeach model similarly are listed in Table 9.

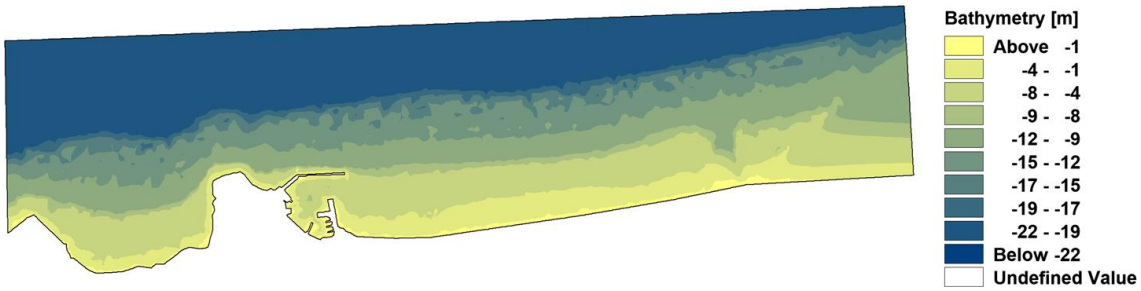

Figure 2-7 Initial Bathymetry of MIKE 21 model (Afentoulis et al., 2017).

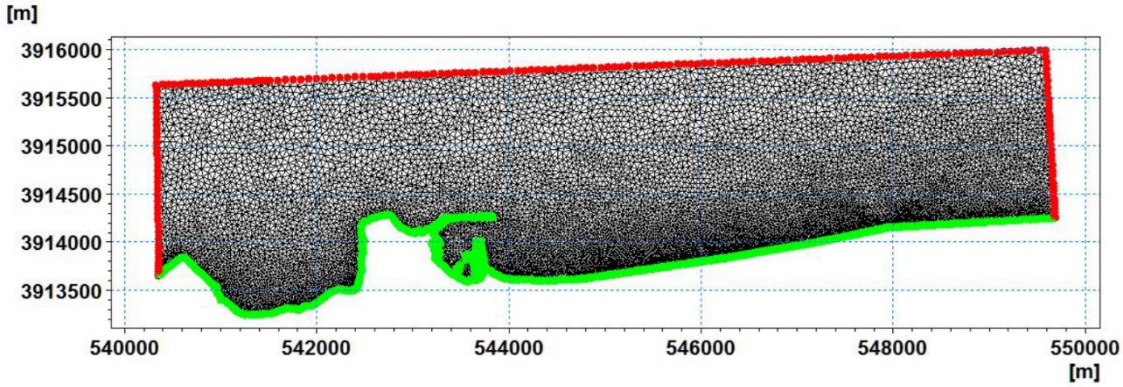

Figure 2-8 Mike 21 Unstructured Mesh with Boundary conditions (Afentoulis et al., 2017).

Mean Grain Diameter	Porosity	Relative Sediment Density	Bed Resistance - Chezy No.
0.2 mm	0.4	2650 kg/m ^{3}	32 m $^{0.5}$/s

Table 9 Main input parameters for MIKE 21 and XBeach.

2.2.3.1.5 XBeach model

XBeach (Roelvink et al., 2009) is an open-source code, developed to model near-shore wave propagation, hydrodynamics, sediment transport and morphodynamics. It has been initially tailored for storm impacts on sandy beaches in the United States (McCall et al., 2010), but has been widely used for the evaluation of morphodynamic conditions for sandy beaches (Mickey et al., 2020; Afentoulis et al., 2017). In recent years, important features were added, such as an efficient phase-resolving wave solver, allowing to estimate intra-wave motions on the incident-band wave time scale. XBeach in Surf Mode does not solve the short waves individually, thus, their phase information cannot be obtained. XBeach-SB calculates short wave motions using a

wave action equation with time-dependent forcing. This equation solves the variation in the short wave envelope on the scale of wave groups:

$$\frac{\partial A}{\partial t}+\frac{\partial cxA}{\partial y}+\frac{\partial cyA}{\partial y}+\frac{\partial c\theta A}{\partial \theta}=-Dw+Df\sigma, \tag{2.6}$$

$$A(x,y,t,\theta)=\frac{Sw(x,y,t,\theta)}{\sigma(x,y,t)} \tag{2.7}$$

Where, A is the wave action density, c is the group velocity associated with the peak frequency, θ represents the angle of incidence with respect to the x-axis, and Dw and Df are dissipation terms for the respective waves and bottom friction [34]; Sw is the wave energy density in each directional bin, and intrinsic frequency σ is calculated as:

$$\sigma=\sqrt{gktanhkh} \tag{2.8}$$

The low-frequency waves and mean flows are solved in the time domain using the nonlinear shallow water equation as follows:

$$\frac{\partial \eta}{\partial t}+\frac{\partial hu^L}{\partial x}+\frac{\partial hv^L}{\partial y}=0, \tag{2.9}$$

$$\frac{\partial u^L}{\partial t}+u^L\frac{\partial u^L}{\partial x}+v^L\frac{\partial u^L}{\partial y}-fv^L-vh\left(\frac{\partial^2 u^L}{\partial x^2}+\frac{\partial^2 u^L}{\partial y^2}\right)=\frac{\tau_{sx}}{\rho h}-\frac{\tau^E bx}{\rho h}-g\frac{\partial \eta}{\partial x}+\frac{Fx}{\rho h}, \tag{2.10}$$

$$\frac{\partial u^L}{\partial t}+u^L\frac{\partial u^L}{\partial x}+v^L\frac{\partial u^L}{\partial y}-fv^L-vh\left(\frac{\partial^2 u^L}{\partial x^2}+\frac{\partial^2 u^L}{\partial y^2}\right)=\frac{\tau_{sy}}{\rho h}-\frac{\tau^E bx}{\rho h}-g\frac{\partial \eta}{\partial x}+\frac{Fy}{\rho h} \tag{2.11}$$

where u^L and v^L represent the Lagrangian velocities, vh is the horizontal viscosity, f is the Coriolis coefficient, τ_{sx} and τ_{sy} are wind shear stresses, $\tau^E bx$ and $\tau^E by$ are the bed shear stresses determined by the Chezy coefficient C. η is the water level and h is the water depth. ρ represents the water density and g the gravitational constant. F_x and F_y are the wave forces due to radiation stress.

In the present version of XBeach, two sediment transport formulations are available. For both methods the total equilibrium sediment concentration is calculated using a depth-averaged advection-diffusion scheme with a source-sink term. In this study, the Soulsby-Van Rijn sediment transport formulation (keyword: form = soulsby_vanrijn) was employed.

XBeach SETUP

The computational grid, over which the available bathymetrical and topographical data were interpolated, is constructed with spatial dimensions of 1500 × 5160 m in cross-shore- and alongshore direction, respectively, while the spatial steps are uniforms ($dx = dy = 5m$). This domain has a total surface that is relatively smaller than that of MIKE 21, because of the model's limitation to use a structured grid. A 3D view of the initial bathymetry is illustrated in Figure 2-9. Similarly to the set-up of MIKE21 ST module, the sediment properties represent here a uniform sand with a porosity of 0.4 and a particle size of 0.2 mm (Table 9). XBeach is 2DH model that runs under stationary and hydrostatic conditions, for simulation of the two selected storm scenarios (Table 8). This configuration is based on a sequence of time-varying wave groups generated using a JONSWAP spectrum (keyword: *wbctype* = *jons_table*). As in the case of MIKE21, waves can enter in the computational domain through the northern offshore open boundary, which is parallel to the shoreline. For a more precise investigation of the flow effects on wave propagation nearshore, the wave-current interaction option was activated (keyword: *wci* = 1). MPI (Message Passing Interface) function was enabled, allowing XBeach grid to be divided into parts, which are simulated on different cores, speeding up the total simulation time. Wave height, velocities, sediment transport and bathymetry updates are the output variables of interest for the selected wave scenarios.

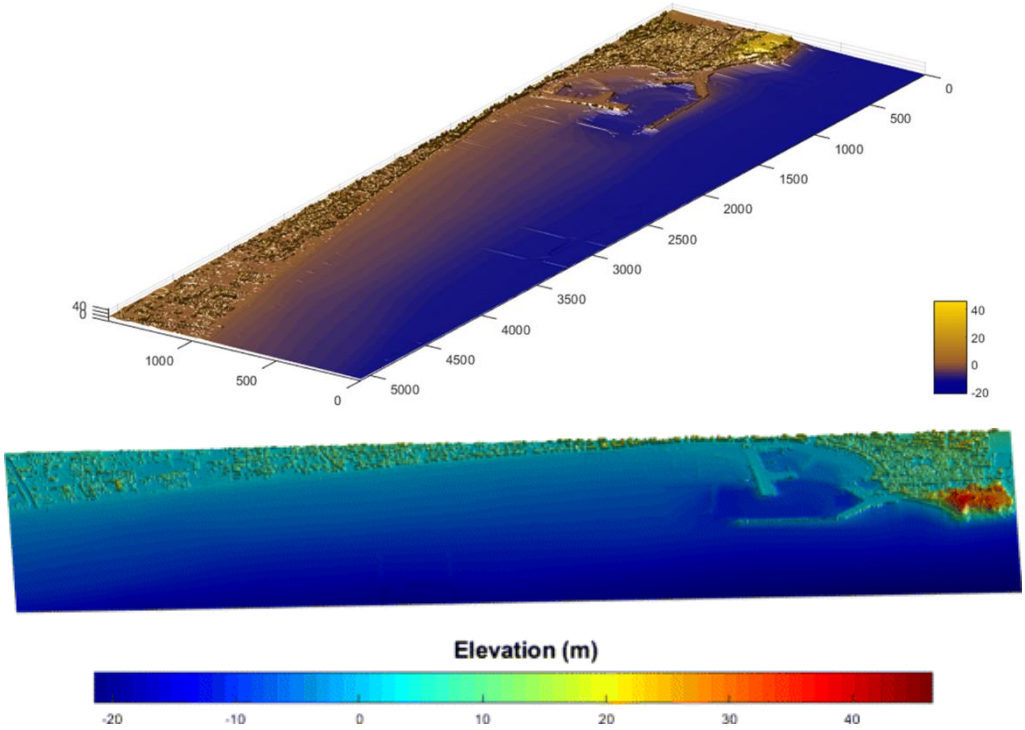

Figure 2-9 3D view of initial bathymetry of XBeach model (Afentoulis et al., 2017).

2.2.3.2 *Model Performance and Comparison*

The two models offer different capabilities of simulating the coastal response during extreme storm events. The capacity of the models to simulate basic nearshore processes is compared in Table 10. Regarding the simulation of sediment transport under storm events, XBeach provides key information on the cross-shore limits, while MIKE 21 provides important information on alongshore scheme impacts (Williams et al. 2014).

Additionally, the two models differentiate on how deep water wave propagation can be predicted. MIKE21 SW module takes into consideration a number of phenomena, occurring in deep water, such as white capping and nonlinear energy transfer amongst the different wave components of a directional-frequency spectrum that plays a crucial role for the temporal and spatial evolution of a wave field. On the other hand, XBeach model does not sufficiently account for these phenomena. Finally, an important aspect in order to accurately simulate the hydrodynamic processes, is wave-current interaction. XBeach provides a limited representation of this process, when non-stationary conditions was not considered in 'surf beat' mode, as it was still on experimental state at the time of writing of this research. More specifically, XBeach in surf beat mode is based on a short-wave averaged and wave-group resolving concept, which put significant difficulties in predicting nonlinear wave-wave interactions, as well as intra-wave effects on hydrodynamics and morphology. Additionally, diffraction and dispersion phenomena cannot be adequately simulated using XB model in surfbeat mode. Although small-scale morphological processes in the inner surf and swash zone can be precisely evaluated using this device, as special focus was placed on avalanching and slope-limited sediment mobilization, while the forcing of wave breaking-induced roller energy dissipation on the hydrodynamic circulation, was considered in the calculations of gradients of radiation stresses. Moreover, overwash, inundation, vegetation and hard structure impact, and breaching were included in computations.

Simulated processes	Mike21	XBeach SB
Shoaling and Refraction	✓	✓
Wave Breaking	✓	✓
Wave diffraction	✓	×
White Capping	✓	×
Wave-Current interaction	✓	✓
Alongshore Sediment Transport	✓	✓
Cross-shore Sediment Transport	✓	✓

Table 10 Comparison of the two models: capacity to simulate basic processes.

2.2.3.3 Numerical predictions and proposed solution methods.

The obtained numerical findings concerning the parameters of wave heights, wave-induced current velocities, sediment transport rates and bottom evolution. These variables are time-averaged over several wave periods and they were extracted after the simulations have reached a quasi-steady state. The first 30 minutes were omitted from the analysis to allow the waves to pass through the domain.

2.2.3.3.1 Wave propagation

The maps of computed wave height across the computational domain, as generated during MIKE21 SW and XBeach simulations, are illustrated in Figure 2-10. These Figures depicts the distribution significant wave height (H_S) and the root mean square wave height (H_{rms}) for MIKE21and XBeach model results, respectively.

Wave height value range is similar in the output of the two models, taking into account that H_S is slightly higher than H_{rms} ($H_S \approx 1.41\ H_{rms}$). However, MIKE 21 wave heights tend to steadily decrease as waves propagate nearshore, while in XBeach the wave decay is not directly proportional to the decrease of the water depth. This is due to the nature of the wave generator, employed by XBeach model, which incroporates the role of different directional bins (keyword:'multi-dir with a directional bin size of 10 deg.'). The way the directional wave groups are treated leads to an excessive smoothing of the longshore wave groupiness, whilst the wave energy from different directional bins is added up, without considering the interference of the distinct wave components (Roelving et al., 2018). The final distribution of wave energy (or action) in x, y and θ space can be achieved by in-stationary runs where the time-varying wave energy balance equation is solved, as it is described in paragraph 2.2.3.1.5.

Thus, considering wave height differentiations in a small spatial scale, XBeach shows a non-uniform image of wave height distributions, while MIKE 21 shows a smooth transformation of wave height values. Waves significantly affect the harbour basin and the outer region in front of the windward breakwater. Wave heights reach the values of 2.0 and 1.4 meters for the North and North-East storm scenarios, respectively, and this energetic wave field can trigger considerable overtopping discharges, followed by high wave run-up heights. More precisely, for the N storm scenario, the harbour basin seems to be well protected, which is not the case for the NE scenario, where disturbance is caused by incoming waves. As it can be deduced by the

results of Figure 2-10-C, XBeach model does not account for simulating the diffraction phenomenon.

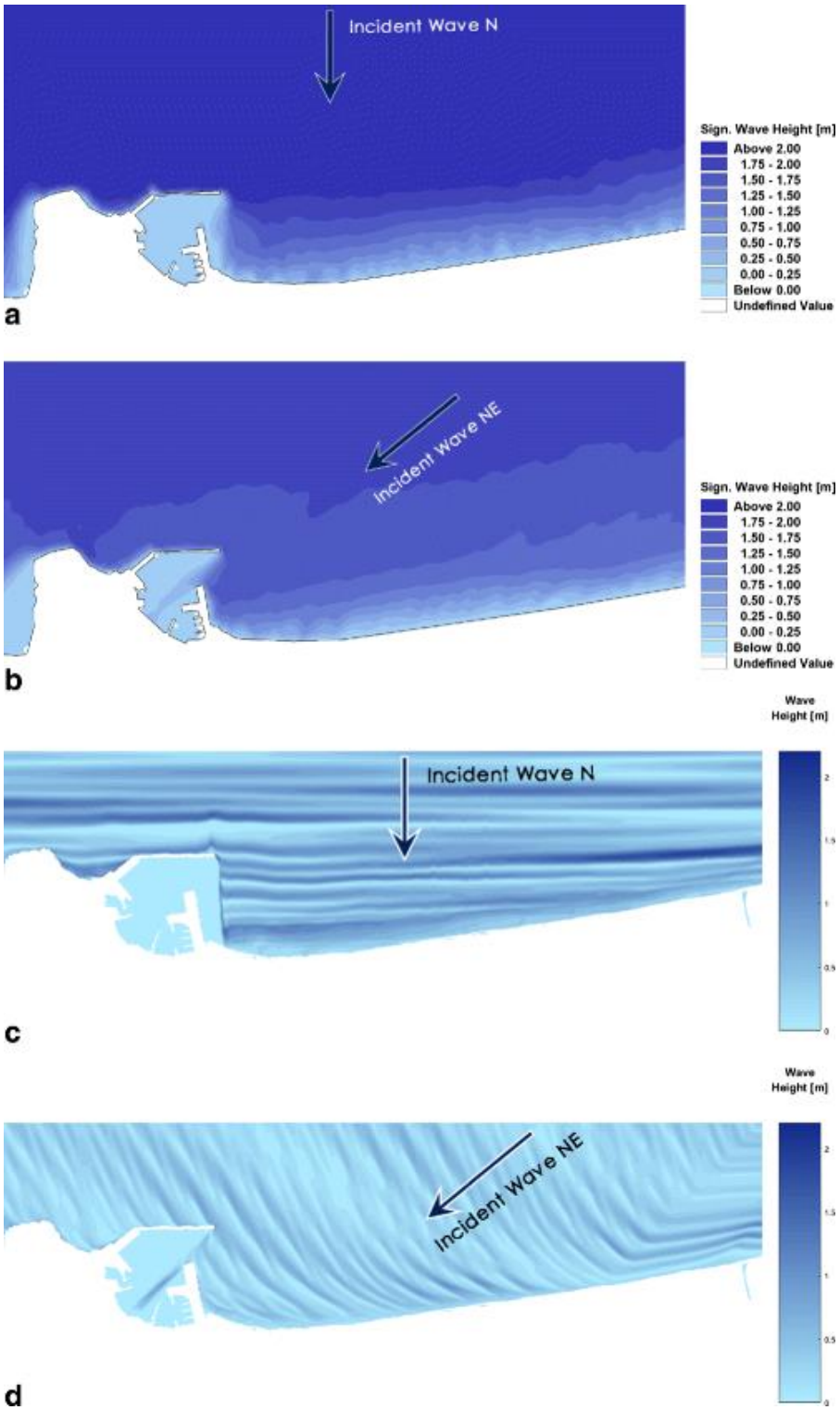

Figure 2-10 Spatial distribution of significant wave height (Hs) by MIKE 21 SW for the North (a) and North-East (b) storm scenarios. Spatial distribution of the root mean square of wave height (Hrms) by XBeach for the North (c) and North-east (d) storm scenarios (Afentoulis et al., 2017).

2.2.3.3.2 Hydrodynamics

The spatial distribution of alongshore and cross-shore depth-averaged and time-averaged velocity components U, V of wave-induced currents is presented in Figure 2-11 and Figure 2-12, respectively. The colour map depicts the magnitude of each velocity component (in U figures positive values represent eastward direction, while in V figures positive values represent northward direction). The black arrows represent the velocity net vector of both alongshore and cross-shore components, whose magnitude was calculated as: $\boldsymbol{V} = \sqrt{\vec{u}^2 + \vec{v}^2}$. The numerical results of the two models validate the existence of an intense alongshore current to the west, caused by both the N and the NE storm scenarios, which can be a dominant factor for sediment motion. Additionally, the model's outputs indicate the presence of strong undertow currents at the East windward side of the main breakwater.

Finally, the mean values of the depth-averaged velocities are in good agreement between the two models, as they do not exceed an absolute of 2 m/s for both models. However, the two models do also exhibit significant differences:

1. There is a lack of information on offshore hydrodynamic circulation in XBeach model results;

2. In nearshore areas, velocity values from MIKE 21 are significantly lower than the corresponding ones of XBeach;

3. The velocity vectors form irregular patterns in the case of XBeach, whereas MIKE 21 results exhibit well-regulated nearshore current patterns;

4. Although for the NE storm scenario, westward current propagation results are similar between the two models, for the N storm scenario, XBeach results present an intense cross-shore movement, whereas MIKE 21 results present mainly an alongshore movement.

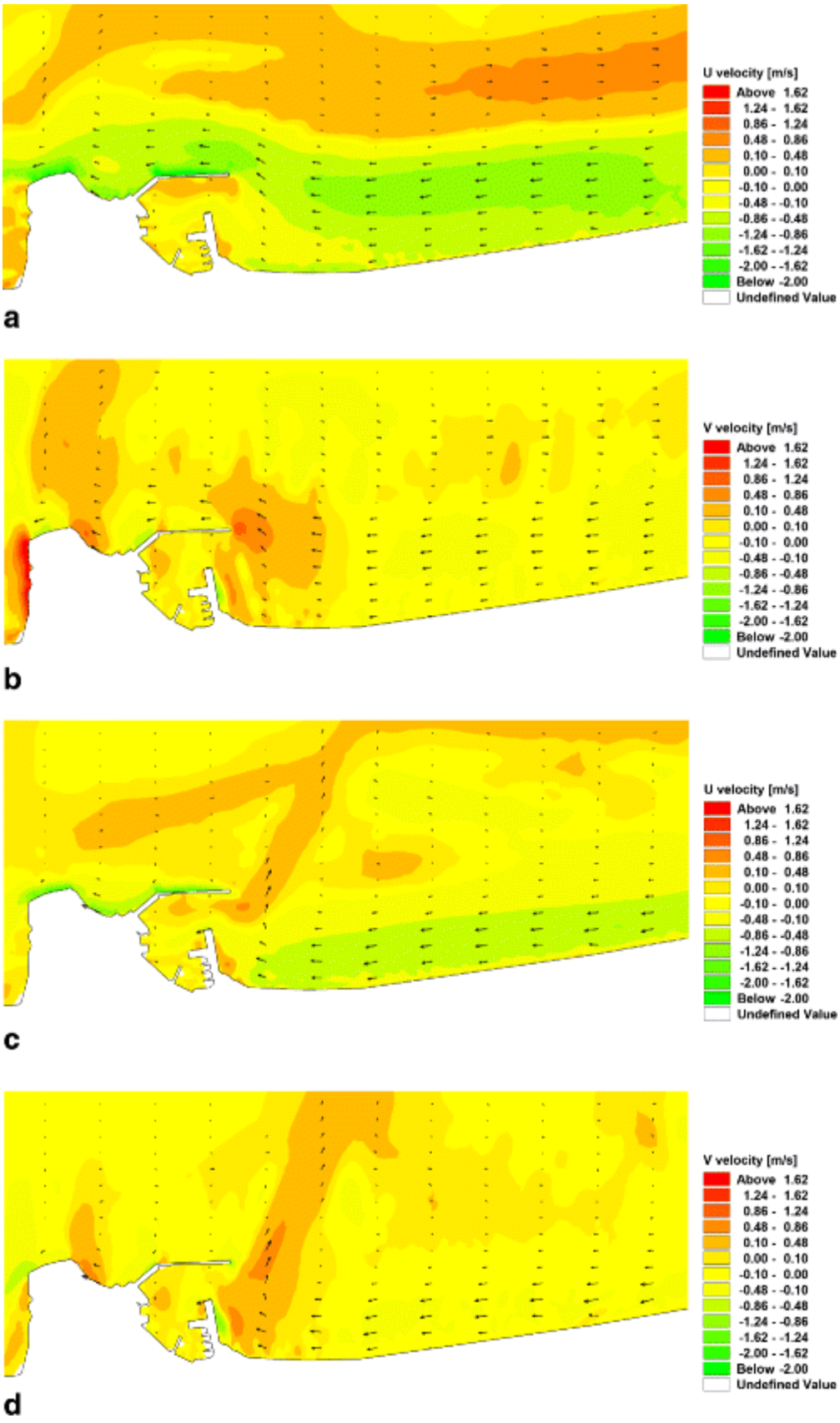

Figure 2-11 a,b) Northern Storm Scenario - Spatial distribution of alongshore velocity U and cross-shore velocity V - MIKE 21 FM HD model. c,d) North-Eastern Storm Scenario - Spatial distribution of alongshore velocity U and cross-shore velocity V - MIKE 21 FM HD model

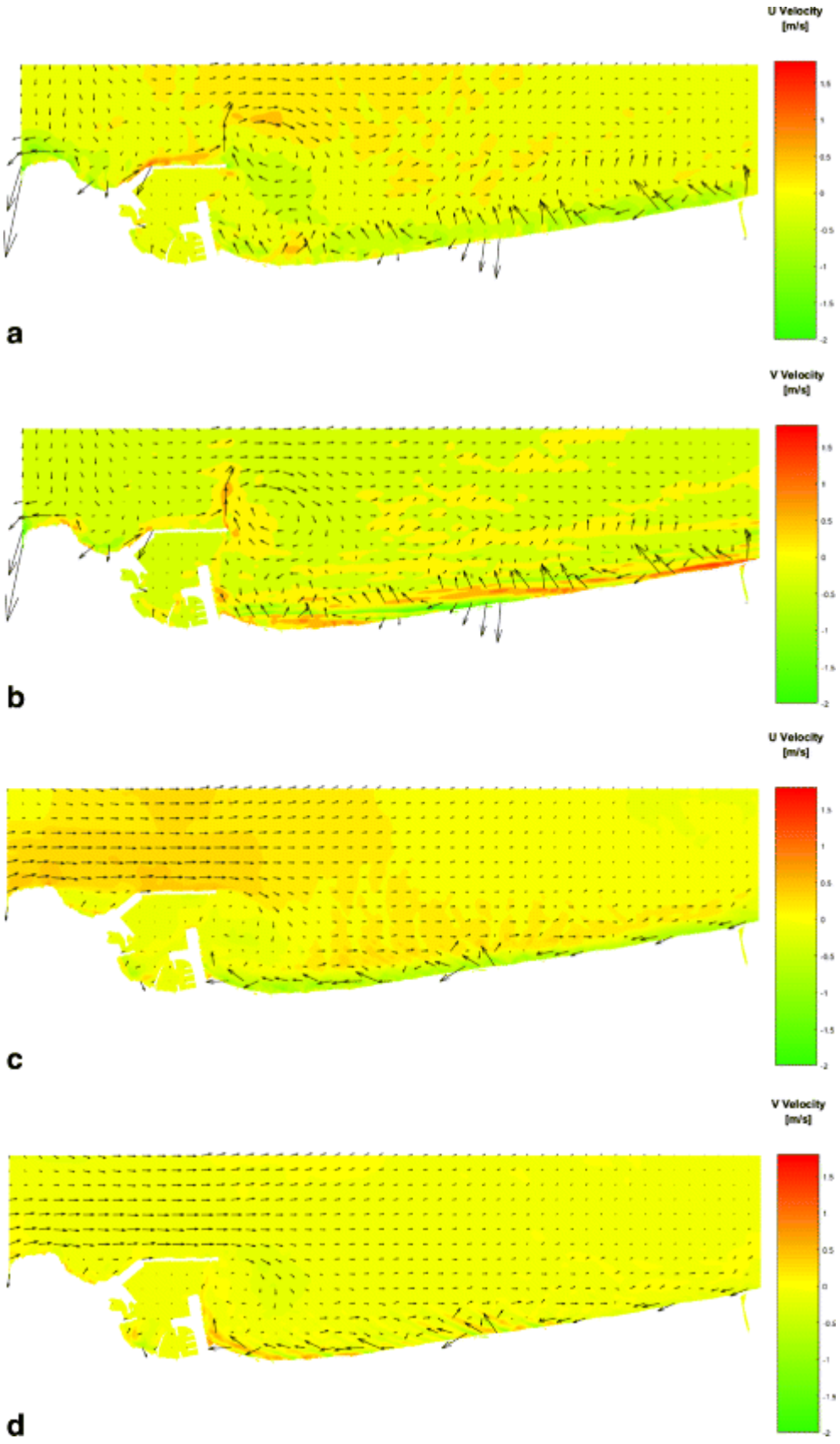

Figure 2-12 a, b) Northern Storm Scenario- Spatial distribution of alongshore velocity U and cross-shore velocity V - XBeach model. c, d) North-Eastern Storm Scenario - Spatial distribution of alongshore velocity U and cross-shore velocity V - XBeach model

2.2.3.3.3 Sediment transport fluxes

The alongshore and cross-shore components of the sediment transport rates, as extracted by the numerical simulation, are illustrated in Figure 2-13, Figure 2-14. Once more, the arrows represent the sediment drift net vector of both alongshore and cross-shore components, whose magnitude is calculated as: $\boldsymbol{S} = \sqrt{\overrightarrow{S_x}^2 + \overrightarrow{S_y}^2}$. The sediment transport, in x- and y-directions, includes both bed and suspended load. As shown in the below Figures, the cross-shore sediment motion is significantly intense for the case of the N storm scenario where the rates reach values of 0.005 m3/s/m in front of the leeward breakwater and 0.014 m^3/s/m at the east area of the shoreline, which signifies the storm-induced erosion phenomena that the area is facing.

The formation of these offshore drifts is induced by the undertow currents that were identified in the analysis of the hydrodynamic processes. Our findings appear to be well substantiated by a number of studies in the literature of coastal engineering, as it has been observed that the offshore sand bar migration, which is driven by strong offshore-directed mean currents, can be observed when incident waves are more energetic (Gallagher et al., 1998; Thornton et al., 1996). Furthermore, as it was expected from the observation of the hydrodynamic patterns, the alongshore sediment transport fluxes attain high values in the southeast part of the case study area, indicating a westward sediment circulation. Comparing the sediment transport results of the two models, a good agreement can be seen in the values of alongshore transport. On the contrary, in terms of cross-shore sediment transport, XBeach provides results only in shallow water depths, while MIKE 21 shows mild sand movements in deep waters. Finally, the obtained numerical outputs are in good agreement with field observation, which reveals an important deposition of sediment particles in the entrance of harbor basin.

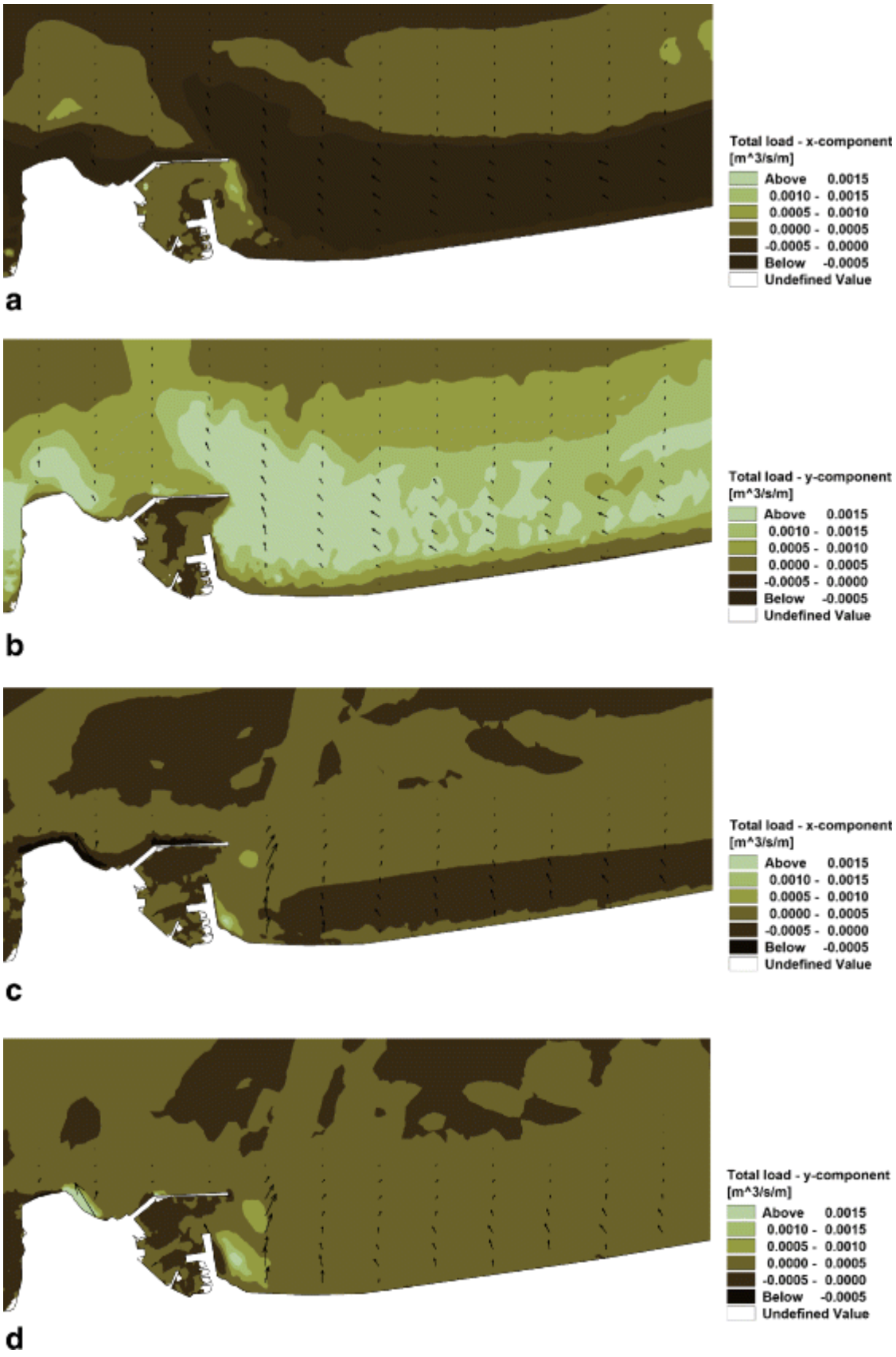

Figure 2-13 a, b) Northern Storm Scenario - Spatial distribution of sediment transport total load x and y component - MIKE 21 ST model. c, d) Northern Storm Scenario - Spatial distribution of sediment transport total load x and y component - MIKE 21 ST model

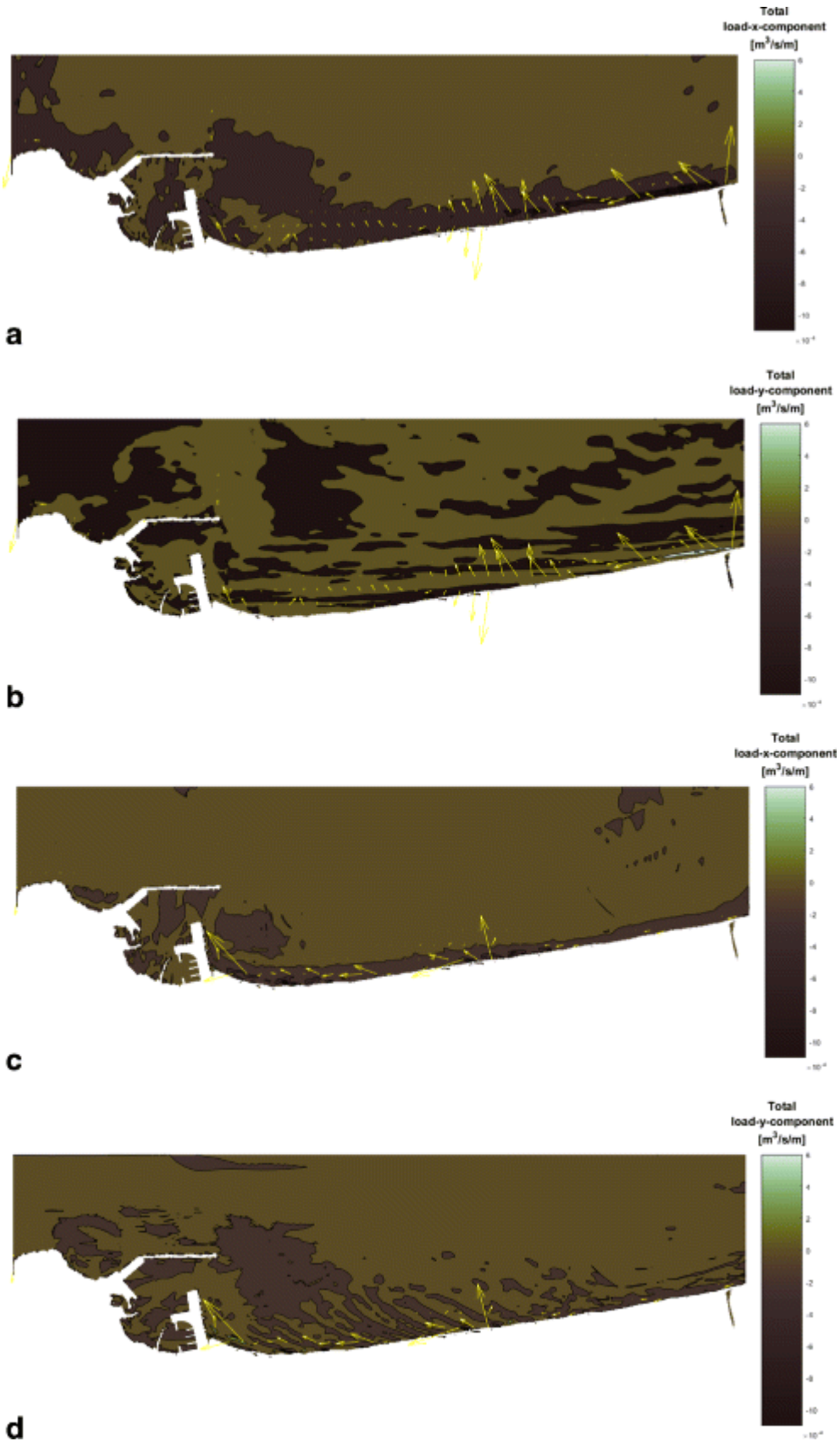

Figure 2-14 a, b) North-Eastern Storm Scenario - Spatial distribution of sediment transport total load x and y component - XBeach model. c, d) North-Eastern Storm Scenario - Spatial distribution of sediment transport total load x and y component - XBeach model

2.2.3.3.4 Tested configurations – Harbour design

The existing layout of the harbour is especially vulnerable to severe weather events, as significant wave-induced overtopping discharges have been encountered over the windward breakwater (Tsoukala et al. 2016). Furthermore, the sediment drifts that were numerically investigated in this study force a high volume of sediment, which is stored in the area east of the leeward breakwater, to move inside the harbour basin. This process can lead to a subsequent decrease of the water depth and the shoaling of the harbour entrance, which can obstruct or hinder the navigation. Moreover, the high amount of the transported sand triggers significant erosion phenomena along the adjacent eastern coasts. Figure 2-15 depicts an overview of the identified vulnerable areas of our study zone.

Both satellite image of Figure 2-16 and the MIKE 21 ST bed level change results for the case of the N storm (Figure 2-16 - down) validate the existence of a sediment longshore movement and deposition of sand towards the west past part of the computational domain, in front of the leeward breakwater. In order to control these sediment transport phenomena, an alternative harbour layout was proposed, including breakwaters with a curved shape reinforced with XBlocks concrete armour. Moreover, the solution- configuration of a submerged breakwater system was evaluated in order to combact erosion phenomena in the eastern low-lying coastal area. Figure 2-17 depicts the reinforcement of the breakwater's embankment and alteration of the harbour geometric properties, as well as the drawing of the projected system of submerged detached breakwaters along the coast.

Figure 2-15 Identification of Vulnerable areas

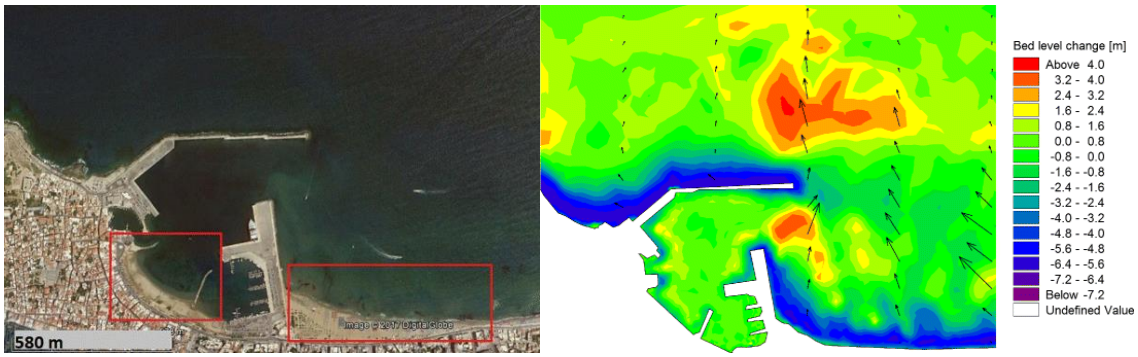

Figure 2-16 Up: Satellite image from Google Earth (31/08/2015), displaying sediment deposition inside the harbor basin (Google Earth Engine Team 2015). Down: Bed level change for the Northern Storm Scenario with the current harbour layout –MIKE21 predictions.

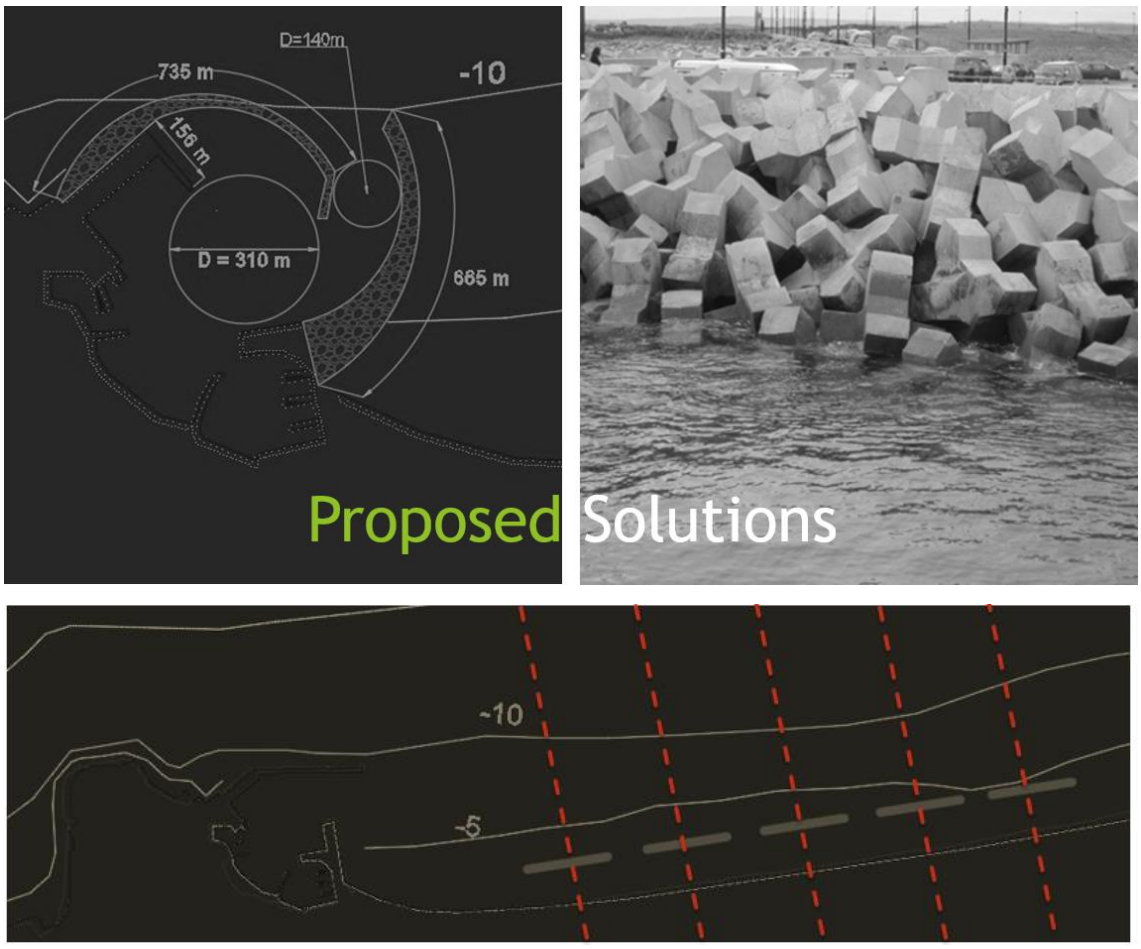

Figure 2-17 Up: reinforcement of the breakwater's embankment and alteration of the harbour geometric properties. Down: Scheme of the projected system of submerged detached breakwaters along the coast.

The response of the proposed harbour layout against storm-induced hydro-morphodynamics was evaluated in order to investigate sediment transport patterns and assess the sedimentation tendency in the harbour entrance. For the worst-case of North Storm Scenario, the numerical investigations were carried out using the MIKE 21 SW-HD-ST module chain. Through the reshaping of the breakwaters, the main direction of hydrodynamic circulation is altered, and a sufficient tranquility of the harbour entrance was achieved. The results of wave propagation show a smooth transformation of wave height values towards the shallow water regions (Figure 2-18). Waves do not affect the harbour basin and the outer region in front of the windward breakwater is well protected.

Our investigations show that the reinforcement of the breakwaters dissipates wave energy reducing the wave run-up, overtopping and reflection phenomena. Wave heights reach the values of 1.0-1.4 meters close to the breakwater area for the originated from North storm scenario. As it can be deduced by the results of Figure 2-19, net velocity vectors follow altered patterns, comparing to the initial state, which leads to avoid significant spatial velocity gradients close to the harbour that drive the sediment deposition. Bed level changes and the patterns of the sediment transport fluxes during the selected extreme storm event are illustrated in Figure 2-20 as obtained by MIKE21 ST module. The morphological evolution shows what was expected from the analysis of the hydrodynamic patterns, the accumulated amount of sediment in front of the entrance is significantly decreased for this configuration and some erosion can be identified in the toe of the windward breakwater.

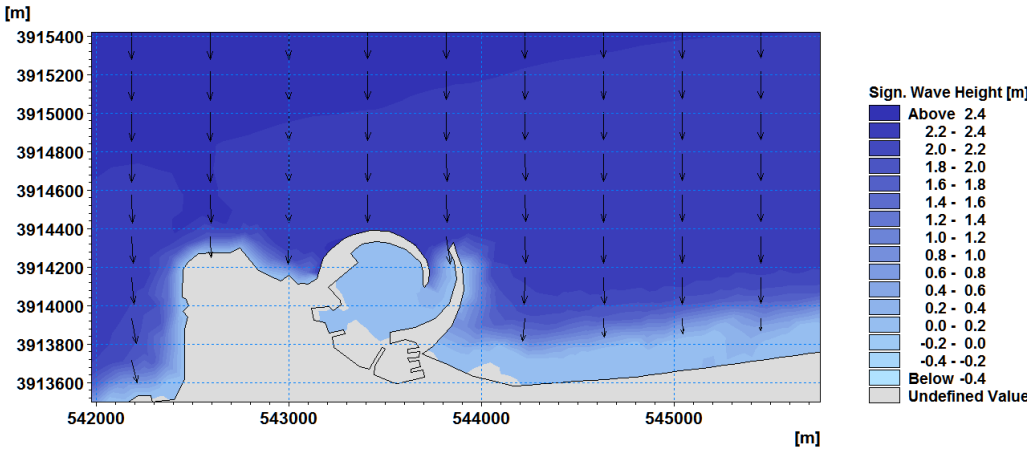

Figure 2-18 Map of Wave Height distribution for the case of the North wave scenario as obtained by MIKE21 SW module.

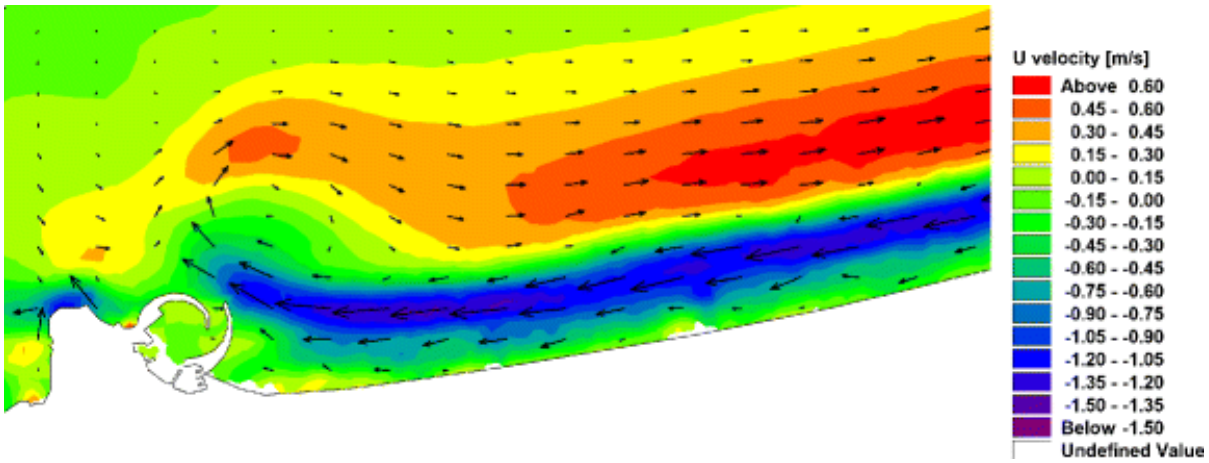

Figure 2-19 MIKE 21 HD results: U velocity contours and net velocity vectors for the reshaped harbour layout, for the case of the North wave scenario.

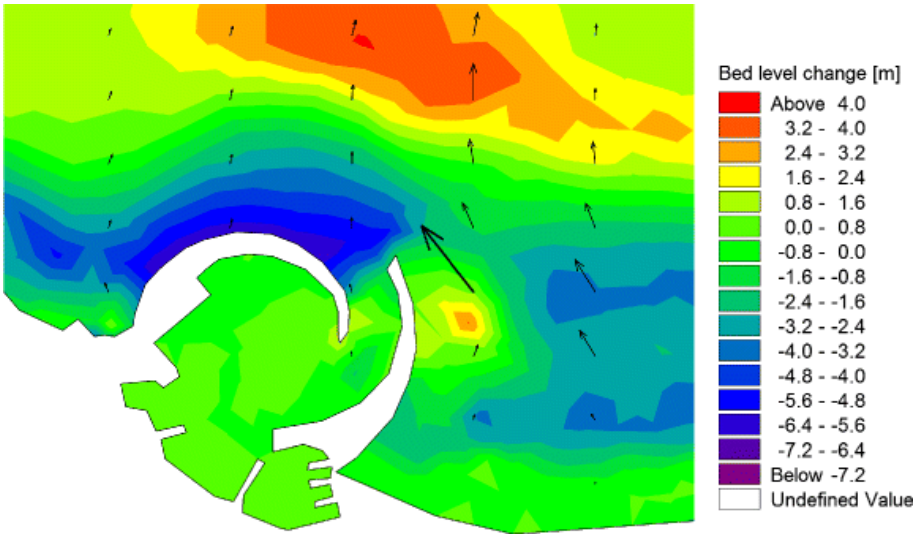

Figure 2-20 Bed level change for the Northern Storm Scenario with the proposed harbour layout as obtained by MIKE21 ST module. Vectors: patterns of the sediment transport fluxes.

2.2.3.3.5 Tested configurations – Coastal defences

Modelling and simulation of fluid-sediment seabed interactions is essential for the design and construction of defence structures against coastline retreat, which result in the reduction of the incoming wave energy in the shoreward zones. For the optimization of form and geometric properties of the detached submerged breakwaters (Figure 2-17) the numerical formulation of Bouharguane and Mohammadi (2013) was utilized. This device is based on shallow water equations and it was herein employed in order to investigate the wave - fluid and structure interactions using minimization principles (Mohammadi and Bouchette, 2014). Minimization principles have been used many times in the past to design defence structures against beach erosion (Azerad et al., 2005), (Isebe et al., 2008). In these works, designed structures were independent of time and were built once for all. Hence, this method goes one-step further giving the possibility to the structure to change in time. It is worth pointing out that the fundamental assumption of Bouharguane and Mohammadi (2013) formulation is the fact that bed adapts to the flow by some sort of optimal sand transport in order to minimize some energy expression. Optimal transport is seen here as minimal change in the bed shape. The time scales of interest are below a day and recoveries between storms or seasonal and inter-annual variabilities are out of scope. A detailed description of this numerical model is presented in the next chapter.

The computational grid, over which the available bathymetrical data of the characteristic 1D-cross-shore profile of

Figure **2-22** were interpolated, is constructed with an uniform spatial step of $dx = 0.5$ m and the computational domain has a total length of 1 Km . The sediment properties represent here a uniform sand with a porosity of 0.4 and a particle size of 0.2 mm (Table 2 8). Irregular waves were generated at inlet that are characterized by JONSWAP spectrum. The wave conditions in the offshore boundary of this 1-D model were obtained by the numerical outputs of the MIKE21 SW model and the worst-case scenario was considered for a total duration of 72 hours.

Figure **2-22** depicts the morphological evolution of the seabed for three different locations (distance to the shore) of the submerged breakwater after the period of 72 hours that corresponds to the N – worst-case wave scenario. An overview of the evaluated configurations is illustrated in Figure 2-23, this analysis has as main variable the breakwater's distance to the shore, so that the optimisation process concerns the definition of the optimal distance that

provides a better protection of littoral system in the leeside area. The distance of 200 meters to the shoe was proven to provide a sufficient protection of the coast.

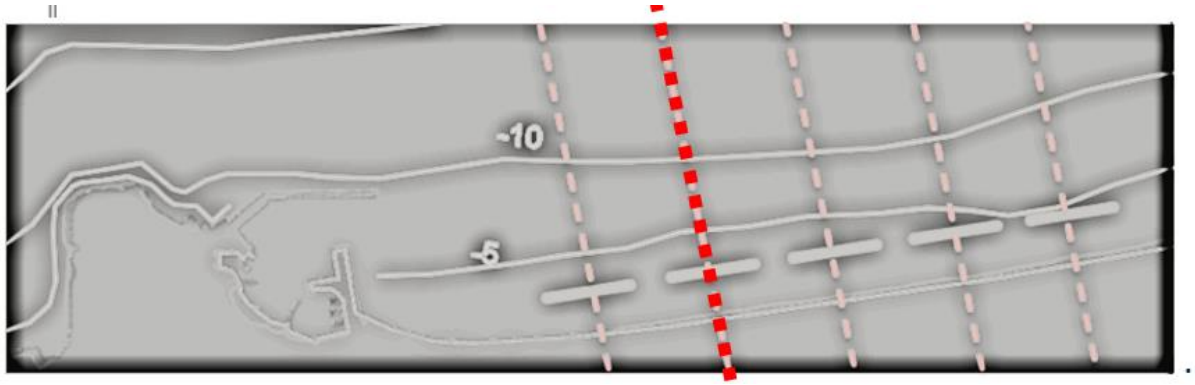

Figure 2-21 Scheme of the projected system of submerged detached breakwaters along the coast and selected characteristic profile.

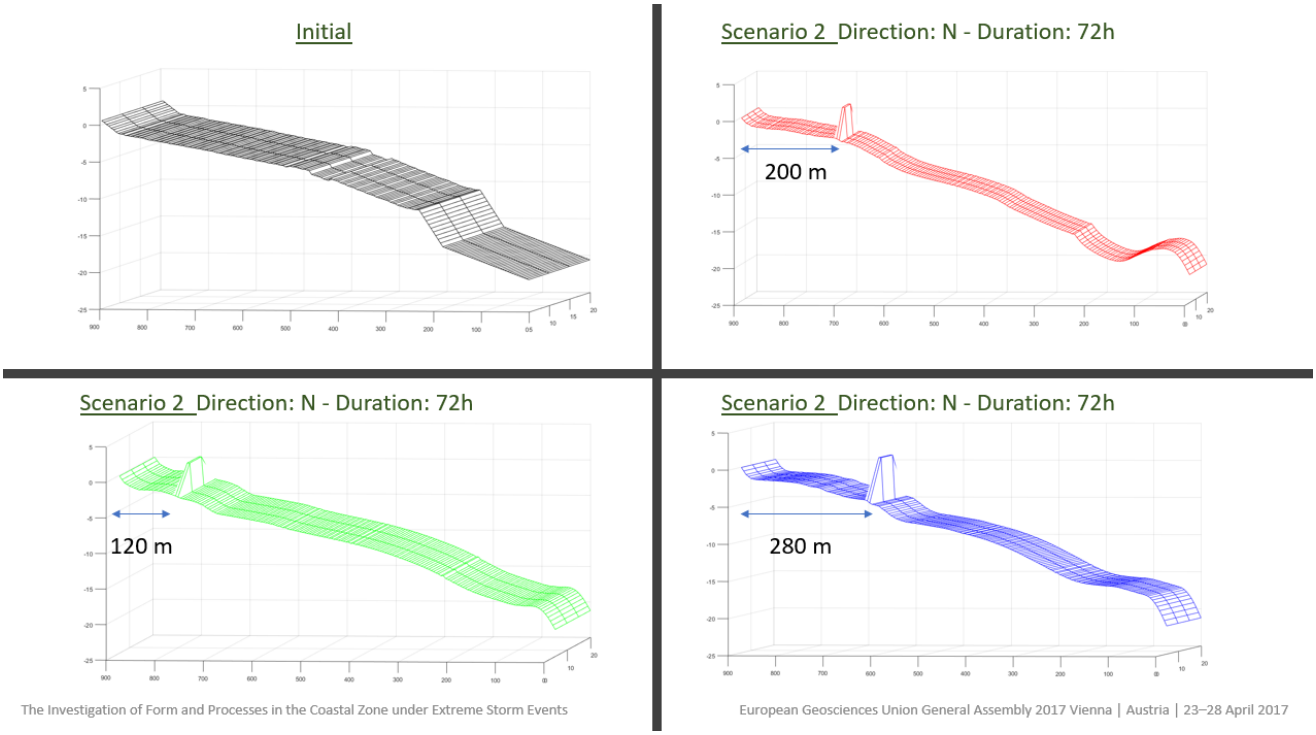

Figure 2-22 Bottom evolution for 3 distinct locations of the submerged breakwater after the period of 72 hours of the N – worst-case wave scenario.

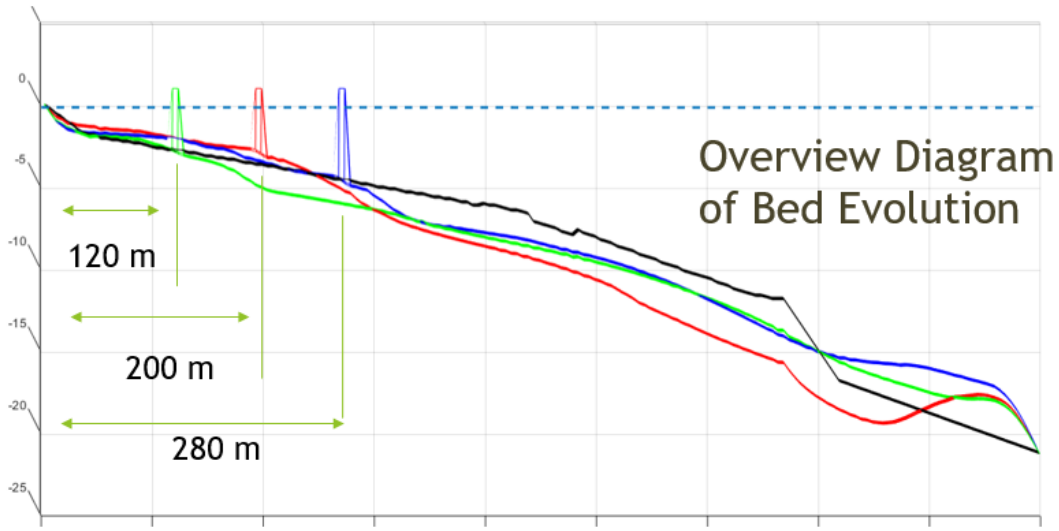

Figure 2-23 Superimposed bottom evolutions for the three selected configurations with a variable breakwater's distance to the shore.

2.3 Assessment of the morphological response under the presence of a detached breakwater, applying a probabilistic design methodology in northern Greece.

For the assessment of the morphological beach response in the leeside of an emerged detached breakwater, four different wave scenarios – sea states were simulated over a characteristic beach profile in the coastal area of Avdera in northern Greece (Figure 2-24). In our case, the determination of the boundary offshore wave conditions issued by the use of an advanced probabilistic theory, while two different data sets were examined and compared. The first set concerns wave data of joint frequencies of H_s and T_p during 7 years (1999-2006) derived from the electronic Wind and Wave Mediterranean Atlas (WWM Atlas), while the second one was wind data of frequencies of wind velocity and direction for 64 years (1951-2014) derived from Hellenic National Meteorological Service (HNMS). It is noted that T_m has been extracted from T_p considering their relationship based on Jonswap energy spectrum of wind waves. The second data set combined with fetch length, has been used to calculate the long-term joint probability density function of H_s and T_m in wind waves at a location in deep waters in Northen Aegean Sea (40.50N, 25.00E).

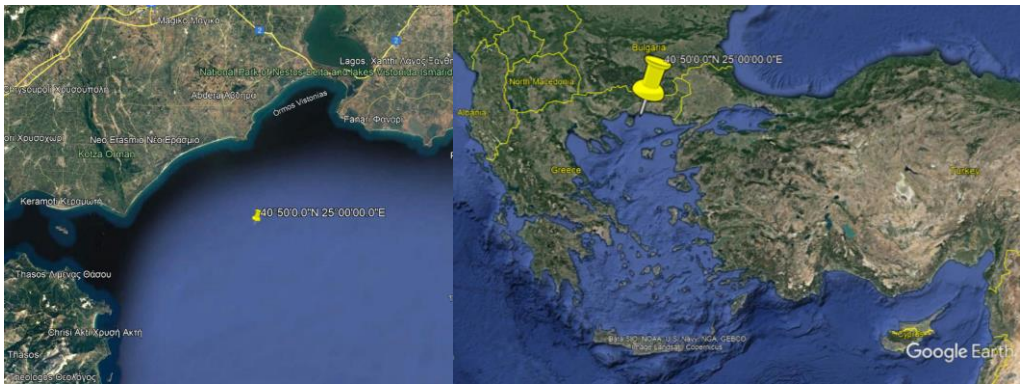

Figure 2-24 Location, coordinates and size of the case study area - Satellite image from Google Earth 31/08/2020 (Google Earth Engine Team 2021)

Results from the two data sets treated by the conditional model transmitted to 1-year period, via the notion of return period associated to each sea state are depicted in Figure 2-25, where the marginal probability density function of H_s from the two data sets is presented. In conditional modelling, the Weibull distribution was fitted to the marginal H_s data, being an extreme value distribution that could cope with climate change, while the conditional distribution of T_m given H_s followed the lognormal. The Pearson correlation coefficient between H_s and Tm is equal to 0.823 in the case of atlas wave data and 0.868 in the other set. Results are presented in Figure 1, after the exclusion of swell waves in WWM Atlas data set following Zaslavskii (2000).

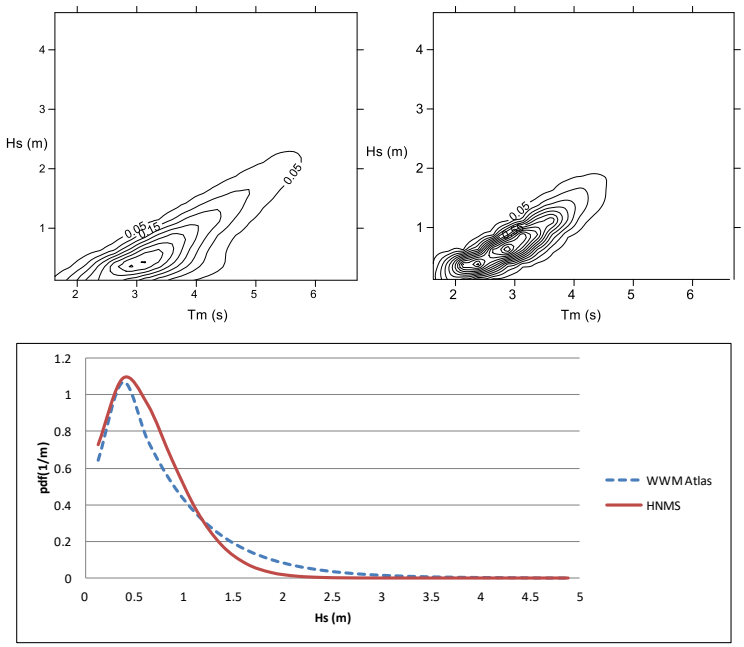

Figure 2-25 Up: Joint probability density function of Hs(m) and Tm(s) estimated via conditional modelling using Atlas wave data (left) and HNMS wind data (right). Down: Comparison of probability density function of Hs (m) estimated via conditional modeling using Atlas wave data and HNMS wind data (Weibull distribution).

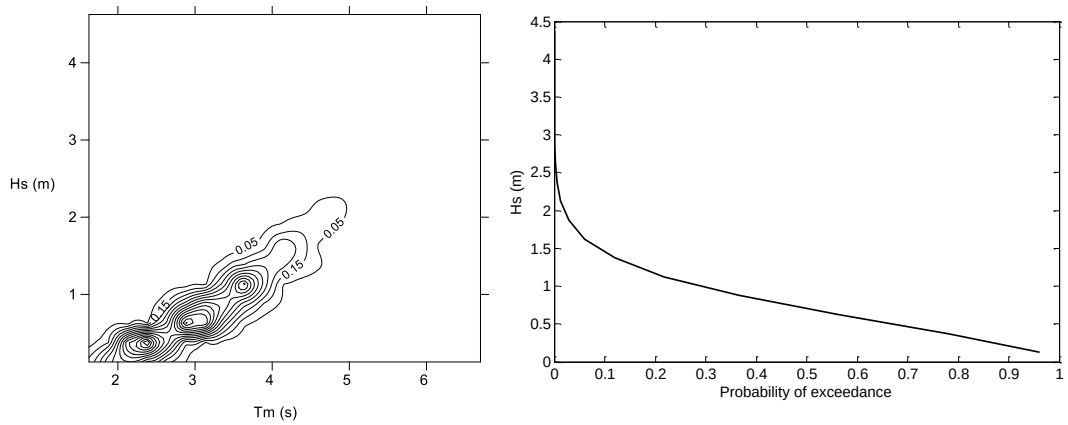

Figure 2-26 Joint probability density function of Hs(m) and Tm(s) at the depth of 7.5m, estimated via conditional modelling using HNMS wind data (left) and Hs exceedance probability curve (right).

The results of Figure 2-25 show a good agreement of the estimations calculated via conditional modelling using WWM Atlas wave data against the HNMS data. Although, the correlation coefficient is slightly higher in HNMS data than WWM Atlas data. This is due to the structure of the methodology applied to determine waves from wind data, which considers a high correlation between *Hs* and *Tm*. Furthermore, HNMS data give also information on the wind direction and therefore of the main wave direction. Thus, the joint probability density distribution of *Hs* and *Tm* can be estimated in intermediate waters considering such processes as wave propagation, wave shoaling and refraction. Following this, the joint probability density distribution of *Hs* and *Tm*, directed from the open sea towards the structure at the depth of 7.5 m, the supposed site of the structure under design is presented in Figure 2-26 (left). This depth lies outside the surf zone; to take wave breaking into account would demand knowledge of short term additionally to long-term wave statistics. The corresponding *Hs* and *Tm* at certain exceedance probabilities can be extracted from Figure 2-26, e.g. from the right panel it is obtained that *Hs* 2.4 m corresponds to a 0.01 probability of exceedance, while from left panel that the most probable Tm associated to this *Hs* is 5.1 s.

The characteristics of the four scenarios are listed in **Table 11**. It is noted that scenario 4 is the sequence of the first three scenarios, tested to provide the accumulated erosion of these three scenarios as it happens in nature. The occurrence probabilities of scenarios 1, 2, and 3 have been derived from Figure 2-26. These three scenarios are considered to be correlated but not fully dependent. Therefore, the probability of occurrence of scenario 4 is estimated here as approximately 80% of the probability of sea state 3.

Sea sate scenario	Hs (m)	Tm(s)	Duration (hr)	Probability
1	1.5	4.08	6	0.019
2	2.0	4.58	6	0.0056
3	2.5	5.11	6	0.0012
4	1.5,2.0,2.5	4.08, 4.58, 5.11	18	0.0010

Table 11 Characteristics of the four sea state scenarios tested

The numerical simulation of the bed evolution was carried out using the XBeach model. For the needs of this application the height of the breakwater and the distance between the structure and the shoreline have been set equal to 8.3 meters and 200 meters respectively. the sediment properties represent here a uniform sand with a porosity of 0.4 and a particle size of 0.2 mm. The goal of this task is to combine the stochastic analysis of sea states with the corresponding impact on the shoreline. The results of bed evolution under the four scenarios tested are presented in Figure 2-27. As it was expected, the higher level of beach erosion is observed for the sea state 4 (Figure 2-27.d). The beach profiles obtained show that the amount of erosion is dependent on the intensity of sea states, and the change of the bed shape becomes negligible as the wave height decreases (see Figure 2-27.a).

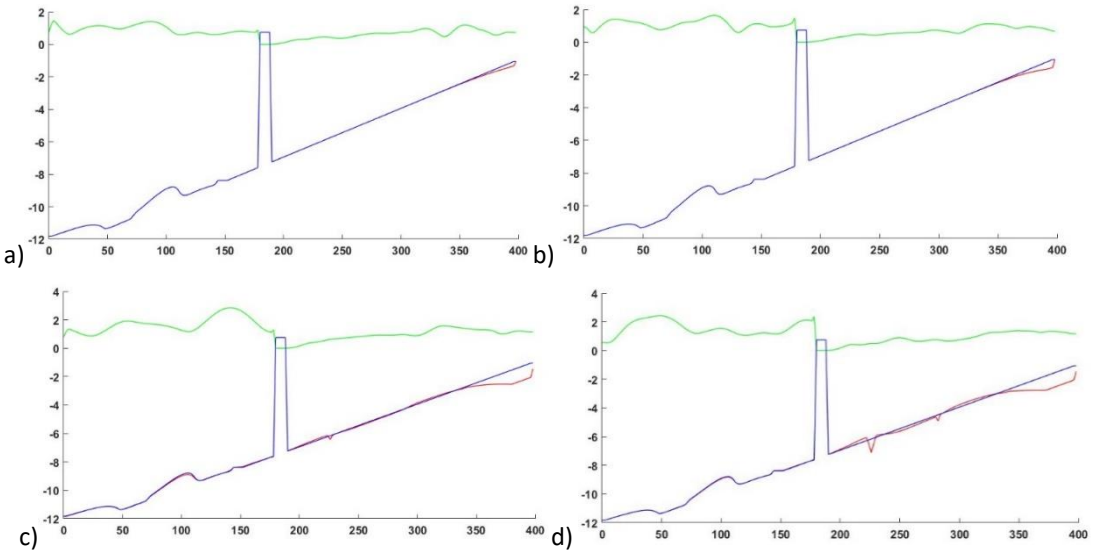

Figure 2-27 Bed evolution for scenario 1(a), scenario 2 (b), scenario 3 (c) and scenario 4 (d) obtained by XBeach model, under four selected sea states. Initial bed (blue lines), final bed (red lines) and wave height (green lines), illustrated for the last time step of each simulation.

2.4 Discussion

In this chapter, different methodologies and numerical approaches were applied for the investigation of nearshore physical processes, such as wave propagation, hydrodynamics and morphodynamics. The storm-induced coastal vulnerability was analyzed for the study area of Rethymno in Greece, where different solutions (configurations of coastal structures) were evaluated via advanced numerical modeling, in terms of their capacity to combat storm-induced damages. Wave propagation and hydro-morphodynamic patterns were investigated through two distinct numerical models: MIKE 21 and XBeach, and a comparison between their outputs was performed in view of their ability to evaluate nearshore physical processes, under extreme storm events. Additionally, for the optimization of form and geometric properties of the detached submerged breakwaters a numerical formulation based on minimization principles of (Bouharguane and Mohammadi, 2013) was utilized.

The obtained results reveal that the coastal system in our study area is exposed to intense erosion due to energetic waves and strong hydrodynamic currents, the existence of which can be validated by the available field measurements and satellite photos. The main direction of the sediment drifts was accurately identified, as it has been observed that large volumes of sedimentary mobilization occur from high to low wave energy areas during extreme meteorological events. Agreement between the two model results, do provide, in principle, more confidence in the estimation of the physical processes. However, as anticipated, some deviations do exist between the outputs of the two models, caused by their different capabilities and purposes: XBeach provides information on the processes in the nearshore area, while MIKE 21 better simulates the transformation of information from deep water to shallow water regions. For this reason, a nesting method could combine the advantages of the two models.

Our findings suggest that the proposed solution of reshaping the harbour layout with curved and reinforced breakwaters provides a better protection of the harbour basin, through wave energy dissipation and by altering of the current patterns and sediment drifts directions. Regarding the design of the breakwater system, the obtained results show favorable tendencies to sediment accretion near the shoreline, as well as at the inward areas for a distance to the shore equal to 200 meters. Moreover, a probabilistic theory was applied to define offshore conditions and wave events that can initiate the sediment in northern Greece. Thus, the assessment of the hydrodynamic and morphological impact of the structures was based on a probabilistic framework of wave climate.

We argue that the methodology presented here can be an important tool to assess impacts of extreme storm events in study areas that face erosion problems. In particular, the advanced numerical models, applied here, can be a valuable asset for engineers and scientists desiring to obtain accurate bed level evolution predictions in complex bathymetries with the presence of a variety of coastal protection structures, both in experimental and in field cases thus improving their design and configuration. The existing numerical devices, employed here, are based on linear model, which wave-averaged parameters for the simulation of nearshore hydrodynamics and subsequently the obtained sediment transport rates do not consider intra-wave effects and nonlinear wave -current interactions. In particular, morphological changes, especially near the shoreline and in the presence of coastal structures, are more precisely predicted when a phase-resolving model is utilized as wave driver. This can be attributed to different fundamental aspects discussed in chapter 4. Therefore, new models and numerical tools were developed within the context of the present dissertation to deal with non-linear – phenomena across the nearshore zone.

References

Afentoulis, V., Eleftheria, K., Eleni, S., Evangelos, M., Archontia, L., Christos, M., & Vasiliki, T. (2017). Coastal Processes Assessment Under Extreme Storm Events Using Numerical Modelling Approaches. Environmental Processes, 4(3), 731-747.

Afentoulis, V., Papadimitriou, A., Belibassakis, K., & Tsoukala, V. (2022). A coupled model for sediment transport dynamics and prediction of seabed morphology with application to 1DH/2DH coastal engineering problems. *Oceanologia*.

Azerad, P., Isebe, D., Ivorra, B., Mohammadi, B., & Bouchette, F. (2005). Optimal shape design of coastal structures minimizing coastal erosion.

Athanassoulis, G. A., Belibassakis, K. A., Gerostathis, T. P., & Kapelonis, Z. G. (2014, November). Application of SWAN wave model for climatic simulation of sea condition at coastal areas of the Mediterranean. In 6th Panhellenic Conf. Coastal Zones Manage. Improvement (Vol. 24, p. 27).

Athanassoulis, G. A., Belibassakis, K. A., Gerostathis, T. P., & Kapelonis, Z. G. (2015). Wave climate analysis in the Mediterranean Sea based on wave model simulation driven by climatological winds. Technical Report WP 2.2. Res. Program CCSEAWAVS.(in Greek).

Bouharguane, A., & Mohammadi, B. (2013). Minimisation principles for the evolution of a soft sea bed interacting with a shallow sea. International Journal of Computational Fluid Dynamics, 26(3), 163-172.

Castelle, Bruno, et al. "Impact of the winter 2013–2014 series of severe Western Europe storms on a double-barred sandy coast: Beach and dune erosion and megacusp embayments." Geomorphology 238 (2015): 135-148.

de Alegria-Arzaburu, A. R., Williams, J. J., & Masselink, G. (2011). Application of XBeach to model storm response on a macrotidal gravel barrier. Coastal Engineering Proceedings, (32), 39-39.

De Michele C, Salvadori G, Passoni G, Vezzoli R (2007) A multivariate model of sea storms using copulas. Coast Eng 54(10):734–751

Dolan, R., & Davis, R. E. (1992). An intensity scale for Atlantic coast northeast storms. Journal of coastal research, 840-853.

Isebe, D., Azerad, P., Bouchette, F., Ivorra, B., & Mohammadi, B. (2008). Shape optimization of geotextile tubes for sandy beach protection. International journal for numerical methods in engineering, 74(8), 1262-1277.

Karambas, Th., & Kampanis, N., (2010). Research Project for the solution of the erosion problem, the protection and regeneration of the coastline (In Greek).

Kragiopoulou, E. V., Skarlatou, S., Lykou, A., Makropoulos, C., & Tsoukala, V. K. (2016). Assessing coastal zone response under extreme storm events for flood risk management. The case study

of Rethymno, Greece. In 13th International conference on protection and restoration of the environment Mykonos Island, Greece.

Li, F., Van Gelder, P. H. A. J. M., Ranasinghe, R. W. M. R. J. B., Callaghan, D. P., & Jongejan, R. B. (2014). Probabilistic modelling of extreme storms along the Dutch coast. Coastal Engineering, 86, 1-13.

Martzikos, N., Afentoulis, V., & Tsoukala, V. (2018). Storm clustering and classification for the port of Rethymno in Greece. Water Util. J, 20, 67-79.

Lončar, G., Carević, D., Bekić, D., Babić, M., Grbić, N., & Pranjić, V. (2016). A morphodynamic stability analysis of gravel beach cross-section by 1D numerical model. Građevinar, 68(02.), 113-124.

Makropoulos, C., Tsoukala, V., Belibassakis, K. A., Lykou, A., Chondros, M., Gourgoura, P., & Nikolopoulos, D. (2015). Managing flood risk in coastal cities through an integrated modelling framework supporting stakeholders'involvement: the case of rethymno, Crete. 36th IAHR World Congrees.

Makropoulos, C., Tsoukala, V. K., Lykou, A., Chondros, M., Manojlovic, N., & Vojinovic, Z. (2014, March). Extreme and rare events in coastal regions due to climate change—a case study application in Rethymno. In Int. Conf. ADAPTto CLIMATE (pp. 27-28).

McCall, R. T., De Vries, J. V. T., Plant, N. G., Van Dongeren, A. R., Roelvink, J. A., Thompson, D. M., & Reniers, A. J. H. M. (2010). Two-dimensional time dependent hurricane overwash and erosion modeling at Santa Rosa Island. Coastal Engineering, 57(7), 668-683.

Mickey, R. C., Dalyander, P. S., McCall, R., & Passeri, D. L. (2020). Sensitivity of storm response to antecedent topography in the XBeach model. Journal of Marine Science and Engineering, 8(10), 829.

Mohammadi, B. (2017). Uncertainty quantification in littoral erosion. Computers & Fluids, 143, 120-133.

Velikou, K., Tolika, K., Anagnostopoulou, C., Tegoulias, I., & Vagenas, C. (2014). High resolution climate over Greece: assessment and future projections. In 12th International Conference on Meteorology, Climatology and Atmospheric Physics (COMECAP 2014), Heraklion.

Prinos, P. (2014, November). Climate change effects on the Greek seas and coastal areas–the research project THALIS-CCSEAWAVS. In 6th Panhellenic Conference on Coastal Zones Management and Improvement (pp. 24-27).

Rangel-Buitrago, N., & Anfuso, G. (2011). An application of Dolan and Davis (1992) classification to coastal storms in SW Spanish littoral. Journal of Coastal Research, 1891-1895.

Roelvink, D., Reniers, A., Van Dongeren, A. P., De Vries, J. V. T., McCall, R., & Lescinski, J. (2009). Modelling storm impacts on beaches, dunes and barrier islands. Coastal engineering, 56(11-12), 1133-1152.

Roelvink, D., McCall, R., Mehvar, S., Nederhoff, K., & Dastgheib, A. (2018). Improving predictions of swash dynamics in XBeach: The role of groupiness and incident-band runup. Coastal Engineering, 134, 103-123.

Sallenger Jr, A. H. (2000). Storm impact scale for barrier islands. Journal of coastal research, 890-895.

Smit, P. B., Stelling, G. S., Roelvink, D., van Thiel de Vries, J., McCall, R., van Dongeren, A., ... & Jacobs, R. (2010). XBeach: Non-hydrostatic model. Delft University of Technology and Deltares.

Warren, I. R., & Bach, H. (1992). MIKE 21: a modelling system for estuaries, coastal waters and seas. Environmental Software, 7(4), 229-240.

Williams, J. J., Esteves, L. S., Conduche, T., Barber, P., & Tindle, A. (2014). Using combined modelling approaches to improve coastal defence design: a case study at Hopton, UK. Journal of Coastal Research, (70 (10070)), 18-23.

Zaslavskii, M. M. (2000). Nonlinear evolution of the spectrum of swell. Izvestiya. Atmospheric and Oceanic Physics, 36(2), 253-260.

3 Numerical assessments of sandbar systems and rip channel dynamics

3.1 Context

The evolution of seabed under the combined action of waves and currents has been extensively studied in the literature, but until nowadays is still not fully understood. Historically, many studies were carried out on the sediment transport pathway investigation, generation and migration of different bed forms, such as ripples and dunes (Sleath, 1984; Nielsen 1992; Fredsøe and Deigaard, 1992; Soulsby, 1997; Van Rijn 1993, 2007). Due to the complex nature of these phenomena, it is difficult to strictly interpret their mechanisms with a rational theory. Sand fluxes can be generated and driven by the combination of steady flows (currents) and oscillatory flows (waves). However, several other processes need to be taken into consideration, such as the mean water level variations (tide, wave set- up and set-down), breaking effects, and influence of the bed slope and form (Camenen and Larroudé, 2003).

Beach states have been observed to present a wide variety as it was shown by Wright and Short (1984) and Lippmann and Holman (1989). This observation was further corroborated via experimental procedures (Castelle et al., 2010; Michallet et al., 2013), numerical investigations (Dodd et al., 2003; Damgaard et al., 2002; Dronen and Deigaard, 2007; Reniers et al., 2004; Calvete et al., 2007; Roelving, 2012; Afentoulis et al., 2016) and video observations (Lippmann and Holman, 1989; Ranasinghe et al., 2000; Van Enckevort and Ruessink 2003; Turner et al., 2006).

The beach types can be classified into 13 beach states utilizing the dimensionless fall velocity (Ω) (Gourlay, 1968): $\Omega = H_b/(W_s T)$, with W_s = sediment fall velocity, H_b = breaker wave height, and T = wave period. Ω represents the relative contribution of wave height and period and sediment properties via the sediment fall velocity to beach morphodynamics. Using Ω wave-dominated beaches can be classified into six beach states. For low waves associated with long periods and coarse sand $(\Omega < 1)$, beaches can be considered reflective. When waves are moderate to high ($\Omega = 2 - 5$) beaches become rip-dominated – intermediate, while for the case

of high waves and fine sediments ($\Omega < 6$) beaches are characterized by a dissipative profile. It has to be mentioned that this beach classification concerns the wave-dominated coasts, which is also the area of interest of the present study, while tide-dominated beaches go through a similar transition, divided into three categories and characterized by the presence of a wide low tide bar (Klein and Short, 2016).

Wright and Short (1984) used a high number of visual field observation of waves, nearshore currents, and sandbar morphology of several wave-dominated beaches to carry out the most widely accepted sequential beach state classification scheme. The concept of two end states, the dissipative (D) and reflective (R) coast, are related to storms with periods of low-energy wave conditions, respectively, with the absence of bars and rip currents. The reflective beach state (R) lacks any dissipative characteristics, as breakers are only surging to collapsing and the turbulence due to the breaking is confined into the zone of high run-up on the beachface. On the other hand, the dissipative state (D) is associated with waves that break by spilling, dissipate progressively, while they enter in a wide surf zone, and reach the beachface with a low amplitude (Wright and Short, 1984).

In between, intermediate states can be identified, while bars and rip currents are observed. Intermediate beaches can be classified into four substates as, from the more reflective to the more dissipative, low tide terrace (LTT), transverse bar and rip (TBR), rhythmic bar and beach (RBB), and longshore bar trough (LBT). This classification scheme was also corroborated by high-frequency video observations (Ranasinghe et al., 2004). It was also extended to take into consideration the tide effects (Masselink and Short, 1993). Figure 3-1 illustrates the six wave-dominated beach states. A List of the 6 wave-dominated beach states and their environmental characteristics is presented in Table 12. The Ω and H_b are all approximate and can vary between wave environments (Klein and Short, 2016).

No.	Abbreviation	Beach state	Ω	H_b (m)
Wave dominated			1–6	
1	D	Dissipative	>6	>2
	I	Intermediate		
2	LBT	Longshore bar & trough	~5	<2
3	RBB	Rhythmic bar & beach	~4	>1.5
4	TBR	Transverse bar & rip	~3	~1.5
5	LTT	Low tide terrace	~2	~1
6	R	Reflective	~1	<1

Table 12 List of the 6 beach states and some of their environmental characteristics

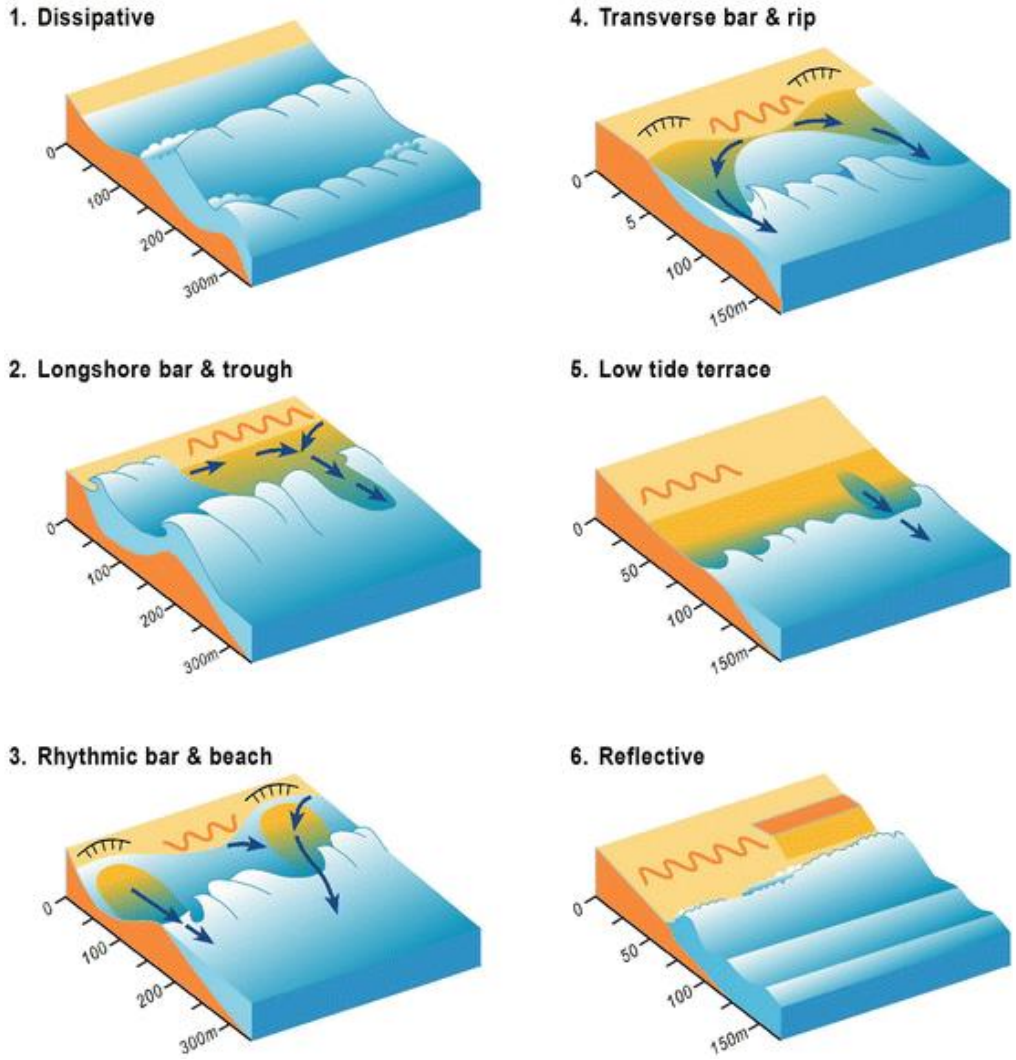

Figure 3-1 Schematic sketch of wave-dominated beach states (1–6), (Source: Short and Woodroffe, 2009).

Furturmore, conceptual models were developed to analyze the morphology and behaviour of sandbars, associated with each state (Brocchini, 2020; Wijnberg, 1997; Aagaard et al., 2004; Certain et al., 2005;Melito et al., 2020). In the widely recognized Net Offshore Migration (NOM) model, a sand bar undergoes a three-stage cycle often ranging from years to decades. The bar is firstly generated close to the shore, then it migrates offshore droven by intense wave conditions and finally, it disappears in the outer nearshore. Moreover, the Net Onshore Migration (NOnM) model suggests that sandbars are generated near the breakpoint and migrate towards the shore as a result of dominant onshore sediment transport due to wave skewness during storms. Contrary to the NOM and NOnM models, the Oscillation around a Point of Equilibrium model applies while a bar oscillates around a long term equilibrium position regardless of the incoming wave energy.

Castelle et al. (2010) carried out a 3D laboratory experiment to investigate rip current circulations over a moveable bed at the facilities of SOGREAH (LHF facility, G-INP, France), based on the pioneer work of Wright and Short (1984). Nearshore current patterns over several nature-like beach morphologies were assessed, while seabed varied from reasonably alongshore uniform to strongly alongshore non-uniform with crescentic patterns and bar-rip morphologies, representative of a full morphological down-state sequence. Both accretive and erosive shore-normal wave conditions were applied, the experiments conducted through all the states within the intermediate beach classification, during both up-state and downstate transitions (from a reflective to a dissipative beach profile and vice-versa). Results showed that any prescribed change in the wave conditions drastically increased the rate at which the morphology changes. This was the first 3D laboratory experiment providing extensive measurements of hydrodynamics and beach morphology through all the states within the intermediate beach classification. The investigation of hydro-morphodynamic phenomena revealed the subtle interplay between several feedback mechanisms associated to wave-driven rip current circulations, wave nonlinearities, sediment transport, and the seabed evolution.

To date, available morphodynamic model cannot simulate sufficiently the range of dynamics related to intermediate beach morphodynamics. The detailed morphodynamic data collected by Castelle et al., (2010) and Michallet et al., (2013) served here as an important benchmark for numerical investigations. Two different numerical approaches were used in the present study, to further evaluated the hypothesis that raised concerning the respective contribution of wave-driven circulation and to the positive and negative feedback mechanisms involved in both down-state and up-state morphology sequences. Thus, the main objective of the present research is to provide a comprehensive understanding of seabed-fluid interactions, and thus two distinct numerical devices were employed to simulate hydrodynamic conditions and morphological seabed changes under erosive and accretive wave sequences.

To deal with this type of interaction phenomenon, a numerical model based on shallow water equations, was exploited, providing a formulation for the seabed updates based on fluid and structure coupling using minimization principles (Bouharguane and Mohammadi, 2013), (Mohammadi and Bouchette, 2014). Minimization principles have been used many times in the past to design defence structures against beach erosion (Azerad et al., 2005), (Isebe et al., 2008). In these works, the designed structures were independent of time and were built once for all. Hence, this method goes one-step further giving the possibility to the structure to change in

time. It is worth pointing out that the fundamental assumption of this proposed method is the fact that bed adapts to the flow by some sort of optimal sand transport in order to minimize some energy expression, optimal transport is seen here as minimal change in the bed shape. The time scales of interest are below a day and recoveries between storms or seasonal and inter-annual variabilities are out of scope

Furthermore, a second numerical approach, based on the conventional formulations for sediment dynamics, was employed herein to simulate the hydrodynamic conditions and bathymetric evolution under erosive and accretive wave sequences. For the hydrodynamic predictions, a device that solve the two-dimensional non-linear shallow water equations (NSWE) in conservative form was applied (Marche and Bonneton, 2006), (Marche et al., 2007). These equations are discretized by a finite volume formulation, which preserve steady state solutions on non-flat sea beds in the absence of perturbations. A wave-maker was also implemented for the generation of irregular waves using directional spectral data. The mode of sediment movement was assessed using two different transport formulas. The first one is based on a quasi-steady approximation suggested by Ribberink, (1998) for the estimation of bed load transport, while the suspended transport was calculated from Camenen and Larson's (2005, 2007, 2008) formula. The second approach is based on Soulsby-Van Rijn approximation (Soulsby, 1997).

3.2 Experimental modelling and facilities

3.2.1 Description of experimental set-up

The laboratory experiment (Castelle et al., 2010; Michallet et al., 2013) was conducted during a period of 5 weeks in a multidirectional wave basin at the SOGREAH (LHF facility, G - INP, France). The basin's dimensions were 30 m in both cross - shore (y-axis) and alongshore (x-axis) directions with an offshore wall constituted of 60 independently controlled piston - type wave-makers (Figure 3-2). A beam sliding on rails supporting the instruments was applied for measuring the waves along cross-shore transects and the bottom elevation (Figure 3-3). The still water level was set at $h = 0.765$ m for all experiments. Natural sediment was used with a sand density of $ps = 2.65\ 10^3\ kg/m^3$, and a median diameter of $D_{50} = 164mm$ that corresponds to a settling velocity of $ws = 2cm\ s^{-1}$), while sand ripples were identified on the bed surface (Figure 3-3). The artificial coast was constructed with a basement of gravels covered with a geotextile. The seabed consisted of a fine-sand layer of at least 10 cm thick.

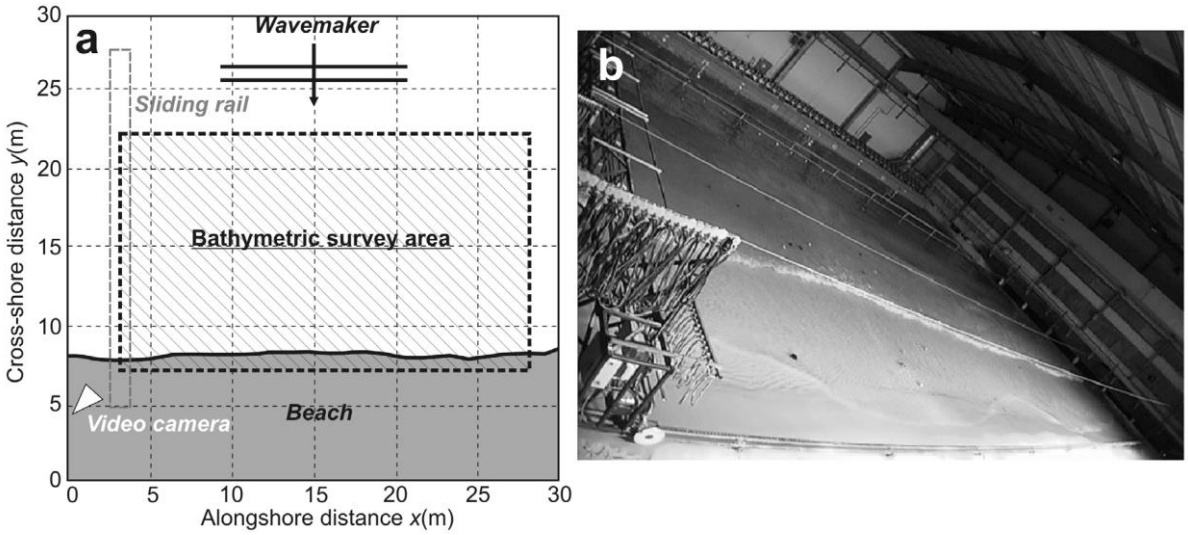

Figure 3-2 (a) Schematic of setup for the laboratory experiment with delimitations of the bathymetric survey area (dashed box) and location of the video camera. (b) Sample of captured video image with drifters (Castelle et al., 2010).

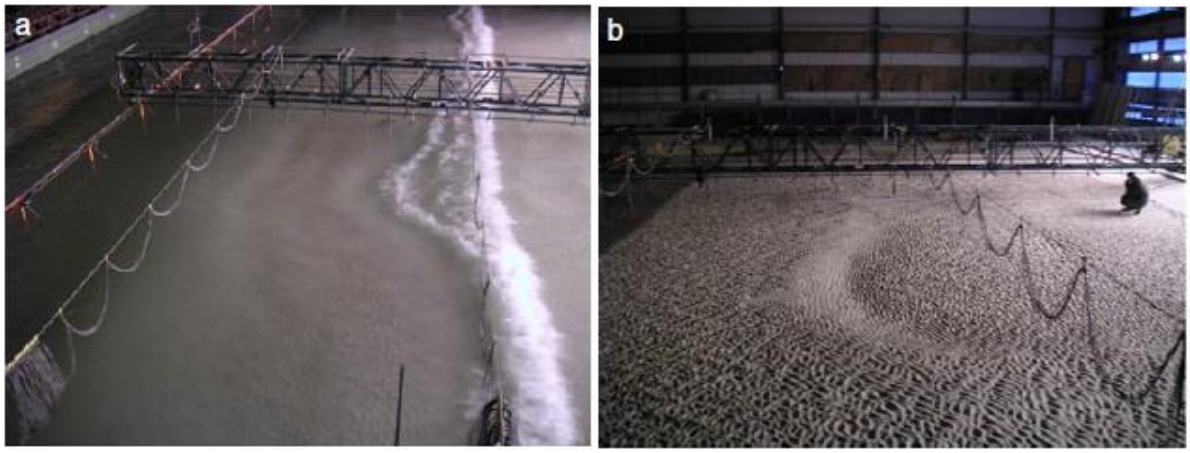

Figure 3-3 (a) View of a breaking wave front over the three-dimensional bathymetry. Wave paddles are shown in the top left corner and the sliding beam supporting the wave gauges (1 m apart) and velocimeters are seen on top of the picture. (b) View of the emptied basin during a bathymetric survey showing the presence of a crescentic sandbar and sand ripples (Michallet et al., 2013).

Shore-normal irregular waves complying with JONSWAP spectrum were applied in the offshore boundary. Three categories of wave conditions were considered, characterized by their significant wave height and peak period, namely as:

- energetic conditions (***A: Hm0 = 23 cm / Tp = 2.3 s, Ω=5);***
- moderate conditions with a large period (***B: Hm0 = 18 cm / Tp = 3.5 s, Ω=2.5***);
- Short period waves (***C: Hm0 = 17 cm / Tp = 2.1 s, Ω=4***).

These conditions were based in the criterion of dimensionless fall velocity or Dean Number ($\Omega=Hm0/Tp$) which is limited in the intermediate range ($A: \Omega = 5; B: \Omega = 2.5; C\,\Omega = 4$) as suggested by the study of Wright and Short (1984). A linear combination of 350 random sinusoidal components was utilized to generate each 20 minutes wave series. Each wave series was repeated until a preset duration. Moreover, the applied irregular waves were forced to have less energy at the center of the wave front by imposing a damped motion on selected wave paddles. Thus, an alongshore non-uniformity in the wave breaking was achieved, which drove nearshore circulations and induced the initial development of the 3-D bed patterns. The designed wavemaker conditions are shown in Figure 3-4 for the seven considered wave climates.

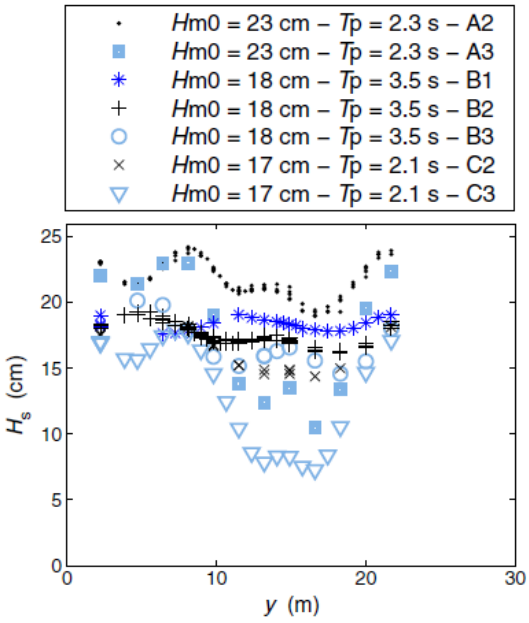

Figure 3-4 Alongshore distribution of significant wave height measured at x = 7.3 m (for a mean water depth of about 0.6 m) for the different wave climates (Michallet et al., 2013).

3.2.2 Experimental outputs

The initial bed geometry utilized for the purposes of the experiment is illustrated in Figure 3-5. The beach face has a slope, which is particularly steep, between 10% -15%, while mild slopes can be encountered in deeper water. In order to obtain this initial and realistic bed form mild wave conditions (C2) were applied for a duration of 4 hours. Figure 3-6 depicts the experimental results of seabed morphology deviation during an accretive wave sequence of 66 hours, with superimposed Eulerian (black arrows) and Lagrangian (white arrows) mean flow velocities. The applied wave climate (indicated on top of each panel) corresponds to moderate conditions associated with a large wave period. The beach is alongshore uniform at the beginning and at the end of this wave sequence. The transition between the intermediate states (from a reflective to a dissipative profile) is associated with the formation of three-dimensional hydro-morphodynamic patterns. In particular, a rip channel is clearly visible between t = 26:00 and 40:00.

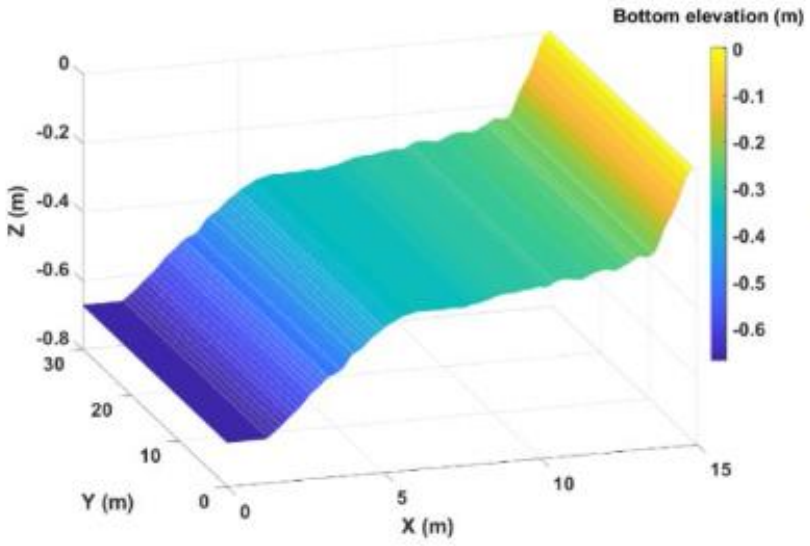

Figure 3-5 3D view of bottom elevation at t = 0 h

Figure 3-7 illustrates the measured seabed morphology deviation and bottom evolution velocity during an erosive wave sequence of 28 hours, with superimposed Eulerian (black arrows) mean flow velocities. The applied wave climate (indicated on top of each panel) refers to energetic conditions associated with a short wave period. The measured bathymetrical updates show an overall accretion offshore, while an increase of water depth can be observed nearshore, related to the offshore migration of the sandbar system. The rate morphological evolution decreases with time. This is due to the fact that the most rapid morphological adjustment occurs immediately after the change in wave conditions, which is in agreement with other studies in

the literature of coastal engineering (Afentoulis et al., 2017; Castelle and Ruessink, 2011). Finally, Figure 3-8 depicts the obtained measured alongshore-averaged beach profiles at the end of the main stages of the experiments (erosive and accretive sequences).

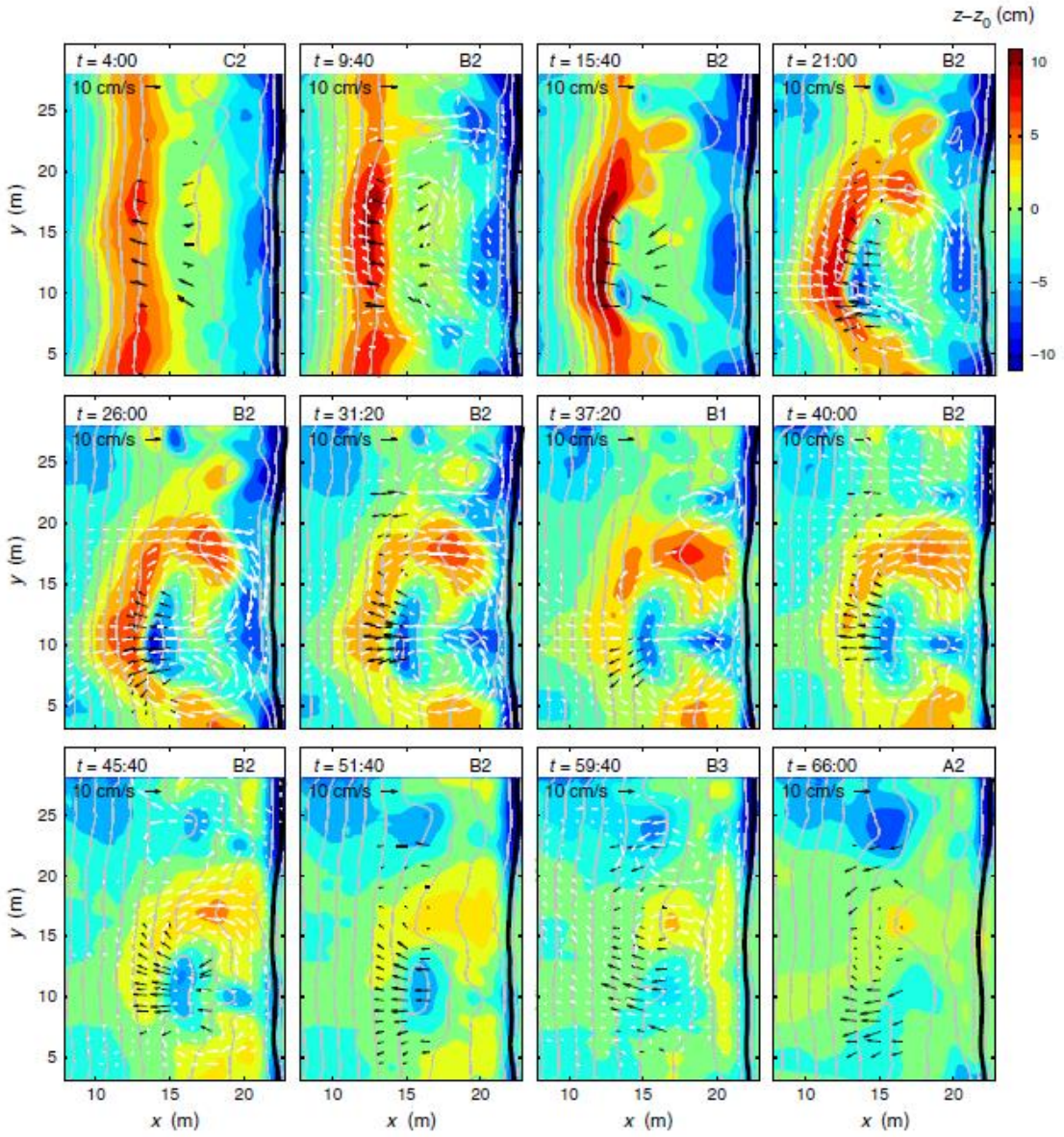

Figure 3-6 Seabed morphology deviation, with superimposed mean Eulerian (black arrows) and Lagrangian (white arrows) flow velocities during the accretive sequence of 66 hours. The wave climate is indicated on top of each panel (Michallet et al., 2013).

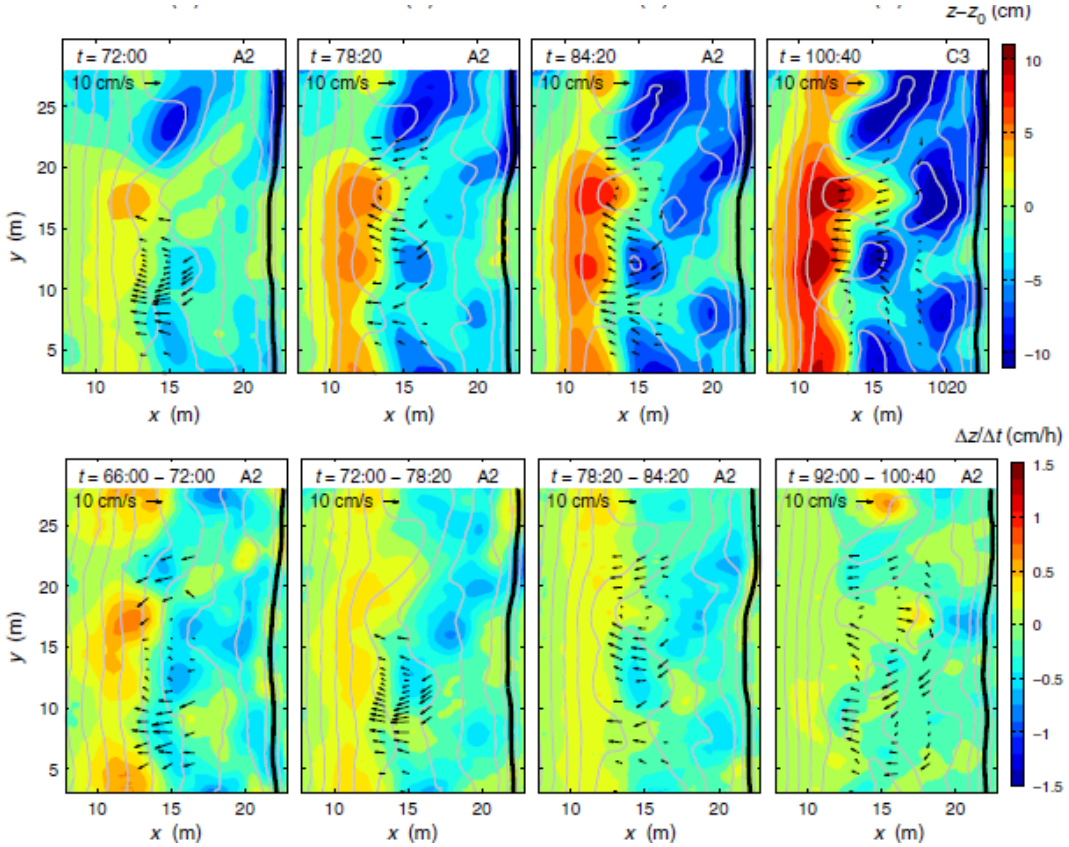

Figure 3-7 Bottom evolution velocity (up) and seabed morphology deviation(down), with superimposed mean Eulerian (black arrows) flow velocities during the erosive sequence of 66 hours. The wave climate is indicated on top of each panel (Michallet et al., 2013).

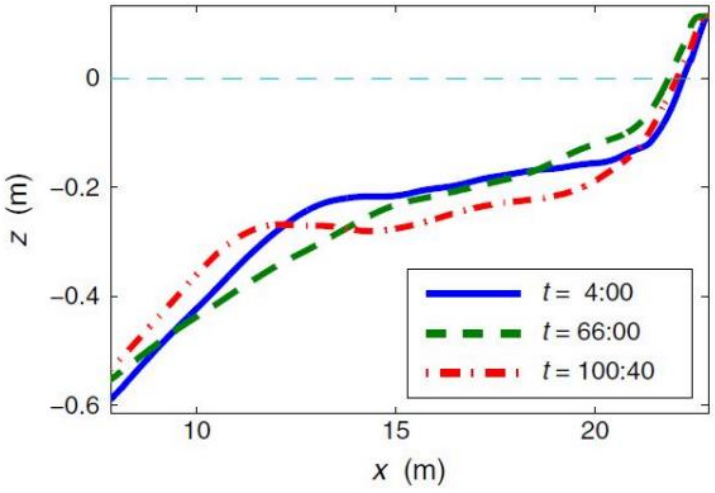

Figure 3-8 Alongshore-averaged beach profiles at the end of the three main stages of the experiment (Michallet et al. 2013) .

3.3 Numerical assessment of flow-seabed interactions using minimization principles.

3.3.1 Numerical modelling for fluid-seabed interactions

The present approach concerns an application of control theory to the evolution of sandy bed and the main aim is to exploit a formulation for the wave motion based on flow and structure coupling using minimization principles. The time scales of interest are below a week and recoveries between storms or seasonal and inter-annual variabilities are out of research's scope. Minimization principle have been used many times in the past to design defense structures against beach erosion. In these works, the designed structures were independent of time and were built once for all. Hence, the numerical formulation of Bouharguane and Mohammadi (2013) goes one-step further giving the possibility to the structure to change in time. One particular case is then the sea bed is seen as a structure with low stiffness. It's really necessary to describe precisely the fundamental assumption of this method which is the fact that bed adapts to the flow by some sort of optimal sand transport in order to minimize some energy expression, optimal transport is seen here as minimal change in the bed shape.

The approach is defined by considering a 2DH domain in shallow water. The sea bed (ψ: $\Omega \subset R^2 \rightarrow R^+$) changes in time following the variations in the state given by the flow conditions U. ψ is a univocal function with some regularity. A bed parameterization is used, based on the bathymetry given at all the nodes of the flow mesh. The model for the seabed evolution is based on minimization of a time dependent functional $J(\psi, U(\psi))$ where $U(\psi) = U(\psi, \tau, x, y), \tau \in [t - T, t], (x, y) \in \Omega$ gathers the state evolution in time, solution of a state equation.

Shallow water equations were employed as state equation for the flow (Saint-Venant equation): $= (h, hu)^t$, where u = $(h, hu)^t$ is the depth-averaged velocity with u and v the scalar components in the horizontal directions and h the water elevation.

$$F(U, \psi) = \begin{pmatrix} \nabla(hu) \\ \nabla(hu \times u) + gh\nabla(h + \psi) \end{pmatrix} \quad (3.1)$$

Where, $g = m/s$ is acceleration due to gravity.

Minimization of J can be seen as a solution of:

$$\begin{pmatrix} \partial_t \psi = -\rho(t, x)\, \nabla_\psi J(\psi, U(\psi)) \\ \psi(t = 0, x), \psi_0(x) = given \end{pmatrix} \quad (3.2)$$

Where ρ a positive parameter which depends on the porosity of the bed (Bouharguane and Mohammadi, 2013). The physical time scales for the flow and structure (bed motion) are quite different. Indeed, the flows have time scales of the order of seconds and the seabed motion takes place over hours.

$$J(\psi, U(\psi)) = \int_{t-T}^{t} j(\psi, U(\psi, \tau))d\tau \tag{3.3}$$

Where T indicates a time dependency window and permits to introduce a difference in time scales between seabed and flow motions.

3.3.2 Flow solver and hydrodynamics

The numerical approach of Bouharguane and Mohammadi (2013) incorporated a flow solver based on nonlinear shallow water equations (NSWE) (Marche et al., 2006). Previous studies have showed that NSWE give a good account of all the processes of wave transformation in coastal areas: shoaling, wave breaking run-up and two-dimensional wave-induced mean-currents over complex topography. These equations were discretized using a finite volume numerical scheme and they can be written as follows:

$$\boldsymbol{U}t \; + \; F(\boldsymbol{U})x \; + \; G(\boldsymbol{U})y \; = \; S(\boldsymbol{U})$$

$$\text{With, } \boldsymbol{U} = \begin{pmatrix} h \\ hu \\ hv \end{pmatrix}, F(\boldsymbol{U}) = \begin{pmatrix} hu \\ hu^2 + \frac{g}{2}h^2 \\ huv \end{pmatrix}, G(\boldsymbol{U}) = \begin{pmatrix} hv \\ huv \\ hv^2 + \frac{g}{2}h^2 \end{pmatrix}, \tag{3.4}$$

$$S(\boldsymbol{U}) = \begin{pmatrix} 0 \\ -gh\partial_x\psi \\ -gh\partial_y\psi \end{pmatrix}$$

Where (),x (resp. (),y) stands for the derivate along the x direction (resp. the y direction), $\boldsymbol{U} = (u, v)^t$ is the depth-averaged velocity with u and v the scalar components in the horizontal directions and h is the water elevation (Figure 3-9). $\boldsymbol{U}$ is the vector for the conservative variables, $F(\boldsymbol{U})$ and $G(\boldsymbol{U})$stand for the flux functions respectively along the x and y directions and $G(\boldsymbol{U})$ is the bed slope source term with the bed slope ($\partial_x\psi, \partial_y\psi$).

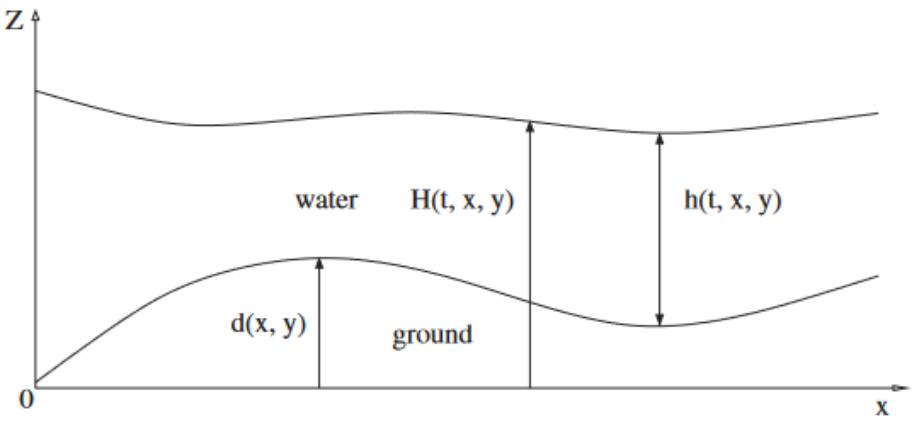

Figure 3-9 Surface elevation, water depth and topography

Numerical non-linear shallow water equations simulations based on shock-capturing schemes to predict wave breaking, and this theoretical framework shows good results in comparison with both field data (Bonneton and Dupuis, 2001) and laboratory data. Two types of boundary conditions were utilized. In the outlet region a transmissive boundary was employed, thus values at boundary cells can be obtained by second order extrapolations normal to the boundary from the values inside the domain. It leads to a simple absorbing boundary condition, efficient for outflows configurations. To describe incoming waves absorbing/generating inlet boundary condition were used, so that in offshore area reflected waves are allowed to freely exit the domain. Moreover, wet drying conditions were applied to describe the swash mechanisms close to the shoreline.

For the offshore boundary, Bouharguane and Mohammadi (2013) developed a wave generator and the free surface water elevation at the inlet is represented by the addition of N monochromatic shore-normal waves:

$$h(t) = h_0 + 2A \sum_{i=1}^{N-1} sin(\frac{\omega_i + \omega_{i+1}}{2} t)\, cos(\frac{\omega_i + \omega_{i+1}}{2} t) \tag{3.5}$$

Where A is the wave amplitude at inlet and h_0 the still water level. Time integration is explicit for the flow. Due to the difference of time scales between fluid motion and seabed updates, a duration of wave action equal to several wave periods (typically 40-70) is simulated by the flow solver before a new time step by the morphological model described by the minimization iterations.

3.3.3 Numerical validation based on experimental findings

For the needs of the numerical investigations, the case of the wave basin of 30 m side that was presented in paragraph *3.2.1* was considered and the mean water depth was set to $h_0 = 0.765$ m, in order to compare the computed and measured hydrodynamic and morphodynamic characteristics in the same domain. The same wave conditions as that of the experiment were applied in the offshore boundary, thus, the total duration of wave action (96.4 h) was divided into 2 phases, the 62 hours of the accretive wave sequence with B-moderate wave conditions ($Hs = 18\ cm\ /\ T\ p = 3.5\ s$) and 34.4 hours of the erosive sequence with A-energetic wave conditions ($Hs = 23\ cm\ /\ T\ p = 2.3\ s$). In Figure 3-10 the wave time series at a specific point of the basin ($x = 18.33, y = 9.27$) is presented, as obtained by the experiment and the numerical model. Moreover, fine sand with a median diameter of $D50 = 164mm$ was considered, similar the one utilized in the experiment.

The first set of validation concerning the model's capacity to predict the wave behaviour along offshore and nearshore areas, as well as in the transition zone. It is important to mention that only shore-normal waves were numerically generated in the offshore boundary due to the nature of the model. The computed wave record agrees reasonably well with the measured surface elevation. Simply by visual inspection, enough concordance can be identified between the numerical and measured wave periods, but a number of differences are presented regarding the wave amplitude. In Figure 3-11 the cross-shore distribution of significant wave height for the case of the erosive wave sequence is depicted. A good agreement of experimental and numerical results was obtained offshore while significant discrepancies can be seen close to the shore. The observed inaccurate predictions of the model in nearshore area can be caused due to dispersion phenomena that cannot be simulated via the non-linear shallow water equations. This level of precision continue for all the locations of the wave gauges along the cross-shore profiles, thus the selected numerical model could be considered sufficiently accurate to take to the next level of comparison, looking at the evolution of the bed shape.

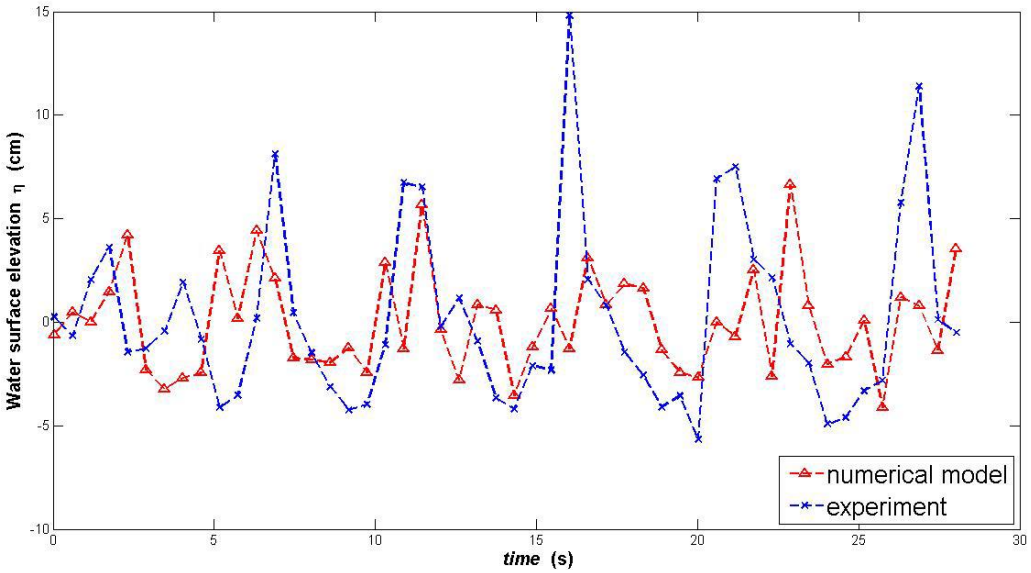

Figure 3-10 Wave record at (x =18.33, y =9.27), as obtained by the numerical model (red line) and experimental data (blue line).

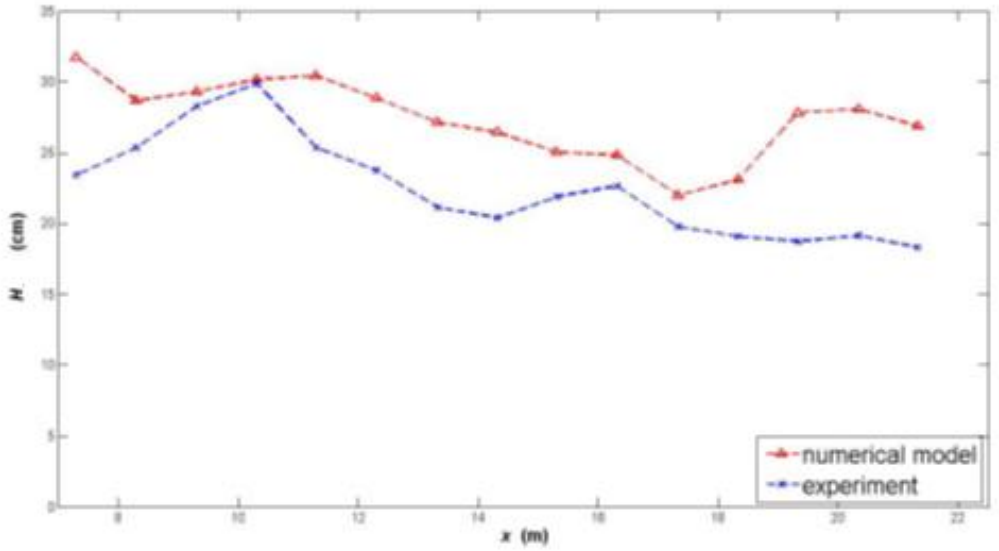

Figure 3-11 Cross-shore distribution of significant wave height for the erosive wave sequence (Hs =2.3 m, Tp =2.3s) of experimental data (blue line) and numerical outputs (red line), at y = 9:27 m .

For the estimation of sediment transport dynamics and the evolution of the beach profile, the wave climates of the experiments were reproduced numerically. Only the area between 6 ≤ x ≤ 26 m was taken into account, where the sandy bottom extends and where measurements conducted (Figure 3-2). It is also worth mentioning that the wave front at the inlet of the numerical model was considered uniform, while for the needs of the experiment, the wave forcing at the wave-maker is set to be alongshore non-uniform. However, some alongshore fluctuations were observed, after the first steps of the numerical simulation before the sandbar three-dimensionality starts to decrease. In other words, wave driven circulations were therefore assumed to be essentially guided and constrained by the 3D sandbar morphology, with negligible effect of the alongshore non-uniform wave generation at the wavemaker (Castelle et al., 2010).

The most striking feature of the results illustrated in Figure 3-12, is that the evolution of the bed shape over the time, follows the same sequence as that of the experiment. During the first phase, an overall accretion of the beach face was observed over a time period of 62 hours of mainly B moderate and long period wave conditions (Hm0 = 18 cm / T p = 3.5 s). During this stage, the obtained results show an onshore migration of the sediments and a significant erosion of the seaward section (x ≤10 m). For this wave sequence, by the comparison of the obtained three-dimensional bathymetry with that of the experiment (Figure 6), it can be concluded that the accretion in the case of the numerical findings, is more intense and extends further seaward. Concerning the second stage between 62 ≤T ≤96.4 hours with A energetic and short period wave conditions (Hm0 = 23 cm / T p = 2.3 s), an overall erosion is obtained for the case of numerical predictions. As it can be derived from Figure 3-13, sandbar system was migrated seaward. The comparison with the experimental data of Figure 3-8, shows that the erosion is less intense shoreward in the case of the numerical model and the sediment concentration in the section x ≤6 is higher than that of the experiment.

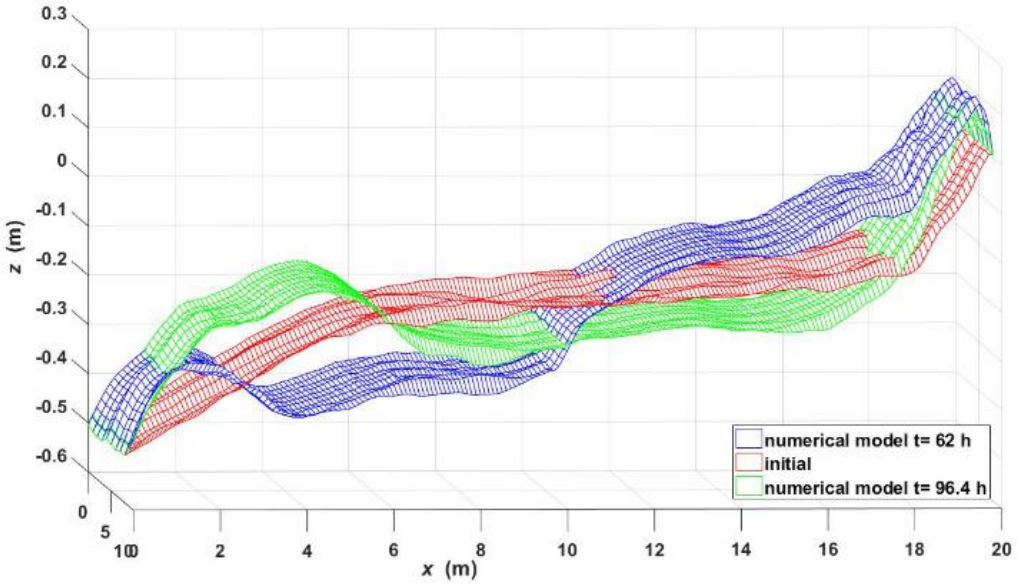

Figure 3-12 Three dimensional shape of the bed (bathymetry) during the first simulation phase (accretive wave sequence). Initial (red lines), numerical model (blue lines) and experiment (green lines).

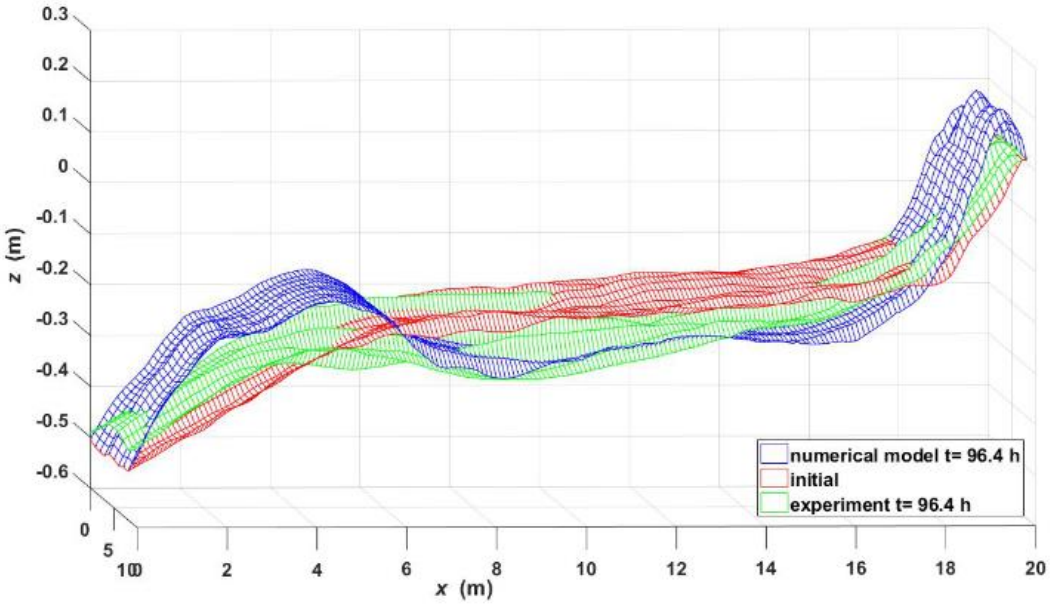

Figure 3-13 Three dimensional shape of the bed (bathymetry) during the second first simulation phase (erosive wave sequence). Initial (red lines), numerical model (blue lines) and experiment (green lines).

The present results are direct in agreement with existing studies (Russell, 1993), (Thornton et al., 1996), which have revealed that the beach erosion is proportional to the amount of the wave energy in the coastal zone. Furthermore, it is not a simple task to compare the characteristics of the alongshore morphology, since the wave caracteristics at the inlet of the numerical model were not identical. However, conversely to the study of (Michallet et al., 2013), these results seem to be compatible with that of (Wright and Short, 1984), as a decrease of the beach three dimensionality was presented during the morphological evolution. As concluded from the present work, applying the same wave climate for a long time period resulted in a decrease in the bottom evolution velocity. Hence, the beach tends towards a steady state, by reshaping the bar into an alongshore-uniform pattern. Additionally, for the comparison of the alongshore morphological characteristics, it has to be considered that the lateral boundaries in the physical model act as headlands, increasing the beach three-dimensionality. It was assumed that the differences in the morphological evolution within and between beaches during storms, are related to embayment geometry and orientation of the shore, while the sediment transport can be driven by marked alongshore gradients in breaking wave height and interaction with embayment boundaries (Loureiro et al., 2012). This phenomenon was not numerically predicted, since the values at boundary cells are obtained by second order extrapolations normal to the boundary from the values inside the domain.

3.4 Numerical approaches for the evaluation of sediment transport mechanisms on a shallow sloping sea bottom based on quasi-steady approximations.

In this section, the seabed evolution due to wave - current interaction was examined for the case of the gently sloping bottom of the aforementioned experiment (paragraph 3.2). Here, an attempt was made to estimate bed level changes over a duration of 96 hours, under accretive and erosive wave sequences applying Jonswap-type incident waves and quasi-steady formulations for the investigation of sediment fluxes. The flow solver, which is based on the non-linear shallow water equations (NSWE), was utilized (paragraph 3.3.2) in order to simulate the wave propagation and hydrodynamic conditions. Two different approaches were employed for the detailed investigation of sediment transport rates and seabed-fluid interactions, using the formula of Soulsby (1997) for the total load, while the approximations of Camenen and Larson (2005, 2007, 2008) and Ribberink (1998) were also employed for the assessment of suspend and bed load sediment fluxes. The simulation was carried out on a variable coastal bathymetry corresponding to the wave basin experiments of Michallet et al. (2013) at LHF facility (Grenoble INP, France), whilst obtained results were qualitatively compared with laboratory observations.

3.4.1 Hydrodynamic solution

For the assessment of hydrodynamic conditions, the model, described in paragraph 3.3.2, which solves the two-dimensional non-linear shallow water equations (NSWE) in conservative form was applied (Marche and Bonneton 2006; Marche et al. 2007). These equations are discretized by a finite volume formulation, which preserves steady state solutions on non-flat sea beds in the absence of perturbations. The main advantage of this numerical approach is that breaking events can be modelled as the development of a free-surface and current discontinuity (Bonneton et al. 2010). It has to be noted, however, that dispersion effects are not considered, which a limitation of this approach is. A wave-maker was implemented also for the generation of irregular waves using directional spectral data. These irregular waves can be obtained by superposing a series of wave components with different frequencies and directions, using random phases.

3.4.2 Morphodynamics

In the present work, the mode of sediment movement is investigated using two different transport approaches. The first one is based on a quasi-steady approximation suggested by Ribberink (1998) for the estimation of bed load transport, while the suspended transport is calculated from Camenen and Larson's (2005, 2007, 2008) formula. The second approach is based on Soulsby - Van Rijn approximation (Soulsby 1997). This formula applies to total (bed and suspended load) sediment transport in combined waves and currents on sloping beds. Averaged sediment fluxes were obtained, by integrating the transport load over N wave periods (typically $N \geq 50$). Furthermore, a slope limiting methodology was applied to control the maximum bottom slope, which is considered equal to the sediment repose angle (≈32 deg) (Bailard and Inman 1981). This module is of high importance, especially for the needs of the simulated morphodynamics in the inner surf and swash zone, where the mechanism of avalanching is dominant.

3.4.2.1 Formulas of Ribberink and Camenen – Larson

3.4.2.1.1 Bed load transport

Ribberink suggested a quasi-steady model of bed load transport where the solid flux is proportional to a function of the difference between the actual time-dependent bed shear stress and the critical bed shear stress. This formula is described by the following expression for the sand transport rate:

$$\boldsymbol{q_{SB}} = m_{Rib}\sqrt{(s-1)gd^3}\left\langle(\left|\overrightarrow{\theta(t)}\right| - \theta_{cr})^{n_{Rib}}\frac{\overrightarrow{\theta(t)}}{|\theta(t)|}\right\rangle \quad (3.6)$$

where, $\overrightarrow{\theta(t)} = 0.5f_{cw}|u(t)|\overrightarrow{u(t)}/[(s-1)gd]$ is the time-dependent Shields parameter with the instantaneous velocity $\overrightarrow{u(t)} = \overrightarrow{U_c} + \overrightarrow{u_W(t)}$, s the relative density of sediment and f_{cw} the wave –current friction factor. ⟨ ⟩: Time-averaged over several wave periods; and m_{Rib} = 11, n_{Rib} = 1.65: adjusted coefficients.

3.4.2.1.2 Suspended load transport

The Camenen and Larson (2005, 2007, 2008) transport rate formula is adopted for estimating suspended load. This formula is described by the following expression for the suspended load transport:

$$\boldsymbol{q_{SB}} = \overrightarrow{u(t)}\frac{C_R\varepsilon}{W_s}[1 - e^{-\frac{W_s h}{\varepsilon}}] \quad (3.7)$$

Where, $c_R = 3.51^{-3}e^{-0.3d*}\theta_{cw,m}e^{-4.5\frac{\theta_{cr}}{\theta_{cw}}}$ is the reference concentration at the bottom with $d_* = \sqrt[3]{(s-1)g/v^2d_{50}}$ the dimensionless grain size, v the kinematic viscosity of water, $\theta_{cw,m}$ and θ_{cw} the mean and maximum Shields parameters due to wave-current interaction and ε the sediment diffusivity.

3.4.2.2 Formula of Soulsby-Van Rijn

Soulsby-Van Rijn's formula (Soulsby, 1997) was derived for total (suspended and bed load) sediment transport in combined wave and currents on horizontal and sloping beds. This approach is described by the following expression for the sand transport rate:

$$\boldsymbol{q_t} = A_s\overline{U}\left[\sqrt{\overline{U}^2 + \frac{0.018}{C_D}{U_{RMS}}^2} - \overline{U}_{CR}\right]^{2.4}(1 - 1.6tan\beta) \quad (3.8)$$

Where, $A_S = A_{SB} + A_{SS}$ with $A_{SB} = \frac{0.005h(\frac{d50}{h})^{1.2}}{[(s-1)gd_{50}]^{1.2}}$ and $A_{SS} = \frac{0.012d_{50}d_*^{-0.6}}{[(s-1)gd_{50}]^{1.2}}$. $\overline{U}$ is the depth averaged velocity, U_{RMS} the root-mean-square wave orbital velocity, C_D the drag coefficient due to current alone, $\overline{U}_{CR}$ the threshold current velocity and β the bed slope.

3.4.3 Morphology

The estimation of bathymetrical updates requires maintaining a budget of sediment fluxes that calculated via the instantaneous flow parameters. Thus, these sediment transport rates were integrated over a number of time steps, which correspond to several wave periods. The

bathymetry update was calculated by solving the sediment mass conservation equation which reads:

$$\frac{\partial z_b}{\partial t} = -\frac{\text{Morfac}}{1-n_p}\nabla \cdot \boldsymbol{q}_{tot} \ , \tag{3.9}$$

where, n_p is the sediment porosity, $\boldsymbol{q}_{tot}$=$(q_{tot,x}, q_{tot,y})$ denotes the total volumetric sediment transport rate equal to the sum of suspended and bed load transport rate, z_b is the local bottom elevation and Morfac is a morphological acceleration factor. This nonunity factor (Morfac) applies a scalar multiplier to the sediment continuity equation and speeds up the depth change rates, multiplying them by a constant value. In this study, Morfac values (ranging from 1 to 30) were systematically adapted to be compared with a baseline condition of no acceleration. Care must be taken not to exaggerate with extreme Morfac values, in order to describe realistically the interaction of the wave, hydrodynamic and morphology modules.

3.4.4 Model's setup

The scenarios of the experimental series, conducted by Michallet et al. (2013) at LHF facility (Grenoble INP, France) were considered here. 3D bottom topography with colour map and alongshore-averaged beach profiles during the three main stages of the experiments are depicted in Figure 3-5 and Figure 3-8, respectively. The applied offshore wave climates, defined by their significant wave height and peak period, are divided into two main categories: energetic conditions (A:$Hs = 18\,cm\,/\,T\,p = 3.5\,s$) and moderate conditions with a large period (B:$Hs = 23\,cm\,/\,T\,p = 2.3\,s$). These wave characteristics correspond to the so-called down-state and up-state wave transitions respectively (i.e. the change from high to low wave energy in the case of the accretive sequence and the change from low to high wave energy in the case of the erosive sequence). The still water depth is set to $h_0 = 0.765$ m and the length and time scales are $1/10$ and $\approx 1/\sqrt{10}$ respectively, using Froude similarity law. Fine sand is considered, with a specific gravity (Gs) of 2.65 and a median diameter $D50$ of $164mm$ which corresponds to a settling velocity ($Ws = 2$ cm/s). The total simulation time is 96.4 hours and it is divided into two parts, 62 hours duration of B wave conditions and 34.4 hours duration of A wave conditions. In order to create alongshore non-uniformity in the wave breaking spatial pattern, the wave directional spreading at the inlet varies from 20 to 30 degrees.

3.4.5 Numerical validation based on experimental findings

In Figure 3-14 the evolution of wave height distribution during the erosive and accretive sequence, as well as the initial bottom topography are depicted. The modification of computed significant wave height distribution during the 36 hours of erosive wave conditions is due to wave-bed evolution joint actions. The wave generator, which was tailored for the needs of our assessments, contributes to the application of a more realistic wave climate, in comparison with the one generated using the numerical model of Bouharguane and Mohammadi (2013) (paragraph 3.3.2). Figure 3-15 presents the numerically produced time series of surface elevation at the inlet. The implementation of direction spreading plays a crucial role for the displacement of breaking zone with an alongshore irregularity, which in turn drive the nearshore hydrodynamic circulation. Although the limitation of the model, concerning the prediction of dispersion effects in the transition water between offshore and shallow water depths, results in an abrupt bottom-induced wave breaking in the zone where significant bathymetric gradients are presented, at x=∼ 5 m.

The initial wave-induced current field after 1 hour of wave action, superimposed with bathymetrical updates, is depicted in Figure 3-16, for the accretive wave sequence. A formation of a parallel to the shore wave-induced current filed can be observed nearshore. This formation is generated due to the wave breaking and the spatial bathymetric gradient of the beach face, that drive the circulation. Additionally, weak rip currents with a velocity of about 0.05m/s can be identified toward the offshore boundary of the computational domain, while the alongshore-oriented velocities detected close to the shore, reflected from the beach face with a maximum velocity of 0.1m/s.

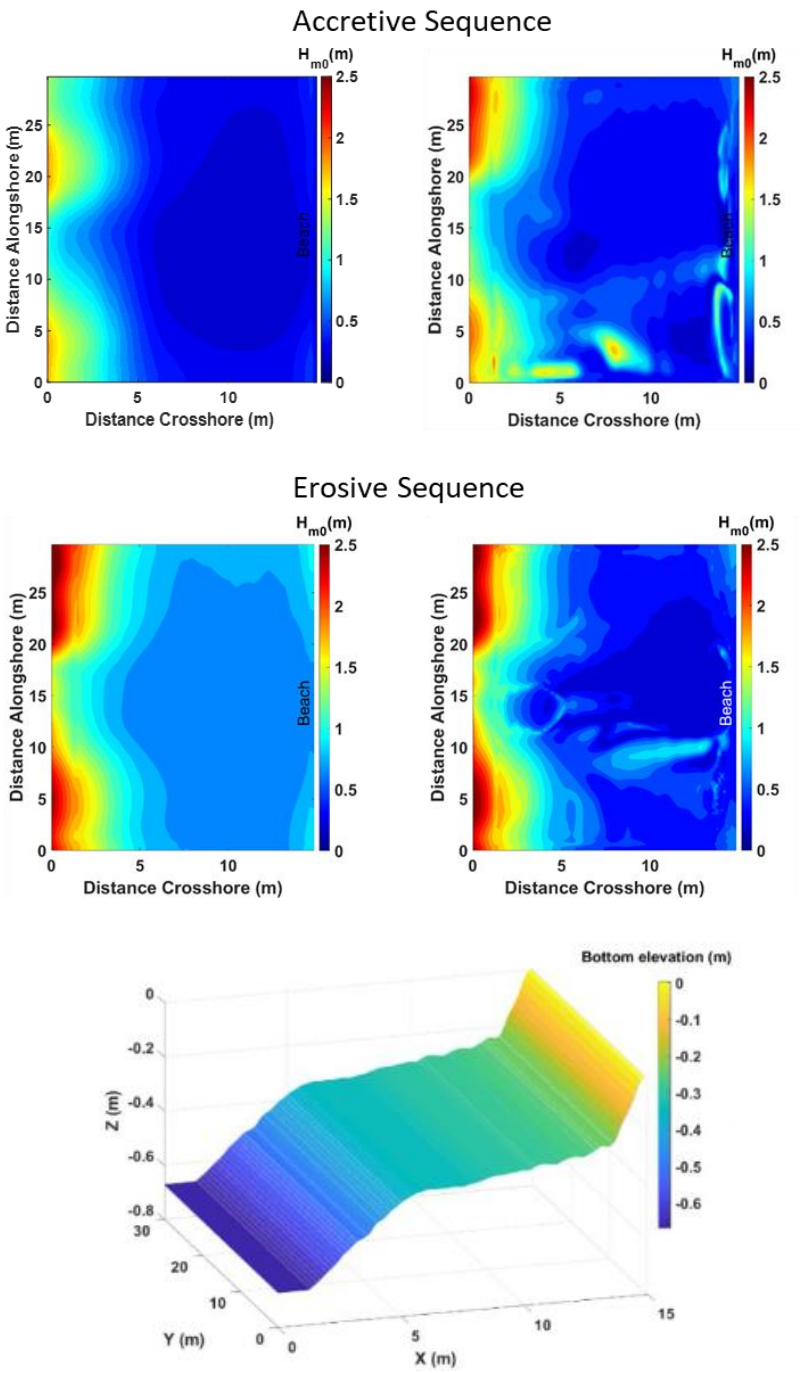

Figure 3-14 Map of evolution of wave height distribution during the accretive (up) and erosive (middle) initial bottom elevation (down).

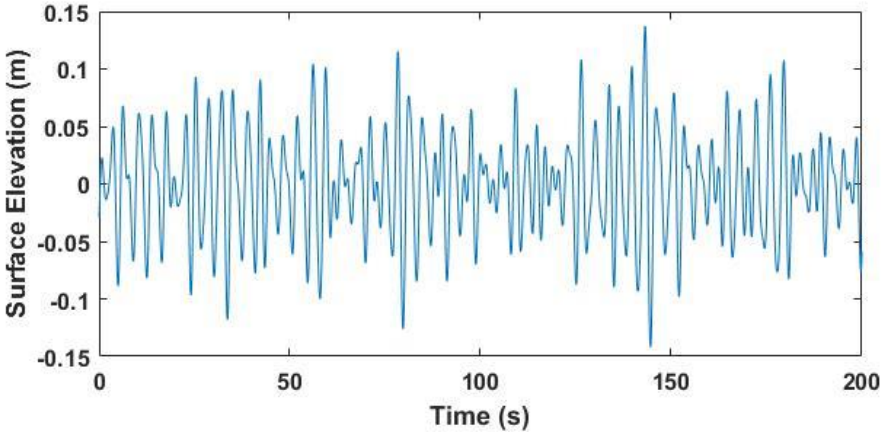

Figure 3-15 Wave record at the inlet.

Figure 3-16 depicts the wave-induced current field after 7 and 30 hours of wave action, superimposed with seabed changes during this time. The seabed evolution is more intense in the zones where significant spatial velocity gradients occur. Close to the shore, the seaward oriented currents resulted in the altering of the uniformity of the beach in the alongshore direction, with associated erosion conditions close to the lateral boundaries. It should be mentioned that the initial geometry with a cross-shore constant slope is not realistic, thus the wave-current-seabed system tends to find an equilibrium by altering the beach slopes near the shoreline. Therefore, dissipative conditions are observed in the foreshore beach morphology after 30 hours. This three-dimensional beach form forces alongshore nearshore currents with a magnitude of 0.1m/s. It can be observed that no significant differences of sea bottom geometry take place between 30 and 60 hours and it is concluded that the rate of bottom level change was high initially and slowed down as equilibrium approached. Close to the equilibrium stage, relatively weak velocities of about 0.07m/s characterize the wave induced current field.

In Figure 3-17 the wave-induced current field after 1, 5, 15, and 30 hours of erosive wave conditions is illustrated, superimposed with bathymetrical updates contour. It can be observed that the numerical simulation performs reasonably well, as an offshore sediment movement characterizes the erosive sequence. The intensity and direction of the wave-induced currents are determinant for the morphological changes of the sea bottom. The flow is characterized by a rip current, which has a relatively shore-normal orientation and a magnitude of about 0.05 m/s and 0.1 m/s. The intensity of seaward currents causes an offshore sandbar migration under energetic wave conditions. The mean circulations obtained during the experiments of Michallet et al. (2013) have a same mean flow magnitude but their directions are highly variable during each sequence. This is to some extent due to the imposed wave conditions of the experiment,

where the wavemaker is designed to have a varying damping at the center of the wave front. Thus, the seabed alongshore non-uniformity obtained by the numerical simulation is more intense.

The seabed evolution at the end of the accretive and erosive sequence using Ribberink's and Camenen – Larson's formulas is presented in Figure 3-18. Seabed changes at the end of each experimental stage are in the same order of magnitude as that of the measured ones, putting in evidence the dominant role of hydrodynamic patterns in nearshore morphology. The obtained results yield information on the emergence of nearshore periodic patterns, corresponding to the fastest growing mode, subject to the irregular sediment transport patterns over the initial bathymetry. The observed deviations of final bottom geometry are between -0.1 m and +0.1 m. Overall, a good agreement between both experimental (Figure 3-8) and numerical results was achieved, as the seabed adapts correctly to the wave climate changes. Further numerical investigations are needed to investigate the inverse transition from the dissipative to the reflective beach state and back again, considering the intermediate sub-states according to the work of Wright and Short (1984).

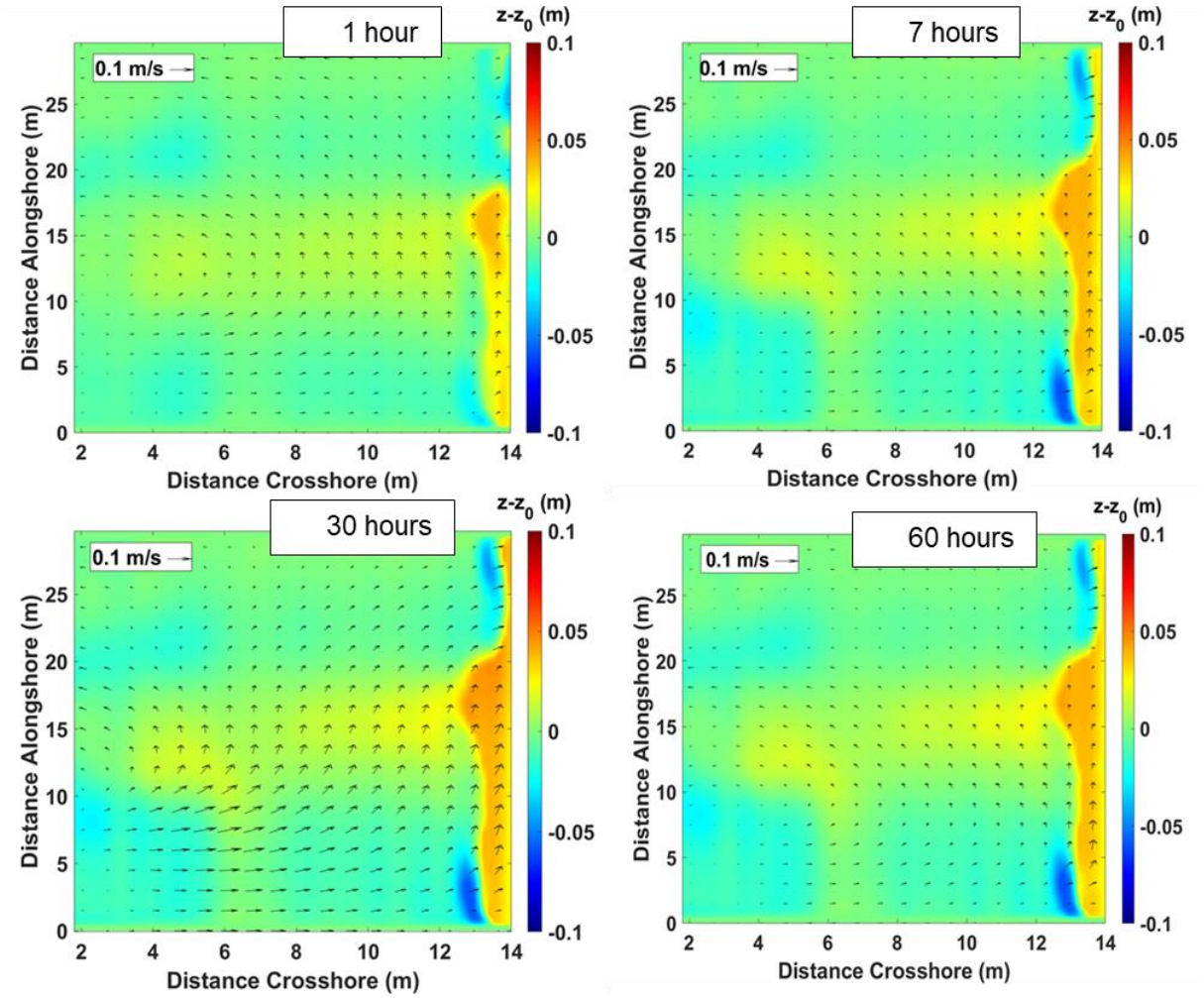

Figure 3-16 Simulated hydrodynamics after 1, 7, 30, 60 hours of accretive wave conditions. Colours: Computed Bathymetrical evolution, Vectors: calculated wave induced current intensity and direction

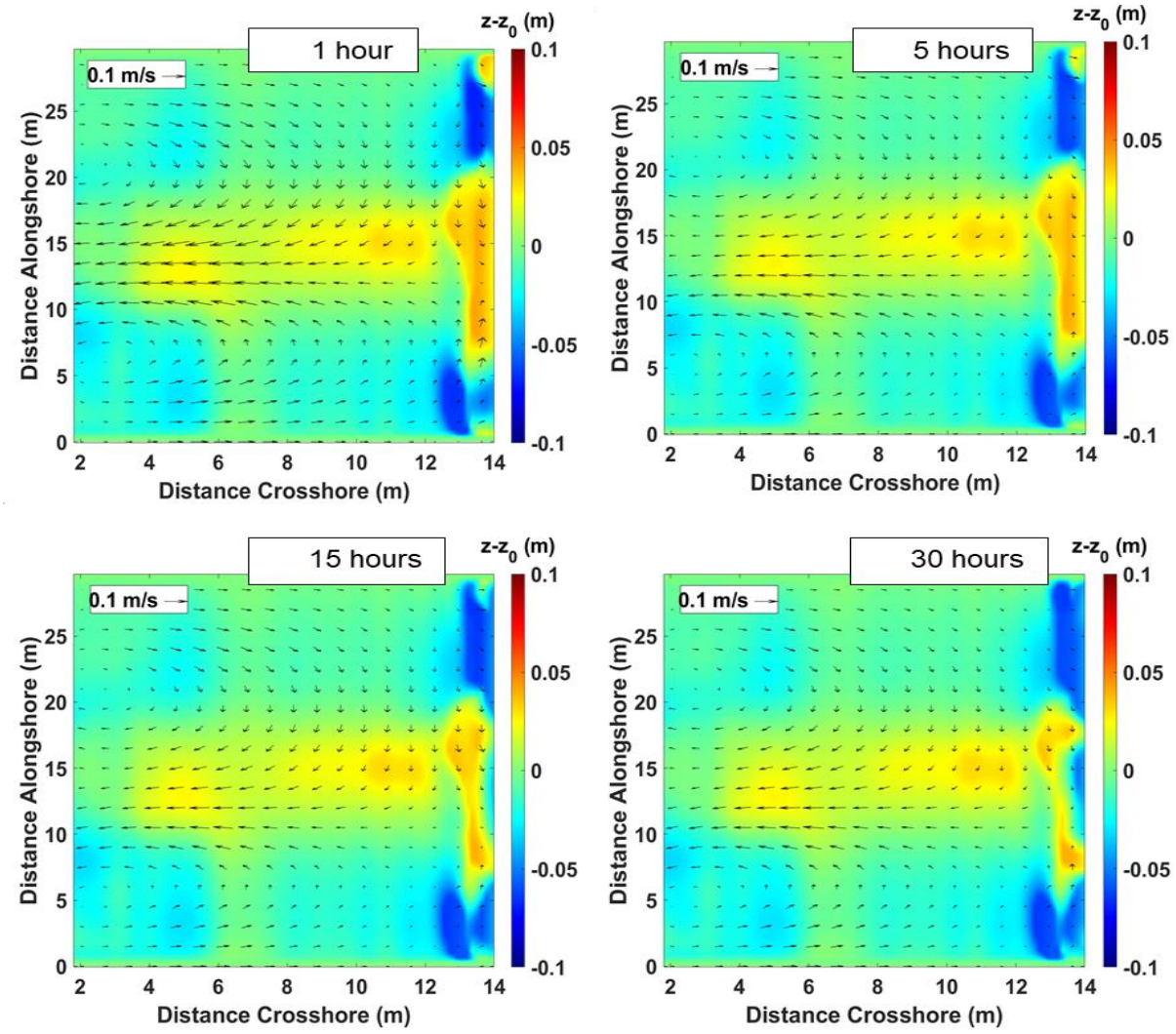

Figure 3-17 Simulated hydrodynamics after 1, 7, 30, 60 hours of erosive wave conditions. Colours: Computed Bathymetrical evolution, Vectors: calculated wave induced current intensity and direction

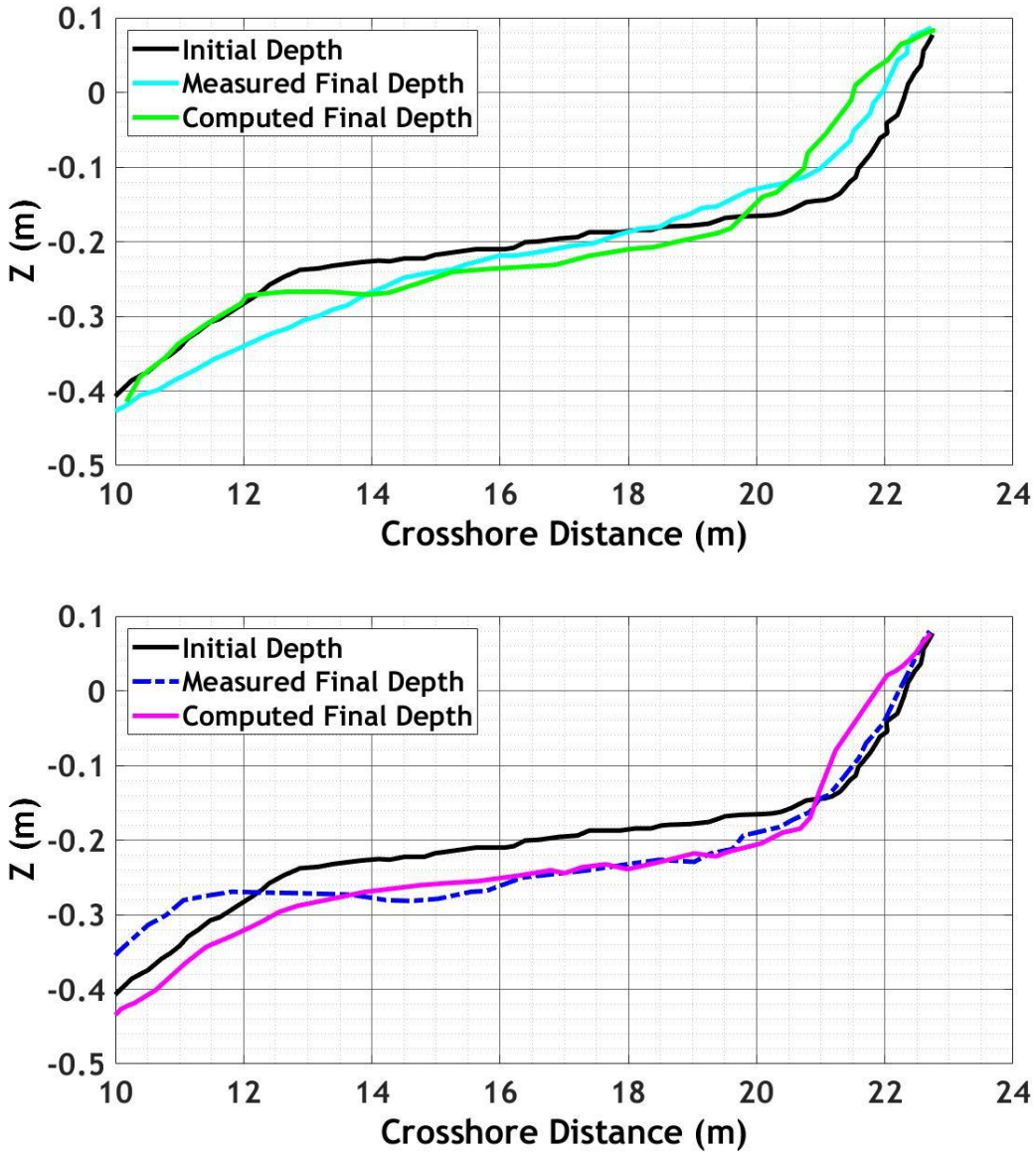

Figure 3-18 Alongshore-averaged beach profiles at the two main stages of the simulation Ribberink's and Camenen – Larson's formulas.

3.5 Discussion

As already discussed previously in this study, the main scope of the present research is to develop a reliable tool for assessing the coastal sediment transport and morphology. The complexity and uncertainty of the various processes is so intense that predictions of sediment fluxes within a factor of 2, or even 5, can be considered as satisfactory, especially for field measurements (Klonaris, 2016). However, nowadays, novel techniques for an integrated coastal zone management, or shoreline and sediment management, require sediment loads to be estimated realistically, despite the level of uncertainty. Therefore, in this section an attempt was made to further our ability to understand wave-sandy bed interaction on a shallow sloping bottom without the presence of coastal structures and investigate the effect of rip channels an nearshore currents on sand bar systems. Following the work of Wright and Short (1984), which put in evidence the role of erosive and accretive wave sequence that drive the transition from a dissipative to a reflective beach profile and vice versa, numerical modelling techniques were applied to validate this statement. The numerical outputs were validated against the experimental findings of Michaellet et al., (2013).

Two distinct approaches were employed for the evaluation of nearshore morphodynamics and particularly the impact of wave climate variations on nearshore morphology. The first device, which was utilized herein, is based on minimization principles for the assessment of bed morphology. The fundamental assumption of this method is the fact that bed adapts to the flow by some sort of optimal sand transport in order to minimize an energy expression, optimal transport is seen here as minimal change in the bed shape This numerical method provided reliable results, concerning the identification of the nearshore zones, in which accretion or erosion prevail. Although, the limitation of this model to reproduce a realistic wave climate offshore (only shore-normal waves were considered), makes difficult the simulation of nearshore hydrodynamic currents that follow the patterns, which were observed during the experimental campaign. Concerning the computed final alongshore bed geometry, a good agreement between computed and measured parameters was achieved. This can lead to the conclusion that this numerical technique can provide accurate prediction for 1DH coastal applications., with and without the presence of coastal structures, as it was demonstrated in chapter 2 (paragraph 2.3: 2.3Tested configurations – Coastal defences).

In addition, another numerical compound model, was utilized in this study for the investigation of hydrodynamic and morphodynamic 2DH phenomena, based on nonlinear

shallow water equations (NSWE) and a numerical wave-maker was developed for the needs of this research to generate irregular waves, using directional spectral data. These irregular waves can be obtained by superposing a series of wave components with different frequencies and directions, using random phases. Moreover, the author developed a new sediment transport model that was utilized in tandem with the hydrodynamic model. This device accounts for the prediction of the combined action of waves and currents and the evaluation of wave unsteady effects on sediment transport rates

The nearshore processes of wave propagation, hydrodynamic circulation, sediment transport and morphology were investigated using the coupled model. The obtained maps of wave height distribution show a good agreement in comparison with the experimental data, although the observed bottom-induced wave breaking results in a less energetic wave field nearshore, as opposed to measured one. Nearshore wave-induced hydrodynamic circulation drove the solid fluxes and the computed bottom elevation is in line with the measured one, as erosion or accretion was identified close to the shore under the corresponding prevailing wave conditions. This technique yields information on the emergence of nearshore periodic patterns, corresponding to the fastest growing mode, subject to the irregular sediment transport patterns over the initial bathymetry. Thus, the computed morphodynamics are sensitive to initial bottom geometry, wave height, period and direction, limiting the predictive capability of this numerical model in a deterministic sense, as the nonlinear hydrodynamic and morphological interactions observed throughout the duration of the experimental procedure, cannot be precisely predicted. Although, the findings are valid for the initial stages of the evolution of rhythmic patterns, associated with the infinitesimal changes in the bed elevation. As the bed-perturbations accelerates, the finite amplitude effects on the wave transformation and flow circulation can be observed.

This study evinced a need to incorporate a more advanced hydrodynamic and wave model to capture nonlinear wave properties, dispersive characteristics, as well as the flow effects on wave propagation. Moreover, periodic later boundary conditions must be applied in order to hinder the boundary effects on hydrodynamic circulation, that were observed using the present numerical tools. An absorbing layer is also needed offshore to absorb the energy of reflected waves that propagate out of the domain. Concerning the sediment transport phenomena, different advanced formulas, especially for the case of suspended load can be utilized to predict numerically the vertical distribution of sediment concentration. The conclusion of the research that described in the present chapter constituted the basis for the development of a novel

coupled 2DH model incorporating quasi-3D sediment characteristics, which is introduced in the next chapter.

References

Aagaard, T., Davidson-Arnott, R., Greenwood, B., & Nielsen, J. (2004). Sediment supply from shoreface to dunes: linking sediment transport measurements and long-term morphological evolution. Geomorphology, 60(1-2), 205-224.

Afentoulis, V., Eleftheria, K., Eleni, S., Evangelos, M., Archontia, L., Christos, M., & Vasiliki, T. (2017). Coastal Processes Assessment Under Extreme Storm Events Using Numerical Modelling Approaches. Environmental Processes, 4(3), 731-747.

Afentoulis, V., Tsoukala, V., & Mohammadi, B. (2016, November). Experimental and numerical modeling of fluid-seabed international in shallow water. In 35th International Conference on Coastal Engineering. Coastal Engineering Research Council.

Azerad, P., Isebe, D., Ivorra, B., Mohammadi, B., & Bouchette, F. (2005). Optimal shape design of coastal structures minimizing coastal erosion.

Bailard, J. A., & Inman, D. L. (1981). An energetics bedload model for a plane sloping beach: local transport. Journal of Geophysical Research: Oceans, 86(C3), 2035-2043.

Bouharguane, A., & Mohammadi, B. (2013). Minimisation principles for the evolution of a soft sea bed interacting with a shallow sea. International Journal of Computational Fluid Dynamics, 26(3), 163-172.

Bonneton, P., & Dupuis, H. (2001). Transformation of irregular waves in the inner surf zone. In Coastal Engineering 2000 (pp. 745-754).

Bonneton, P., Bruneau, N., Castelle, B., & Marche, F. (2010). Large-scale vorticity generation due to dissipating waves in the surf zone. Discrete & Continuous Dynamical Systems-B, 13(4), 729.

Brocchini, M. (2020). Wave-forced dynamics in the nearshore river mouths, and swash zones. Earth Surface Processes and Landforms, 45(1), 75-95.

Calvete, D., Coco, G., Falqués, A., & Dodd, N. (2007). (Un) predictability in rip channel systems. Geophysical research letters, 34(5).

Camenen, B., & Larroudé, P. (2003). Comparison of sediment transport formulae for the coastal environment. Coastal Engineering, 48(2), 111-132.

Camenen, B., & Larson, M. (2005). A bedload sediment transport formula for the nearshore. Estuarine, Coastal and Shelf Science, 63(1-2), 249-260.

Certain, R., & Barusseau, J. P. (2005). Conceptual modelling of sand bars morphodynamics for a microtidal beach (Sète, France). Bulletin de la société Géologique de France, 176(4), 343-354.

Damgaard, J., Dodd, N., Hall, L., & Chesher, T. (2002). Morphodynamic modelling of rip channel growth. Coastal Engineering, 45(3-4), 199-221.

Dodd, N., Blondeaux, P., Calvete, D., de Swart, H., Falques, A., Hulscher, S., Rozynski, G. & Vittori, G. (2003). Understanding coastal morphodynamics using stability methods, J. of Coast. Res. 19, 4, pp. 849-865.

Drønen, N., & Deigaard, R. (2007). Quasi-three-dimensional modelling of the morphology of longshore bars. Coastal Engineering, 54(3), 197-215.

Isebe, D., Azerad, P., Bouchette, F., Ivorra, B., & Mohammadi, B. (2008). Shape optimization of geotextile tubes for sandy beach protection. International journal for numerical methods in engineering, 74(8), 1262-1277.

Camenen, B. (2007). A unified sediment transport formulation for coastal inlet application (Vol. 7, No. 1). [US Army Corps of Engineers, Engineer Research and Development Center], Coastal and Hydraulics Laboratory.

Camenen, B., & Larson, M. (2008). A general formula for noncohesive suspended sediment transport. Journal of Coastal Research, 24(3), 615-627.

Castelle, B., Michallet, H., Marieu, V., Leckler, F., Dubardier, B., Lambert, A., ... & Bouchette, F. (2010). Laboratory experiment on rip current circulations over a moveable bed: Drifter measurements. Journal of Geophysical Research: Oceans, 115(C12).

Castelle, B., & Ruessink, B. G. (2011). Modeling formation and subsequent nonlinear evolution of rip channels: Time-varying versus time-invariant wave forcing. Journal of Geophysical Research: Earth Surface, 116(F4).

Fredsoe, J., & Deigaard, R. (1992). Mechanics of coastal sediment transport (Vol. 3). World scientific publishing company.

Gourlay, M. R., & Meulen, T. (1968). Beach and dune erosion tests (I). M0935.

Klein, Antonio Henrique da F., and Andrew D. Short. "Brazilian Beach Systems: Introduction." Brazilian Beach Systems. Springer, Cham, 2016. 1-35.

Loureiro, C., Ferreira, Ó., & Cooper, J. A. G. (2012). Geologically constrained morphological variability and boundary effects on embayed beaches. Marine Geology, 329, 1-15.

Lippmann, T. C., & Holman, R. A. (1989). Quantification of sand bar morphology: A video technique based on wave dissipation. Journal of Geophysical Research: Oceans, 94(C1), 995-1011.

Marche, F., & Bonneton, P. (2007). A simple and efficient well-balanced model for 2DH bore propagation and run-up over a sloping beach. In Coastal Engineering 2006: (In 5 Volumes) (pp. 998-1010).

Marche, F., Bonneton, P., Fabrie, P., & Seguin, N. (2007). Evaluation of well-balanced bore-capturing schemes for 2D wetting and drying processes. International Journal for Numerical Methods in Fluids, 53(5), 867-894.

Masselink, G., & Short, A. D. (1993). The effect of tide range on beach morphodynamics and morphology: a conceptual beach model. Journal of coastal research, 785-800.

Melito, L., Parlagreco, L., Perugini, E., Postacchini, M., Devoti, S., Soldini, L., ... & Brocchini, M. (2020). Sandbar dynamics in microtidal environments: Migration patterns in unprotected and bounded beaches. Coastal Engineering, 161, 103768.

Michallet, H., Castelle, B., Barthélemy, E., Berni, C., & Bonneton, P. (2013). Physical modeling of three-dimensional intermediate beach morphodynamics. Journal of Geophysical Research: Earth Surface, 118(2), 1045-1059.

Mohammadi, B., & Bouchette, F. (2014). Extreme scenarios for the evolution of a soft bed interacting with a fluid using the Value at Risk of the bed characteristics. Computers & Fluids, 89, 78-87.

Klonaris, G. (2016). Morphodynamics in a beach with submerged breakwaters (Doctoral dissertation.

Nielsen, P. (1992). Coastal bottom boundary layers and sediment transport (Vol. 4). World scientific.

Ranasinghe, R., Symonds, G., Black, K., & Holman, R. (2001). Processes governing rip spacing, persistence, and strength in a swell dominated, microtidal environment. In Coastal Engineering 2000 (pp. 454-467).

Reniers, A. J., Roelvink, J. A., & Thornton, E. B. (2004). Morphodynamic modeling of an embayed beach under wave group forcing. Journal of Geophysical Research: Oceans, 109(C1).

Ribberink, J. S. (1998). Bed-load transport for steady flows and unsteady oscillatory flows. Coastal Engineering, 34(1-2), 59-82.

Russell, P. E. (1993). Mechanisms for beach erosion during storms. Continental Shelf Research, 13(11), 1243-1265.

Short, A. D. (2006). Australian beach systems—nature and distribution. Journal of Coastal Research, 22(1), 11-27.

Short, A. D., & Woodroffe, C. D. (2009). The coast of Australia. Cambridge University Press.

Sleath, J. F. (1984). Sea bed mechanics.

Soulsby, R. (1997). Dynamics of marine sands.

Turner, I. L., Aarninkhof, S. G., & Holman, R. A. (2006). Coastal imaging applications and research in Australia. Journal of Coastal Research, 22(1), 37-48.

Thornton, E. B., Humiston, R. T., & Birkemeier, W. (1996). Bar/trough generation on a natural beach. Journal of Geophysical Research: Oceans, 101(C5), 12097-12110.

Van Enckevort, I. M. J., & Ruessink, B. G. (2003). Video observations of nearshore bar behaviour. Part 1: alongshore uniform variability. Continental Shelf Research, 23(5), 501-512.

Van Rijn, L. C. (1993). Principles of sediment transport in rivers, estuaries and coastal seas (Vol. 1006, pp. 11-3). Amsterdam: Aqua publications.

Van Rijn, L. C. (2007). Unified view of sediment transport by currents and waves. I: Initiation of motion, bed roughness, and bed-load transport. Journal of Hydraulic engineering, 133(6), 649-667.

Ranasinghe, R., Symonds, G., Black, K., & Holman, R. (2004). Morphodynamics of intermediate beaches: a video imaging and numerical modelling study. Coastal Engineering, 51(7), 629-655.

Wijnberg, K. M. (1997). On the systematic offshore decay of breaker bars. In Coastal Engineering 1996 (pp. 3600-3613).

Wright, L. D., & Short, A. D. (1984). Morphodynamic variability of surf zones and beaches: a synthesis. Marine geology, 56(1-4), 93-118.

4 A novel coupled non-linear model for sediment transport dynamics in coastal areas

4.1 Context

Coastline retreat poses a threat to nearshore environment and the assessment of erosion phenomena is required to plan the coastal engineering works. The hydro-morphodynamic response of a beach to natural and artificial forcing factors differ considerably, as the nearshore processes are especially complex and depended on a multitude of parameters, including prevailing wave and hydrodynamic conditions, beach topography, sediment characteristics and the presence of coastal protection works.

In the present chapter, a new numerical integrated model is introduced, which serves the purpose of numerically evaluating nearshore morphological processes and ultimately assessing the capacity of coastal defence structures to control beach erosion. For this reason, a new sediment transport model including sediment transport dynamics in the swash zone, was coupled to the highly nonlinear Boussinesq wave model FUNWAVE-TVD, providing integrated predictions of bed level evolution, across various timescales of interest. The integrated model was validated thoroughly, and results were compared with laboratory data and numerical investigations present in literature to assess swash and surf zone sediment dynamics as well as the effect of coastal protection structures. Overall, a good agreement between experimental and numerical results was achieved for a variety of test cases with or without the presence of coastal protection structures, rendering the proposed integrated model a valuable tool for engineers and scientists desiring to obtain accurate bed level predictions.

4.1.1 Setting out research issue

Sandy coasts have been constantly modified as a result of natural processes involving wind waves or swell, currents, sea level variability and aeolian sediment transport (Divinsky et al., 2021; Divinsky and Kosyan, 2020; Roelvink and Costas, 2019). Erosion of the coastal seabed and ultimately a retreat of shoreline position is caused by a combination of the abovementioned processes and has strong implications to the economy, environment and community safety since a multitude of activites are concentrated at the coastal zones. Additionally, anthropogenic unplanned infrastructures in the coastal zone, along with jetties and other obstacles to longshore transport, reflective vertical walls that accelerate offshore sand bar migration (Seabergh and Kraus, 2003), as well as devegetation along coasts are key causes intensifying beach erosion in the long term (Gabriel Ruiz-Martínez et al., 2016).

The most widely applied engineering technique to control beach erosion is the construction of coastal defense structures, which can also provide sufficient protection against flooding phenomena to the inland (Charlier and De Meyer, 1989; van Rijn, 2013; Nordstrom, 2014; Pranzini et al., 2015; Servold et al., 2017). A variety of coastal defenses can be encountered in the literature of coastal engineering, such as detached emerged and submerged breakwaters, groynes, seawalls, riprap and wave attenuators. Emerged breakwaters, the presence of which leads to reduce wave agitation alters the patterns of the nearshore breaking wave-induced current field and creates the appropriate conditions for sediment deposition, thus enabling shoreline advance. It should be noted that emerged breakwaters have been used at a lesser extent in the recent decades as a protection solution, due to their negative impact on the aesthetic characteristics of coastal landscape. Hence, submerged structures provide a good compromise between the need to reduce the wave energy close to the shore and the aim to ensure landscape preservation and a good water quality though the exchange of water between offshore and inshore areas. Moreover, in case the longshore sediment transport dominates the sediment transport regime, groynes are employed to retain the beach and maintain the stability of the littoral system.

The investigation of nearshore hydrodynamic and morphodynamic patterns, associated with the presence of coastal structures, has been carried out through laboratory experiments during the last decades. In the studies of Ming and Chiew (2000) and Birben et al. (2007) a series of experiment were used to analyze the effect of offshore breakwaters on beach morphology and sediment accumulation ratio. Cáceres et al. (2008) carried out an experimental research to

assess wave overtopping and wave-induced current field in the breaker zone around low-crested structures. A new dimensionless parameter (β) was proposed by Mahmoudof and Hajivalie (2021), through experimental investigations in order to describe wave transmission and reflection phenomena over submerged breakwaters. However, scaling effects inherently linked to the experimental conditions and the sediment transport processes (Gorrick et al., 2014) render the long-term prediction of coastal bed evolution through experimental procedures a difficult task. As a consequence, process-based models that can advance understanding of the dominant process response (and feedbacks) of littoral systems to a wide range of costal defense structures, have been extensively used in coastal engineering (Zyserman and Johnson, 2002; Lesser et al., 2004; Nam et al., 2011; Kobayashi, 2016; Postacchini et al., 2016; Tang et al., 2017).

These composite nearshore models are usually comprised of wave propagation, hydrodynamic, and sediment transport / morphology models. A variety of sophisticated numerical tools have been utilized for the simulation of wave transformation processes, taking into consideration that for most coastal configurations waves are the dominant driving factor, inducing morphological changes. Two distinct approaches have been highlighted (Hotlhiujsen, 2003) for the numerical investigation of the dominant processes governing wave transformation:

1) The phase-averaged approach that describes wave propagation in the spatial and time domain using the variance-density spectrum, which is the Fourier transformation of the auto-covariance function of free-surface elevation. The most notoriously used models following this approach are 3rd generation spectral wave models (Benoit et al., 1996).

2) The phase resolving deterministic approach describing details of the wave field in the spatial and temporal domain at a resolution that is a small fraction of the wavelength / period. In this category, models solving the mild slope, shallow water (SWE) or Boussinesq equations have been employed.

It should be noted that despite the plethora of modeling tools available, each one is associated with flaws, which have to be taken into serious consideration for the purpose of predicting the morphological evolution of coastal areas. Models based on the phase averaging approach are computationally efficient but omit a large amount of dominant wave processes in the nearshore, especially considering that wave diffraction, reflection and run-up are not usually accounted for. In addition, coherencies observed in the wave field and caused by abrupt bottom

variations and strong current gradients are unable to be simulated in these models (Smit et al., 2015).

Phase resolving models are able to resolve many of the aforementioned important wave transformation processes but are often associated with major constraints, i.e. mildly sloping bottoms (for models based on the mild slope wave equations) and satisfaction of the shallow water approximation (for the SWE wave models). It should be mentioned that the phase-resolving models, which are based on shallow water equations, put significant restrictions on the maximum relative depth kh (k the wavenumber, and h depth) that can be approximated. In the case of high kh values, the vertical accelerations or wave dispersion cannot be neglected, and the usage of non-dispersive shallow-water equations to compute the hydrodynamic parameters becomes inaccurate. From deep to shallow water, dispersive nonlinear wave effects can be simulated satisfactorily using Boussinesq models (Madsen et al., 1997; Kennedy et al., 2001) since they are sufficiently accurate in resolving nearshore wave phenomena, such as refraction and diffraction (Do, 2019). However, until recent decades, their application to hydrodynamic modeling in engineering projects was limited due to high computational cost (Klonaris et al., 2018, 2020) rendering their use in practical applications almost impossible.

Nowadays, several Boussinesq-type models coupled with a sediment transport module, suitable for coastal engineering applications, can be encountered in the literature of coastal engineering (Kobayashi et al., 2001; Karambas, 2002; Karambas, 2012; Gallerano et al. 2016; Klonaris et al., 2016; Malej et al., 2019). Based on this concept, different researches have successfully predicted the shoreline evolution and beach morphology in the vicinity of detached breakwaters, groynes or vertical quay walls (Du et al., 2010; Karambas and Samaras, 2017; Bouvier et al., 2019; Hieu et al., 2020). Tsiaras et al., (2020) used a nonlinear breaking wave and morphodynamic model, including unsteady aspects of the sand transport for evaluating the potential influence of the transmission coefficient and of the net mass influx over structure in the design process of submerged breakwaters. Moreover, Klonaris et al. (2020) provided a detailed experimental and numerical investigation about the effects of rubble-mound submerged breakwaters on beach morphology, using a compound Boussinesq-type model. Although up to present, numerical predictions of wave-current interactions and morphological responses, with and without the presence of coastal structures, are still associated with considerable uncertainty related to the high non-linear nature of these physical processes. In the above mentioned studies, either the wave and hydrodynamic module does not consider the reflection and transmission (e.g. permeability) characteristics of emerged breakwaters and

vertical obstacles, or the utilized sediment transport approximations are not suitable to capture the wave non-linear effects on sand transport and simulate the 3D characteristics of the suspended sediment transport loads.

In the present study, a fully nonlinear Boussinesq model- FUNWAVE-TVD (Shi et al., 2012) tasked with the simulation of wave propagation and hydrodynamic circulation was directly coupled to a quasi-3-D sediment transport and morphology model, which was developed by the authors of this study. Thus, taking advantage of FUNWAVE model's capacity to provide information on coastal structure's reflection and transmission behavior and employing advanced sediment transport approximations, including unsteady sand transport aspects, this study seeks to reduce the uncertainty in hydro-morphodynamic predictions. Special attention was given to the role of sediment transport dynamics across the swash zone, incorporating them in the morphodynamic model, while advanced techniques were utilized to model the three-dimensional patterns of suspended load fluxes and incorporate wave nonlinear and unsteady effects on bed load transport rates. Our scope is to introduce an integrated model that can be utilized to a wide range of maritime engineering applications, both for soft engineering (beach replenishment, sand dune management, drainage) and hard engineering techniques (design of groynes, breakwaters, seawalls, revetments). A particular effort was made to keep the computational complexity at a reasonable level by utilizing morphological acceleration techniques and exploiting the efficient parallel scheme of the wave model. Moreover, in order to ensure the reliability of our numerical modelling approach, the compound model was extensively validated for five distinctive test cases, covering a wide range of coastal engineering applications in both experimental and field scales and providing significant insights into the morphological response of sandy beaches to the combined action of waves and currents.

4.2 Description of models and formulations

A fully coupled method for simulation of wave-current-seabed interaction was developed within the context of our research. The numerical output of FUNWAVE-TVD model is used as forcing for a two-dimensional sediment transport model in an interactive mode, while the computation of sediment fluxes and morphological changes provides the feedback of bathymetry updates on wave computations. Particularly, the seabed morphology is updated over a morphological time step (Δt_{mor}) and for every bed level update, simulations by three numerical tools are performed: FUNWAVE-TVD model, followed by a sediment transport model and a bathymetry updating module. This process is repeated until a preset duration, coinciding

with the simulation end time is reached. The relevant flow chart outling the model interaction and feedback is illustrated in Figure 1. The implementation of a morphological acceleration factor (Morfac) serves to multiply bed level changes by a nonunity integer quantity and therefore alters the morphology time scale. In this research, three different time scales and steps were utilized in order to simulate nearshore processes of a different nature, the time step (Δt) of the wave model (FUNWAVE-TVD), the time interval of wave action which is necessary to obtain the time averaged (mean) velocities that are referred here as currents (Δt_{cur}) and the morphological time step (Δt_{mor}) which is required to calculate bathymetry updates.

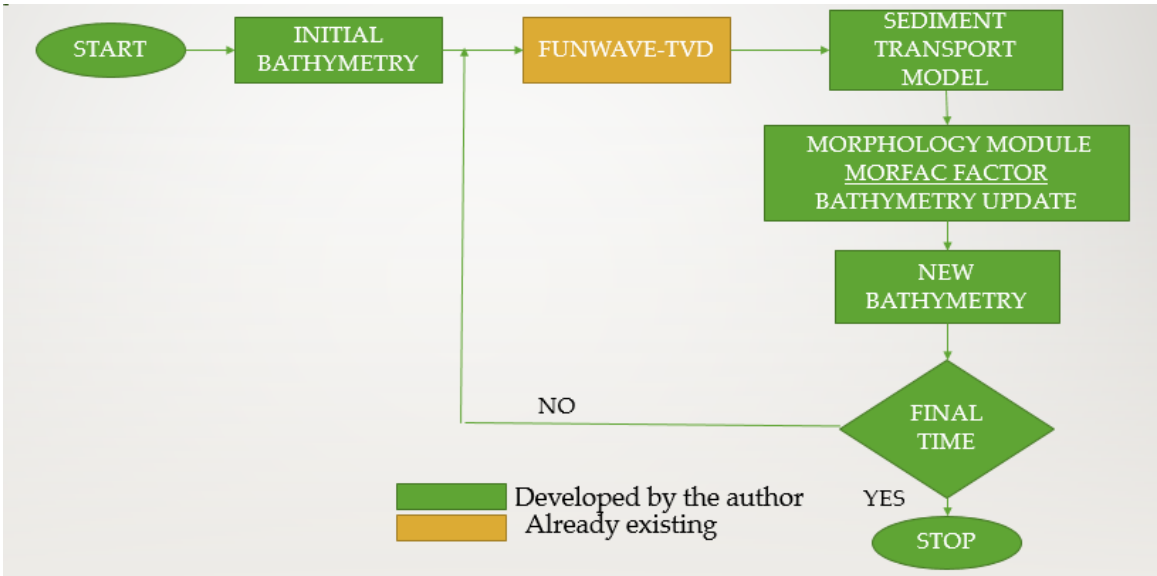

Figure 4-1 Flow chart of wave-current, sediment transport and morphology models.

4.2.1 Hydrodynamics

Wave propagation and hydrodynamic circulation can be simulated by FUNWAVE-TVD model from deep to shallow water, including surf and swash zones. The governing equations of the above model were based on the fully nonlinear Boussinesq equations (Nwogu et al. 1992), modified by Chen et al. (2003) and Chen (2006) and extended to incorporate a moving reference level (Kennedy et al. 2001). FUNWAVE-TVD is a nonlinear wave model that operates with a hybrid finite-volume and finite-difference TVD-type scheme developed by Shi et al. (2012). The shock–capturing wave breaking scheme, chosen for this study, was based on the work of Tonelli and Petti (2009). This method takes advantage of the sock capturing ability of non-linear shallow water equations (NSWE) and can simulate the moving hydraulic jumps. Bottom friction for wave attenuation was calculated by a quadratic friction law incorporating a Manning coefficient. An adaptive time step was implemented, based on a third order Runge–Kutta method. The model includes wetting–drying moving boundary conditions with incorporation of Harten-Lax-van Leer

(HLL) construction method into the scheme. The option for parallel computation was also activated. The sponge layer technique introduced by Larsen and Dancy (1983) is used by FUNWAVE-TVD model to deal with internal wave reflection problems. The governing equations of the wave model are presented below:

$$\eta_t + \nabla \cdot \boldsymbol{M} = 0 \tag{4.1}$$

$$\boldsymbol{u}_{a,t} + (\boldsymbol{u}_a \cdot \nabla)u_a + g\nabla\eta + \boldsymbol{V}_1 + \boldsymbol{V}_2 + \boldsymbol{V}_3 + \boldsymbol{R} = 0 \tag{4.2}$$

Equation (4.1) represents the depth integrated mass conservation, while Equation (4.2) denotes the depth-averaged horizontal momentum. The symbol $\boldsymbol{M}$ of Equation (4.1) is the horizontal flux and can be further expressed as:

$$\boldsymbol{M} = (h+\eta)[\boldsymbol{u}_a + \mu^2\{\left(\frac{{z_a}^2}{2} - \frac{1}{6}(h^2 - \eta h + \eta^2)\right)\nabla(\nabla \cdot \boldsymbol{u}_a)\big) + (z_a + \frac{1}{2}(h-\eta))\nabla(\nabla \cdot (h\boldsymbol{u}_a))\}], \tag{4.3}$$

Where, η is the sea-surface elevation, h is the water depth, $\boldsymbol{u}_a$ the horizontal velocity at the adaptive reference elevation, z_a and μ denotes a dimensionless measure of dispersion. In addition, $\boldsymbol{V}_1$ and $\boldsymbol{V}_2$ are the dispersive Boussinesq terms, $\boldsymbol{V}_3$ accounts for the second-order effect of vertical vorticity, and $\boldsymbol{R}$ represents diffusive and dispersive terms and subgrid lateral mixing. It also includes bottom friction that is approximated using a quadratic friction equation. Moreover, in order to simulate wave-generated nearshore currents such as rip current or alongshore currents, a Smagorinsky-type (1963) subgrid turbulent mixing algorithm is employed. The eddy viscosity associated with the subgrid mixing is determined by breaking-induced current field (Chen et al., 1999). A more detail description of the utilized formulas is provided in Appendix A.

In recent studies, Boussinesq models have been utilized to model rip currents (Johnson and Pattiaratchi, 2006; Geiman et al., 2011) and alongshore currents (Chen et al., 2003; Feddersen et al., 2011) in the nearshore zone. Geiman et al., (2011) presented a numerical study on wave averaging effects on estimates of the surf zone mixing. Their study revealed that FUNWAVE model is able to reproduce 1-h time-averaged mean Eulerian velocities consistent with field measurements and numerical findings.

4.2.2 Morphodynamics

In the present study, a new numerical model developed by the authors of this paper, was applied to assess nearshore morphodynamics. The mode of sediment movement is investigated using Van Rijn's (1993, 2007, 2013) formula, while a quasi-steady approximation, suggested by Ribberink (1998) for the estimation of bed load transport, was implemented. The usage of Van Rijn's approximation serves to distinguish suspended load transport that is computed above a reference height α and bed load transport, which is estimated using the near-bottom hydrodynamic parameters. It is also suited to assess sediment transport rates in combined breaking or non-breaking wave and current conditions. In the following subsections the governing equations will be presented. Moreover, it has to be mentioned that the Boussinesq-type 2DH model provided depth-averaged hydrodynamic parameters that were exploited to extract near-bed flow characteristics and nonlinear time-varying near-bottom wave velocities using the parameterisation suggested by Karambas and Samaras (2017) and initially proposed by Isobe and Horikawa (1982).

4.2.2.1 Suspended load transport

Van Rijn (1993) suggested a multi-layer model, describing the time-averaged sediment concentration profile. This profile can be obtained by the integration of the time averaged convection-diffusion under equilibrium (stationary) conditions. The three-dimensional convection -diffusion (mass-balance) equation for the suspended sediment can be written, as follows:

$$\frac{\partial(c)}{\partial t}+\frac{\partial(uc)}{\partial x}+\frac{\partial(vc)}{\partial y}+\frac{\partial[(w-w_s)c]}{\partial z}-\frac{\partial}{\partial x}\left[\varepsilon_{s,x}\frac{\partial(c)}{\partial x}\right]-\frac{\partial}{\partial y}\left[\varepsilon_{s,y}\frac{\partial(c)}{\partial y}\right]-\frac{\partial}{\partial z}\left[\varepsilon_{s,z}\frac{\partial(c)}{\partial z}\right]=0 \qquad (4.4)$$

In which, (u, v, w) = local flow velocities, $(\varepsilon_{s,x}, \varepsilon_{s,y}, \varepsilon_{s,z})$ = local turbulent sediment mixing, w_s = particle fall velocity, and c = sediment concentration.

Integration of Equation (4) with respect to z leads to:

$$\frac{\partial(Cave)\mathrm{h}}{\partial t}+\frac{\partial(UCave)\mathrm{h}}{\partial x}+\frac{\partial(VCave)\mathrm{h}}{\partial y}-\frac{\partial}{\partial x}\left[\varepsilon_{s,x}h\frac{\partial(Cave)}{\partial x}\right]-\frac{\partial}{\partial y}\left[\varepsilon_{s,y}h\frac{\partial(cave)}{\partial y}\right]=S \qquad (4.5)$$

Where, C_{ave} is the depth-averaged concentration and (U, V, W) the depth-averaged velocities, and S represents the source term of the convection diffusion equation that is based on the mismatch between a current and an equilibrium concentration (Galappatti and

Vreugdenhil, 1985; Galappatti, 1983). In order to estimate the equilibrium concentration, we need to prescribe the boundary conditions of the problem. Considering that the concentration presents variability in a timescale much larger than the representative wave period stationary conditions in the surface and in the bed boundary are assumed. Thus, the longitudinal diffusion terms can be neglected in relation to the vertical diffusion term, whilst the unsteady concentration term ($Cave/\partial t$) is relatively small with respect to the other terms. Moreover, at water surface, the vertical diffusive flux through the free surface is equal to zero:

$$-w_s c - \varepsilon_{s,cw}\frac{dc}{dz} = 0, \qquad \text{at: } z = \eta, \tag{4.6}$$

At bed boundary surface, the vertical mixing or the exchange of sediment fluxes, according to Galappati 1983, can be described as:

$$-w_s c - \varepsilon_{s,cw}\frac{dc}{dz} = D - E, \qquad \text{at: } z = zb, \tag{4.7}$$

Where, D is the sediment deposition rate and E being the sediment erosion rate.

The sediment erosion rate was evaluated explicitly, while the deposition rate was included in the transport equation implicitly (Lesser et al., 2004), as follows:

$$\text{Erosion rate: } c_\alpha \frac{\varepsilon_s}{\Delta z}, \qquad \text{Deposition rate: } c_k\left(\frac{\varepsilon_s}{\Delta z} + w_s\right), \tag{4.8}$$

in which, ε_s =sediment vertical diffusion coefficient, Δz = vertical distance from the reference level α to the center of reference cell, and c_k = sediment concentration in the reference cell.

Erosion and deposition rates are responsible for the vertical readjustment of the concentration distribution and they were used, herein, in order to estimate sediment source and sink terms throughout the vertical. It should be noted that source and sink terms are not normally time invariant over depth. However, in this study we consider the existence of an equilibrium concentration profile, which is adjusted to current conditions within a specific time interval. Katopodi and Ribberink (1991) described the adjustment of the depth-averaged concentration to its equilibrium value, for specific time and space scales.

For oscillatory flows, the concentration at the reference level α is expressed as:

$$c_a = 0.015\rho_s \frac{D_{50}}{\alpha} \frac{\left(\frac{\theta - \theta_{cr}}{\theta_{cr}}\right)^{1.5}}{D_*^{0.3}} \tag{4.9}$$

Where, ρ_s= sediment density, α= reference level, D_{50} = median particle diameter of bed material, θ = Shields parameter, θ_{cr} = critical Shields parameter , D_*= non-dimensional particle diameter

The vertical distribution coefficient due to the total wave and current mixing can be calculated following Lesser at al. (2004) and Van Rijn (1993).

Thus, the vertical distribution coefficient due to currents can be calculated as:

$$\begin{aligned} &\varepsilon_{s,c} = k\beta u_{*,c} z(1 - z/h) && \text{for } z < 0.5h \\ &\varepsilon_{s,c} = 0.25k\beta u_{*,c} z(1 - z/h) && \text{for } z \geq 0.5h \end{aligned} \tag{4.10}$$

Where, $\varepsilon_{s,c}$= vertical diffusion coefficient due to currents, k= Von karman constant (0.4), $u_{*,c}$ =current related bed shear velocity, β van Rijn's factor (used to describe the difference between fluid and granular diffusion; van Rijn, (1993).This formula can generate similar turbulent mixing values to those generated by the standard algebraic turbulence (Lesser at al., 2004).

The vertical distribution coefficient due to waves is calculated as:

$$\begin{aligned} &\varepsilon_{s,w} = \varepsilon_{s,bed} = 0.004 D_* \delta_s \widehat{U_\delta}, && \text{for } z \leq \delta_s \\ &\varepsilon_{s,w} = \varepsilon_{s,max} = 0.035 h H_s / T_P, && \text{for } z \geq 0.5h \\ &\varepsilon_{s,w} = \varepsilon_{s,bed} + \left(\varepsilon_{s,max} - \varepsilon_{s,bed}\right)\left(\frac{z - \delta_s}{0.5h - \delta_s}\right), && \text{for } \delta_s < z < 0.5h \end{aligned} \tag{4.11}$$

Where, $\varepsilon_{s,w}$ = vertical distribution coefficient due to waves, δ_s = thickness of the near-bed sediment mixing layer, which is equal to three times the ripple height ($\delta_s = 3 * \Delta_r$), $\widehat{U_\delta}$ = near-bed wave velocity, D_*= non-dimensional particle diameter. The total vertical diffusion coefficient can be expressed as:

$$\varepsilon_{s,Tot} = \sqrt{{\varepsilon_{s,w}}^2 + {\varepsilon_{s,c}}^2} \tag{4.12}$$

Ultimately, after integration of the convection diffusion equation over the time the net suspended sediment fluxes per unit area can be expresses as follows:

$$\boldsymbol{q}_s = (\overline{c_{ave}h - \varepsilon_{s,x}h\frac{\partial Cave}{\partial x}},\ \overline{c_{ave}h - \varepsilon_{s,y}h\frac{\partial Cave}{\partial y}}) \tag{4.13}$$

4.2.2.2 Bed load transport

Following the approach suggested by Ribberink (1998), bed load sediment transport can be calculated using a formula for unsteady oscillatory flows where the instantaneous solid flux is assumed to be proportional to a function of the difference between the actual time-dependent bed shear stress and the critical bed shear stress (Figure 4-2). Therefore, the nonlinear effects of wave asymmetry on bedload transport rates can be satisfactory predicted using the proposed approach. Ribberink's (1998) formulation has been calibrated towards several flume data sets including wave-current interaction in a plane regime (suspended load negligible) and field data (unidirectional flows in rivers). In total, more than 75 bed-load transport measurements in oscillating water tunnels were utilized to corroborate the validity of this approach (Ribberink, 1998). The solid fluxes a can be calculated, as follows:

$$\boldsymbol{q_{SB}} = m_{Rib}\sqrt{(s-1)gd^3}\left\langle(\left|\overrightarrow{\theta(t)}\right| - \theta_{cr})^{n_{Rib}}\frac{\overrightarrow{\theta(t)}}{|\theta(t)|}\right\rangle \tag{4.14}$$

where, $\overrightarrow{\theta(t)} = 0.5 f_{cw}|u(t)|\overrightarrow{u(t)}/[(s-1)gd]$ is the time-dependent Shields parameter with the instantaneous velocity $\overrightarrow{u(t)} = \overrightarrow{U_c} + \overrightarrow{u_W(t)}$, s the relative density of sediment and f_{cw} the wave –current friction factor. ⟨ ⟩: Time-averaged over wave period; and m_{Rib} = 11, n_{Rib} = 1.65: adjusted coefficients.

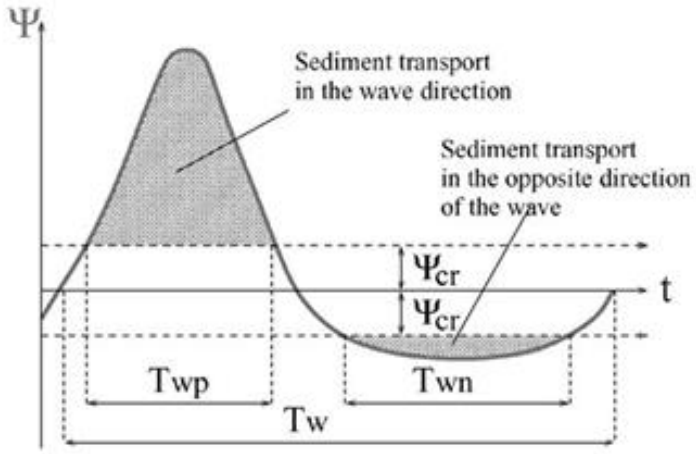

Figure 4-2 Profile of the time-dependent shear stress (case where wave and current directions are the same).

4.2.2.3 Swash zone sediment dynamics

The swash zone is the zone of the coastal environment where the waves run up and down, dissipating or reflecting their energy after moving towards the shore. The sediment fluxes are often large close to the shoreline because of swash uprush and backwash phases. Sediment transport generated from bed evolution at a swash time scale can be several orders of magnitude larger than those derived from the most of available sediment transport formulas, applied in the surf zone. Thus, numerical models often underestimate this sediment migration and tend to yield sediment transport that decreases too rapidly from the swash zone towards the offshore (Nam et al., 2009; Masselink et al., 2009; Klonaris, 2016). For the estimation of longshore and cross-shore sediment transport in swash zone the approximation proposed by Larson and Wamsley (2007) has been used. The net transport rates can be expressed as follows:

$$q_{tc,net} = K_c \frac{tan\,\varphi_m}{tan^2\,\varphi_m - \left(\frac{dh}{dx}\right)^2} \frac{u_0^3}{g} \left(\frac{dh}{dx} - tan\,\beta_e\right) \frac{t_0}{T}, \tag{4.15}$$

$$q_{tl,net} = K_l \frac{tan\,\varphi_m}{tan^2\,\varphi_m - \left(\frac{dh}{dx}\right)^2} \frac{u_0^2 v_0}{g} \frac{t_0}{T}, \tag{4.16}$$

Where, K_c, K_l are cross-shore and long-shore empirical coefficients, respectively, φ_m is the internal friction angle (≈ 30◦). v_0, u_0 and t_0 are scaling velocities and time, T is the swash duration (considered equal to the incidence wave period), $tan\,\beta_e$ is the foreshore equilibrium slope. Equation (4.15) implies that the cross-shore sediment transport rate is zero if foreshore slope is in equilibrium, while longshore transport still occurs if the transporting velocity v_0 is not zero during the uprush and backwash phase. In order to define the foreshore equilibrium slope

the assumption of Camenen et al. (2004) was followed. Therefore, an equilibrium is assumed to occur when $q_{t,net} = 0$ at all points across the foreshore, thus the equilibrium slope can be expressed as:

$$tan\,\beta_e = \frac{I_U - I_B}{I_U + I_B} tan\,\varphi_m, \tag{4.16}$$

where,

$$I_U = \frac{1}{T}\int_{t_s}^{t_m} (|\theta(t)|)^{3/2}\mathrm{dt}$$

$$I_B = \frac{1}{T}\int_{t_m}^{t_e} (|\theta(t)|)^{3/2}\mathrm{dt} \tag{4.17}$$

in which T is the wave period, $t_s$and $t_e$the start and end time of the swash oscillation, and $t_m$the moment at which uprush changes to backwash.

Klonaris et al. (2018) proved that the application of the latter quasi-empirical formulation is especially efficient in predicting swash morphodynamics, in conjunction with a phase resolving Boussinesq-type model, ensuring the continuity of sediment fluxes throughout the surf and swash zones and providing a smooth transition between them. The main advantage of this approximation is that the computed sediment transport rates do not decrease too rapidly from the swash to offshore zones, guaranteeing the stability of the solution throughout the entire coastal zone.

The investigation of sediment dynamics in this zone is of high interest for engineering applications. Swash dynamics determine the shoreline position, thus the precise evaluation of the natural processes in this zone contribute in the performance evaluation of coastal defence structures in terms of their capacity to maintain or advance the shoreline seaward. Hence, it is considered that combining a highly nonlinear Boussinesq wave model with a sophisticated representation of wetting-drying conditions, along with a quasi-3D sediment transport formula incorporating sediment fluxes in the swash zone is crucial in obtaining accurate bed level predictions in the presence of coastal engineering structures, therefore improving engineering design.

4.2.3 Morphology

Total sediment transport rates are computed as the sum of the bed and suspended loads in the intermediate depths and surf zone. In swash zone, the sediment rates, estimated using the Larson and Wamsley's (2007) approximation, are also added to the total sum of sediment fluxes in cross-shore and alongshore direction. The variables of FUNWAVE-TVD model have been used to estimate these rates following the time scale of hydrodynamic circulation. However, morphological changes vary at a different and slower rate compared to the short-term variations of hydrodynamics. Thus, the estimation of bathymetry update requires to maintain a budget of the sediment fluxes that have been derived by averaging the instantaneous flow parameters. Thus, these sediment transport fluxes were integrated over a number of time steps, which correspond to several wave periods. The bathymetry update was calculated by solving the sediment mass conservation equation which reads:

$$\frac{\partial z_b}{\partial t} = -\frac{\text{Morfac}}{1-n_p}\nabla \cdot \boldsymbol{q}_{tot} \ , \tag{4.18}$$

where, n_p is the sediment porosity, $\boldsymbol{q}_{tot}$=($q_{tot,x}$, $q_{tot,y}$) denotes the total volumetric sediment transport rate equal to the sum of suspended and bed load transport rate, z_b is the local bottom elevation and Morfac is a morphological acceleration factor (Lesser, 2004). This nonunity factor (Morfac) applies a scalar multiplier to the sediment continuity equation and speeds up the depth change rates, multiplying them by a constant value. In this study, Morfac values (ranging from 1 to 30) were systematically adapted to be compared with a baseline condition of no acceleration. Care must be taken not to exaggerate with extreme Morfac values, in order to describe realistically the interaction of the wave, hydrodynamic and morphology modules.

The Morphological Acceleration Factor (Morfac) concept is widely used in morphodynamic simulations involving coupled models of wave propagation, hydrodynamic circulation and sediment transport/morphology. Lesser (2004), who was the first to develop this concept, defined an upper limit of Morfac values at 100, stating though that for cases where waves are the most important factor driving the morphological evolution these values may be even lower. This holds true particularly for highly energetic wave conditions and storm events where values should be even lower due to the non-linear response of the morphology to the wave forcing. Additionally, the upper limit of the Morfac values is depended among others on the discretization spatial step, the solution scheme of the sediment continuity (Exner) equation as

well as the local hydrodynamic Froude and Courant numbers (Ranasinghe et al., 2010) and are therefore model specific. This is also evident on studies performed to investigate the critical values of Morfac for different models and for a variety of input forcing conditions. Knaapen and Joustra (2012) define the critical value of Morfac at around 20 for a tidal flow simulation for the Sisyphe model, whereas the CMS-Flow model User Manual states that it should not exceed 20-30 (CMS Flow User Manual, 2012). In the absence of clearly defined limits in the literature, Morfac values were adopted with particular caution in this study by performing trial & error simulations of a few hours, to define the upper allowable values of Morfac in order to obtain a good compromise between simulation speed and accurate results.

The effect of the bed slope on sediment transport has been included following Watanabe (1988). Following Leont'yev (1996) and Karambas et al. (2002) the sediment mass conservation equation can be obtained from Equation (4.18) as follows:

$$\frac{\partial z_b}{\partial t} = -\frac{\partial}{\partial x}\left(q_{tot,x} - \varepsilon\left|q_{tot,x}\right|\frac{\partial z}{\partial x}\right) - \frac{\partial}{\partial y}\left(q_{tot,y} - \varepsilon\left|q_{tot,y}\right|\frac{\partial z}{\partial y}\right) \ , \qquad (4.19)$$

In which, ε is an empirical coefficient that varies within the range of 2.0 to 5.0. The second term in each of the parentheses in the right part of Equation (4.19) describes the diffusion term, as well as additional gravitational term reflects the effect of local bed slope on sediment transport.

4.3 Model validation

For the validation of the presented composite model, four different test cases were evaluated, both in 1DH and 2DH configurations. Our results were compared to experimental and numerical findings involving hydrodynamic, sediment transport loads and short and medium-term bathymetry changes. Taking advantage of FUNWAVE-TVD model's capacity to employ rapidly varying terrains and steep slopes in the surf zone, this study provides significant insights for the sediment transport dynamics in a variety of coastal engineering applications. Sediment transport and morphology evolution was analyzed for the case of large-scale wave flumes using

the experimental findings of Alsina et al. (2012) and Dette et al. (2002). These test cases were also utilized for the calibration of several empirical factors and formulas, as the required computational cost for the performed simulations was significantly lower than that of the 2DH cases.

The present numerical model was applied afterwards, in the case of the physical experiments of Baidei et al. (1994), concerning the effect of a groyne on shore morphology. Ultimately, the effect of shore parallel emerged and submerged breakwaters on the hydrodynamics and morphology was evaluated. For this purpose, our numerical results were quantitatively compared to the empirical models from previous related studies (Deltares/Delft Hydraulics 1997; Bos et al., 1996, Cáceres et al., 2005). Thus, the efficiency of the proposed coupled model was tested under real field dimensions and for a total duration of 50 days, providing significant conclusions about the time scale of the achieved morphological equilibrium.

4.3.1 1DH Surf and swash zone morphological processes in cross-shore direction

4.3.1.1 Large Wave Flume experiment

The first set of comparisons refers to the experimental campaign carried out at the Grosser Wellenkanal in Hannover within the context of the EU SAFE project. The results of this work were presented in the study of Dette et al. (2002). The main objective of that study was to investigate the effectiveness of beach nourishment as a soft protection technique to combat coastline erosion. The experiments were performed in a wave flume 324m long, while the width and the depth of the flume were 5m and 7m respectively. Figure 4-3 depicts a layout of the flume bathymetry. Herein, the test B2 of the experimental campaign was reproduced in order to evaluate the results of our numerical coupled model. Irregular waves were applied ($H_s = 1.20$m and $T_p = 5.5$s) using a TMA spectrum internal wavemaker (Wei and Kirby, 1999), for a total duration of 23 hours. The initial bathymetry was characterized by a horizontal bed of 5 m depth followed by the theoretical Bruun equilibrium profile (Bruun, 1954; Dean, 1977) below the water level. The sea bottom was represented by well-sorted sand with a median sediment size of $D_{50} = 0.30$mm. A summary of the retrieved experimental wave and bathymetry data that were used as input for the numerical simulation is given in Table 13.

H_s (m)	1.20
T_p (s)	5.5
Water depth at wavemaker (m)	5.0
D_{50} (mm)	0.25
Total duration (h)	23
Bed slope	Varying

Table 13 Summary of the retrieved experimental wave and bathymetry data from the study of Dette et al. (2002).

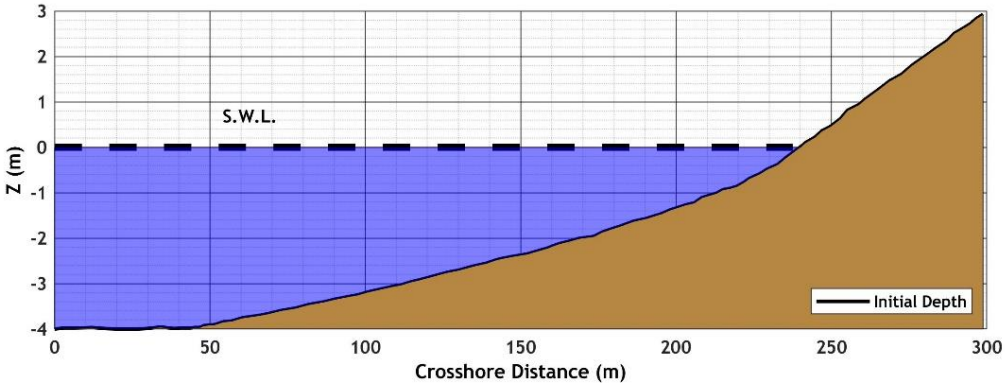

Figure 4-3 Initial beach profile setup in the Dette et al. (2002) experiments.

The bathymetry data were discretized on an equispaced grid with a spatial step of $\Delta\chi = 0.5m$ and a fixed bottom friction coefficient was utilized and set equal to $C = 0.008$, as it was found that it leads to the best agreement with the experimental data. The minimum water depth used to represent wetting-drying conditions was set equal to 0.01m. The selected Courant number in the time-stepping scheme of the FUNWAVE-TVD model was relatively low ($CFL = 0.3$) to achieve numerical stability. A low morphological factor was utilized (Morfac = 2) to ensure the stability of the numerical simulation and calibrate the sediment transport model. The empirical coefficient ε of equation (4.19) was set equal to 5, in order to represent the effect of the bed slope on seabed morphology.

Figure 4-4 shows the distribution of significant wave height along the flume profile and the comparison between the computed and measured data for the test B2 of Dette et al. (2002). Computed and measured values of sediment transport rates and seabed geometry are depicted in Figure 4-5 and Figure 4-6, respectively. The wave height distribution was accurately computed using FUNWAVE-TVD model taking advantage of its high order nonlinearity. Moreover, the sediment transport model reproduced adequately the peaks of the sediment load distribution

along the cross-shore profile. The bar formation is well predicted, although the model overestimates the shoreline erosion in swash zone.

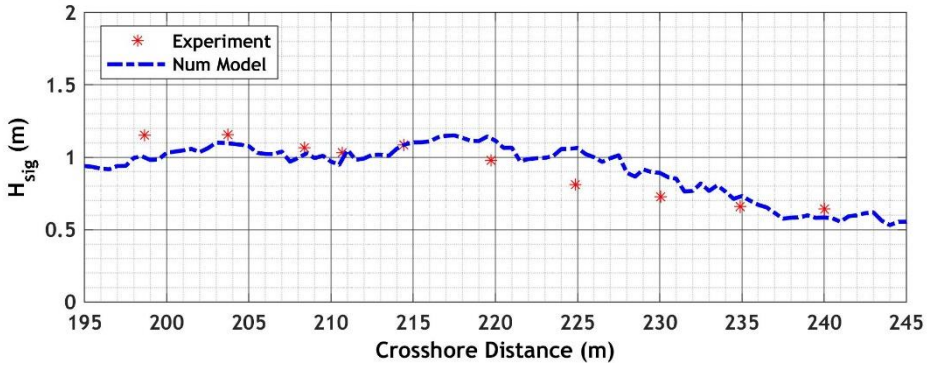

Figure 4-4 Computed and measured significant wave height after 19 h 45min of wave action for test case B2 in Dette et al. (2002).

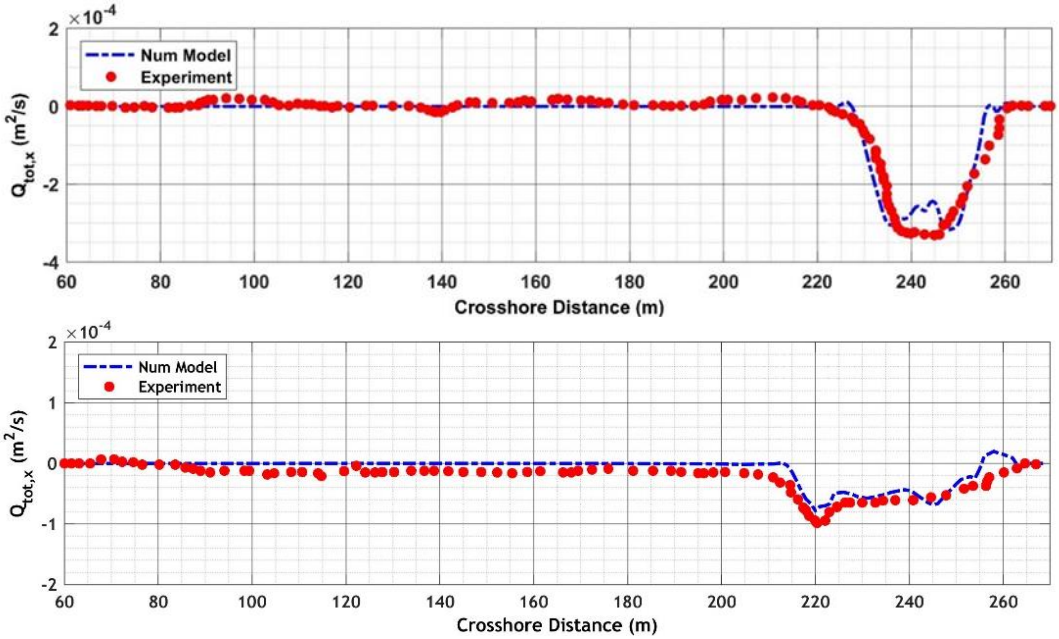

Figure 4-5 Computed and measured total sediment transport rate after 1.5 h (up) and after 19 h 45min (down) for test case B2 in Dette et al. (2002).

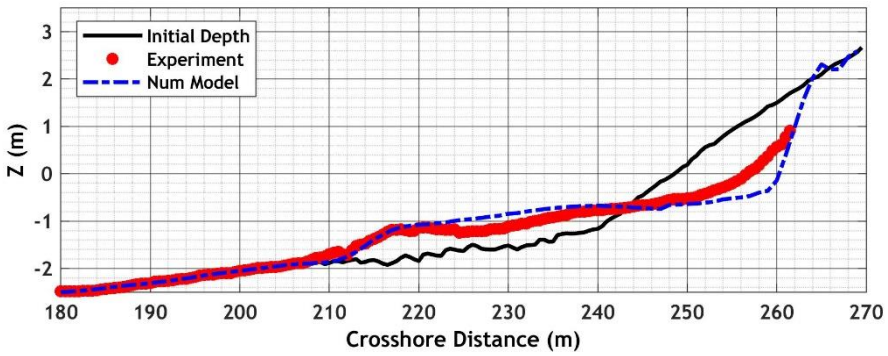

Figure 4-6 Computed and measured bottom elevation after 19 h 45min of wave action for test case B2 in Dette et al. (2002).

4.3.1.2 SANDS experiment

This test case refers to the Hydralab III SANDS project (Scaling and Analysis and New instrumentation for Dynamic bed testS). The experiment was carried out in the Canal de Investigacion y Experimentacion Maritima (CIEM) at the Universidad Politecnica de Cataluña (UPC), Barcelona. The dimensions of the large-scale wave flume were: 100m long, 3m wide and 4.5m deep. Figure 4-7 shows a snapshot of the initial bathymetry in the laboratory flume. The experimental findings were presented in the study of Alsina et al. (2012). The main purpose of this physical experiment was to investigate the link between swash zone dynamics and surf zone morphodynamics and how dissipative beaches with mild-sloping beach face tend to decrease the rate of sand bar migration towards the sea, while more reflective swash conditions intensify sediment transport erosive rates.

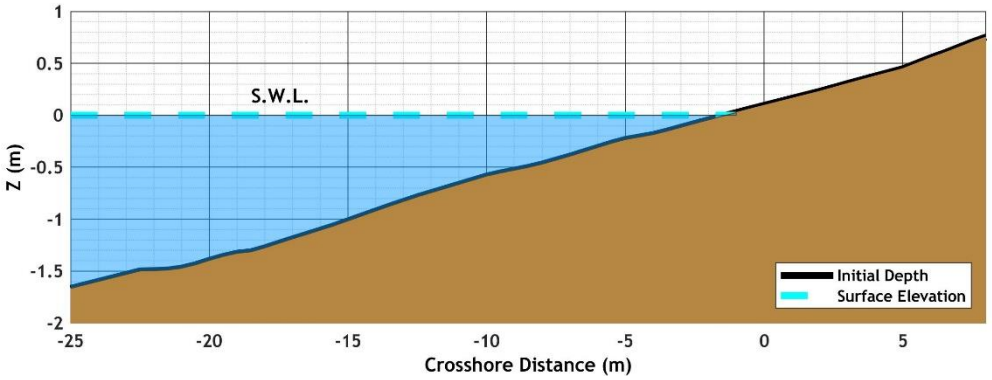

Figure 4-7 Initial beach profile used for SANDS experiment (Alsina et al. 2012).

During the experiment, moderately energetic random waves were applied ($H_s = 0.53$m and $T_p = 4.14$s) and the same wave conditions were repeated for a series of 47 tests. Each test was comprised of 500 waves with a total duration equal to 27 min. The random wave time series corresponded to a JONSWAP spectrum with a peak factor of γ= 3.3. The initial bathymetry was characterized by a constant sloping beach with a gradient of 1:10. The sea bottom was represented by well-sorted sand with a median sediment size $D_{50} = 0.25$mm. A summary of the retrieved experimental wave and bathymetry data that were used as input for the numerical simulation is given in Table 14.

H_s (m)	0.53
T_p (s)	4.14
Water depth at wavemaker (m)	2.47
D_{50} (mm)	0.25
Total duration (h)	21.15
Bed slope	1:10

Table 14 Summary of the retrieved experimental wave and bathymetry data from the study of Alsina et al. (2012).

In order to reproduce the experimental procedure numerically, the bathymetric data were interpolated on a fine grid with a spatial step of $\Delta x = 0.2$m. The initial bathymetry consisted of a horizontal bottom of 2.47m depth followed by a uniform slope of 1:10. A fixed bottom friction coefficient was utilized and set at 0.009 and the minimum water depth for wetting-drying conditions was considered equal to 0.01m. Once again, the Courant number used in the time-stepping scheme of the FUNWAVE-TVD model was relatively low ($CFL = 0.3$) in order to achieve numerical stability. No morphological acceleration factor (Morfac = 1) was employed, as the total simulation time was relatively low (Duration= 21.15h). Similar wave conditions to that of the experiment were generated ($H_s = 0.53$m and $T_p = 4.14$s) by an irregular wavemaker in a water depth of 2.47m, producing a JONSWAP spectrum. The empirical coefficient ε of Equation (4.19) was set equal to 5. in order to consider the impact of the bed slope on seabed morphology.

The initial computed and measured cross-shore distribution of significant wave height after 21.15 hours of wave action are both depicted in Figure 4-8. The initial beach profile, as well as the computed and measured final beach profiles at 21.15 hours are also shown in Figure 7. The present test case corresponds to erosive conditions close to swash zone due to the initial reflective beach profile that, in turn, force significant sediment quantities into deeper water. FUNWAVE-TVD model estimated accurately the cross-shore wave height distribution due to its higher order of nonlinearity. However, it should be noted that some discrepancies between measurements and numerical results appear in the area where water depth is less than 0.5 m. A breaking event takes place just after x = -20 m leading to the formation of the inner bar.

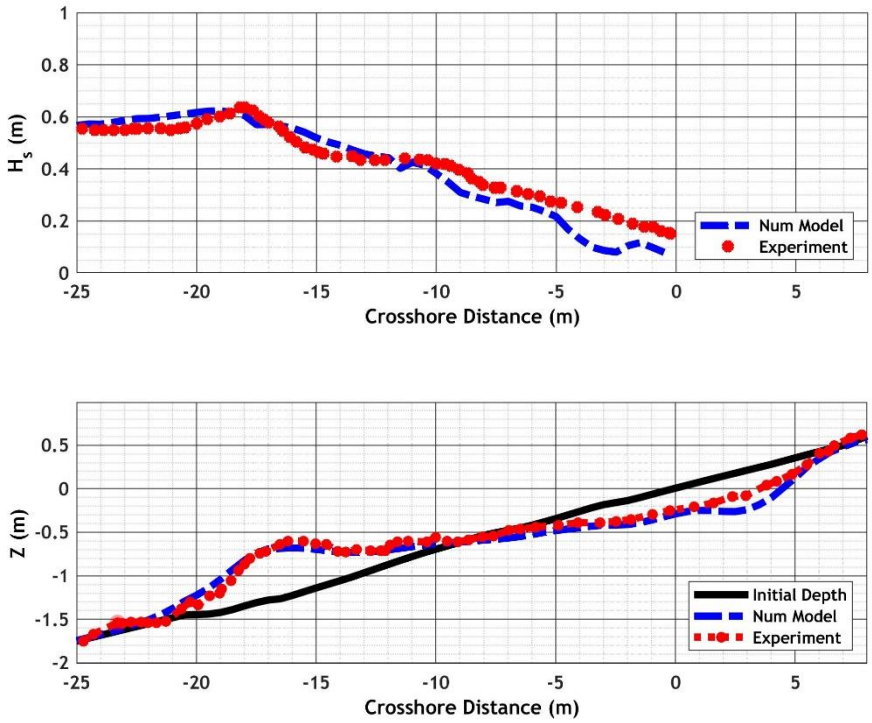

Figure 4-8 Computed and measured cross-shore distribution of significant wave height after 21.15 hours (up), Computed and measured final beach profile after 21.15 hours (down).

The numerical outputs of sediment transport model are in good agreement with experimental results, as an accurate prediction of the sandbar formation was achieved. Overall, the evolution of the bed shape over time follows the same sequence as that of the experiment, since a seaward sandbar migration was observed. However, a bed-change over-estimation of ± 0.10cm can be detected in the swash and surf zone.

4.3.2 2DH numerical simulations for the effect of a single groyne structure on the shore

The impact of a groyne structure, which acts as an artificial obstacle to the longshore sediment transport and affects the subsequent shoreline evolution, was numerically investigated in our study and compared with the experimental findings of Baidei et al. (1994). Single groynes are referred to as the structures that are usually placed normal to the shoreline and block the littoral drift partially or completely (Kristensen et al., 2016). Groynes are employed to produce sediment cells in which the shore can turn against the locally predominant wave direction. These structures can also be situated close to a river mouth to aid the canalization of the flow into the sea (Valsamidis et al., 2017), or as terminal structures (jetties) which limit the amount of sediment, deposited in harbor basin. An accretive or erosive trend is expected to occur in the vicinity of a groyne due to the presence of a source or sink, respectively. Moreover, in coastal management, a system of multiple groynes is typically used to advance the shore seaward and trap large amounts of sediments by blocking alongshore sediment fluxes. A thorough research of groyne system functionality was conducted by French (2001).

The physical model presented by Baidei et al. (1994) concerns nearshore sediment transport dynamics and morphological effects of groynes on a mobile bed with an initial straight beach, which was exposed to obliquely incident irregular waves at an angle of 11.6 degrees (with respect to the shore-normal). The test NT2 of the experimental study was reproduced numerically in the scope of the present work. The median particle diameter of bed material (D_{50}) was 0.12 mm and the initial cross-shore constant beach slope was 1:10.

The integrated coupled model was applied to reproduce the hydrodynamic and morphodynamic conditions of the experiment. The spatial domain has been discretized with a spatial step of Δx = 0.2m and Δy = 0.5m in cross-shore and alongshore direction, respectively. Irregular waves (characterized by a JONSWAP spectrum at the wave-maker), were generated with $H_s = 0.8$m and $T_p = 1.15$s, whilst the angle between the normal to the coast and the main direction of wave propagation was set at 11.6°. For the absorption of the wave energy propagating out of the model area, a sponge layer of about 5m was applied at the offshore boundary of FUNWAVE-TVD model and periodic lateral boundary conditions were employed. In Figure 4-9 the initial bathymetry with a constant slope of 1:10 is illustrated. The wave-maker was placed at X = 7m and in the deep water region a flat bottom of 2m was considered. The total

duration of the simulation was 12 hours, equal to that of the experiment and a morphological acceleration factor in the order of 5 was employed.

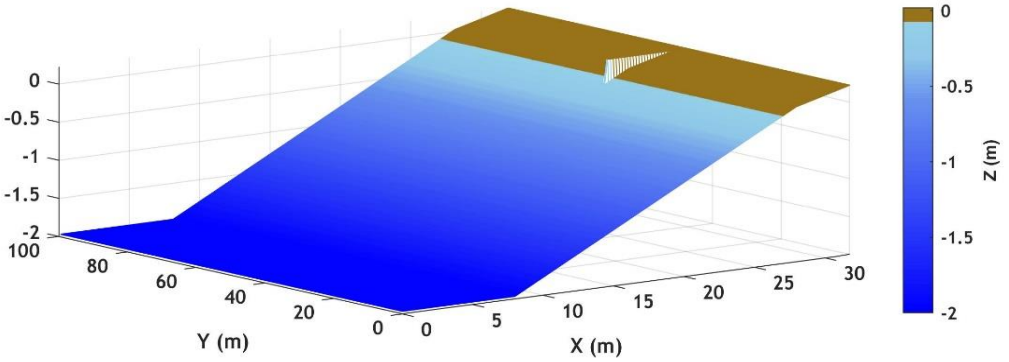

Figure 4-9 3D view of model's initial bathymetry.

Figure 4-10 depicts the wave induced current field after 1 hour of wave action. The groyne structure alters the longshore currents' direction in its vicinity, as decreased velocities can be seen in the lee side of the structure. The nearshore currents reach a maximum velocity of about 0.1m/s. Moreover, offshore-oriented velocities are observed in the swash zone, reflected from the beachface, with a maximum velocity of 0.06m/s. The direction and order of magnitude of computed currents are in line with the numerical findings of the study of Karambas and Samaras (2017), in which the present experimental test case was also reproduced. However, reflection phenomena in the vicinity of groyne are less intense in our study, due to the application of inner sponge layers that represent flow friction and energy dissipation within the structure.

Figure 4-11 shows the final bottom evolution after 12 hours of wave action. The sediment accretion updrift of the structure contributes to an advance of the shoreline seaward, whilst the lack of sediments at the lee side of the structure results to a shoreline retreat. Overall, the numerical findings are in a very good agreement with the experimental results, as is evident in Figure 10. The computed final shoreline position is almost identical to that of the experiment, with some small discrepancies encountered close to the lateral boundaries.

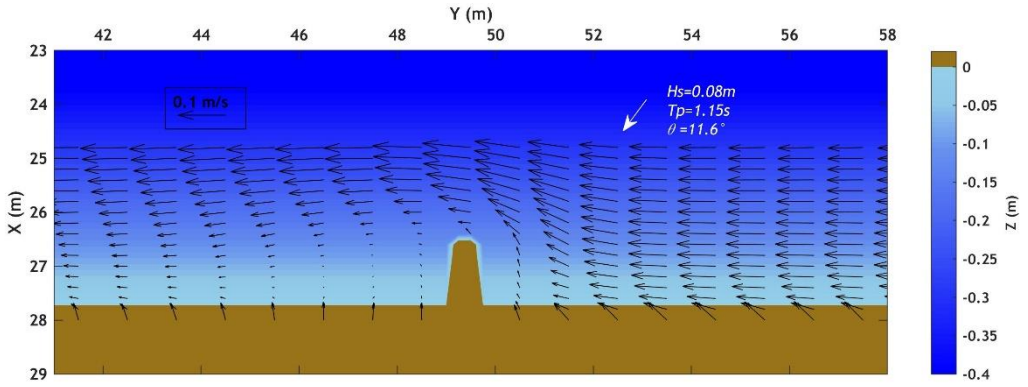

Figure 4-10 Simulated hydrodynamic circulation after 1 hour of wave action for a groyne field subject to waves with a 11.6° angle of incidence. Colourmap corresponds to the initial bathymetry.

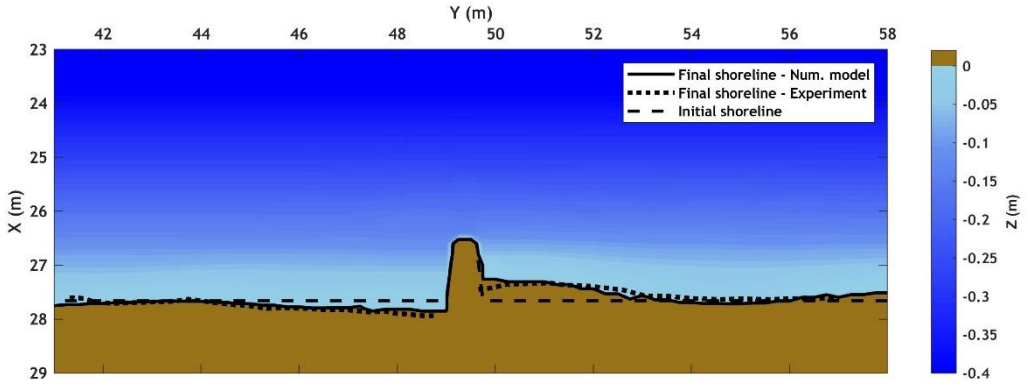

Figure 4-11 Simulated bathymetry for a groyne field subject to waves with a 11.6° angle of incidence depicting the measured (dot line) and computed (solid line) final shoreline position. Colourmap indicates the final bathymetry.

4.3.3 2DH numerical simulations for the effect a detached breakwater on the shore

4.3.3.1 Single emerged breakwater

To provide significant protection against erosion phenomena in the littoral environment, layout optimization of a breakwater is necessary. Previous studies have revealed that breakwater geometry affects hydrodynamic processes and evolution of bottom topography, resulting in a plan form development (formation of tombolo or salient) in the lee of the breakwater (Deltares/Delft Hydraulics, 1997; Bos et al., 1996; Cáceras et al., 2005; Zyserman et al., 2002). The type of beach plan form strongly depends on dimensions and location of structure. In the case of emerged detached breakwaters, the beach can extend and come in contact with the structure (formation of tombolo). Permanent tombolo is expected for $L/D > 1$ and salient for $L/D < 1$ according to Van Rijn (2011) with L being the breakwater length, and D the offshore distance to original shoreline. However, the morphological evolution in the lee of breakwaters is a complex physical process that cannot be analyzed in terms of only two parameters (L, D). The beach response relies on several environmental factors, such as three-dimensional bathymetry characteristics, prevailing hydrodynamic conditions and sediment supply. Additionally, geometric properties of the structure, including freeboard, structure slopes, crest width, length of the gap between segments of the breakwater system, and breakwater porosity are known to be influential in beach morphology (Afentoulis et al., 2019).

Deltares/Delft Hydraulics (1997) and Bos et al. (1996) carried out a study about the effect of a detached emerged breakwater on coastal hydro-morphodynamics, using numerical modeling approaches. Herein, this work is used as benchmark test for the validation of our numerical model in field conditions. This application is of high interest, as model's behavior may vary from laboratory to field dimensions. It has been revealed that the achievement of moveable bed equilibrium is slower in the field than in the laboratory's-controlled conditions, where the use of lightweight sediment can introduce additional scale effects (Gorrick et al., 2014). Hence, the present test case corresponds to a total duration of 50 days, which is deemed a sufficient period to explore the model's capacity to capture fluid-seabed interactions over a relatively larger time scale.

The examined test case consisted of 300 m long breakwater with a crest height of +0.5 m, located on an initially along-shore uniform sloping bottom, with a slope of 1:50 and placed at 200 m offshore the shore. In order to reproduce this test case numerically, the bathymetric data were interpolated over a rectangular grid with a spatial step of $\Delta x = 2m$ and $\Delta y = 5m$ in cross-

shore and alongshore direction, respectively. Irregular waves were generated with $H_{rms} = 2.0$m and $T_p = 8.0$s. Fine sand was considered with median sediment size $D_{50} = 0.25$mm. A sponge layer 100m wide was applied at the offshore side to absorb the reflected waves from the breakwater. The dissipation of wave energy at the breakwater location was achieved using large bottom friction locally (a high drag coefficient of C_d =10 was considered) and periodic lateral boundary conditions were applied. A morphological acceleration factor (Morfac = 30) was employed to reduce the relatively high computational cost. The morphological acceleration option was activated after 7 days of wave action when quasi-steady flow conditions prevailed. In Figure 4-12 the initial bathymetry along with the breakwater configuration is illustrated.

Figure 4-13 shows a snapshot of the computed instantaneous free surface elevation. The nearshore processes that can be identified in this Figure are the wave shoaling, diffraction into the sheltered area as well as run-up and run-down. The wave breaking over the breakwater can be observed at X = 400m. Subsequently, Figure 4-14 depicts the mean sea level during the 1st hour of wave action. Wave set-up of about 0.08m can be observed in the lee part of the breakwater and in the illuminated area due to the wave-induced flux nearshore.

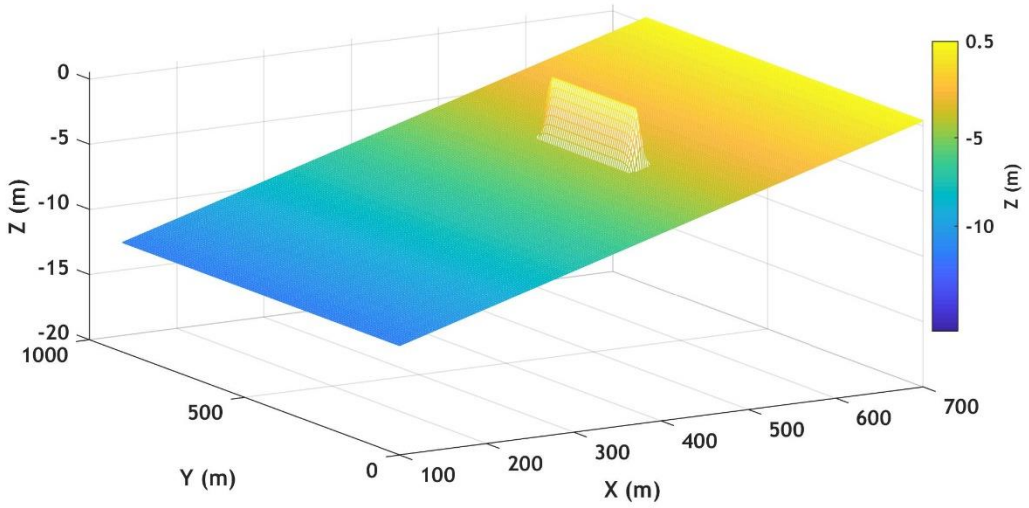

Figure 4-12 3D illustration of Initial bathymetry (breakwater at 200 m from shore).

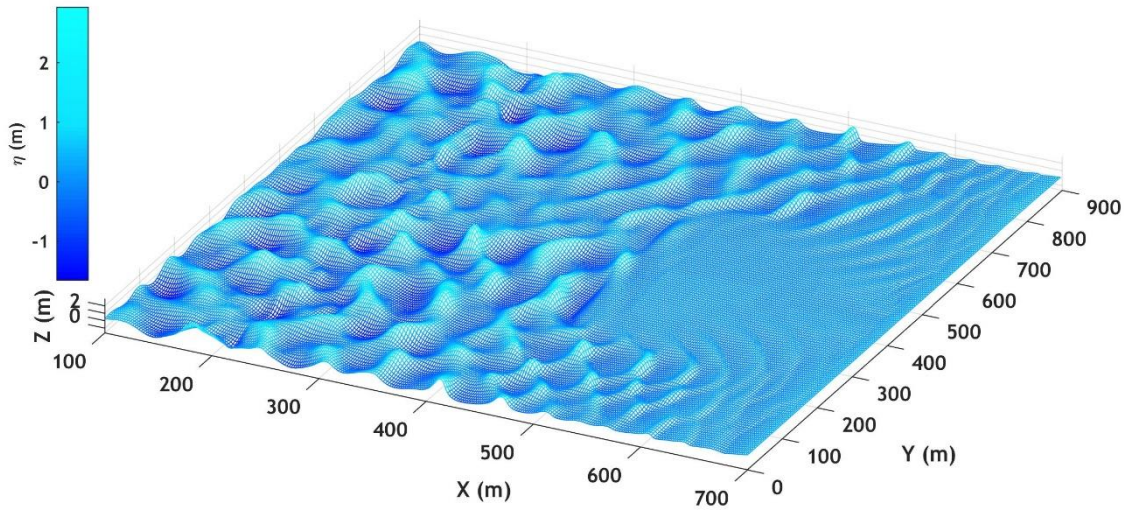

Figure 4-13 Snapshot of the instantaneous computed free surface elevation.

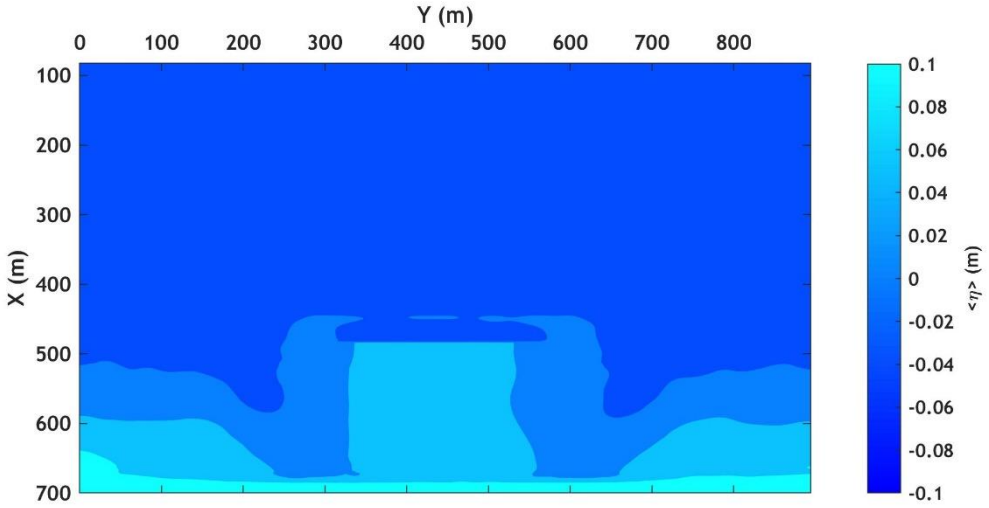

Figure 4-14 Mean surface elevation during the 1st hour of wave action.

The initial wave-induced current field after 1 hour of wave action, superimposed with bathymetry contours, is depicted in Figure 4-15. A formation of two eddies can be observed in the lee of the breakwater. The generation of eddies is due to the current circulation towards the sheltered area, parallel to the shoreline and across both sides. This formation is generated due to the gradient of the mean sea level between the illuminated area and the sheltered area, which leads to diffraction effects with a consequent forcing of currents towards the down-wave of the structure (Karambas, 2012). Additionally, weak rip currents with a velocity of about 0.2m/s can be identified between the lateral boundaries of the model and the structure, while

offshore-oriented velocities are detected close to the shore, reflected from the beachface with a maximum velocity of 0.75m/s.

Figure 4-16 shows the wave-induced current field after 1 day of wave action, superimposed with seabed changes during this time. The seabed evolution is more intense in the zones where significant spatial velocity gradients occur. The developed plan form results to a shortening in the shore-normal direction of the two eddies, which are shifted towards the two gaps, with a slight decrease of the relevant velocities compared to the initial current field. Close to the shore, the seaward oriented currents resulted in the altering of the uniformity of the beach in the alongshore direction, with associated erosion conditions. Figure 4-17 shows the seabed elevation after 10 days of wave action and the associated wave induced currents. Behind the structure, the shoreline extends out and a tombolo starts to be formed. It should be mentioned that the initial geometry with a cross-shore constant slope is not realistic, thus the wave-current-seabed system tends to find an equilibrium by altering the beach slopes near the shoreline. Therefore, dissipative conditions are observed in the foreshore beach morphology after 10 days and the computed erosion of the beach face at both sides is about 1m. This three-dimensional beach form forces alongshore nearshore currents with a magnitude of 0.3m/s. In addition, strong rip currents with a megnitude of about 0.9m/s are detected in the vicinity of breakwater.

The bathymetry obtained after 50 days of wave action is illustrated in Figure 4-18. It can be observed that no significant differences of sea bottom geometry take place between 10 and 50 days. It is concluded that the rate of bottom level change was high initially and slowed down as equilibrium approached. Close to the equilibrium stage, relatively weak velocities of about 0.3m/s characterize the wave induced current field. During this phase, the waves break out of the shadow zone due to the presence of the tombolo, resulting in a less energetic current field in the protected area. Consequently, since the current velocities are relatively weak, the sediment fluxes are insignificant and there is no noticeable change of the seabed geometry.

The agreement between the obtained results and the corresponding retrieved data of the study of Deltares/Delft Hydraulics (1997) seem quite satisfactory, concerning the accretion close to the center-line of the wave tank and the observed erosion of the beach face at both sides. Overall, a formation of tombolo was achieved for L/D >1, which is in line with the available field data used in the study of Deltares/Delft Hydraulics (1997). Furthermore, the outcome of our numerical investigation is consistent with the computed bottom evolution and hydrodynamics revealed in the study of Razak et al. (2018), concerning a similar test case. Razak et al. (2018)

used XBeach model to assess beach response in the lee part of breakwater under the same wave conditions as that used in our study. Once again a single tombolo was formed after 50 days of wave action whilst the computed currents followed flow patterns (discrete vortices) close to our estimates.

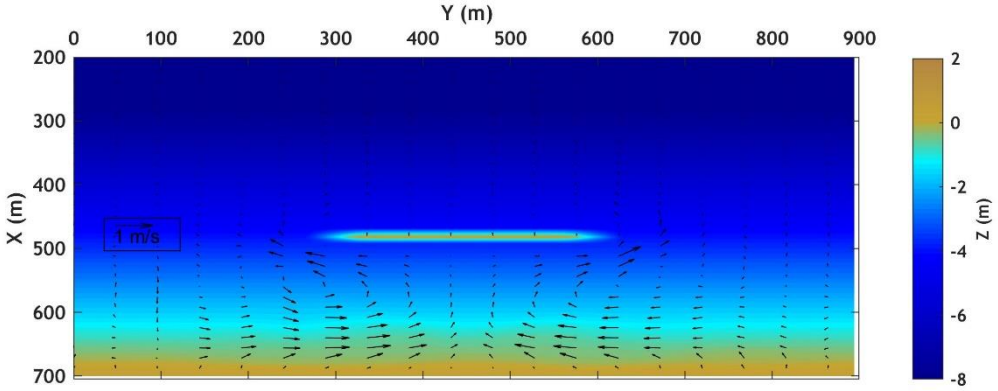

Figure 4-15 Simulated hydrodynamics after 1 hour of wave action. Colors: Initial Bathymetry, Vectors: calculated wave induced current intensity and direction.

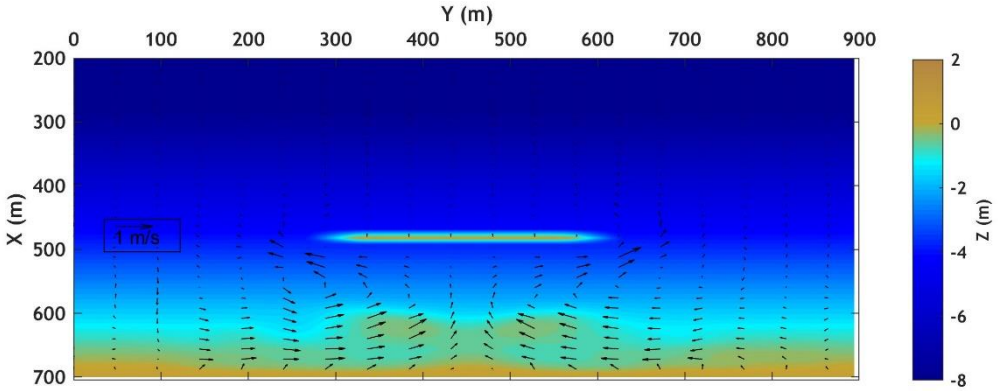

Figure 4-16 Simulated morphodynamics after 1 day of wave action. Colors: Sea bed elevation, Vectors: calculated mean wave induced current intensity and direction.

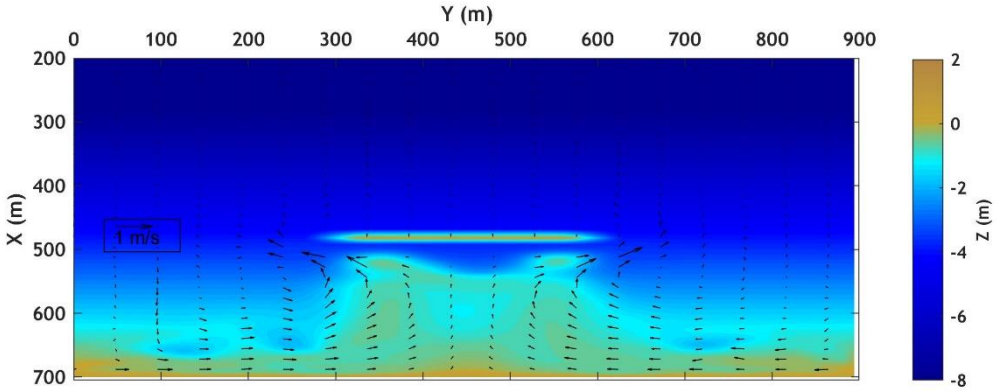

Figure 4-17 Simulated morphodynamics after 10 days of wave action. Colors: Sea bed elevation, Vectors: calculated mean wave induced current intensity and direction.

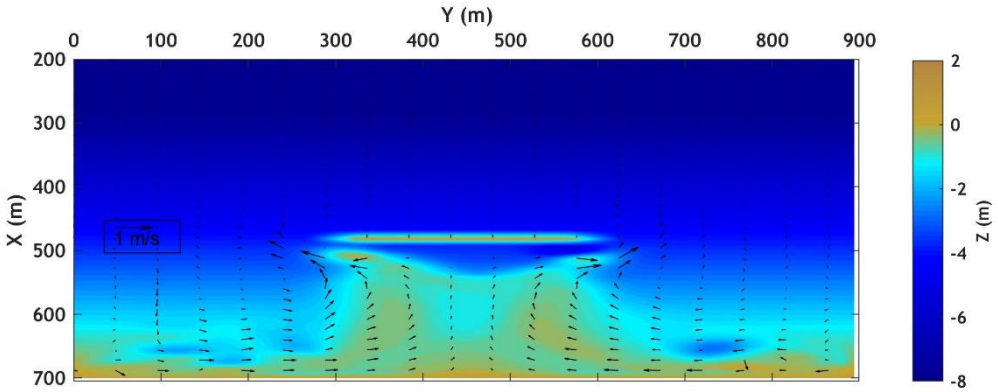

Figure 4-18 Simulated morphodynamics after 50 days of wave action. Colors: Sea bed elevation, Vectors: calculated mean wave induced current intensity and direction.

4.3.3.2 Single submerged breakwater

The proposed coupled model was utilized to investigate the hydrodynamic and morphodynamic patterns as well as the beach morphology in the vicinity of a submerged offshore breakwater. These structures lead in wave energy reduction through depth-induced wave breaking and the shoreline response to submerged breakwater is governed by hydrodynamic processes such as wave setup, wave set-down, onshore mass flux, and nearshore currents (Ranasinghe et al., 2010). The effect of structure freeboard is also dominant in shaping hydrodynamic patterns shoreward of the breakwaters. When a submerged breakwater is located close to the beach, strong erosion behind the structure appears and high turbulence levels occur due to wave breaking associated with high sediment suspension, which can be driven outwards the sheltered area by diverging fluxes (Tsiaras et al., 2020). Thus, potential erosion could occur for the case of short structure distances relative to the shore. Cáceres et al. (2005) used numerical modeling approaches, based on a phase averaged wave driver, to investigate the bed evolution behind low-crested structures. The effect of structure freeboard and significant wave height were thoroughly analyzed.

In order to evaluate the effect of submerged structures on beach morphology, the study of Cáceres et al. (2005) was utilized as a benchmark case. A smooth cross-shore slope, around 2:100, characterized the seabed and the bathymetric data were interpolated over a rectangular grid with a spatial step of Δχ = 2m and Δy = 4m in cross-shore and alongshore direction, respectively. Irregular waves were generated with $H_{rms} = 1.0$m and $T_p = 4.0$s with a shore-normal direction. The breakwater crest height was set at - 0.5m (freeboard = 0.5 m) and the structure was placed in a distance of 230m to the shore. The bottom evolution was computed for a duration of 200 hours and a morphological acceleration factor (Morfac = 15) was employed to reduce the computational cost. No sponge layers were employed in the location of the structure to simulate the depth–induced wave breaking and discharge flux over the submerged breakwater.

In Figure 4-19, a snapshot of the free surface elevation is illustrated. It can be observed that some wave breaking is initiated on the breakwater crest at X=470m while a portion of incident wave energy is reflected from the front breakwater face. The transmission of waves from the downstream side of the breakwaters is highly nonlinear, where free and bound transmitted waves travel into the shore (Christou et al., 2008). Nearshore phenomena such as wave shoaling, diffraction, run-up and run-down can also be identified in Figure 18. In contrast to emerged structures, submerged breakwater leads to wave transmission and overtopping. These

processes can be reproduced more accurately through the highly nonlinear phase resolving wave driver proposed in this study in contrast to the phase averaged one utilized in Cáceres et al. (2005). Thus, the net mass transport that occurs above the structure increases wave-setup in the lee zone, which in turn forces outward rip currents around the heads of the structures and through the gaps.

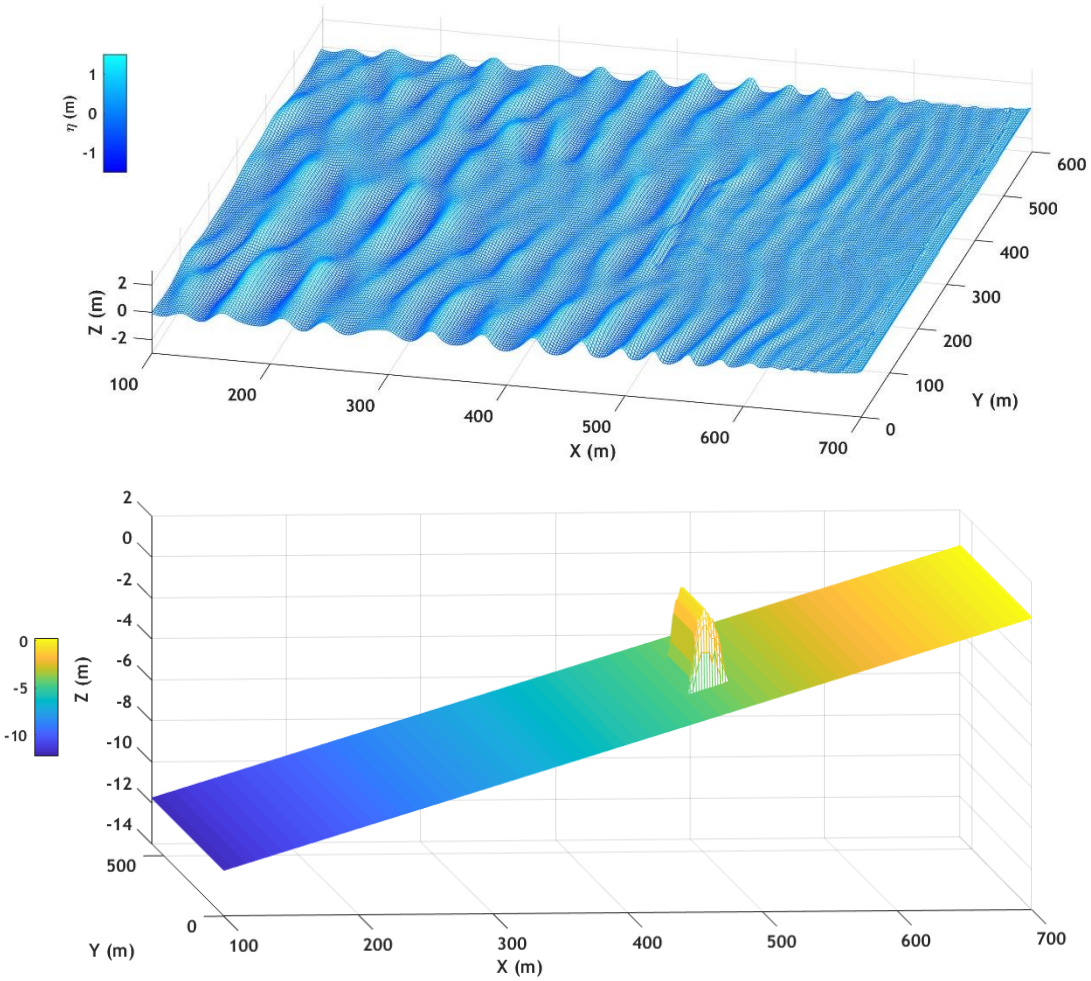

Figure 4-19 Snapshot of the instantaneous computed free surface elevation and initial seabed geometry.

Figure 4-20 presents seabed geometry and the wave-induced current field after one hour of wave action. Two symmetric eddies can be identified associated with strong currents of about 0.8m/s. This is in line with the other studies, which have revealed that the dominant source of vorticity, in the case of submerged breakwaters, is located around the edges of the structure (Bouvier et al., 2019). In contrast to the case of emerged breakwater, the nearshore vortex is hindered, and the order magnitude of nearshore velocities is relatively low, of about 0.3m/s.

This is due to the fact that the overtopping flux extends in a limited area around the structure and governs the circulation, suppressing the nearshore currents.

The computed bathymetry and the associated wave-induced current field after 200 hours of wave action are presented in Figure 4-21. The model results are in good agreement with the findings of Cáceres et al. (2005), as the integrated model succeeded in reproducing all morphological and hydrodynamic patterns behind the breakwater and up to the shore. Once again two symmetric eddies can be identified outside of the sheltered area, while strong diverging erosive currents, with a velocity of 0.8m/s, prevail through the gaps. The overall bottom evolution reveals erosion close to the structure, while the shoreline is accreting, and the formation of salient can be observed.

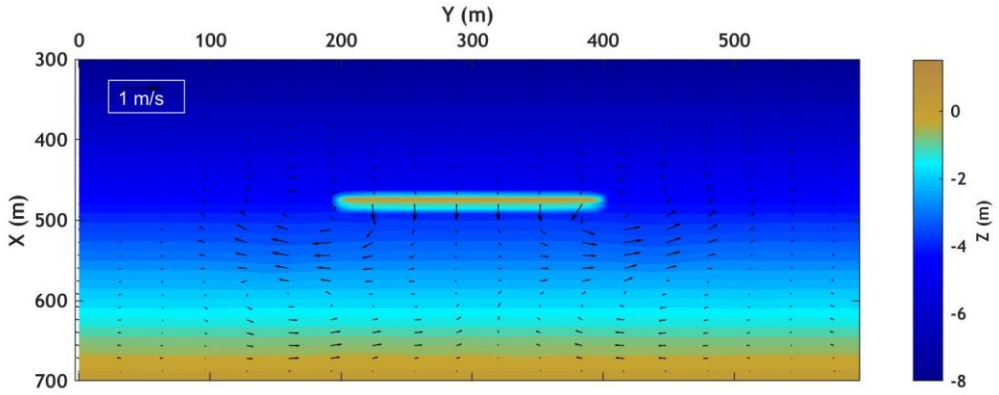

Figure 4-20 Simulated hydrodynamics after 1 hour of wave action. Colors: Initial Bathymetry, Vectors: calculated wave induced current intensity and direction.

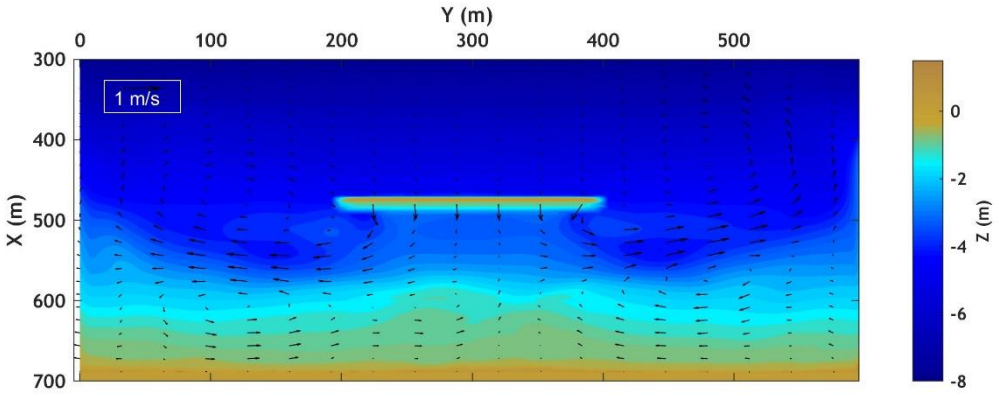

Figure 4-21 Simulated hydrodynamics after 200 hours of wave action. Colors: Final Bathymetry, Vectors: calculated wave induced current intensity and direction.

4.3.3.3 Extended applications with submerged breakwaters

The compound numerical model, utilized herein, was proven to be a valuable tool to predict shoreline morphology, as bed level changes were precisely predicted for a variety of test cases and coastal applications, while the obtained numerical investigations are in line with a large number of existing studies in the broader literature. Therefore, this device was employed for the evaluation of the submerged breakwater effects on nearshore morphology, in terms of two distinct parameters: the distance of the structure to the shore (*S*), keeping a constant longshore breakwater length (*B*), and the cross-shore slope of the initial bathymetry *tan(β)*. Previous studies (Pilarczyk, 2003; Ranasinghe et al., 2010; Klonaris et al., 2016; Tsiaras et al.; 2020; Hieu et al., 2021) have extensively focused on the role of the distance parameter (*S*), and the impact it has on the structure's hydrodynamic effects and ultimately on the capacity of immerged breakwaters to control beach erosion. However, only a limited amount of research attempts was carried out to analyze the sensitivity of this parameter in combination with the cross-shore bed slope, as this latter can dominantly drive nearshore morphodynamics and thus alter breakwater-induced sediment transport patterns. For instance, the performance of a submerged breakwater system, placed in the offshore zone of a reflective coast, differs considerably from the case of a dissipative beach, for a given cross-shore distance to the shore.

In order to assess the morphological evolution in the lee part of a submerged breakwater, the compound nonlinear process-based model, presented in this chapter was applied. The selected breakwater geometrical characteristics correspond to a freeboard of 0.5 m and a transmission coefficient Kt =0.4. This coefficient, Kt, is defined as the ratio of the transmitted wave height to the incident wave height. Irregular waves were generated at the inlet ($H_{rms} = 2.0$m and $T_p = 8.0$s), corresponded to a JONSWAP spectrum with a peak factor of γ= 3.3. In order to create alongshore non-uniformity in the wave breaking spatial pattern, the wave directional spreading at the inlet varies from 10 to 20 degrees. The following Table summarizes the obtained results for six selected cases.

The conclusions derived from the application of the model to the submerged breakwater case are in line with other studies, already published in the literature of coastal engineering (Tsiaras et al., 2020; Ranasinghe et al., 2010; Villani et al., 2012). Within these studies, it was pointed out that Kt, values near 0.4 (corresponding to a low budget structure) are sufficient for successful beach protection for *B /S* values of 0.9-1.3. Another conclusion, derived from this

application is that a small distance to the shore (*S)* in combination with a transmission coefficient relatively large (above 40%, corresponding to larger overtopping rates), significantly affects the structure's performance, as breakwater fails to protect the beach and erosion is predicted leeward. This is due to high overtopping fluxes that extend in a limited space and drive the circulation, in a way to suppress nearshore vortices, which are responsible for the accretive sediment transport patterns.

Test	*Hs(m)*	*Tp(s)*	*B(m)*	*S(m)*	*B /S*	*tan(β)*	Shoreline response to structure
1	*1.4*	*6.5*	*200*	*80*	*2.5*	*2/100*	No response
2	*1.4*	*6.5*	*200*	*80*	*2.5*	*6/100*	Erosion
3	*1.4*	*6.5*	*200*	*150*	*1.3*	*2/100*	Uniform Protection
4	*1.4*	*6.5*	*200*	*150*	*1.3*	*6/100*	Salient
5	*1.4*	*6.5*	*200*	*230*	*0.9*	*2/100*	Well-developed salient
6	*1.4*	*6.5*	*200*	*230*	*0.9*	*6/100*	Erosion

Table 15 Conditions for shoreline response behind submerged breakwater with a free board Sb = 0.5 m and Kt =0.4.

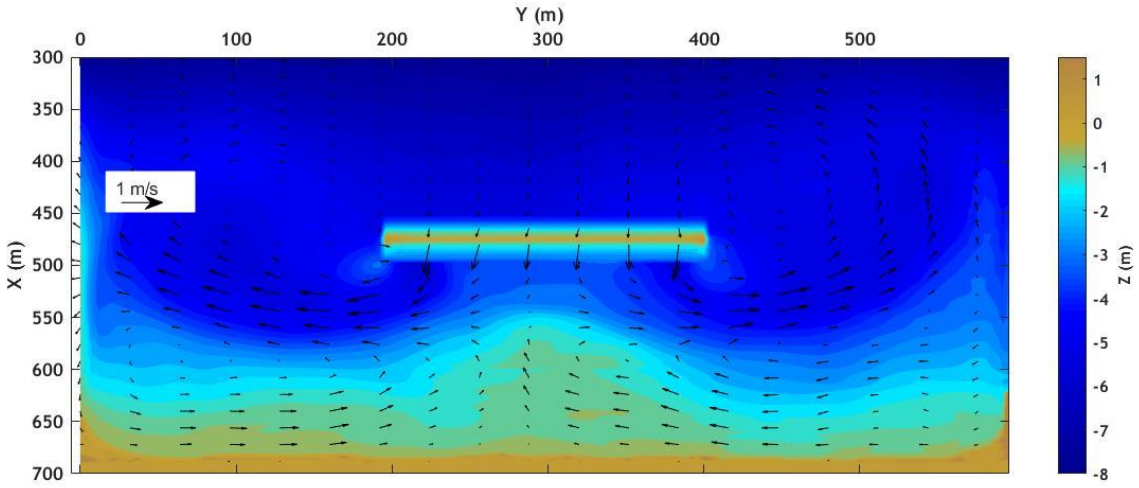

Figure 4-22 Simulated hydrodynamics after 200 hour of wave action. Colors: Final Bathymetry, Vectors: calculated wave induced current intensity and direction. Bed slope: 2/100. Breakwater's distance to the shore: 230m.

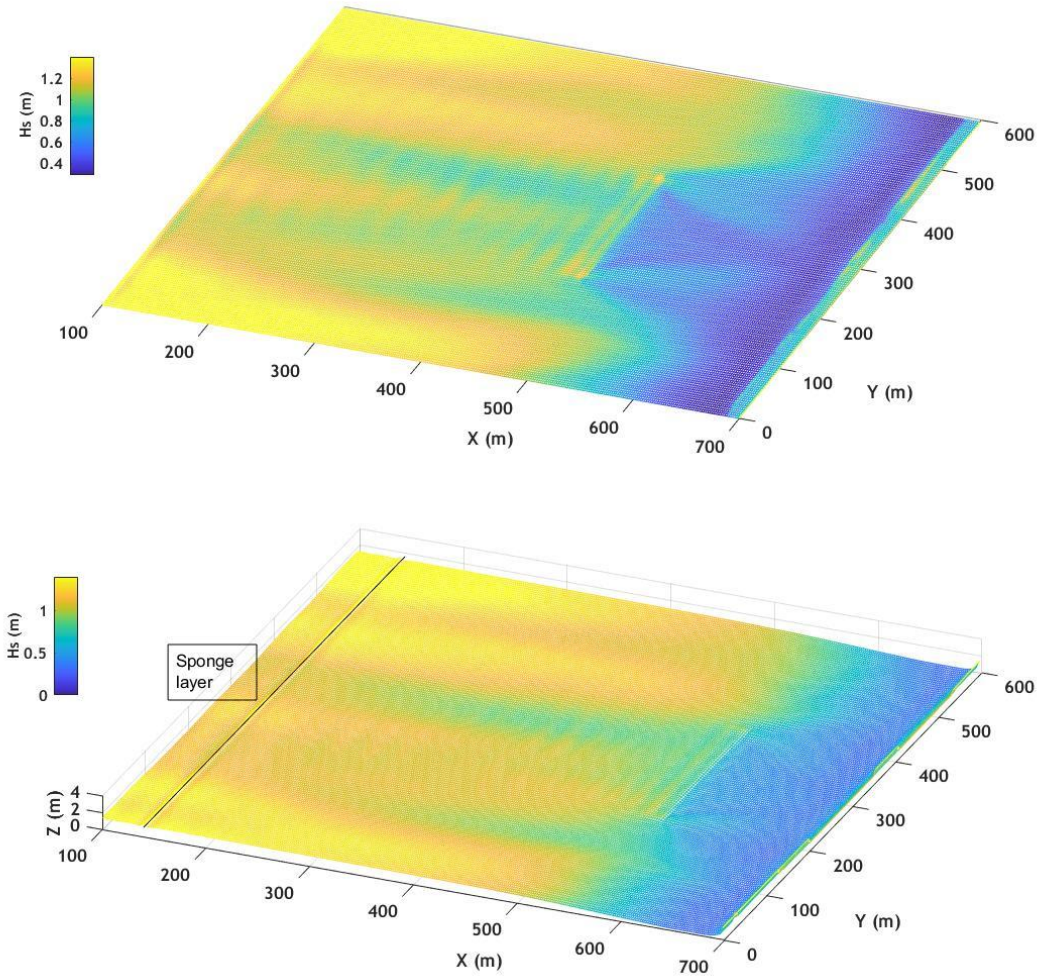

Figure 4-23 Simulated significant wave height distribution maps.. Breakwater's distance to the shore: 230m (up) and 150 (down). Bed slope: 2/100

4.4 Discussion

In this chapter, a newly developed sediment transport model was introduced and coupled to a highly nonlinear Boussinesq wave model to assess the combined effect of waves and currents and ultimately the bed level evolution of coastal areas. Special attention was given to the swash zone dynamics which are considered dominant in shaping the morphological bed level changes, as well as to the unsteady wave effects on the bed load sediment transport rates. The combination of the sophisticated Boussinesq model along with a quasi-3D sediment transport model incorporating swash zone dynamics is considered to be extremely valuable in obtaining accurate bed level predictions in complex coastal areas. Of particular interest was the investigation of the interaction between hydrodynamics, seabed, and coastal structures, with

the obtained results having strong implications on the improvement of the structures' design and performance in protecting the shoreline.

The model was validated against the experimental data of Alsina et al. (2012) and Dette et al. (2002) in order to assess seabed morphology in the inner and swash zone. The prediction of erosion or accretion close to the shoreline is crucial for engineering applications and can affect the solution throughout the whole computational domain. The effect of swash zone dynamics was embedded, and the good agreement between model results and laboratory measurements enhance the robustness of our numerical approach. For the evaluation of the morphological influence of groyne structures, the physical experiment of Baidei et al. (1994) was reproduced. The numerical model results are in very good agreement with the experimental findings in the context of an accurate prediction of the measured bed evolution and shoreline position. Moreover, the performance of the composite model was evaluated in terms of its capacity to estimate the effects of detached emerged and submerged breakwaters on morphological features under real field conditions. The computational results were quantitatively compared to those of other studies (Cáceres et al., 2005; Deltares/Delft Hydraulics, 1997) and a good agreement was achieved. The formation of tombolo/salient was reproduced accurately and agreed with the limits defined in literature.

Regarding the several parameters/coefficients that utilized in this research, special attention should be given to the choice of the empirical coefficient of Equation (16), where values up to 3 should be employed for intermediate beaches and up to 5 for reflective beach profiles, in order to represent avalanching phenomena associated with steep slopes. This element was proven particularly important in order to guarantee the stability of the numerical simulations and the accuracy of the final solution, in combination with a proper selected time step of the continuity equation (Exner), which was set equal or slightly higher than the corresponding one, used in hydrodynamic simulations. Furthermore, the application of periodic boundary conditions allowed us to obtain a realistic wave-induced current field and minimize boundary effects in 2DH simulations. In addition, the acceleration techniques utilized in this research, were significantly effective to reduce computational burden, although a sensitivity analysis that was carried out herein, revealed that the values of the non-unity factor (Morfac) greater than 30 affects unrealistically the hydrodynamic solution. In the absence of clearly defined limits in the literature, Morfac values were adopted with caution in this work by performing trial and error simulations of a few hours, to define the upper allowable values of Morfac. This analysis served

to consider non-linear morphological responses to wave forcing, and obtain a good compromise between simulation speed and accurate results.

In this study, swash and nearshore morphodynamics were investigated over dissipative and reflective beaches, as well as in transition profiles between the two states, where the formation of wave-breaking induced sandbars under the shoreface was accurately predicted, especially in the case of 1DH applications that allow us to assess small-scale physical processes. Although further investigations are needed to model sand ripple morphology using finer grids and accretive wave sequences during the transition from reflective to dissipative beach states, knowing that the simulation of nearshore accretion phenomena is generally a more demanding task that requires the implementation of groundwater processes. Moreover, in order to extend the limitation of the present numerical approach, the role of aeolian sediment transport has to be considered in case of dune erosion and further benchmark test cases need to be evaluated, including estuary dynamics and gravel beaches.

Considering all the above, it is believed that the presented integrated model can be an asset for engineers and scientists desiring to obtain accurate bed level evolution predictions in complex bathymetries with the presence of a variety of coastal protection structures, both in experimental and in field

References

Afentoulis, V., Eleftheria, K., Eleni, S., Evangelos, M., Archontia, L., Christos, M., & Vasiliki, T. (2017). Coastal Processes Assessment Under Extreme Storm Events Using Numerical Modelling Approaches. Environmental Processes, 4(3). https://doi.org/10.1007/s40710-017-0253-8

Alsina, J. M., Cáceres, I., Brocchini, M., & Baldock, T. E. (2012). An experimental study on sediment transport and bed evolution under different swash zone morphological conditions. Coastal Engineering, 68. https://doi.org/10.1016/j.coastaleng.2012.04.008

Badiei, P., Kamphuis, J. W., & Hamilton, D. G. (1995). Physical experiments on the effects of groins on shore morphology. In Proceedings of the Coastal Engineering Conference (Vol. 2). https://doi.org/10.1061/9780784400890.129

Benoit, M., Marcos, F., & Becq, F. (1997). Development of a third generation shallow-water wave model with unstructured spatial meshing. In Proceedings of the Coastal Engineering Conference (Vol. 1). https://doi.org/10.1061/9780784402429.037

Birben, A. R., Özölçer, I. H., Karasu, S., & Kömürcü, M. I. (2007). Investigation of the effects of offshore breakwater parameters on sediment accumulation. Ocean Engineering, 34(2). https://doi.org/10.1016/j.oceaneng.2005.12.006

Bos, K. J., Roelvink, J. A., & Dingemans, M. W. (1997). Modelling the impact of detached breakwaters on the coast. In Proceedings of the Coastal Engineering Conference (Vol. 2). https://doi.org/10.1061/9780784402429.157

Bouvier, C., Castelle, B., & Balouin, Y. (2019). Modeling the impact of the implementation of a submerged structure on surf zone sandbar dynamics. Journal of Marine Science and Engineering, 7(4). https://doi.org/10.3390/jmse7040117

Bruun, P. (1954). Coast Erosion and the Development of Beach Profiles. US Army Corps of Engineers.

Cáceres, I., Sánchez-Arcilla, A., Zanuttigh, B., Lamberti, A., & Franco, L. (2005). Wave overtopping and induced currents at emergent low crested structures. Coastal Engineering, 52(10–11). https://doi.org/10.1016/j.coastaleng.2005.09.004

Cáceres, I., Stive, M. J. F., Sánchez-Arcilla, A., & Trung, L. H. (2008). Quantification of changes in current intensities induced by wave overtopping around low-crested structures. Coastal Engineering, 55(2). https://doi.org/10.1016/j.coastaleng.2007.09.003

Charlier, R. H., & de Meyer, C. P. (1989). Coastal defense and beach renovation. Ocean and Shoreline Management, 12(5–6). https://doi.org/10.1016/0951-8312(89)90029-5

Chen, Q. (2006). Fully Nonlinear Boussinesq-Type Equations for Waves and Currents over Porous Beds. Journal of Engineering Mechanics, 132(2). https://doi.org/10.1061/(asce)0733-9399(2006)132:2(220)

Chen, Q., Dalrymple, R. A., Kirby, J. T., Kennedy, A. B., & Haller, M. C. (1999). Boussinesq modeling of a rip current system. Journal of Geophysical Research: Oceans, 104(C9). https://doi.org/10.1029/1999jc900154

Chen, Q., Kirby, J. T., Dalrymple, R. A., Shi, F., & Thornton, E. B. (2003). Boussinesq modeling of longshore currents. Journal of Geophysical Research: Oceans, 108(11). https://doi.org/10.1029/2002jc001308

Christou, M., Swan, C., & Gudmestad, O. T. (2008). The interaction of surface water waves with submerged breakwaters. Coastal Engineering, 55(12). https://doi.org/10.1016/j.coastaleng.2008.02.014

Dette, H. H., Larson, M., Murphy, J., Newe, J., Peters, K., Reniers, A., & Steetzel, H. (2002). Application of prototype flume tests for beach nourishment assessment. Coastal Engineering, 47(2). https://doi.org/10.1016/S0378-3839(02)00124-2

Ding, Y., & Wang, S. S. (2008). Development and application of a coastal and estuarine morphological process modeling system. Journal of Coastal research, (10052), 127-140.

Do, J. D., Jin, J. Y., Hyun, S. K., Jeong, W. M., & Chang, Y. S. (2020). Numerical investigation of the effect of wave diffraction on beach erosion/accretion at the Gangneung Harbor, Korea. Journal of Hydro-Environment Research, 29. https://doi.org/10.1016/j.jher.2019.11.003

French, P. (2001). Coastal Defences Processes, Problems and Solution. Taylor & Francis Group (Vol. 53).

Gallerano, F., G. Cannata, and F. Lasaponara. "A new numerical model for simulations of wave transformation, breaking and long-shore currents in complex coastal regions." International Journal for Numerical Methods in Fluids 80.10 (2016): 571-613.

Galappatti, G., & Vreugdenhil, C. B. (1985). A depth-integrated model for suspended sediment transport. Journal of Hydraulic Research, 23(4). https://doi.org/10.1080/00221688509499345

Galappatti, R. (1983). A depth integrated model for suspended transport. Communications on Hydrology - Delft University of Technology, Department of Civil Engineering Report, 83–7.

Geiman, J. D., Kirby, J. T., Reniers, A. J. H. M., & MacMahan, J. H. (2011). Effects of wave averaging on estimates of fluid mixing in the surf zone. Journal of Geophysical Research: Oceans, 116(4). https://doi.org/10.1029/2010JC006678

Hieu, P. D., Phan, V. N., Nguyen, V. T., Nguyen, T. V., & Tanaka, H. (2020). Numerical study of nearshore hydrodynamics and morphology changes behind offshore breakwaters under actions of waves using a sediment transport model coupled with the SWASH model. Coastal Engineering Journal, 62(4), 553-565.

Holthuijsen, L. H., Herman, A., & Booij, N. (2003). Phase-decoupled refraction-diffraction for spectral wave models. Coastal Engineering, 49(4). https://doi.org/10.1016/S0378-3839(03)00065-6

Johnson, D., & Pattiaratchi, C. (2006). Boussinesq modelling of transient rip currents. Coastal Engineering, 53(5–6). https://doi.org/10.1016/j.coastaleng.2005.11.005

Isobe, M., & Horikawa, K. (1982). Study on water particle velocities of shoaling and breaking waves. Coastal Engineering in Japan, 25(1), 109-123.

Karambas, T. v. (2012). DESIGN OF DETACHED BREAKWATERS FOR COASTAL PROTECTION: DEVELOPMENT AND APPLICATION OF AN ADVANCED NUMERICAL MODEL. Coastal Engineering Proceedings, 1(33). https://doi.org/10.9753/icce.v33.sediment.115

Karambas, T. v., & Koutitas, C. (2002). Surf and Swash Zone Morphology Evolution Induced by Nonlinear Waves. Journal of Waterway, Port, Coastal, and Ocean Engineering, 128(3). https://doi.org/10.1061/(asce)0733-950x(2002)128:3(102)

Karambas, T. v., & Samaras, A. G. (2017). An integrated numerical model for the design of coastal protection structures. Journal of Marine Science and Engineering, 5(4). https://doi.org/10.3390/jmse5040050

Katopodi, I., & Ribberink, J. S. (1992). Quasi-3D modelling of suspended sediment transport by currents and waves. Coastal Engineering, 18(1–2). https://doi.org/10.1016/0378-3839(92)90006-G

Kennedy, A. B., Kirby, J. T., Chen, Q., & Dalrymple, R. A. (2001). Boussinesq-type equations with improved nonlinear performance. Wave Motion, 33(3). https://doi.org/10.1016/S0165-2125(00)00071-8

Klonaris, Georgios Th., Memos, C. D., & Drønen, N. K. (2016). High-Order Boussinesq-Type Model for Integrated Nearshore Dynamics. Journal of Waterway, Port, Coastal, and Ocean Engineering, 142(6). https://doi.org/10.1061/(asce)ww.1943-5460.0000349

Klonaris, Georgios Th, Metallinos, A. S., Memos, C. D., & Galani, K. A. (2020). Experimental and numerical investigation of bed morphology in the lee of porous submerged breakwaters. Coastal Engineering, 155. https://doi.org/10.1016/j.coastaleng.2019.103591

Klonaris, Georgios T., Memos, C. D., Drønen, N. K., & Deigaard, R. (2018). Simulating 2DH coastal morphodynamics with a Boussinesq-type model. Coastal Engineering Journal, 60(2). https://doi.org/10.1080/21664250.2018.1462300

Kobayashi, H., Watanabe, A., Isobe, M., Sato, S., & Ishii, T. (2001). Three-Dimensional beach deformation model for nonlinear multi-directional waves. In Coastal Engineering 2000 (pp. 2728-2739).

Kristensen, S. E., Drønen, N., Deigaard, R., & Fredsoe, J. (2016). Impact of groyne fields on the littoral drift: A hybrid morphological modelling study. Coastal Engineering, 111. https://doi.org/10.1016/j.coastaleng.2016.01.009

Larsen, J., & Dancy, H. (1983). Open boundaries in short wave simulations - A new approach. Coastal Engineering, 7(3). https://doi.org/10.1016/0378-3839(83)90022-4

Larson, M., & Wamsley, T. v. (2007). A formula for longshore sediment transport in the Swash. In Coastal Sediments '07 - Proceedings of 6th International Symposium on Coastal Engineering and Science of Coastal Sediment Processes. https://doi.org/10.1061/40926(239)151

Leont'yev, I. O. (1996). Numerical modelling of beach erosion during storm event. Coastal Engineering, 29(1–2). https://doi.org/10.1016/S0378-3839(96)00029-4

Lesser, G. R., Roelvink, J. A., van Kester, J. A. T. M., & Stelling, G. S. (2004). Development and validation of a three-dimensional morphological model. Coastal Engineering, 51(8–9). https://doi.org/10.1016/j.coastaleng.2004.07.014

Madsen, P. A., Sørensen, O. R., & Schäffer, H. A. (1997). Surf zone dynamics simulated by a Boussinesq type model. Part I. Model description and cross-shore motion of regular waves. Coastal Engineering, 32(4). https://doi.org/10.1016/S0378-3839(97)00028-8

Malej, M., Shi, F., & Smith, J. M. (2019). Modeling ship-wake-induced sediment transport and morphological change–sediment module in FUNWAVE-TVD.

Masselink, G., Russell, P., Turner, I., & Blenkinsopp, C. (2009). Net sediment transport and morphological change in the swash zone of a high-energy sandy beach from swash event to tidal cycle time scales. Marine Geology, 267(1–2). https://doi.org/10.1016/j.margeo.2009.09.003

Ming, D., & Chiew, Y.-M. (2000). Shoreline Changes behind Detached Breakwater. Journal of Waterway, Port, Coastal, and Ocean Engineering, 126(2). https://doi.org/10.1061/(asce)0733-950x(2000)126:2(63)

Nam, P. T., Larson, M., Hanson, H., & Hoan, L. X. (2009). A numerical model of nearshore waves, currents, and sediment transport. Coastal Engineering, 56(11–12). https://doi.org/10.1016/j.coastaleng.2009.06.007

Nordstrom, K. F. (2014). Living with shore protection structures: A review. Estuarine, Coastal and Shelf Science. https://doi.org/10.1016/j.ecss.2013.11.003

Postacchini, M., Russo, A., Carniel, S., & Brocchini, M. (2016). Assessing the Hydro-Morphodynamic Response of a Beach Protected by Detached, Impermeable, Submerged Breakwaters: A Numerical Approach. Journal of Coastal Research, 32(3). https://doi.org/10.2112/JCOASTRES-D-15-00057.1

Pranzini, E., Wetzel, L., & Williams, A. T. (2015). Aspects of coastal erosion and protection in Europe. Journal of Coastal Conservation, 19(4). https://doi.org/10.1007/s11852-015-0399-3

Raffourt, C., Vergnet, C., Afentoulis, V., & Bardey, P. (2020). Hydrodynamics of an Innovative Discontinuous Double Breakwater, Mixed Modeling: 2D Flume Physics and 3D Digital Modelling. https://doi.org/10.1007/978-981-15-5436-0_63

Ranasinghe, R., Larson, M., & Savioli, J. (2010). Shoreline response to a single shore-parallel submerged breakwater. Coastal Engineering, 57(11–12). https://doi.org/10.1016/j.coastaleng.2010.06.002

Razak, M. S. A., & Nor, N. A. Z. M. (2018). XBeach Process-Based Modelling of Coastal Morphological Features Near Breakwater. In MATEC Web of Conferences (Vol. 203). https://doi.org/10.1051/matecconf/201820301007

Ribberink, J. S. (1998). Bed-load transport for steady flows and unsteady oscillatory flows. Coastal Engineering, 34(1-2), 59-82.

Roelvink, Dano, Reniers, A., van Dongeren, A., van Thiel de Vries, J., McCall, R., & Lescinski, J. (2009). Modelling storm impacts on beaches, dunes and barrier islands. Coastal Engineering, 56(11–12). https://doi.org/10.1016/j.coastaleng.2009.08.006

Roelvink, D, & Reniers, A. (2012). A guide to modeling coastal morphology. Advances in Coastal and Ocean Engineering.

Ruiz-Martínez, G., Mariño-Tapia, I., Baldwin, E. G. M., Casarín, R. S., & Ortiz, C. E. E. (2016). Identifying Coastal Defence Schemes through Morphodynamic Numerical Simulations along the Northern Coast of Yucatan, Mexico. Journal of Coastal Research, 32(3). https://doi.org/10.2112/JCOASTRES-D-15-00009.1

Seabergh, W. C., & Kraus, N. C. (2003). Progress in management of sediment bypassing at coastal inlets: Natural bypassing, weir jetties, jetty spurs, and engineering aids in design. Coastal Engineering Journal, 45(4). https://doi.org/10.1142/S0578563403000944

Servold, K. P., Webb, B. M., & Douglass, S. L. (2015). Effects of Low-Crested Living Shoreline Breakwaters on Wave Setup. In Coastal Structures and Solutions to Coastal Disasters 2015: Resilient Coastal Communities - Proceedings of the Coastal Structures and Solutions to Coastal Disasters Joint Conference 2015. https://doi.org/10.1061/9780784480304.045

Shi, F., Kirby, J. T., Harris, J. C., Geiman, J. D., & Grilli, S. T. (2012). A high-order adaptive time-stepping TVD solver for Boussinesq modeling of breaking waves and coastal inundation. Ocean Modelling, 43–44. https://doi.org/10.1016/j.ocemod.2011.12.004

Smagorinsky, J. (1963). General circulation experiments wiht the primitive equations I. The basic experiment. Monthly Weather Review, 91(3).

Smit, P. B., Janssen, T. T., & Herbers, T. H. C. (2015). Stochastic modeling of inhomogeneous ocean waves. Ocean Modelling, 96. https://doi.org/10.1016/j.ocemod.2015.06.009

Tang, J., Lyu, Y., Shen, Y., Zhang, M., & Su, M. (2017). Numerical study on influences of breakwater layout on coastal waves, wave-induced currents, sediment transport and beach morphological evolution. Ocean Engineering, 141. https://doi.org/10.1016/j.oceaneng.2017.06.042

Tonelli, M., & Petti, M. (2009). Hybrid finite volume - finite difference scheme for 2DH improved Boussinesq equations. Coastal Engineering, 56(5–6). https://doi.org/10.1016/j.coastaleng.2009.01.001

Tsiaras, A.-C., Karambas, T., & Koutsouvela, D. (2020). Design of Detached Emerged and Submerged Breakwaters for Coastal Protection: Development and Application of an Advanced

Numerical Model. Journal of Waterway, Port, Coastal, and Ocean Engineering, 146(4). https://doi.org/10.1061/(asce)ww.1943-5460.0000566

Valsamidis, A., & Reeve, D. E. (2017). Modelling shoreline evolution in the vicinity of a groyne and a river. Continental Shelf Research, 132. https://doi.org/10.1016/j.csr.2016.11.010

van Rijn, L. (1993). Principles of Sediment Transport in Rivers, Estuaries and Coastal Seas. Principles of Sediment Transport in Rivers , Estuaries and Coastal Seas.

van Rijn, Leo C. (2007). Unified View of Sediment Transport by Currents and Waves. I: Initiation of Motion, Bed Roughness, and Bed-Load Transport. Journal of Hydraulic Engineering, 133(6). https://doi.org/10.1061/(asce)0733-9429(2007)133:6(649)

Waters, C. N., Zalasiewicz, J., Summerhayes, C., Barnosky, A. D., Poirier, C., Gałuszka, A., Cearreta, A., Edgeworth, M., Ellis, E. C., Ellis, M., Jeandel, C., Leinfelder, R., McNeill, J. R., Richter, D. D. B., Steffen, W., Syvitski, J., Vidas, D., Wagreich, M., Williams, M., Zhisheng, A., Grinevald, J., Odada, E., Oreskes, N., & Wolfe, A. P. (2016). The Anthropocene is functionally and stratigraphically distinct from the Holocene. Science. https://doi.org/10.1126/science.aad2622

Wei, G., Kirby, J. T., & Sinha, A. (1999). Generation of waves in Boussinesq models using a source function method. Coastal Engineering, 36(4). https://doi.org/10.1016/S0378-3839(99)00009-5

Zyserman, J. A., & Johnson, H. K. (2002). Modelling morphological processes in the vicinity of shore-parallel breakwaters. Coastal Engineering, 45(3–4). https://doi.org/10.1016/S0378-3839(02)00037-6

5 Conclusions and future research

Beach erosion is a worldwide and largely discussed issue, caused by both natural processes and anthropogenic activities. Although, the latter was proven to be a significant intensification factor during the last decades, as urban sprawl, unplanned interventions and unregulated structures may alter the littoral drift, constituting an obstacle to the continuity of natural morphodynamic mechanisms. This can result in a deficit of sediment, which ultimately leads to coastal erosion. During next coming years, urbanization, population growth and increase in construction activity will grow the coastal risks, adding more pressure to an already dwindling sediment supply. The choice of the appropriate type of defence to control coastal erosion is the object of an active discussion in many countries, as soft, mild and hard engineering techniques can be used to deal with beach erosion. Sandscaping and sand dunes, mangroves, seagrass, coral, dynamic cobble berm revetment and shellfish reefs are some green solutions that can be utilized to reinforce the stability of coastal environment, while emerged and immerged detached breakwaters, groynes and rock revetments are typically hard interventions that can minimize the erosive wave force. The conception of these works highlighted the necessity of accurate bed level change predictions to estimate the effect of each solution on littoral system. In recent years, the scientific and engineering research has turned to the application of advanced numerical techniques to investigate the performance and efficiency of these structures (mild or hard), in terms of their capacity to combat erosion tendencies. Hence, the present Ph.D. dissertation can be considered as part of this research field.

This study seeks to assist in better understanding non-cohesive sediments movement under wave-current actions. The core aim of the present dissertation is to develop advanced numerical modelling approaches techniques, in order to precisely simulate morphodynamic mechanisms over a variety of complex and irregular bathymetries, considering wave unsteady phenomena and several small-scale physical processes in the inner surf and swash zone. In parallel, the advanced compound models, which were tailored within the context of the present research, served to evaluate the hydrodynamic and morphodynamic effects of a number of coastal defence types, such as submerged and emerged offshore-detached breakwaters, groynes and jetties.

To analyze general sediment phenomena in erosion-dominated coasts, numerical assessments, based on available existing devices, were carried out in selected case studies in Greece (chapter 2); laboratory experimental data analysis and novel coupled models were used to study the incipient motion of fine-sand and morphological evolution from dissipative to intermediate and reflective beach state.(chapter 3). Finally, inspired by the capacities and limitations of the existing numerical devices, the development of a novel and robust numerical model was achieved in purpose of practical applications. In particular, a process-based newly developed sediment transport model, with a quasi-3D approach for the assessment of suspended sediment transport, was utilized in tandem with a fully non-linear Boussinesq model to evaluate wave-current-sediment transport interactions in wave-dominated conditions, with and without the presence of coastal defences (chapter 4). In this context, novel 3D and 2D laboratory experimental investigations were exploited to corroborate the numerical predictions. The model validation against experimental measurements revealed that the main scope of the thesis was fulfilled satisfactorily.

In order to attain this overarching goal, supplementary intermediate objectives were also pre-set, as described in chapter 1. Thus, the conclusions reached on way to all these objectives, undertaken herein, are discussed in the following by answering the preset research questions, listed in Chapter1.

5.1 Answering the research questions

(1) How existing numerical models and software suites perform in terms of the prediction of nearshore complex morphological processes, influenced by the unsteady impact of the wave-current combined action and how they consider coastal structures effects?

As literature review, an analysis of the existing numerical devices and tools as well as their capacities to predict sediment transport phenomena in selected study areas with special morphological interest, was carried out within the context of the present thesis (Chapter 1). Several methodologies and numerical approaches were applied for the investigation of nearshore physical processes, such as wave propagation, wave-structure interactions, hydrodynamics and morphodynamics. The storm-induced coastal vulnerability was analyzed for the study area of Rethymno in Greece, where different solutions (configurations of coastal structures) were evaluated via advanced numerical modeling, in terms of their capacity to

combat storm-induced damages. Wave propagation and hydro-morphodynamic patterns were investigated through two distinct numerical models: MIKE 21 and XBeach, and a comparison between their outputs was performed in view of their ability to evaluate nearshore physical processes, under extreme storm events. These two process-based models performed satisfactory well, as the obtained findings proved it. It was demonstrated that the MIKE 21 and XBeach synergistic numerical modeling can be confidently applied on large scale (domain of a total surface of 14 km^2) to simulate the hydro-morphodynamics of a complex embayment, under extreme conditions. The obtained fields of sediment transport rates and wave-induced currents, computed separately by each model, show a similar behavior, which corroborates the validity of the numerical technique.

The selected approach presented although some limitations, associated with the quasi-linear nature of the MIKE21 and XB numerical models, in which hydrodynamic circulation is calculated via a wave-averaged concept. More specifically, XBeach in surf beat mode is based on a short-wave averaged and wave-group resolving concept, which put significant difficulties in predicting nonlinear wave-wave interactions, as well as intra-wave effects on hydrodynamics and morphology. Additionally, diffraction and dispersion phenomena cannot be adequately simulated using XB model in surfbeat mode. Although small-scale morphological processes in the inner surf and swash zone can be precisely evaluated using this device, as special focus was placed on avalanching and slope-limited sediment mobilization, while the forcing of wave breaking-induced roller energy dissipation on the hydrodynamic circulation, was considered in the calculations of gradients of radiation stresses. The processes of overwash, inundation, vegetation and hard structure impact, and breaching were also included in computations. However, no particular techniques are included in the recent version of this model to analyze the porous nature of coastal structures and defenses, and the associated transmission phenomena.

Furthermore, MIKE21 model takes into consideration a number of processes, occurring in deep and intermediate water depths, such as white capping and nonlinear energy transfer amongst the different wave components of a directional-frequency spectrum that plays a crucial role for the temporal and spatial evolution of a wave field. However, as in the case of XB model, this device provides a wave-averaged approach for the evaluation of hydro-morphodynamic characteristics, as current field is driven by the radiation stresses calculated via the spectral wave model, which is based on the conservation of the wave action balance. This concept put significant limitations in predicting wave phenomena near the coast, where the effects of

medium variations (bathymetry and currents), obstacles, and a transition to dispersive wave motion result in deviations from homogeneous and Gaussian statistics upon which these spectrum-based models are relied. Within this model, the presence of structures, such as piers, breakwaters, caissons or groynes can be modeled by a sub-grid scaling technique, using a source term and convective flux approach or transmission coefficients for 'line' structures.

(2) What are the key approaches for the modelling of beach up-state or down-state transitions and the prediction of sandbar systems and rip channels behaviour?

Beach states have been observed to present a wide variety as it was shown by Wright and Short (1984) and Lippmann and Holman (1989) and further corroborated via experimental and numerical procedures and video observations. These beach state variations differ from alongshore quasi-uniform dissipative beaches to intermediate and reflective coasts, while intermediate sub-sates can appear characterized by pronounced bar-trough (straight or crescentic) topographies, rhythmic bars, shore connected transverse bars intersected by (obliquely oriented) rips and low tide terrace. The transition from one beach state to the next is defined as up-state or down-state. A large number of modeling efforts have been made to explain these transitions of which the downstate transitions have been reasonably successful. To date, available morphodynamic model cannot precisely simulate the range of dynamics related to intermediate beach morphodynamics.

The detailed morphodynamic data collected by Castelle et al., (2010) and Michallet et al., (2013) served here as an important benchmark for numerical investigations. In order to provide a better understanding of these physical processes, two distinct approaches were employed for the evaluation of nearshore morphodynamics and particularly the impact of wave climate variations on nearshore morphology. The first device, which was utilized herein, is based on minimization principles for the assessment of bed morphology. The fundamental assumption of this method is the fact that bed adapts to the flow by some sort of optimal sand transport in order to minimize an energy expression, optimal transport is seen here as minimal change in the bed shape This numerical method provided reliable results, concerning the identification of the nearshore zones, in which accretion or erosion prevail. Although, the limitation of this model to reproduce a realistic wave climate offshore (only shore-normal waves were considered), makes difficult the simulation of nearshore hydrodynamic currents that follow the patterns, which were observed during the experimental campaign. Concerning the computed final alongshore bed geometry, a good agreement between computed and measured parameters was achieved.

This can lead to the conclusion that this numerical technique can provide accurate prediction for 1DH coastal applications.

Moreover, an additional numerical compound model, was utilized in this study for the investigation of hydrodynamic and morphodynamic 2DH phenomena, based on nonlinear shallow water equations (NSWE) and a newly developed sediment transport model was utilized in tandem with the hydrodynamic model. This technique yields information on the emergence of nearshore periodic patterns, corresponding to the fastest growing mode, subject to the irregular sediment transport patterns over the initial bathymetry. Overall, a good agreement between both experimental and numerical results was achieved, as the seabed adapted correctly to the wave climate changes. However, the computed morphodynamics are sensitive to initial bottom geometry, wave height, period and direction, limiting the predictive capability of this numerical model. The wave forcing and the variability in the nearshore bathymetry along the coast has a stochastic nature, and thus is unlikely to be able to predict the rip channel positions in a deterministic sense.

Although, the findings are valid for the initial stages of the evolution of rhythmic patterns, associated with the infinitesimal changes in the bed elevation. The transition process takes place within a relatively short time span of 5-10 hours. It is concluded that the rate of bottom level change was high initially and slowed down as equilibrium approached.

(3) How to develop time-dependent techniques for fine sediment transport modelling, including non-linear wave effects in nearshore region and swash zone, for practical purposes (e.g., to improve the approaches of sediment simulation in 2DH/3D model)?

Nearshore models are usually comprised of wave propagation, hydrodynamic, and sediment transport / morphology models. A variety of sophisticated numerical tools have been tailaored in the literature of coastal engineering, for the simulation of wave transformation processes, taking into consideration that for most coastal configurations waves are the dominant driving factor, inducing morphological changes. Two distinct approaches have been highlighted (Hotlhiujsen, 2003) for the numerical investigation of the dominant processes governing wave transformation: 1) The phase-averaged approach that describes wave propagation in the spatial and time domain using the variance-density spectrum, which is the Fourier transformation of the auto-covariance function of free-surface elevation. 2) The phase resolving deterministic

approach describing details of the wave field in the spatial and temporal domain at a resolution that is a small fraction of the wavelength / period. In this category, models solving the mild slope, shallow water (SWE) or Boussinesq equations have been employed. It should be noted that despite the plethora of modeling tools available, each one is associated with flaws, which have to be taken into serious consideration for the purpose of predicting the morphological evolution of coastal areas. Models based on the phase averaging approach are computationally efficient but omit a large amount of dominant wave processes in the nearshore, especially considering that wave diffraction, reflection and run-up are not usually accounted for. In addition, coherencies observed in the wave field and caused by abrupt bottom variations and strong current gradients are unable to be simulated in these models (Smit et al., 2015).

Phase resolving models are able to resolve many of the aforementioned important wave transformation processes but are often associated with major constraints, i.e. mildly sloping bottoms (for models based on the mild slope wave equations) and satisfaction of the shallow water approximation (for the SWE wave models). From deep to shallow water, dispersive nonlinear wave effects can be simulated satisfactorily using Boussinesq models (Madsen et al., 1997; Kennedy et al., 2001) since they are sufficiently accurate in resolving nearshore wave phenomena, such as refraction and diffraction (Do, 2020). However, until recent decades, their application to hydrodynamic modeling in engineering projects was limited due to high computational cost (Klonaris et al., 2018, 2020) rendering their use in practical applications almost impossible.

Within the context of this dissertation and in order to go one step further in comparison with the most of the presented morphological coastal models that are often relied on wave-averaged methods, phase-resolving sediment transport models were implemented to evaluate wave behavior in transition zones from deep to shallow water areas and obtain the necessary wave input for the estimation of sediment transport rates. To this purpose, a fully non-linear Boussinesq–type wave model (FUNWAVE-TVD) were utilized to simulate wave propagation. The usage of this phase resolving model gave a good account of all the processes of wave transformation in coastal areas: shoaling, wave breaking run-up and run-down, two-dimensional wave-induced mean-currents over complex bathymetries, dispersion, wave skewness and asymmetry. These features were proven significantly necessary for the precise estimation of sediment transport and morphological processes. Furthermore, the fact that the usage of a phase-resolving non-linear model as wave driver, lead to more confident bed elevation changes, can be mainly attributed to three fundamental aspects following Gallerano et al. (2016). The

first one refers to the undertow impact on sediment transport, the second concerns the sediment particle resuspension and settling due to the intra-wave effects and breaking-induced turbulence and the third one concerns the net swash sediment transport dynamics.

Therefore, the fully nonlinear Boussinesq model- FUNWAVE-TVD was directly coupled to a quasi-3-D sediment transport and morphology model, which was developed by the author of this dissertation. This device accounts for sediment transport non-linear processes, while special attention was given to the role of sediment transport dynamics across the swash zone, incorporating them in the morphodynamic model. Moreover, advanced techniques were utilized to model the three-dimensional patterns of suspended load fluxes and incorporate wave nonlinear and unsteady effects on bed load transport rates. The compound model was validated thoroughly against laboratory data and other numerical investigations. Overall, a good agreement between experimental and numerical results was achieved for a number of 1DH and 2DH coastal applications.

(4) How coupled numerical modelling techniques can incorporate the role of coastal structures/obstacles on the mechanisms of wave propagation, wave-induced current, sediment transport by waves and currents, and bed morphology evolution.

The most widely applied engineering technique to control beach erosion is the construction of coastal defense structures, which can also provide sufficient protection against flooding phenomena to the inland. A variety of coastal defenses can be encountered in the literature of coastal engineering, such as detached emerged and submerged breakwaters, groynes, seawalls, rip-rap and wave attenuators. The investigation of nearshore hydrodynamic and morphodynamic patterns, associated with the presence of coastal structures, has been carried out through experimental investigations in order to describe wave transmission and reflection phenomena. However, scaling effects inherently linked to the experimental conditions and the sediment transport processes render the long-term prediction of coastal bed evolution through experimental procedures a difficult task. As a consequence, process-based models that can advance understanding of the dominant process response (and feedbacks) of littoral systems to a wide range of costal defense structures, have been extensively used in coastal engineering.

In the available coastal area models, based on spectral approaches, the role of coastal structures is implemented by the usage of empiric formulas for the estimation of wave transmission over ‘line’ structures. These lines intercept the elements of the computational grid,

as the bathymetry features are represented by a spacing of O(10) to O(100) m, which is considerably higher than the required spatial discretization. Another method, used in the case of nearshore models with a wave drive that relie on mild slope equations (e.g. Artemis, Refonde), is to represent the behavior of structures by a reflection/transmission coefficient. These techniques put significant restrictions in the predictive capability of the numerical models, as the structure's geometry is not well represented, while overtopping phenomena are not included in the simulations.

In the present study, a fully nonlinear Boussinesq model- FUNWAVE-TVD (Shi et al., 2012) tasked with the simulation of wave propagation and hydrodynamic circulation was directly coupled to a quasi-3-D sediment transport and morphology model. Thus, taking advantage of FUNWAVE model's capability to provide information on coastal structure's reflection and transmission behavior and employing advanced sediment transport approximations, including unsteady and 3D sand transport aspects, this study seeks to reduce the uncertainty in hydro-morphodynamic predictions. Using this technique within the context of this dissertation, the updrift entrapment and downdrift erosion, as well as the associated hydrodynamic characteristics in the vicinity of a groyne structure was accurately simulated. Furthermore, this study assessed the mechanisms of how breakwater geometry affects hydrodynamic processes and evolution of bottom topography, resulting in a plan form development (formation of tombolo or salient) in the lee of a submerged or emerged breakwater.

5.2 Intermediate aims

On the way to fulfill the principal objectives of the specific research, some intermediate aims were set and achieved. During this procedure additional conclusions were drawn from the individual parts of the thesis.

Coastal area models and applications in erosion-dominated areas

- The storm-induced coastal vulnerability was analyzed for the study area of Rethymno in Greece, where different solutions (configurations of coastal structures) were evaluated via advanced numerical modeling, in terms of their capacity to combat storm-induced damages. Wave propagation and hydro-morphodynamic patterns were investigated through two distinct numerical models: MIKE 21 and XBeach, and a comparison between their outputs was performed in view of their ability to evaluate nearshore physical processes, under extreme storm events. T

- The optimization of form and geometric properties of a detached submerged breakwater system was analyzed, using a numerical formulation based on minimization principles of (Bouharguane and Mohammadi, 2013).
- Moreover, a probabilistic theory was applied to define offshore conditions and wave events that can initiate the sediment motion. Thus, the assessment of the hydrodynamic and morphological impact of the structures was based on a probabilistic framework , linked to the prevailing wave conditions of a coastal area.

Numerical assessments of sandbar systems and rip channel dynamics

- The outputs of a novel 3D experiment (Castelle et al., 2010; Michallet et al., 2013) were analyzed in order to study wave-sandy bed interactions over a shallow sloping bottom and without the presence of coastal structure. Special focus was placed on the investigation of rip channels effects on sand bar morphology. The analysis of experimental data provided significant insights about the so-called up-state and down-state transitions.
- A literature review of recent studies was carried out to reveal the efficient strategies of wave-dominated sandy beach morphological predictions, including experimental procedures, numerical simulations and video /satellite observations.
- A wave generator was tailored for the needs of the numerical assessments, contributing to the application of a more realistic wave climate. This device was implemented also for the generation of irregular waves using directional spectral data. The irregular waves were obtained by superposing a series of wave components with different frequencies and directions, using random phases.

A novel coupled non-linear model for sediment transport dynamics in coastal areas.

- The FUNWAVE-TVD model was tested in a number of test cases, showing good response including a number of physical wave processes such as wave run-up and rundown, shoaling, refraction, diffraction, breaking, overtopping, and interactions with the wave-induced current field. Therefore, it was verified that this model forms a robust tool for assessing coastal morphodynamics.
- The sediment transport model, developed for the needs of this research, uses as input the results from the Boussinesq-type wave model, which in turn is fed by the updated bathymetry. Therefore, several significant aspects, such as the wave skewness and asymmetry, wave irregularity, bound and free long waves, wave groups and nonlinear interactions are directly taken into account from the intra-wave sediment transport

formulation. In addition, a quasi-3D approach was employed to reconstitute numerically the suspended sediment transport vertical profile.

- The adopted sediment transport formula for the bed load transport incorporates significant unsteady effects. The exclusion of these unsteady effects may lead to inaccurate predictions of sediment transport fluxes. This was corroborated by a sensitivity analysis performed for the sediment transport model.
- The incorporated morphological accelerator technique was proved to be an effective strategy for predicting 2DH short and medium-term changes of bed morphology. In this study, Morfac values (ranging from 1 to 30) were systematically adapted to be compared with a baseline condition of no acceleration. Care must be taken not to exaggerate with extreme Morfac values, in order to describe realistically the interaction of the wave, hydrodynamic and morphology modules
- Regarding the several parameters/coefficients that utilized in this research, special attention was given to the choice of the empirical coefficient of Equation(16), where values up to 3 should be employed for intermediate beaches and up to 5 for reflective beach profiles, in order to represent avalanching phenomena associated with steep slopes. This element was proven particularly important in order to guarantee the stability of the numerical simulations and the accuracy of the final seabed geometry, in combination with a proper selected time step of the continuity equation (Exner), which was set equal or slightly higher than the corresponding one, used in hydrodynamic simulations.
- The application of periodic boundary conditions allowed us to obtain a realistic wave-induced current field and minimize boundary effects in 2DH simulations.
- Concerning the role of submerged breakwaters, it was pointed out that transmission coefficient (Kt) values near 0.4 (corresponding to a low budget structure) are sufficient for successful beach protection for B /S values of 0.9-1.3, with (*B*) breakwater length (S) distance to the shore. Another conclusion, derived from this study is that a small distance to the shore (S) in combination with a transmission coefficient relatively large (above 0.4, corresponding to larger overtopping rates), affects significantly the structure's performance, as breakwater fails to protect the beach and erosion is predicted leeward.

5.3 Recommendations

The previous chapters present the conception, setup, validation and analysis of 2DH process-based models covering the nearshore and swash area, whilst considerable insight has been

gained with regard to the usage of the advanced numerical techniques to predict nearshore wave propagation, nonlinear wave -current interactions and beach morphology. The novel compound model presented in Chapter 4 and the sediment transport tool based on NSWE, discussed in Chapter 3, can be further calibrated at onshore and offshore stations, while filed measurements can be utilized to validate the computed wave, hydrodynamic and sediment transport output parameters. Moreover, additional detailed measurements can give insight in near-bed variations in turbulence energy, turbulence advection and diffusion in time and space and the different behavior of turbulence generated by spilling and plunging breaking waves respectively.

Concerning the investigations of sandbar dynamics, filed measurement can provide a benchmark for numerical validations, since only a restricted amount of data is available about the down-state and up-state transitions in a large scale, at the time of writing of the present thesis. In this dissertation, inner surf and swash zone morphodynamics were investigated over dissipative and reflective beaches, as well as in transition profiles between the two states, where the formation of wave-breaking induced sandbars under the shoreface was accurately predicted. Although further investigations are needed to model sand ripple morphology using finer grids and accretive wave sequences during the transition from reflective to dissipative beach states, knowing that the simulation of nearshore accretion phenomena is generally a more demanding task that requires the implementation of groundwater processes.

Furthermore, the suspended sediment transport formula, introduced in Chapter 4 to predict sediment fluxes, is based on a quasi-3D concept for the identification of the vertical mixing zone and the approximation of sediment concentration gradients. Although, hydrodynamic parameters were computed via a 2DH model and near-bed flow characteristics and nonlinear time-varying near-bottom wave velocities were extracted using the parameterization proposed by Isobe and Horikawa (1982). Therefore, 3D modelling techniques are needed to further assess the flow patterns that drive sediment motions along the water column and trigger small-scale sediment resuspension processes (Wu et al., 2012). In addition to the implementation of 3D modelling techniques, supplementary experimental observations are required to better understand hydro-morphodynamic interactions over the vertical space, within the top layer from wave crest to wave through, the middle layer and the near bed layer. Special focus should be placed on 3D hydrodynamic characteristics in the vicinity and through the porous space of the coastal defences, whose 2DH effects and performance were thoroughly analyzed in Chapter 4.

The numerical approaches introduced in this research, should be utilized with the aim to predict interannual seabed morphology over several tide cycles, to assess model's capability in terms of long-term predictions of shoreline position. For this purpose, it is desirable to reduce the total computational burden required for the simulation of wave phenomena, using more powerful computing resources and parallelization techniques. Concerning the issue of high computational cost, further investigations on the current research topic are already underway to incorporate machine learning techniques, so as to predict wave and hydrodynamic conditions with comparable accuracy to a physics-based numerical model for a fraction of the computational cost.

References

Bouharguane, A., & Mohammadi, B. (2013). Minimisation principles for the evolution of a soft sea bed interacting with a shallow sea. International Journal of Computational Fluid Dynamics, 26(3), 163-172.

Castelle, B., Michallet, H., Marieu, V., Leckler, F., Dubardier, B., Lambert, A., ... & Bouchette, F. (2010). Laboratory experiment on rip current circulations over a moveable bed: Drifter measurements. Journal of Geophysical Research: Oceans, 115(C12).

Do, J. D., Jin, J. Y., Hyun, S. K., Jeong, W. M., & Chang, Y. S. (2020). Numerical investigation of the effect of wave diffraction on beach erosion/accretion at the Gangneung Harbor, Korea. Journal of Hydro-environment Research, 29, 31-44.

Gallerano, F., G. Cannata, and F. Lasaponara. "A new numerical model for simulations of wave transformation, breaking and long-shore currents in complex coastal regions." International Journal for Numerical Methods in Fluids 80.10 (2016): 571-613.

Holthuijsen, L. H., Herman, A., & Booij, N. (2003). Phase-decoupled refraction–diffraction for spectral wave models. Coastal Engineering, 49(4), 291-305.

Lippmann, T. C., & Holman, R. A. (1989). Quantification of sand bar morphology: A video technique based on wave dissipation. Journal of Geophysical Research: Oceans, 94(C1), 995-1011.

Kennedy, A. B., Kirby, J. T., Chen, Q., & Dalrymple, R. A. (2001). Boussinesq-type equations with improved nonlinear performance. Wave Motion, 33(3), 225-243.

Klonaris, G. T., Memos, C. D., Drønen, N. K., & Deigaard, R. (2018). Simulating 2DH coastal morphodynamics with a Boussinesq-type model. Coastal Engineering Journal, 60(2), 159-179.

Klonaris, Georgios Th, et al. "Experimental and numerical investigation of bed morphology in the lee of porous submerged breakwaters." Coastal Engineering 155 (2020): 103591.

Isobe, M., & Horikawa, K. (1982). Study on water particle velocities of shoaling and breaking waves. Coastal Engineering in Japan, 25(1), 109-123.

Michallet, H., Castelle, B., Barthélemy, E., Berni, C., & Bonneton, P. (2013). Physical modeling of three-dimensional intermediate beach morphodynamics. Journal of Geophysical Research: Earth Surface, 118(2), 1045-1059.

Madsen, P. A., Sørensen, O. R., & Schäffer, H. A. (1997). Surf zone dynamics simulated by a Boussinesq type model. Part I. Model description and cross-shore motion of regular waves. Coastal Engineering, 32(4), 255-287.

Roelvink, D., Reniers, A., Van Dongeren, A. P., De Vries, J. V. T., McCall, R., & Lescinski, J. (2009). Modelling storm impacts on beaches, dunes and barrier islands. Coastal engineering, 56(11-12), 1133-1152.

Shi, F., Kirby, J. T., Harris, J. C., Geiman, J. D., & Grilli, S. T. (2012). A high-order adaptive time-stepping TVD solver for Boussinesq modeling of breaking waves and coastal inundation. Ocean Modelling, 43–44.

Smit, P. B., Janssen, T. T., & Herbers, T. H. C. (2015). Stochastic modeling of inhomogeneous ocean waves. Ocean Modelling, 96, 26-35.Warren, I. R., & Bach, H. (1992). MIKE 21: a modelling system for estuaries, coastal waters and seas. Environmental Software, 7(4), 229-240.

Wright, L. D., & Short, A. D. (1984). Morphodynamic variability of surf zones and beaches: a synthesis. Marine geology, 56(1-4), 93-118.

Wu, J., Liu, J. T., & Wang, X. (2012). Sediment trapping of turbidity maxima in the Changjiang Estuary. Marine Geology, 303, 14-25.

Appendix A

In the last version (TVD) of FUNWAVE model, the equations, in which the device is based, are reorganized into a conservative form to facilitate computations with a hybrid numerical scheme. The set of conservative Boussinesq equations in FUNWAVE-TVD can be written as

$$\frac{\partial \eta}{\partial t}+\frac{\partial M(x)}{\partial x}+\frac{\partial M(y)}{\partial y}=0 \tag{A.1}$$

$$\begin{aligned}\frac{\partial M(x)}{\partial t}+\frac{\partial}{\partial x}\left[\frac{1}{H}\left(M^{(x)}\right)^2+\frac{1}{2}g(\eta^2+2\eta h)\right]+\frac{\partial}{\partial y}\left[\frac{1}{H}\left(M^{(x)}M^{(y)}\right)\right] \\ =g\eta\frac{\partial h}{\partial x}+H\left(x^{(x)}-V_1^{(x)}-V_2^{(x)}-V_3^{(x)}\right)+R^{(x)}+R^{b(x)}\end{aligned} \tag{A.2}$$

$$\begin{aligned}\frac{\partial M(y)}{\partial t}+\frac{\partial}{\partial x}\left[\frac{1}{H}\left(M^{(x)}M^{(y)}\right)\right]+\frac{\partial}{\partial y}\left[\frac{1}{H}\left(M^{(y)}\right)^2+\frac{1}{2}g(\eta^2+2\eta h)\right] \\ =g\eta\frac{\partial h}{\partial x}+H\left(x^{(y)}-V_1^{(y)}-V_2^{(y)}-V_3^{(y)}\right)+R^{(y)}+R^{b(y)}\end{aligned} \tag{A.3}$$

In which, $H=\eta+h,\ \eta$ is the surface elevation and h is water depth. In Equations (A.1)–(A.3), the superscript $(x)$and (y) denote x and y components of the variables in vector form, respectively.

$R^{(x)}$, $R^{(y)}$ represent the quadratic form of the bottom friction modeled by $C_d\boldsymbol{u}_a|\boldsymbol{u}_a|$, where $C_d$is the bottom friction coefficient.

$\boldsymbol{M}$ is the horizontal volume flux defined by:

$$\boldsymbol{M}=(M^{(x)},M^{(y)})=H(\boldsymbol{u}_a+\overline{\boldsymbol{u}_2}) \tag{A.4}$$

Where, $\boldsymbol{u}_a=(u_a,v_a)$ is the horizontal velocity vector at a reference elevation $z=z_a$. $\boldsymbol{u}_2$ is the depth-averaged second-order horizontal velocity ($O(\mu^2)$, where μ is the dimensionless parameter for wave dispersion) given by

$$\overline{\boldsymbol{u}_2}=(u_2,v_2)=\frac{1}{H}\int_{-h}^{\eta}\boldsymbol{u}_2(z)dz \tag{A.5}$$

$$= \{{z_a}^2 - \frac{1}{6}(h^2 - h\eta + \eta^2)\}\nabla(\nabla \cdot \boldsymbol{u}_a) + \{z_a + \frac{1}{2}(h - \eta)\}\nabla(\nabla \cdot (h\boldsymbol{u}_a)). \quad \text{(A.6)}$$

The terms $x^{(y)}$ and $x^{(x)}$ in Equations. (A.2) and (A.3) can be expressed as:

$$x^{(x)} = \frac{\partial \overline{u_2}}{\partial t} + u_a \frac{\partial \overline{u_2}}{\partial x} + v_a \frac{\partial \overline{u_2}}{\partial y} + \overline{u_2}\frac{\partial u_a}{\partial x} + \overline{u_2}\frac{\partial v_a}{\partial y}, \quad \text{(A.8)}$$

$$x^{(y)} = \frac{\partial \overline{u_2}}{\partial t} + u_a \frac{\partial \overline{v_2}}{\partial x} + v_a \frac{\partial \overline{u_2}}{\partial y} + \overline{u_2}\frac{\partial v_a}{\partial x} + \overline{u_2}\frac{\partial v_a}{\partial y}, \quad \text{(A.9)}$$

$\boldsymbol{V_1}$ and $\boldsymbol{V_2}$ are terms representing the dispersive Boussinesq terms given by Chen (2006)

$$\boldsymbol{V_1} = \frac{z_a^2}{2}\nabla(\nabla \cdot \boldsymbol{u}_a) + z_a\nabla[\nabla \cdot (h\boldsymbol{u}_{at})] - \nabla\{\frac{\eta^2}{2}\nabla \cdot \boldsymbol{u}_{at} + \eta[\nabla \cdot (h\boldsymbol{u}_{at})]\} \quad \text{(A.10)}$$

$$\begin{aligned}\boldsymbol{V_2} = \nabla\{(z_a - \eta)(\boldsymbol{u}_a \cdot \nabla)[\nabla \cdot (h\boldsymbol{u}_{at})] + \frac{1}{2}(z_a^2 - \eta^2)(\boldsymbol{u}_a \cdot \nabla)(\nabla \cdot \boldsymbol{u}_a)\} \\ + \frac{1}{2}\nabla\{[\nabla \cdot (h\boldsymbol{u}_a) + \eta\,\nabla \cdot \boldsymbol{u}_a]^2\}\end{aligned} \quad \text{(A.11)}$$

It can be noticed that the z-dependent terms do not appear in equations (A.2-A.3) except for the $\boldsymbol{V_3}$ term, which accounts for the second-order effect of the vertical vorticity and may be expressed as:

$${V_3}^x = -u_a\omega_1 - \omega_0\{(z_a - z)\frac{\partial}{\partial_y}[\nabla \cdot (h\boldsymbol{u}_{at})] +)\} + \frac{1}{2}({z_a}^2 - z^2)\frac{\partial}{\partial_y}(\nabla \cdot \boldsymbol{u}_a)\} \quad \text{(A.12)}$$

$${V_3}^y = -u_a\omega_1 - \omega_0\{(z_a - z)\frac{\partial}{\partial_x}[\nabla \cdot (h\boldsymbol{u}_{at})] +)\} + \frac{1}{2}({z_a}^2 - z^2)\frac{\partial}{\partial_x}(\nabla \cdot \boldsymbol{u}_a)\} \quad \text{(A.13)}$$

In which, the vertical vorticities, first order and second order) can be expressed as follows:

$$\omega_0 = \frac{\partial v_a}{\partial x} - \frac{\partial u_a}{\partial y} \quad \text{(A.14)}$$

$$\begin{aligned}\omega_1 = \frac{\partial z_a}{\partial x}\left\{\frac{\partial}{\partial y}[\nabla \cdot (h\boldsymbol{u}_{at})] + z_a\frac{\partial}{\partial y}(\nabla \cdot \boldsymbol{u}_a)\right\} \\ - \frac{\partial z_a}{\partial y}\left\{\frac{\partial}{\partial x}[\nabla \cdot (h\boldsymbol{u}_{at})] + z_a\frac{\partial}{\partial x}(\nabla \cdot \boldsymbol{u}_a)\right\}\end{aligned} \quad \text{(A.15)}$$

z_a was chosen in order to optimize the apparent dispersion relation of the linearized model relative to the full linear dispersion in some sense.

Particularly, the choice $a = \frac{\left(\frac{z_a}{h}\right)^2}{2} + \frac{z_a}{h} = -2/5$ recovers a Padé approximant form of the dispersion relation, while the choice $a = 0.39$, corresponding to the choice $z_a = 0.53h$, minimizes the maximum error in wave phase speed. Kennedy et al. (2001) showed that allowing $z_a$to move up and down with the passage of the wave field allowed a greater degree of flexibility in optimizing nonlinear behavior of the resulting model equations.

The terms $R^{b(x)} + R^{b(y)}$ in Equations (2) and (3) express the eddy-viscosity-type breaking terms as below.

$$R^{b(x)} = \frac{\partial}{\partial x}\left[v\frac{\partial}{\partial x}(Hu_a)\right] + \frac{\partial}{\partial y}\left[v\frac{\partial}{\partial y}(Hu_a)\right] \tag{A.16}$$

$$R^{b(y)} = \frac{\partial}{\partial x}\left[v\frac{\partial}{\partial x}(Hv_a)\right] + \frac{\partial}{\partial y}\left[v\frac{\partial}{\partial y}(Hv_a)\right] \tag{A.17}$$

$$v = B\delta_b^2(h+\eta)\eta_t\,, \qquad B = \begin{cases} 1, \eta_t \geq \eta_t^I \\ 0, \eta_t < \eta_t^I \end{cases} \tag{A.18}$$

Where δ_b = 1.0. B has the value of 0 or 1, representing the switch between non-breaking. and breaking. A breaking event begins when η_t exceeds an initial threshold $\eta_t^I = c_1\sqrt{gH}$. When wave breaking develops, the wave will continue to break until η_t becomes lower than the second threshold $\eta_t^F = c_2\sqrt{gH}$, where $c_2 < c_1$.

The eddy-viscosity-type breaking scheme was found to provide more accurate breaking wave solutions compared to the NSWE-based breaker, particularly for predicting breaking undular bores or solitons as pointed out by Shi et al. (2018).

Time stepping is adaptive based on the Courant–Friedrichs–Lewy (CFL) condition. The time step (Δt) is computed by

$$\Delta t = CFLmin(min\frac{\Delta x}{\left|u+\sqrt{gH}\right|}, min\frac{\Delta y}{\left|v+\sqrt{gH}\right|}) \tag{A.16}$$

where CFL is the Courant number. Δx and v are grid sizes in the x and y directions, respectively.

Spatial derivatives are discretized using a combination of finite-volume and finite-difference methods. A high-order MUSCL (Monotone Upstream-centered Schemes for Conservation Laws)

reconstruction technique, which is accurate up to the fourth-order, is used in the Riemann solver.

The code was parallelized using the Message Passing Interface (MPI) domain decomposition with non-blocking communication.

Appendix B

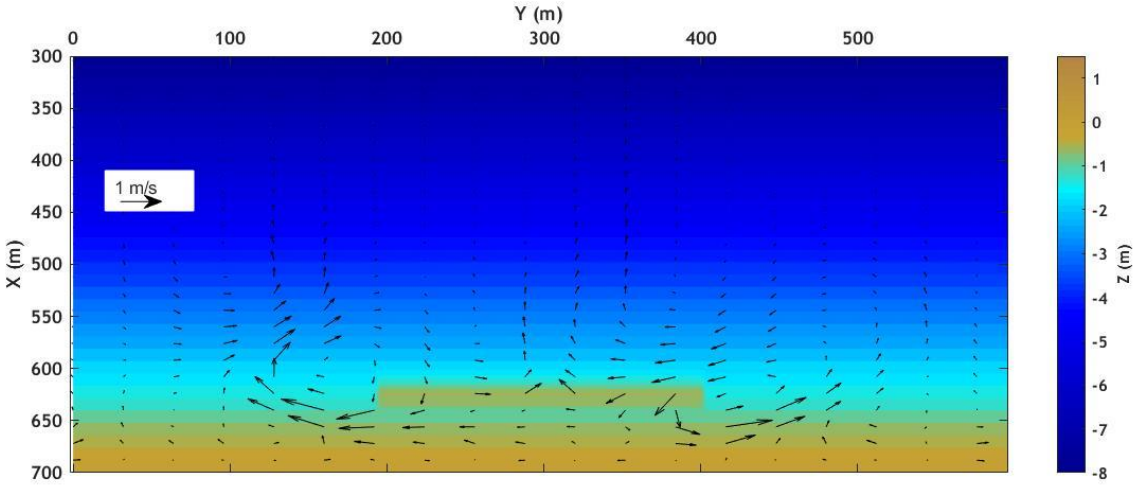

Figure B-1 Simulated hydrodynamics after 1 hour of wave action. Colors: Initial Bathymetry, Vectors: calculated wave induced current intensity and direction. Bed slope: 2/100. Breakwater's distance to the shore: 80m.

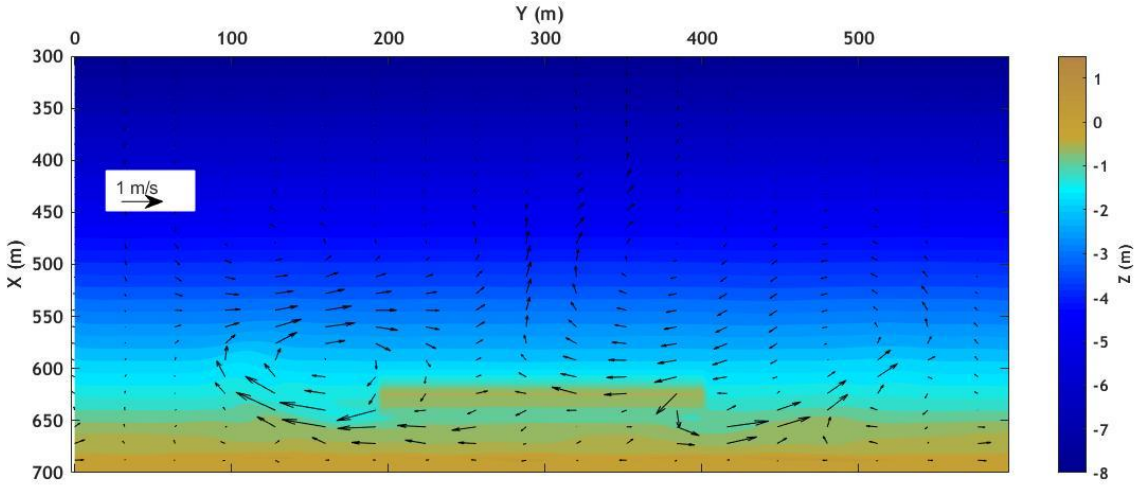

Figure B-2 Simulated hydrodynamics after 200 hour of wave action. Colors: Final Bathymetry, Vectors: calculated wave induced current intensity and direction. Bed slope: 2/100. Breakwater's distance to the shore: 80m.

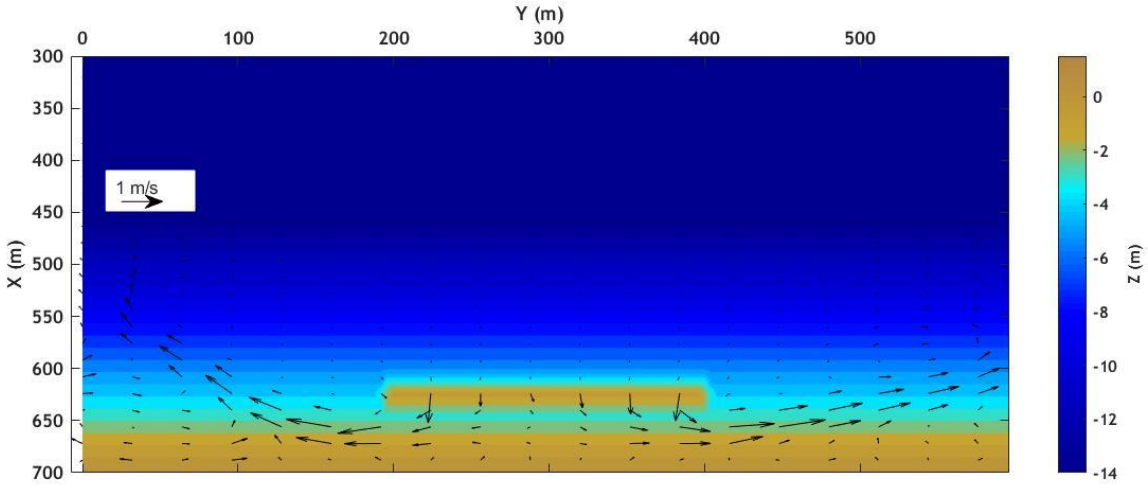

Figure B-3 Simulated hydrodynamics after 1 hour of wave action. Colors: Initial Bathymetry, Vectors: calculated wave induced current intensity and direction. Bed slope: 6/100. Breakwater's distance to the shore: 80m.

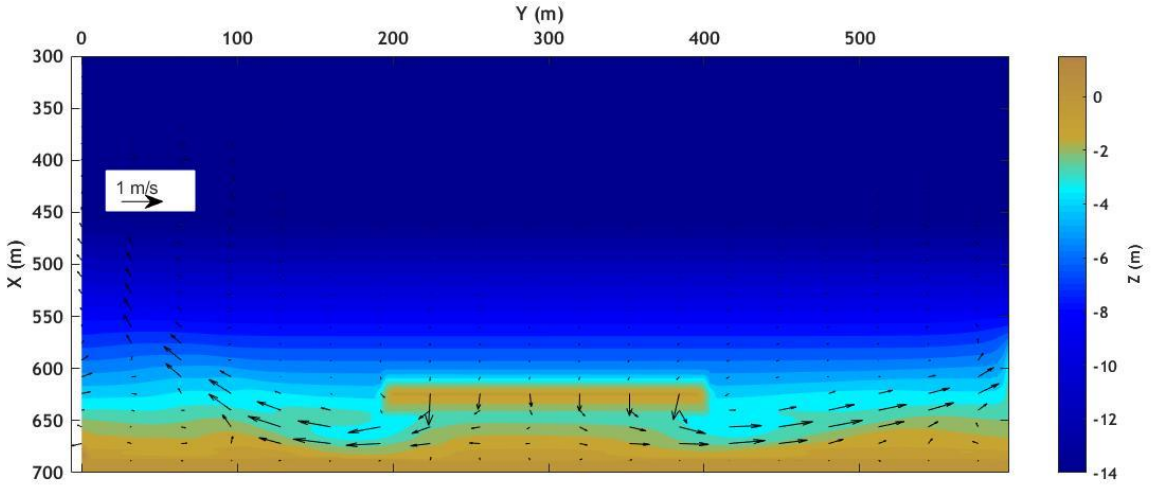

Figure B-4 Simulated hydrodynamics after 200 hour of wave action. Colors: Final Bathymetry, Vectors: calculated wave induced current intensity and direction. Bed slope: 6/100. Breakwater's distance to the shore: 80m.

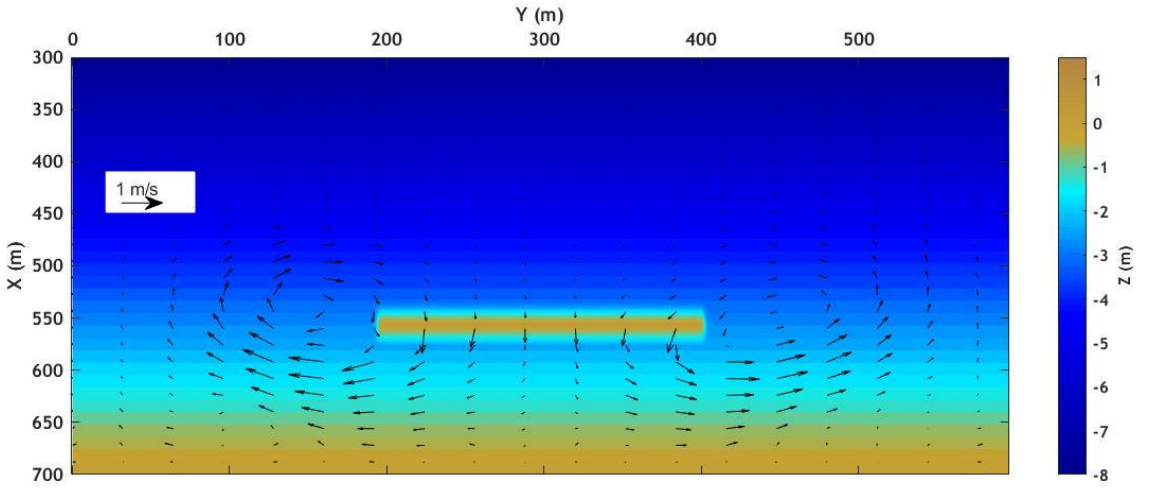

Figure B-5 Simulated hydrodynamics after 1 hour of wave action. Colors: Initial Bathymetry, Vectors: calculated wave induced current intensity and direction. Bed slope: 2/100. Breakwater's distance to the shore: 150m.

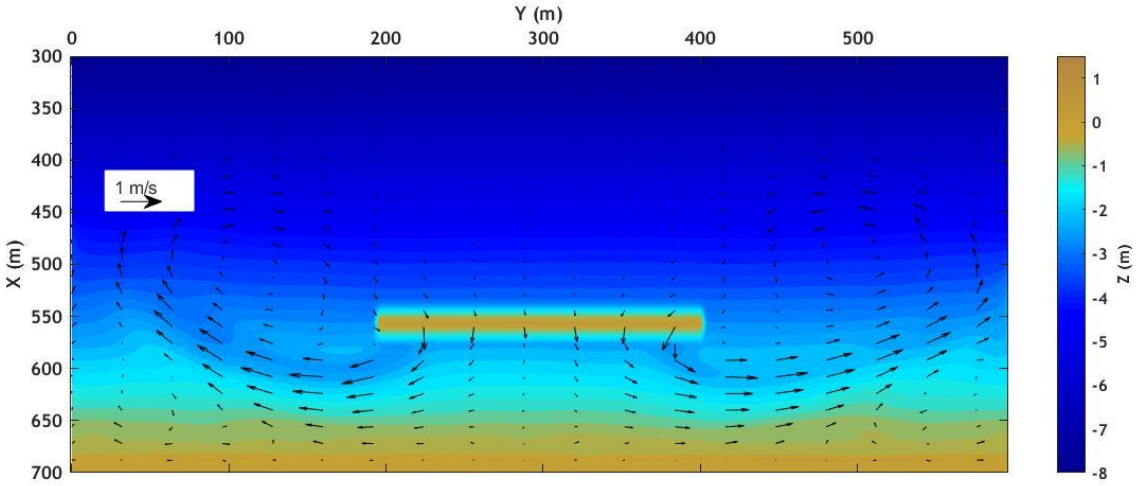

Figure B-6 Simulated hydrodynamics after 200 hour of wave action. Colors: Final Bathymetry, Vectors: calculated wave induced current intensity and direction. Bed slope: 2/100. Breakwater's distance to the shore: 150m.

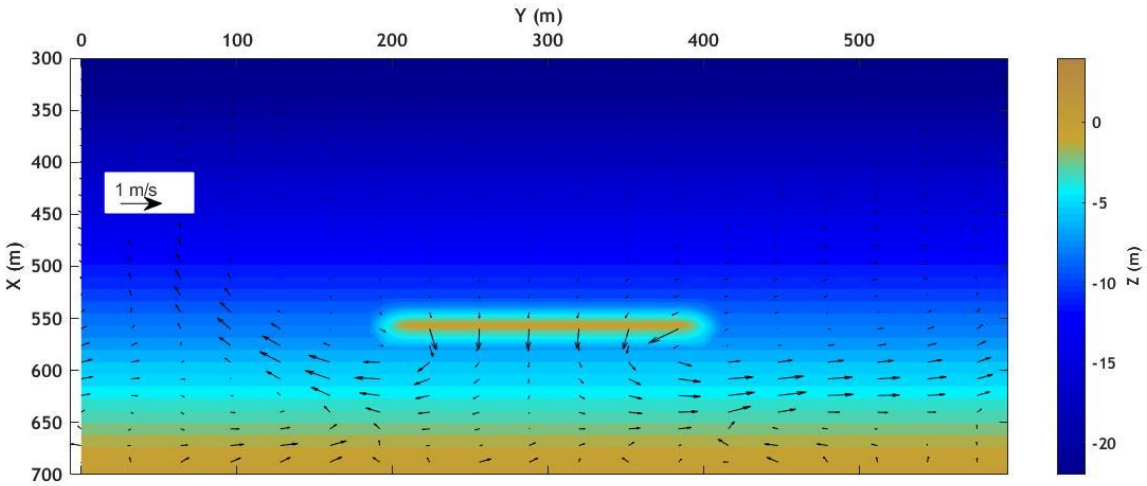

Figure B-7 Simulated hydrodynamics after 1 hour of wave action. Colors: Initial Bathymetry, Vectors: calculated wave induced current intensity and direction. Bed slope: 6/100. Breakwater's distance to the shore: 150m.

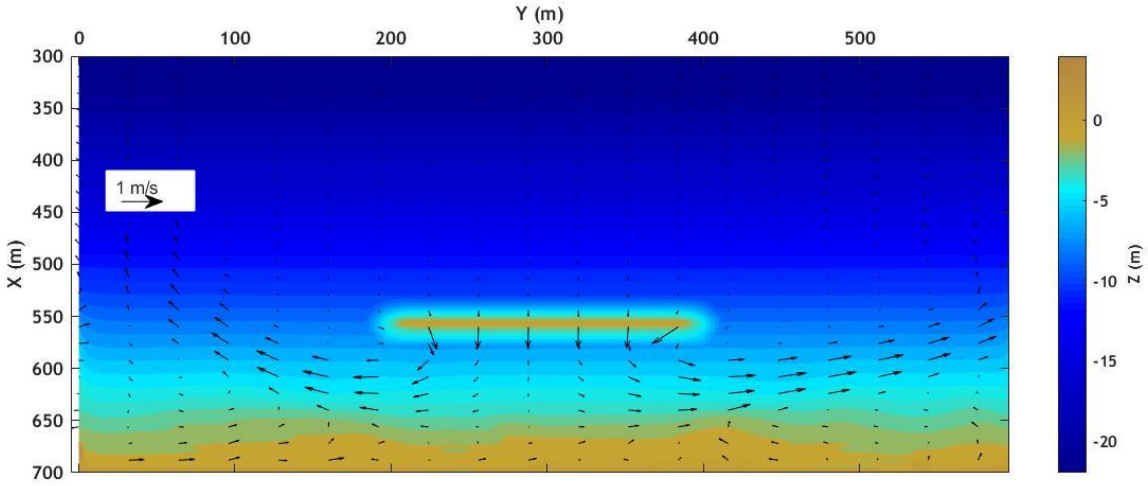

Figure B-8 Simulated hydrodynamics after 200 hour of wave action. Colors: Final Bathymetry, Vectors: calculated wave induced current intensity and direction. Bed slope: 6/100. Breakwater's distance to the shore: 150m.

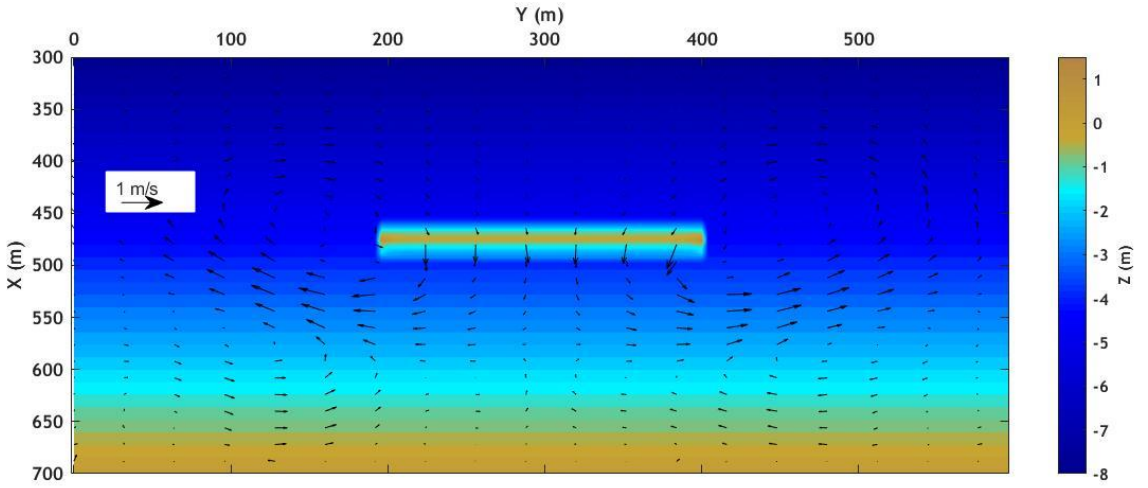

Figure B-9 Simulated hydrodynamics after 1 hour of wave action. Colors: Initial Bathymetry, Vectors: calculated wave induced current intensity and direction. Bed slope: 2/100. Breakwater's distance to the shore: 230m.

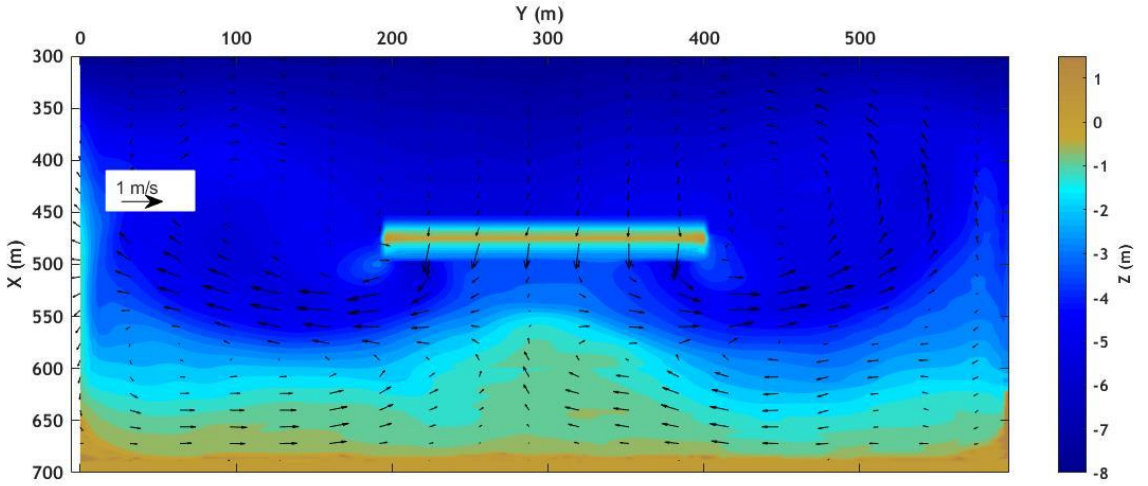

Figure B-10 Simulated hydrodynamics after 200 hour of wave action. Colors: Final Bathymetry, Vectors: calculated wave induced current intensity and direction. Bed slope: 2/100. Breakwater's distance to the shore: 230m.

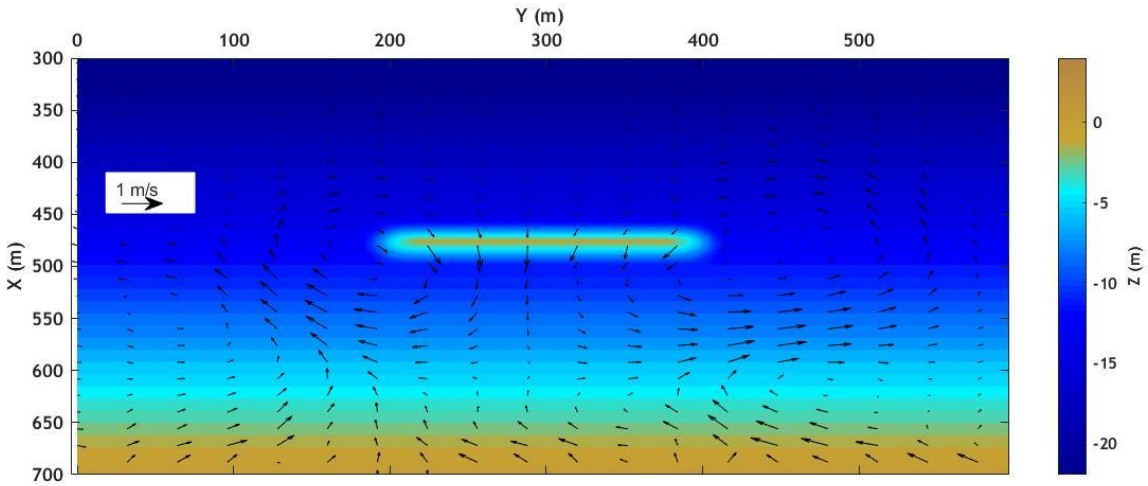

Figure B-11 Simulated hydrodynamics after 1 hour of wave action. Colors: Initial Bathymetry, Vectors: calculated wave induced current intensity and direction. Bed slope: 6/100. Breakwater's distance to the shore: 230m.

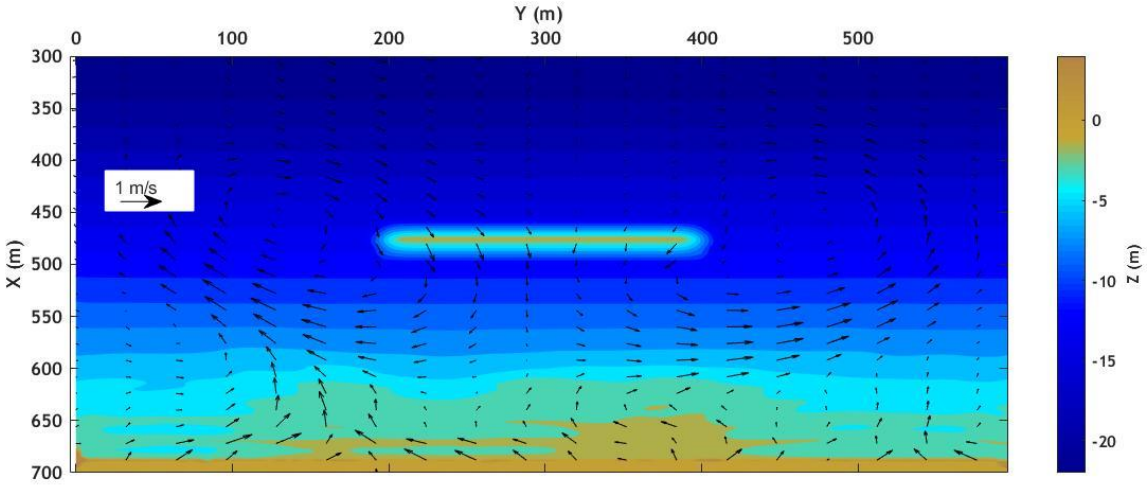

Figure B-12 Simulated hydrodynamics after 200 hour of wave action. Colors: Final Bathymetry, Vectors: calculated wave induced current intensity and direction. Bed slope: 6/100. Breakwater's distance to the shore: 230m.

Appendix C

In the present thesis several numerical codes and tools have been constructed, in Fortran, python and/or Matlab language, to obtain the desired results. The following Table presents these codes.

No	Code Name	Description
1	Q-3D Sediment Transport model	Novel quasi-3d sediment transport model (in Fortran – Python)
2	Bathymetry Update Model	Numerical model for the calculation of bottom changes (in Fortran – Python)
3	Wave generation	Numerical wave-maker for the generation of irregular waves using directional spectral data (in Fortran)
4	Sediment transport	Sediment transport model based on a quasi-steady approximation (in Fortran)
5	Visual-2D	Matlab tool to visualize wave height maps, current fields and bathymetrical updates (in Matlab)

Table 16 List of developed models and tools by the author.

Appendix D

The setup file of FUNWAVE-TVD model for the numerical case of paragraph 4.3.3.1, is presented here below:

```
!INPUT FILE FOR BOUSS_TVD
  ! NOTE: all input parameter are capital sensitive
  ! --------------------TITLE-------------------------------------
  ! title only for log file
TITLE = TEST RUN
  ! -------------------HOT START---------------------------------
HOT_START = F
FileNumber_HOTSTART = 1
  ! -------------------PARALLEL INFO-----------------------------
  !
  !    PX,PY - processor numbers in X and Y
  !    NOTE: make sure consistency with mpirun -np n (px*py)
  !
PX = 4
PY = 2
  ! --------------------DEPTH-------------------------------------
  ! Depth types, DEPTH_TYPE=DATA: from depth file
  !            DEPTH_TYPE=FLAT: idealized flat, need depth_flat
  !            DEPTH_TYPE=SLOPE: idealized slope,
  !                              need slope,SLP starting point, Xslp
  !                              and depth_flat
 DEPTH_TYPE = DATA
 !DEPTH_FLAT = 2.5
 !SLP = 0.0666667
 !Xslp = 62.5
 Mglob = 350
 Nglob = 180
 DX = 2.0
 DY = 5.0
 DEPTH_FILE = depth.txt
 DepthFormat = ELE
  ! if depth is flat and slope, specify flat_depth
!DEPTH_FLAT = 0.54
!  if depth is slope, specify slope and starting point
!SLP = 0.05
!Xslp = 0.0

  ! -------------------PRINT---------------------------------
  ! PRINT*,
  ! result folder
RESULT_FOLDER = r/
```

```
  ! ----------------- TIME---------------------------------
  ! time: total computational time/ plot time / screen interval
  ! all in seconds
TOTAL_TIME = 4320000
PLOT_INTV = 10000.0
!PLOT_INTV_STATION = 0.02
!SCREEN_INTV = 1000.0
!HOTSTART_INTV = 360000000000.0


  ! cartesian grid sizes
  ! --------------- INITIAL UVZ --------------------------
  ! INI_UVZ - initial UVZ e.g., initial deformation
  !        must provide three (3) files
INI_UVZ = F
  ! if true, input eta u and v file names
ETA_FILE = r/etamean_00001
U_FILE = r/umean_00001
V_FILE = r/vmean_00001
  ! ----------------WAVEMAKER-----------------------------
  !  wave makeer
  ! LEF_SOL- left boundary solitary, need AMP,DEP, LAGTIME
  ! INI_SOL- initial solitary wave, WKN B solution,
  ! need AMP, DEP, XWAVEMAKER
  ! INI_REC - rectangular hump, need to specify Xc,Yc and WID
  ! WK_REG - Wei and Kirby 1999 internal wave maker, Xc_WK,Tperiod
  !         AMP_WK,DEP_WK,Theta_WK, Time_ramp (factor of period)
  ! WK_IRR - Wei and Kirby 1999 TMA spectrum wavemaker, Xc_WK,
  !         DEP_WK,Time_ramp, Delta_WK, FreqPeak, FreqMin,FreqMax,
  !         Hmo,GammaTMA,ThetaPeak
  ! WK_TIME_SERIES - fft time series to get each wave component
  !                 and then use Wei and Kirby 1999
  !         need input WaveCompFile (including 3 columns: per,amp,pha)
  !         NumWaveComp,PeakPeriod,DEP_WK,Xc_WK,Ywidth_WK
WAVEMAKER = JON_2D
! WaveMaker
Time_ramp = 1.0
!Delta_WK = 0.5    ! width parameter 0.3-0.6
DEP_WK = 8.00
Xc_WK = 130.0
Ywidth_WK = 10000.0
! Wei and Kirby irregular wave
Hmo = 2.0
FreqPeak = 0.125
FreqMin = 0.0875
FreqMax = 0.375
!Tp=7.262s
!Tperiod = 1.0
```

```
!AMP_WK = 0.1
!Delta_WK = 3.0
  ! 2.95m
!GammaTMA = 3.3
ThetaPeak = 0.0
Sigma_Theta = 0.0
  ! ---------------- PERIODIC BOUNDARY CONDITION ---------
  ! South-North periodic boundary condition
  !
PERIODIC = T
  ! ---------------- SPONGE LAYER -----------------------
  ! DHI type sponge layer
  ! need to specify widths of four boundaries and parameters
  ! set width=0.0 if no sponge
  ! R_sponge: decay rate
  ! A_sponge: maximum decay rate
DIFFUSION_SPONGE = F
FRICTION_SPONGE = T
DIRECT_SPONGE = T
Csp = 0.0
CDsponge = 1.0
Sponge_west_width = 100.0
Sponge_east_width =  0.0
Sponge_south_width = 0.0
Sponge_north_width = 0.0
  ! ----------------OBSTACLES----------------------------
  ! obstacle structures using mask_struc file
  ! mask_struc =0 means structure element
  ! give a file contains a mask array with Mloc X Nloc
BREAKWATER_FILE=Breakwater200.txt
BreakWaterAbsorbCoef=5.0
  ! ----------------PHYSICS-----------------------------
  ! parameters to control type of equations
  ! dispersion: all dispersive terms
  ! gamma1=1.0,gamma2=0.0: NG's equations
  ! gamma1=1.0,gamma2=1.0: Fully nonlinear equations
DISPERSION = T
Gamma1 = 1.0
Gamma2 = 1.0
Gamma3 = 1.0
Beta_ref=-0.531
SWE_ETA_DEP = 0.80
  !----------------Friction----------------------------
Friction_Matrix= T
Cd_file= btrad.txt
!Cd = 0.000

  ! ----------------NUMERICS----------------------------
  ! time scheme: runge_kutta for all types of equations
  !              predictor-corrector for NSWE
```

```
  ! space scheme: second-order
  !               fourth-order
  ! construction: HLLC
  ! cfl condition: CFL
  ! froude number cap: FroudeCap

! Time_Scheme = Runge_Kutta
!Time_Scheme = Predictor_Corrector
  ! spacial differencing
HIGH_ORDER = FOURTH
!HIGH_ORDER = THIRD
 CONSTRUCTION = HLLC
  ! CFL
CFL = 0.64
  ! Froude Number Cap (to avoid jumping drop, set 10)
!FroudeCap = 10.0

  ! --------------WET-DRY-----------------------------
  ! MinDepth for wetting-drying
MinDepth=0.01
  ! -----------------
  ! MinDepthfrc to limit bottom friction
MinDepthFrc = 0.2

  ! -------------- SHOW BREAKING ------------------------
VISCOSITY_BREAKING = F
ROLLER_EFFECT = T
Cbrk1 = 0.65
Cbrk2 = 0.35

BATHY_CORRECTION = F

SmoothBelowDepth = 0

SlopeCap = 0.29

T_INTV_mean = 36000.0
STEADY_TIME= 36000.00

  ! -----------------OUTPUT-----------------------------
  ! stations
  ! if NumberStations>0, need input i,j in STATION_FILE
NumberStations = 0
STATIONS_FILE = nothing
  ! output variables, T=.TRUE, F = .FALSE.
DEPTH_OUT = T
U = T
V = T
ETA = T
Hmax = F
```

Hmin = F
MFmax = F
Umax = T
VORmax = F
Umean = T
Vmean = T
ETAmean = T
MASK = T
MASK9 = F
SXL = F
SXR = F
SYL = F
SYR = F
SourceX = F
SourceY = F
P = T
Q = T
Fx = F
Fy = F
Gx = F
Gy = F
AGE = F
TMP = F
WaveHeight = T